THE INFLUENCE OF REGIONAL STRESS AND STRUCTURAL CONTROL ON THE SHAPE OF MAAR CRATERS

A THESIS IN
Environmental and Urban Geoscience

Presented to the Faculty of the University
Of Missouri-Kansas City in partial fulfillment of
The requirements for the degree

MASTER OF SCIENCE

by
Cody Nichols

B.S., Northwest Missouri State University, 2015

Kansas City, Missouri
2018

THE INFLUENCE OF REGIONAL STRESS AND STRUCTURAL CONTROL ON THE SHAPE OF MAAR CRATERS

Cody Nichols, Candidate for the Masters of Science Degree

University of Missouri-Kansas City, 2018

ABSTRACT

This study aims to gain a better understanding of the factors leading to the expressed shape of individual maars in volcanic fields. Maars are volcanic features produced by phreatomagmatic eruptions which excavate a crater beneath the pre-eruptive surface through the explosive interaction of magma and water. Maar craters take on a wide range of shapes including, circular, elliptical, and polylobate. Across all maar fields, the existence of one or more axis of elongation is commonplace. Identification of the factors which lead to, and control, elongation in individual maars will help improve the accuracy of current hazard mapping and safety protocols. In order to determine

whether the orientations of elongation are controlled by existing structures and regional stress, the primary and secondary directions of elongation of maar craters from a range of tectonic settings were measured. Maars were found to exhibit similar primary elongation orientations within each field. Influence of regional stress was identified in the geographic placement of maars along lineaments in most fields. Although many maars were found in lineaments identified through nearest neighbor analyses, they rarely share primary elongation orientations with the lineaments they compose. Furthermore, maars which shared similar primary elongation orientations with one another were not found to be grouped close together geographically. Overall, the number of maars in each field which share primary elongation orientations with existing structures (faults) and nearest neighbor lineaments does not suggest regional structural control over primary elongation orientation in any field. The tendency of maars to exhibit similar primary elongation orientations within a field, coupled with the lack of correlation with structural controls shows that the elongation orientations of maars are likely governed by more local controls related to host rock material, explosion induced changes to the stress regime, or hydrology.

The faculty listed below, appointed by the Dean of the College of Arts and Sciences, have examined a thesis titled “The Influence of Regional Stress and Structural Control Over the Shape of Maar Craters”, presented by Cody Nichols, candidate for the Masters of Science: Environmental and Urban Geoscience degree, and certify that in their opinion it is worthy of acceptance.

Supervisory Committee

Alison H. Graettinger, Ph.D., Committee Chair
Department of Geoscience

James B. Murowchick, Ph.D.
Department of Geoscience

Tina M. Niemi, Ph.D.
Department of Geoscience

TABLE OF CONTENTS

LIST OF ILLUSTRATIONS

LIST OF TABLES

ACKNOWLEDGEMENTS

This author wishes to acknowledge the contributions of the following people, without whom this thesis would not have been possible. First and foremost, my thanks go out to my advisor, Dr. Alison Graettinger. Without your guidance, continual support, and profound patience this work would never have been realized. Dr.'s Jozua Van Otterloo and Francesco Mazzarini, I cannot thank you enough for making your data available to me. Your generosity not only helped make this paper possible, but also greatly enhanced the accuracy of our findings. To my mother, grandparents, and friends; thank you for all of your love and support in seeing this through. Kadie Bennis, thanks for always lending a listening ear. Megan Medley, thanks for all the tireless hours you've put in on my behalf; I wouldn't be here without your help. Finally, to Brittney Siefker, thanks for your unconditional support, love, and friendship. I never imagined that I would encounter so many extraordinary people over the course of this research. My thanks go out to all of you.

CHAPTER 1

INTRODUCTION

Maars are small volcanic craters, primarily distinguished from other volcanic features in that the floor lies below the pre-eruptive surface (White and Ross, 2011). Maar craters are the product of hundreds of phreatomagmatic explosions resulting from contact between magma and groundwater. Each of these individual explosions excavates the ground above, creating a crater (Figure 1). Although these eruptions generate craters of varying size and shape, one thing that does remain constant across nearly all maars is a general elongation (Graettinger, 2018). For a maar to form, both magma and water must be present at the time of eruption. In vents and cones, as wells as maars, magma is sourced from a larger body and approaches the surface through intrusive processes.

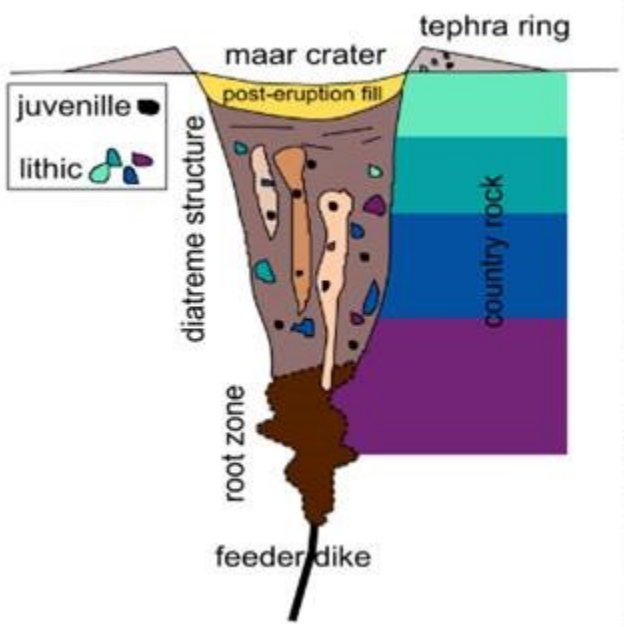

Figure 1 – Illustration showing the structure of maar craters

Previous research has shown that some fields exhibit a correlation between the alignment of volcanic vents and cones, and fault orientation (Connor and Aubele, 1992; Mazzarini and D'Orazio, 2003; Cebriá, J. M., Martín-Escorza, C., López-Ruiz, J., Morán-Zenteno, D. J., & Martiny, B. M., 2011; Hernando, I. R., Franzese, J. R., Llambías, E. J., & Petrinovic, I. A., 2014), demonstrating that regional structures play a role in the distribution of volcanic features within a field. When regional stresses pull apart pre-existing faults, it creates a potential pathway for magma to propagate to the surface.

Alternatively, in the absence of pre-existing structures, dikes cut their own path to the surface under the influence of regional stresses alone. This could be thought of as a macro (or large scale) expression of magma distribution. In a study of the elliptical calderas of the Ethiopian rift, Acocella, V., Korme, T., Salvini, F., & Funiciello, R. (2003) found that E-W pre-rift fractures had been reactivated during development of the magma chambers leading to E-W elongation of the caldera in surface expression. The orientation of structures exploited during the placement of maar craters could control the distribution of magma at the site of an eruption, resulting in a similar elongation orientation between maars and regional structures. It is the purpose of this study to identify whether this correlation can be extended to maars. To this end, seven volcanic fields have been chosen, representing a range of stress regimes, to discern whether a relationship exists between the orientation of stress indicators, including faults and lineations, and the direction in which maars proximally close to those features are elongated. The chosen field are Auckland Volcanic Field, Lamongan Volcanic Field, the Newer Volcanic Province, Pali Aike Volcanic Field, Pinacate Volcanic Field, San Pablo City Volcanic Field, and Serdán Oriental Volcanic Field. Because regional stress plays such a significant role in the formation of faults and volcanic features, it is important that a diversity of settings be represented within the study, as results for one field may not be representative of the whole. A subset of well-preserved maars were chosen from each field. These maars were selected primarily based upon the degree to which their crater rim could be clearly

defined from satellite imagery. It is crucial that the crater's rim be easily ascertained, as the shape of the maars in question is pivotal to the connections this study is aimed at uncovering. What follows is a brief introduction to each of the chosen fields, their geologic history, and tectonic settings.

CHAPTER 2

SETTING

Auckland Volcanic Field

The Auckland Volcanic field of northern New Zealand is an example of intraplate volcanism (Figure 2 and Figure 3). Located roughly 400 km west of the present-day subduction zone (Cassidy and Locke, 2010), the field occupies an area of 336 km^2 and contains roughly 52 small monogenetic volcanic centers (Kereszturi, G., Németh, K., Cronin, S. J., Procter, J., & Agustín-Flores, J., 2014). It is estimated that the field was produced by slow upwelling of the asthenosphere from three different sources of varying depth (Kereszturi et al., 2014). Comprised predominately of alkali basalts or basanites with less common tholeiite, transitional basalt, and nephelinite, the best defined maximum age for the field is 200 ka (Cassidy and Locke, 2010). The youngest volcano, however, is only several hundred years old (Cassidy and Locke, 2010). While the basement region consists of Mesozoic metasedimentary terranes trending NNW, the field is mainly hosted by sedimentary rocks in alternating sequences of sandstones and mudstones of Miocene-Eocene age (Cassidy and Locke, 2010) (Table 1). Faults striking NNW and ENE were produced throughout the region by basement uplift as a consequence of Miocene-Quaternary extensional block faulting to the immediate east (Cassidy and Locke, 2010). A

wide range of eruption styles are exhibited, but phreatomagmatics dominate the region (Cassidy and Locke, 2010).

Table 1 - Host and Basement Rock in Field

Field Name	Basement Rock	Host Rock
Auckland Volcanic Field	Metasedimentary Terranes	Alternating layers of sandstone and mudstone
Lamongan Volcanic Field	Unidentified	Unidentified
Newer Volcanic Province	Metamorphic, Volcanic and Sedimentary	Basin Sediments
Pali Aike Volcanic Field	Metamorphic	Volcanic Sedimentary Infill
Pinacate Volcanic Field	Basalt	Basin Filling Sediment
San Pablo City Volcanic Field	Unidentified	Unidentified
Serdán Oriental Volcanic Field	Limestone	Pyroclastic deposits and basaltic lava flows

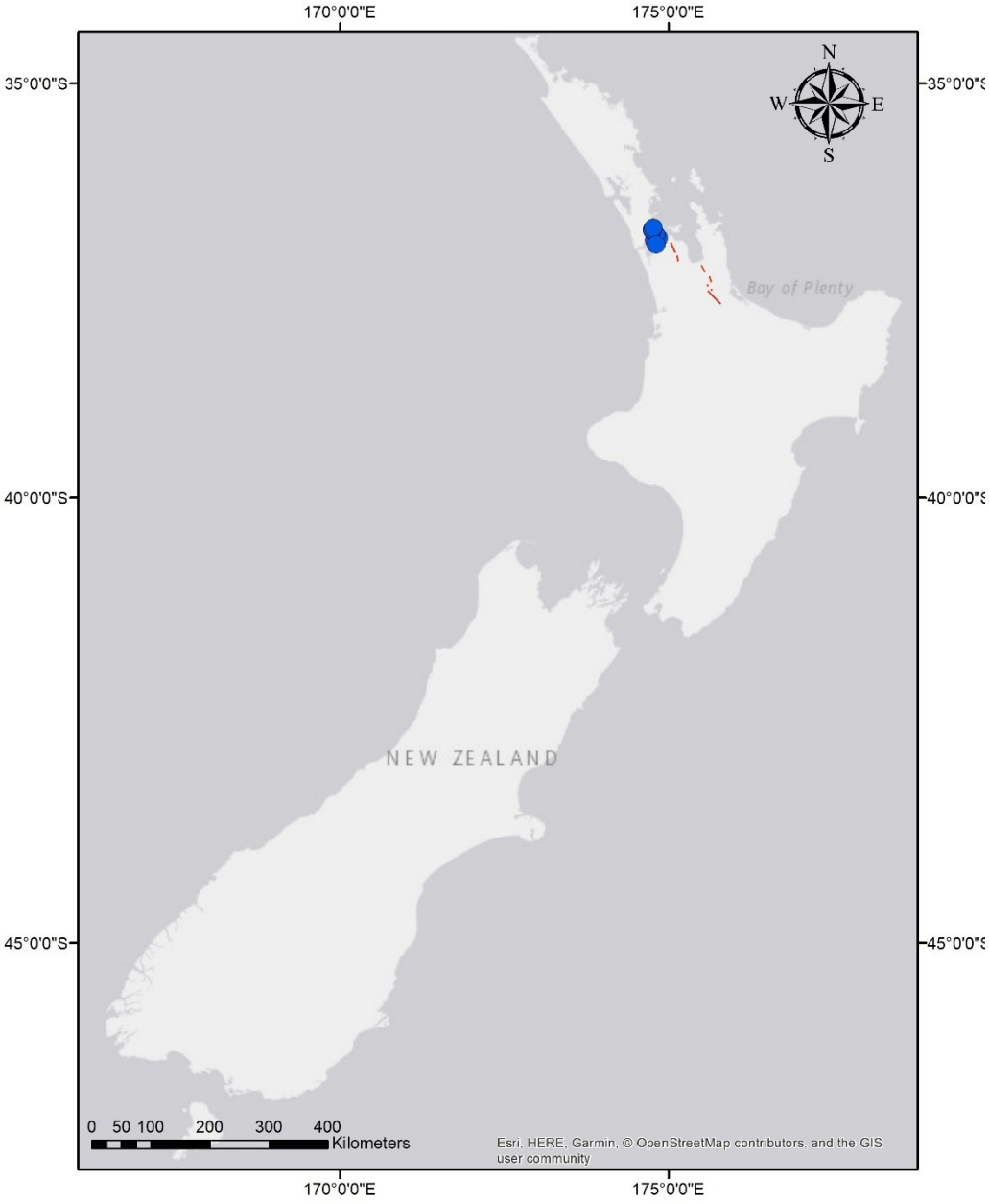

Figure 2 - Auckland Volcanic Field (New Zealand) – Shows a regional view of the field with faults in red and maars in blue.

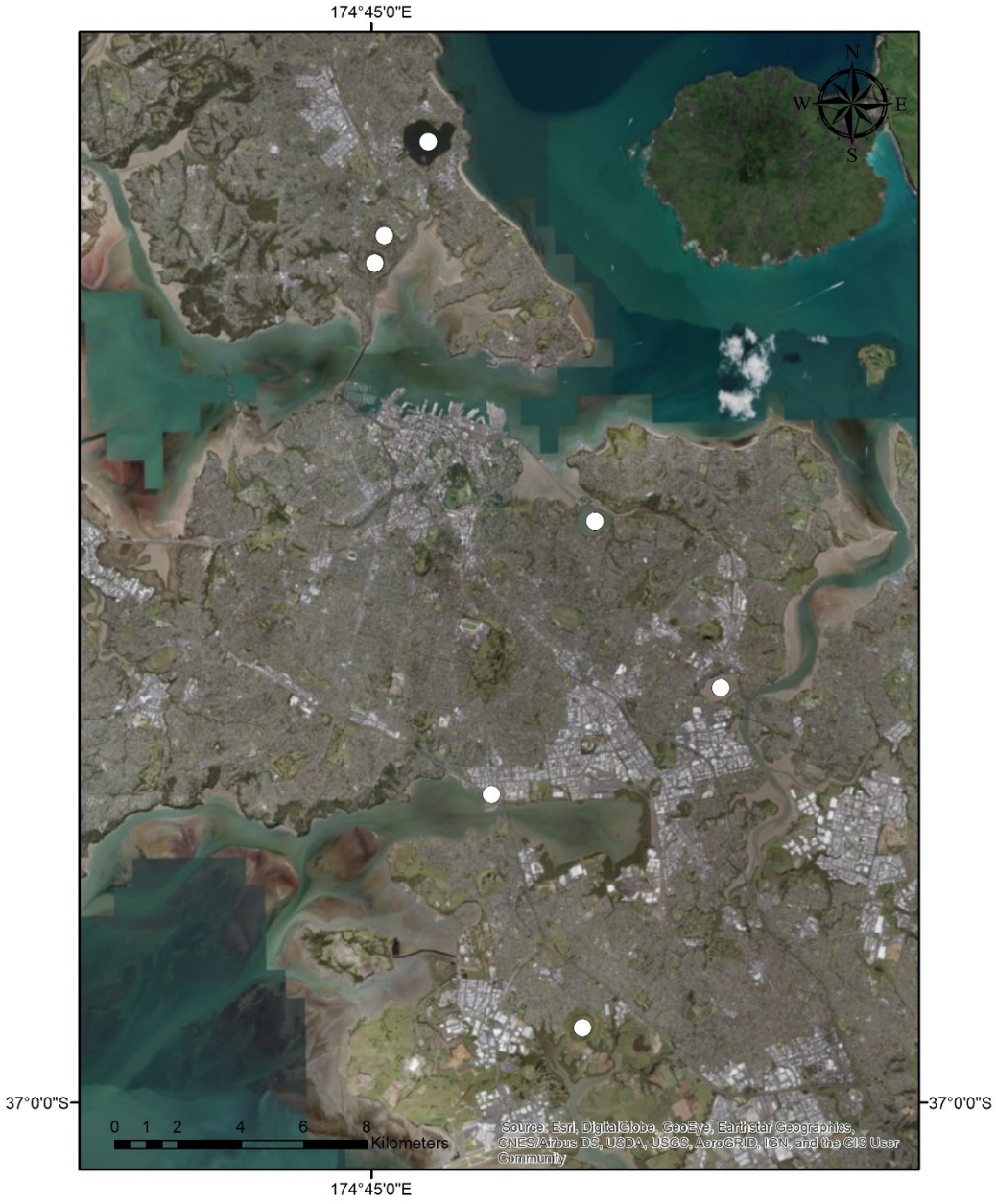

Figure 3 – A satellite view of Auckland Volcanic Field in New Zealand with white dots marking the location of the seven maar craters included in this study.

Lamongan Volcanic Field

In east Java, Indonesia, at the point where the peninsula is pinched into its narrowest section, the Lamongan volcanic field rests within the Sunda Volcanic Arc (Figure 4 and Figure 5). Spanning approximately 260 km^2, the Sunda Arc is the surface expression of the northward subduction of the Indo-Australian Plate beneath the Eurasian Plate (Carn, 1999). The active subduction in this area has been fueling volcanic activity from the Holocene up to present day (Carn, 1999). Lava flows and cones of the Lamongan Volcanic Field exhibit a range of compositions from basalt to basaltic andesite (Carn,1999). Within the field there are 61 basaltic cinder cones, 29 maars, and a stratovolcano with three main vents known as the Central Complex (Carn, 1999). The maars are predominantly circumferential and radial in locations close to the central complex, and are concentrated to the East, North, and West of the complex at elevations between 175 and 700 m above sea level (Carn, 1999). Synoptic radar imagery shows evidence for regional NW-SE and NE-SW faulting (Carn, 1999). Unfortunately, host and basement rock could not be identified for this field owing to the limited publications available on it (Table 1).

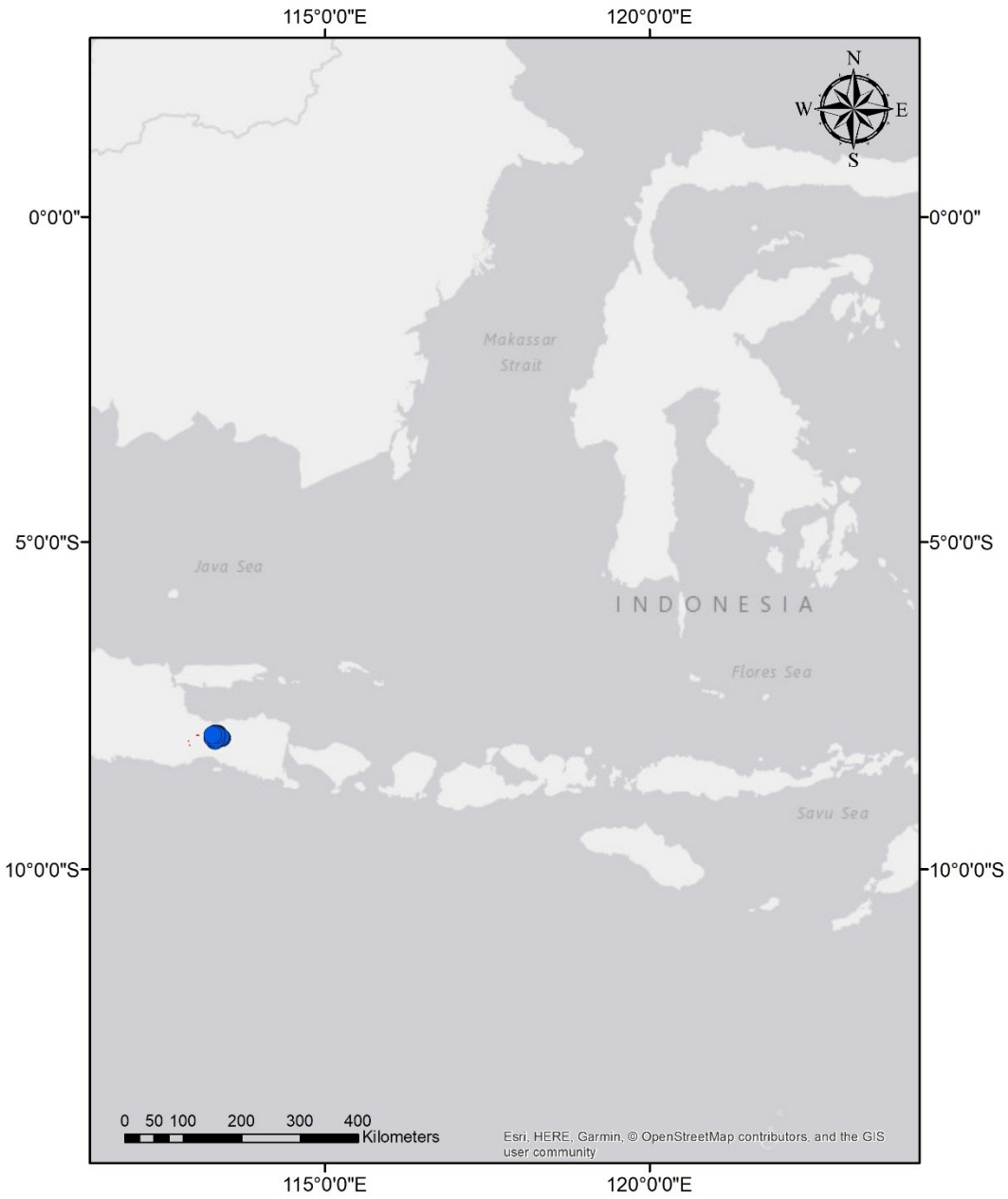

Figure 4 - Lamongan Volcanic Field (Indonesia) – Shows a regional view of the field with faults in red and maars in blue.

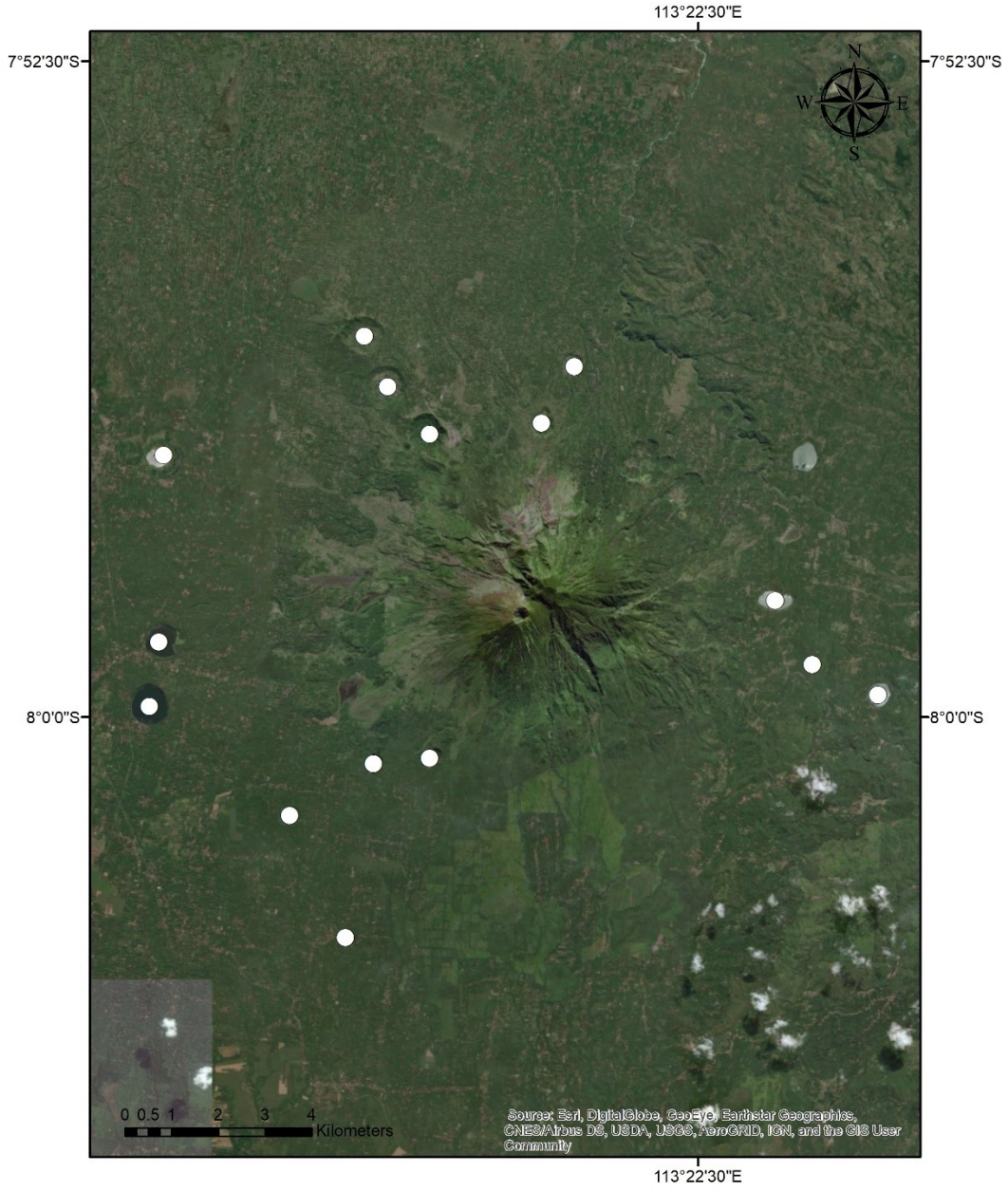

Figure 5 – A satellite view of Lamongan Volcanic in Indonesia with white dots marking the location of the 16 maar craters included in this study.

Newer Volcanic Province

The Newer Volcanic Province is an intraplate volcanic region located in the Victoria province of south eastern Australia (Figure 6, Figure 7, and Figure 8). The area spans roughly 19,000 km^2 and contains over 400 eruption points (Boyce, 2013). Among these eruption points, 23 maars have been identified for use in our study. Most of the maars of NVP (and all the maars utilized in this study) fall within the Otway Basin, along the southern coast of the region. The Otway Basin is an extensional basin formed as part of an intraplate rift system during the break-up of Australia and east Antarctica (Kharazizadeh, N., Schellart, W.P., Duarte, J.C., and Hall, M., 2017). The products of eruptive activity in the Newer Volcanic Province range from tholeiitic to alkalic basalt (Lesti, C., Giordano, G., Salvini, F., & Cas, R., 2008). Volcanic activity in the region dates to the Pliocene-Holocene epochs with evidence supporting the presence of a 32-km-deep thermal anomaly in the mantle (Lesti et al., 2008). Most of the selected maars have near neighbors, exhibiting a strong tendency to occur in clusters. The maars of the Newer Volcanic Province fall toward the southern end of the western plains province, which has extensive lava fields atop the Otway Basin sediments (Boyce, 2013). Beneath the basin sediments the basement is divided between two adjacent Orogens (Kharazizadeh et al. 2017). Under the eastern half of the Otway Basin, the Lachlan Orogen is comprised of oceanic boninitic, tholeiitic volcanic rocks, island arc crust, and deep marine sediments. To the west, the Delamerian Orogen comprises strongly deformed volcanic and sedimentary rocks

(Kharazizadeh et al. 2017) (Table 1). The region is crosscut by multiple major fault lines, predominately oriented in a North-South direction. Of these faults, the Moyston (normal), Avoca (reverse), and Hummocs pass directly through regions populated by the maars outlined for use in this study (Kharazizadeh et al. 2017).

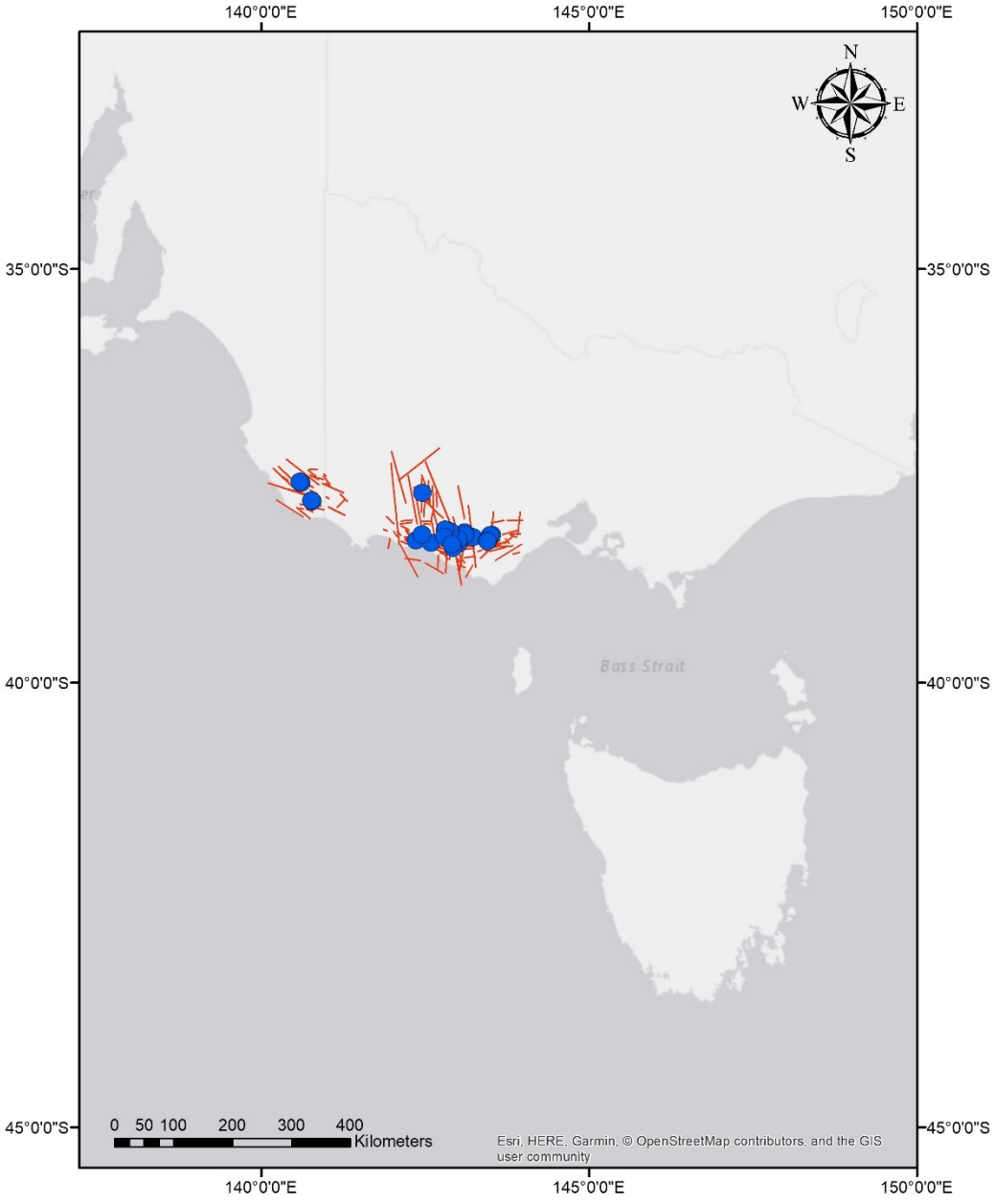

Figure 6 - Newer Volcanic Province (Australia) – Shows a regional view of the field with faults in red and maars in blue.

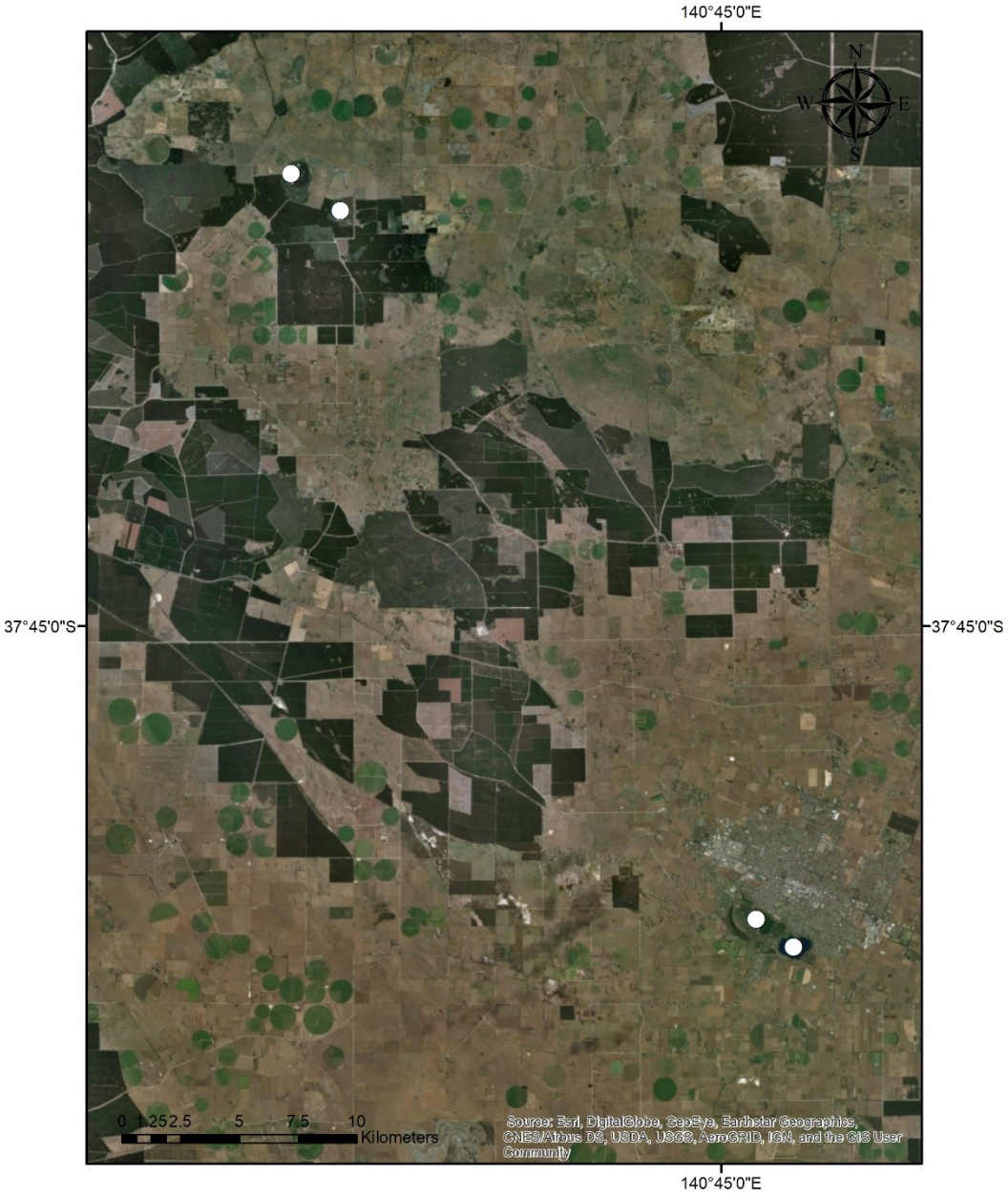

Figure 7 – A satellite view of the western half of the Newer Volcanic Province in Australia with white dots marking the location of the four maar craters.

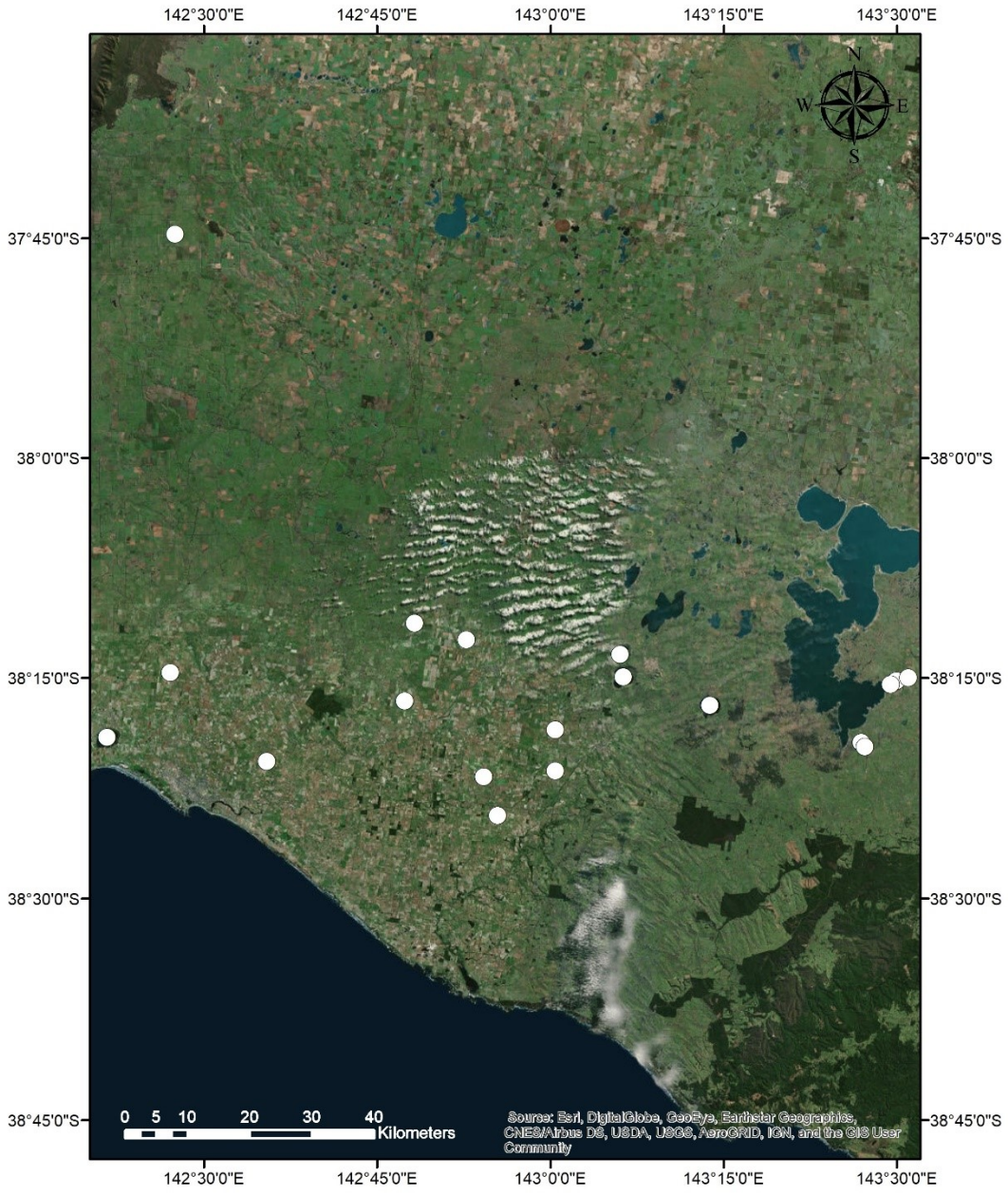

Figure 8 – A satellite view of the eastern half of the Newer Volcanic Province in Australia with white dots marking the location of the nineteen maar craters included in this study.

Pali Aike Volcanic Field

The Pali Aike volcanic field (Figure 9 and Figure 10) marks a major Pliocene – Quaternary phase in the development of the Magellan Neogene rift system in Southern Argentina (Mazzarini and D'Orazio, 2003). Spanning roughly 4500 km^2 (Ross, P. S., Delpit, S., Haller, M. J., Németh, K., & Corbella, H., 2011), the field is mostly built on top of volcano-sedimentary infill with intercalated silicic volcanic rocks with a Paleozoic metamorphic basement (Mazzarini and D'Orazio, 2003) (Table 1). The basin infill sequence reaches 2 to 3 km in thickness in the area of the Pali Aike Volcanic Field (Mazzarini and D'Orazio, 2003). The 476 eruptive features in the field exhibit predominantly primary magma compositions (Mazzarini and D'Orazio, 2003). These alkali basaltic/basanitic magmas likely spent little time in their ascent to the surface (Mazzarini and D'Orazio, 2003). Situated in an area of mutual interaction among four lithospheric plates, the principal stress field of the region is dominated by the convergence between the Antarctic and South American plates and by the strike slip motion between the South American and Scotia plates, generating NE-SW and ENE-WSW principal horizontal compressional stresses (Mazzarini and D'Orazio, 2003). The field, however, is so distanced from the subduction boundary that the principle stresses at play are likely not compressional. Isotopic age determinations (K-Ar and ^{40}Ar-^{39}Ar methods) for the Pali Aike Volcanic Field span from 3.78 to 0.17 Ma, although the youngest and best-preserved lava flows suggest a younger age for the final period of activity (Mazzarini and D'Orazio, 2003).

Maars chosen for elongation orientation analysis in this study likely fall into the latter age group as they still exhibit clearly preserved crater rims. Investigation into the main morphometric features and spatial distribution of the ~450 monogenetic cones reveals that cone alignment and elongation are mainly controlled by ENE-WSW and NW-SE trending structures (Mazzarini and D'Orazio, 2003). Mazzarini et al. (2003), however, did not investigate the maars as an independent population.

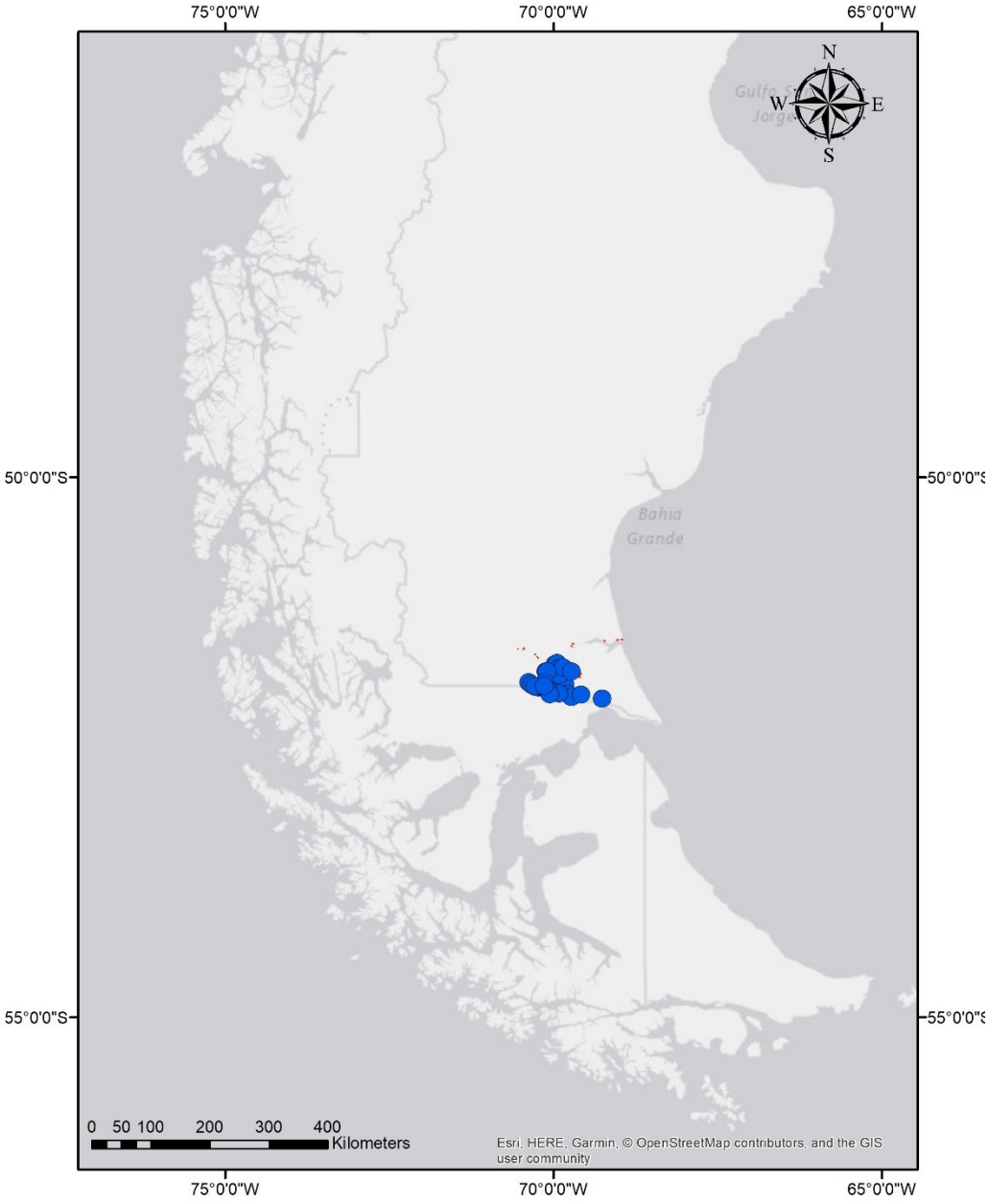

Figure 9 - Pali Aike Volcanic Field (Argentina) – Shows a regional view of the field with faults in red and maars in blue.

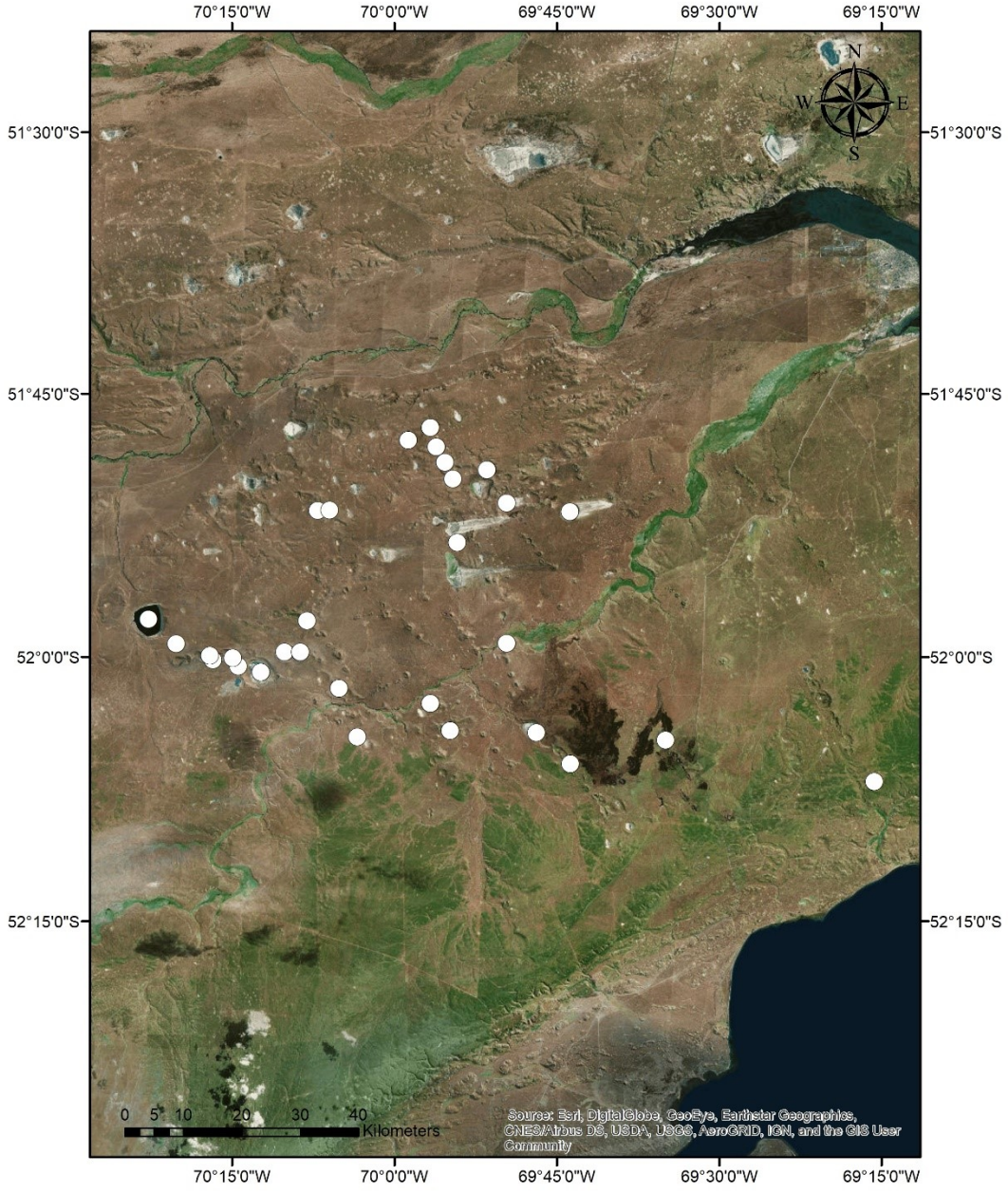

Figure 10 – A satellite view of the Pali Aike Volcanic Field in Argentina with white dots marking the location of the 27 included maar craters.

Pinacate Volcanic Field

The Pinacate volcanic field (Figure 11 and Figure 12) of Sonora Mexico lies in the Sonoran Desert, just a few kilometers east of the Gulf of California (Gutmann, 2002) in the Gulf of California Extensional Province (García-Abdeslem and Calmus, 2015). Here, 400 cinder and spatter cones, eight maar craters, aa and pahoehoe flows (García-Abdeslem and Calmus, 2015) are strewn about over 1500 km^2(Turrin, B. D., Gutmann, J. T., & Swisher, C. C., 2008). All eight maars and one large tuff cone lie across an arcuate path following what is believed to have been the path of the Sonoyta River in years past (Gutmann, 2002). Dating of the Pinacate series yielded an age of 13 +/- 3 ka (Turrin et al. 2008). Isotopic data suggests an asthenospheric source for Pinacate lavas (Lynch, D.J., Musselman, T.E., Gutmann, J.T., and Patchett, P.J., 1993). Along cliffside outcrops the rocks used to interpret the eruptive history of the field are exposed (Gutmann, 2002). Thick basaltic lava flows rest on basin-filling sediment, which itself rests on top of a Miocene basaltic basement (Gutmann, 2002; García-Abdeslem and Calmus, 2015) (Table 1). Nearby, the Pacific – North American plate boundary is defined by the right lateral, NW-SE-trending, Imperial and Cerro Prieto faults (García-Abdeslem and Calmus, 2015).

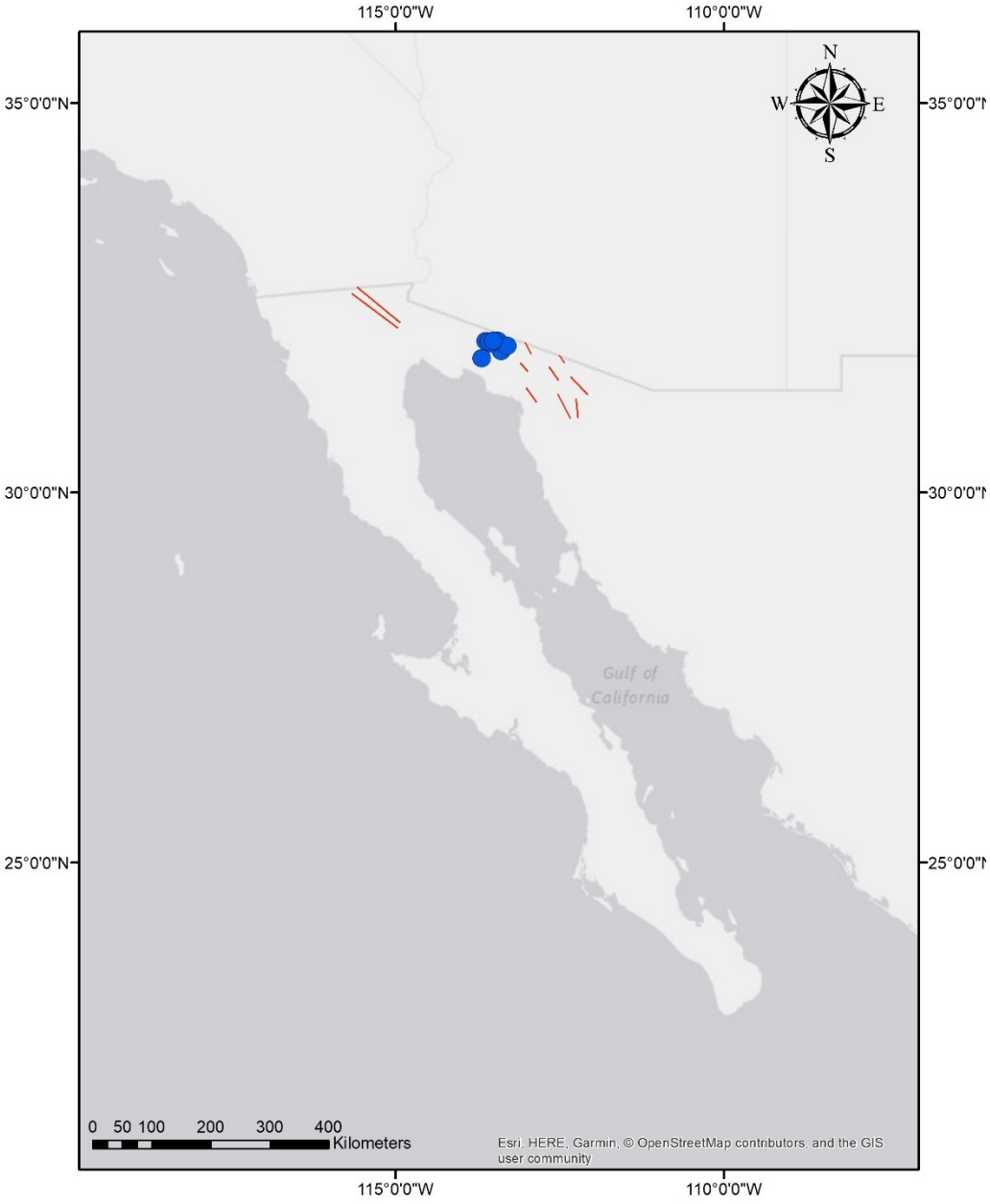

Figure 11 - Pinacate Volcanic Field (Mexico) – Shows a regional view of the field with faults in red and maars in blue.

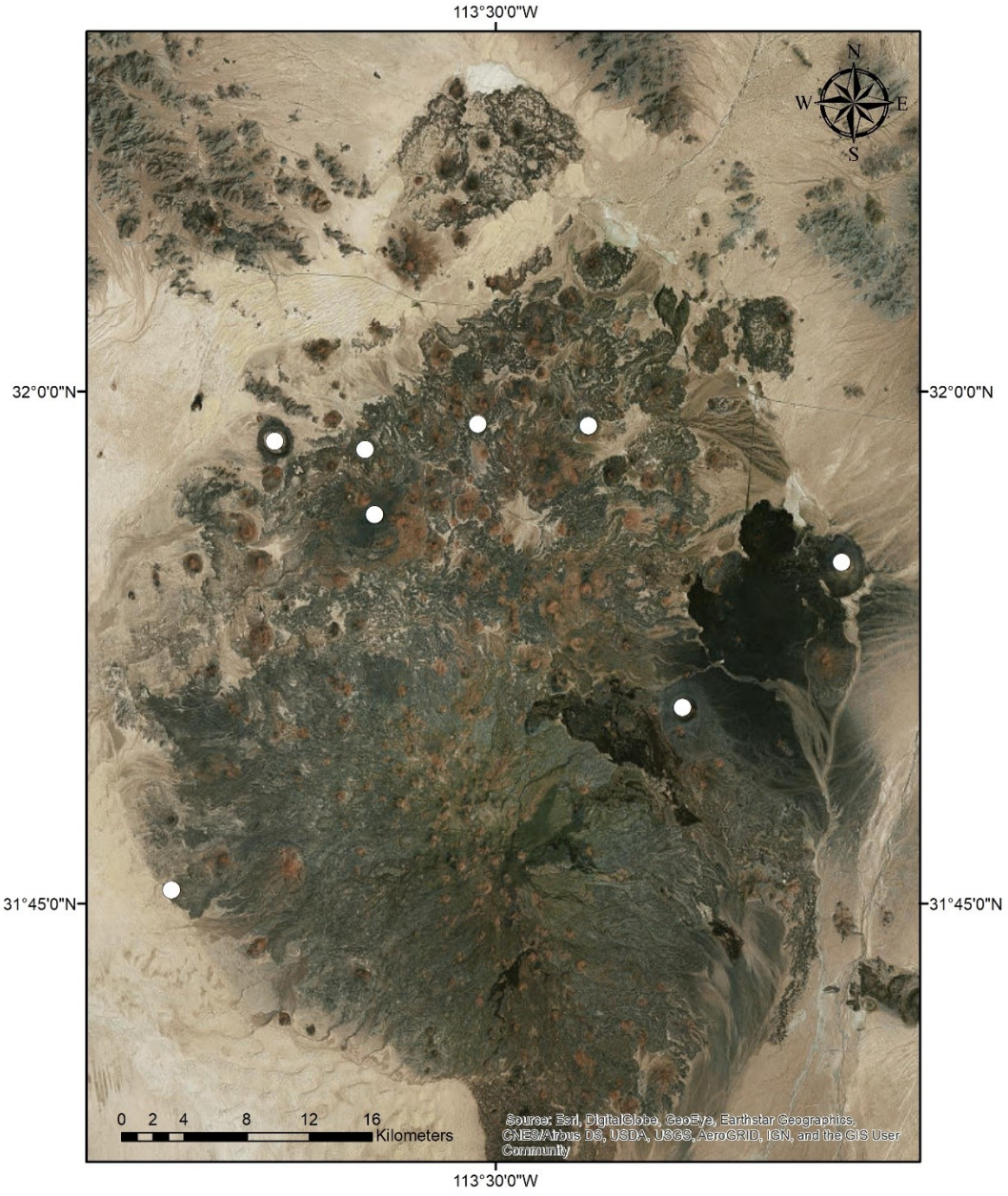

Figure 12 – A satellite view of Pinacate Volcanic Field in Northern Mexico with white dots marking the location of the eight included maar craters.

San Pablo City Volcanic Field

The San Pablo City Volcanic Field (Figure 13 and Figure 14), occurs within the Macolod Corridor on the island of Luzon in the Philippines. The Macolod Corridor, like most of the Philippine Archipelago, lies between two opposing subduction systems (Vogel, T.A., Flood, T.P., Patino, L.C., Wilmot, M.S., Maximo, R.P.R., Arpa, C.B., Arcilla, C.A., and Stimac, J.A., 2006). Torn between Eastward subduction along the Manila Trench, and Westward subduction along the Philippine Trench, the Macolod Corridor is a NE-trending, 80 km wide zone of extensional faulting between these two segments of the Luzon Arc (Vogel et al., 2006). It contains two calderas, three stratovolcanoes, and hundreds of maars and scoria cones (Defant, M. J., De Boer, J. Z., & Dietmar, O., 1988; Förster, H., Oles, D., Knittel, U., Defant, M. J., & Torres, R. C., 1990; Ku, Y. P., Chen, C. H., Song, S. R., Iizuka, Y., & Shen, J. J. S., 2009). The lavas of the Macolod Corridor are almost exclusively basaltic and were generated by relatively small degrees of partial melting of a mantle segment that escaped enrichment by the subducted South China Sea lithosphere (Förster et al., 1990). The San Pablo City Volcanic Field contains 16 maars (14 of which were used for calculating primary elongation orientation) and a handful of scoria cones.

With regard to orientation and location, the volcanoes within the Macolod Corridor older than 1 Ma are formed on N-S and E-W trending fault systems (Förster et al., 1990). An E-W trending left-lateral, strike-slip fault zone is located in the Philippine Sea at about 15^{o}N in the northeastern extension of the Macolod Corridor (Förster et al. 1990). It

connects the Philippine trench and the east Luzon Trough (Lewis and Hayes, 1989). Although publications pertaining to the Macolod Corridor are abundant, the host and basement rock, age of the field, and total area it occupies could not be identified for the San Pablo City Volcanic Field due to the lack of emphasis on this section of the corridor (Table 1).

Figure 13 - San Pablo City Volcanic Field (Philippines) – Shows a regional view of the field with faults in red and maars in blue.

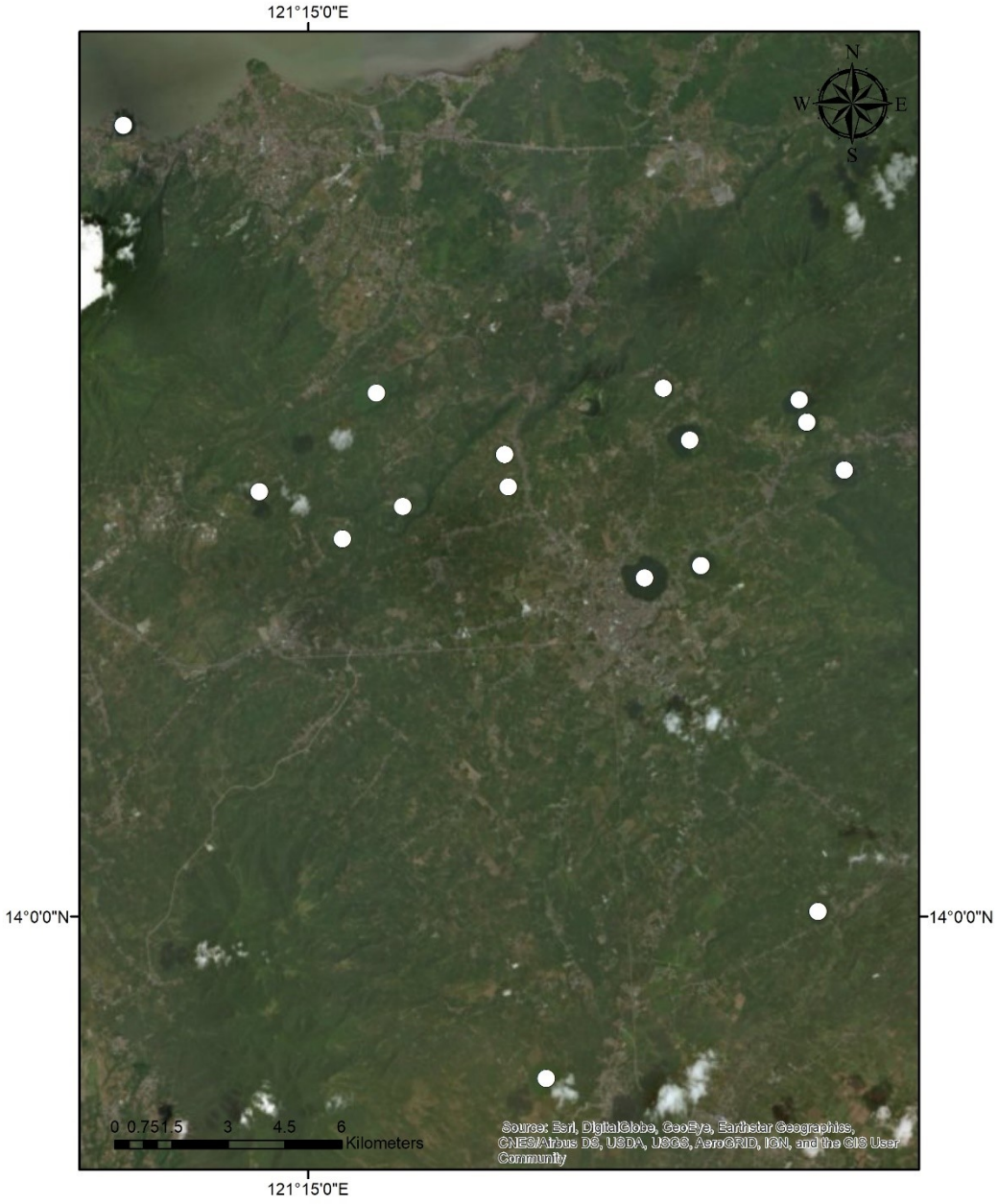

Figure 14 – A satellite view of the San Pablo City Volcanic Field in the Philippines with white dots marking the location of the sixteen included maar craters.

Serdán Orientale Volcanic Field

In the easternmost part of the Trans Mexican Volcanic Belt, the Serdán-Oriental basin (Figure 15 and Figure 16) is a broad, internally drained, intermontane basin of the Mexican High Plain (Carrasco-Núñez, G., Ort, M. H., & Romero, C., 2007). Covering approximately 5250 km^2, the Serdán-Oriental basin is characterized by monogenetic bimodal volcanism (Carrasco- Núñez et al., 2007). Some of the more prominent features of the area include isolated rhyolitic domes, isolated cinder, scoria, and lava cones of basaltic composition, maar craters, tuff rings, and a few tuff cones (Ort and Carrasco-Núñez, 2009). Volcanism in the Serdán Oriental basin has been active since the Pliocene epoch, though the surrounding area has been active since the Miocene (Carrasco- Núñez et al., 2007). The maars are excavated out of pyroclastic deposits and basaltic lava flows, resting on top of a limestone basement (Carrasco- Núñez et al., 2007) (Table 1). Intra-arc active extensional-faulting in the central part of the Mexican Volcanic Belt follows a general E-W or ENE-WSW trend with the least horizontal stress oriented in the N-S direction (Suter et al., 1992; Carrasco- Núñez et al., 2007). These faults controlled the emplacement of the late Miocene mafic lavas, exhibiting boundaries reactivated by oblique extension during the period of placement (Ferrari, L., Conticelli, S., Vaggelli, G., Petrone, C.M., and Manetti, P., 2000).

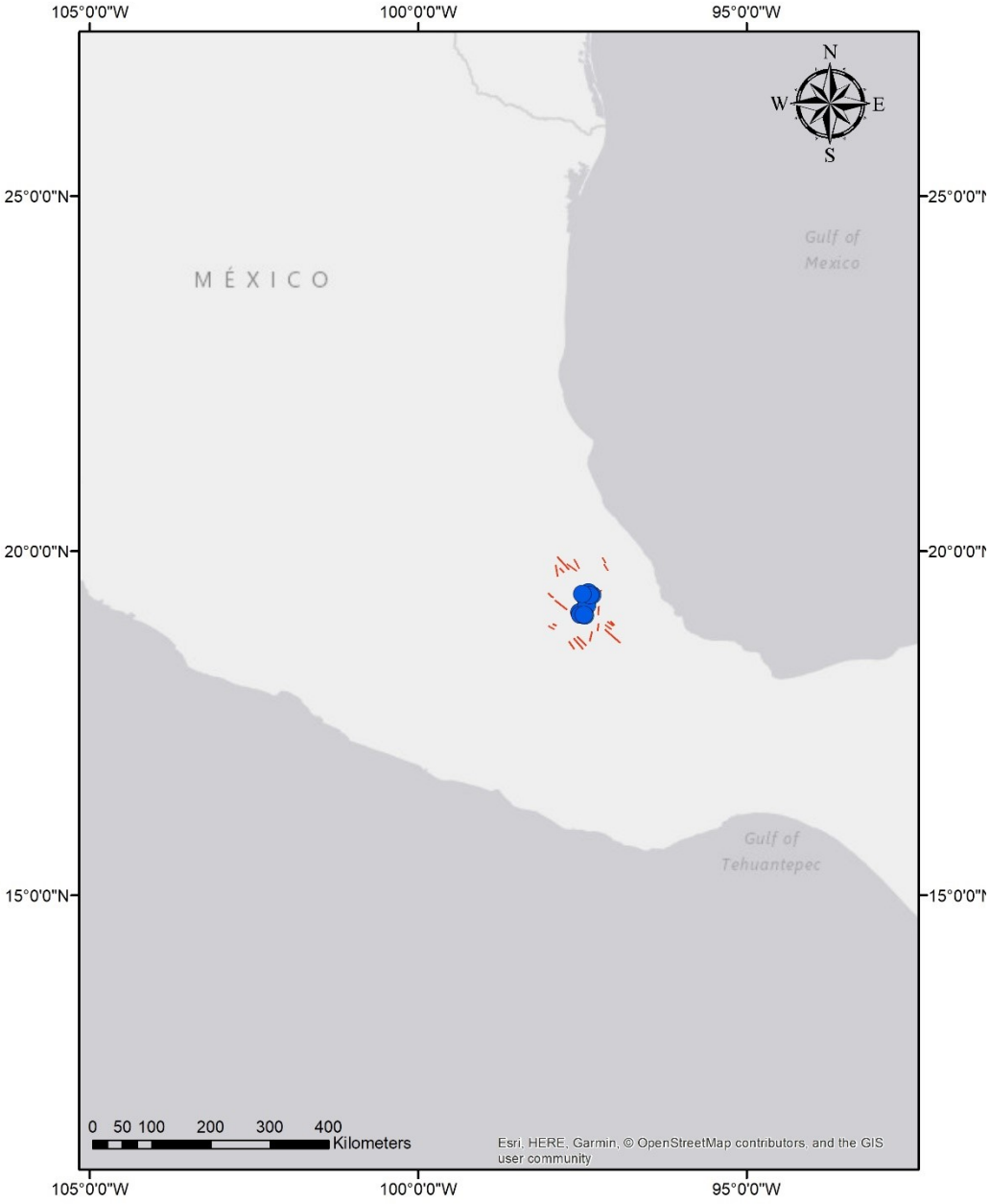

Figure 15 - Serdán Oriental Volcanic Field (Mexico) – Shows a regional view of the field with faults in red and maars in blue.

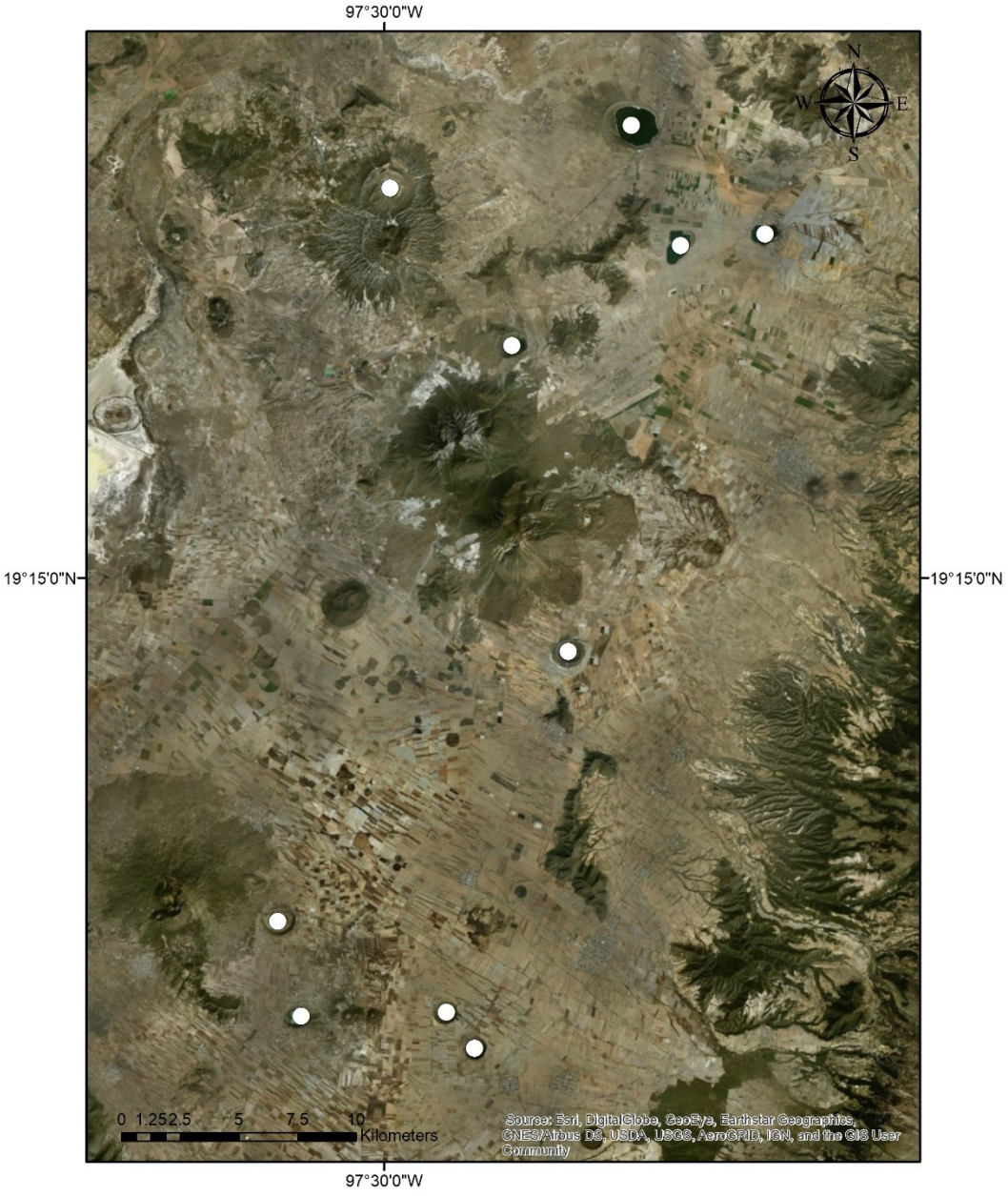

Figure 16 – A satellite view of Serdán Oriental Volcanic in Mexico with white dots marking the location of the ten included maar craters.

CHAPTER 3

METHODOLOGY

Maar craters in each field were manually digitized using the add polygon tool in Google Earth. The maars beneath these polygons were then inspected by visually assessing the crater rim for continuity using satellite imagery from Google Earth. In order for a maar to be eligible for inclusion in elongation orientation analysis, it had to have a visually discernable and complete crater rim that could be accurately traced using satellite imagery. After maars with the necessary characteristics were identified in each field, the polygons for those craters were exported as a KML and imported into Arc GIS. In Arc GIS, an ellipse was fit within each maar such that it occupied the largest possible area without crossing the boundaries of the polygon. This ellipse represents the primary angle of elongation. In cases where the largest area covered by an ellipse proved to be circular, the maar was removed from the data set.

The secondary angle of elongation was calculated using the same methodology for craters that exhibited areas which could not be contained within the initial ellipse. For this study, a secondary angle of elongation is defined as an area in the digitized polygon which could not be covered by the initial ellipse, that has an angle of elongation measured to be equal to or greater than thirty degrees apart from the primary angle of elongation (Figure 17). It is estimated that orientations of elongation determined this way are reasonable within ten degrees.

Figure 17 – Gnotuk (Top) and Bullen Merri (Bottom) maars with polygon of crater outline in transparent blue and light blue ellipse for elongation superimposed. Bullen Meri shows an example of secondary elongation orientation in the Newer Volcanic Province (Australia).

Faults were selected within and around the studied volcanic fields, based on proximity, from published literature and government datasets of mapped faults and lineaments. Most fields have a number of lineaments located within 50 km of the maars selected. In those fields, all fault lineaments within 50 km were digitized as polylines and imported to Arc through KML files. In some fields, there were insufficient numbers of exposed faults within the original radius. For Auckland Volcanic Field and Pinacate Volcanic field, the range was extended to 150 km.

In San Pablo City Volcanic Field and Lamongan Volcanic Field, fault orientations were measured by hand from maps in order to minimize introduced error. The

orientations of all other maars and faults were calculated by utilizing the direction feature of the add line construction tool in Arc GIS. The portion of each ellipse furthest from the center was identified, and a line was drawn such that it bisected the image. Lines were drawn from the lowest end of each ellipse to the highest (from south to north). By right clicking after the line had been drawn, and selecting the direction feature, the direction of the line could be measured. The direction measured was then copied into an excel spreadsheet. Since Arc GIS measures angles counterclockwise starting at ninety degrees East of North, a formula was applied to convert them into an angle measured clockwise from north. For angles less than ninety degrees formula "A" was used. Angles greater than ninety degrees required formula "B".

Formula A: $\Theta_f = (\Theta_i - 90°) \times -1$

Formula B: $(\Theta_f = (\Theta_i - 90°) \times -1) + 180°$

A nearest neighbor analysis was carried out for all maars digitized (not just those used for elongation orientation) using the centroid of the original polygons imported from Google Earth. The digitized maar polygons were used to create a table of the xy coordinate data for each maar. This table was then displayed visually in arc, using the display xy data feature. Then, using the Generate Near Table tool of the Proximity group in the Systems Tool Box, a near table was generated which detailed the angle and distance to the nearest neighbor for each maar.

Orientation data was converted into radians and imported into Matlab from excel. The primary orientation of elongation, secondary orientation of elongation, nearest neighbor angle, and faulting data were each graphed individually using the polar histogram graph type. Each histogram contains 36 ten-degree bins. This bin size was chosen based on the accuracy of our methods, and functions as an effective cap on the resolution with which the data can be resolved.

After this, primary elongation orientations, secondary elongation orientations, fault orientations, and nearest neighbor orientations were tabulated separately in an excel spreadsheet for each field. For each data set, modes were identified by comparing the proximity of orientations to one another. To accomplish this, all orientations for a given data set were sorted from least to greatest between 0 and 180^{o}. Each data point was assigned a number, in order from least to greatest, beginning at one. By graphing the two columns, a line was generated. The slope of the generated line reflects concentration of orientation values (Figure 18). After manually identifying areas in which the slope of the line deviated from average in each data set and comparing those to the rose diagram for that data, it was determined that a data point would be part of a strong mode if its segment of the line had a slope of five or less. Data belonging to weak modes have a slope between five and ten. Because the volume of data for faulting in the Newer Volcanic Province was substantially larger than what was available for all other data sets (more than six times as many data points as other fields), modes were manually determined

with the assistance of the slope method after lowering the required slope threshold to two and a half. When determining which modes identified in nearest neighbor data would be considered, it was determined that, in addition to qualifying by slope as a strong or weak mode, lineaments of three or more aligned maars would also have to be found in field with an orientation (of the lineament) within ten degrees of the mode.

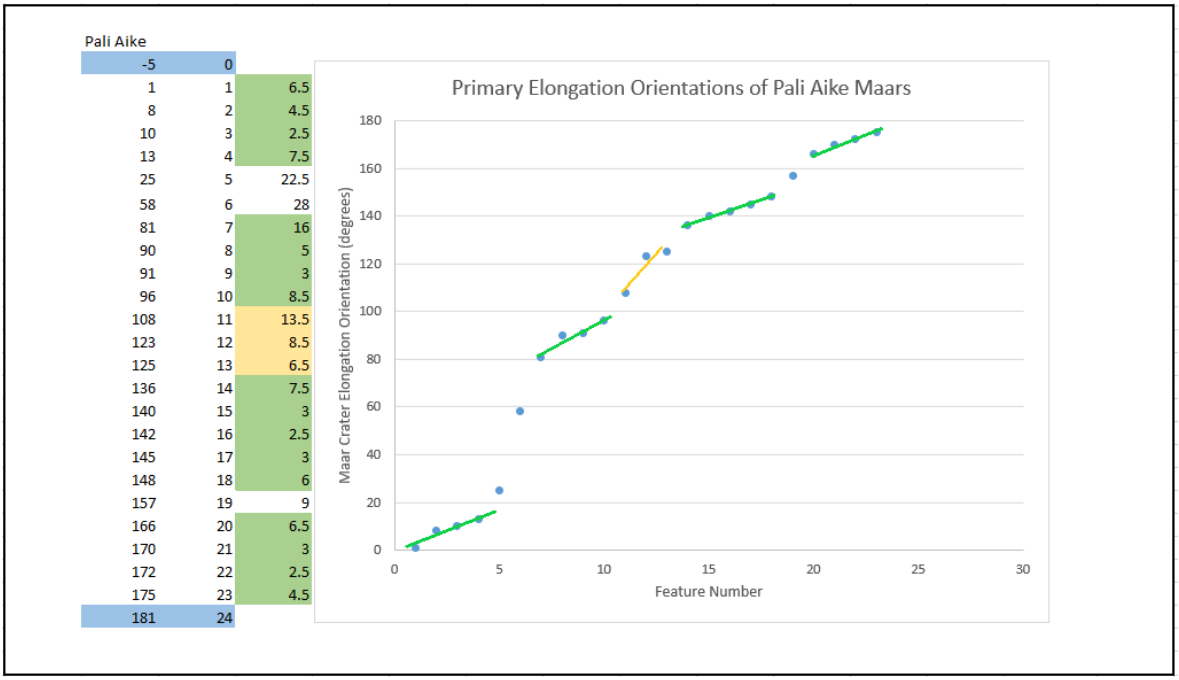

Figure 18 – Graph of primary elongation orientations for maars in the Pali Aike Volcanic Field and line used to identify modes of shared orientations. Areas in which the slope is less than five are highlighted green, making up the strong modes. Areas of the line highlighted yellow have a slope less than ten and make up weak modes.

CHAPTER 4

RESULTS

Auckland Volcanic Field

Auckland volcanic field has a total of six maars with measurable elongation. The maars exhibit no strong or weak modes in either primary or secondary elongation orientation. Five of the maars were found to have secondary elongation orientations. The faulting data exhibits a single strong mode, F_a, from 154-168° (Figure 19 and Figure 20). Nearest neighbor direction data exhibits one strong mode from 19-25° (N_a) and one weak mode from 143-159° (Figure 21). The strong mode is supported by a lineament of three or more aligned maars in field (Figure 22). There are no maar elongation orientation modes. Out of all the maars, only one falls within ten degrees of the faulting mode F_a. Since no nearest neighbor modes could be used, only 1/6 of the maars were found to have similar primary elongation orientations to faulting and nearest neighbor data.

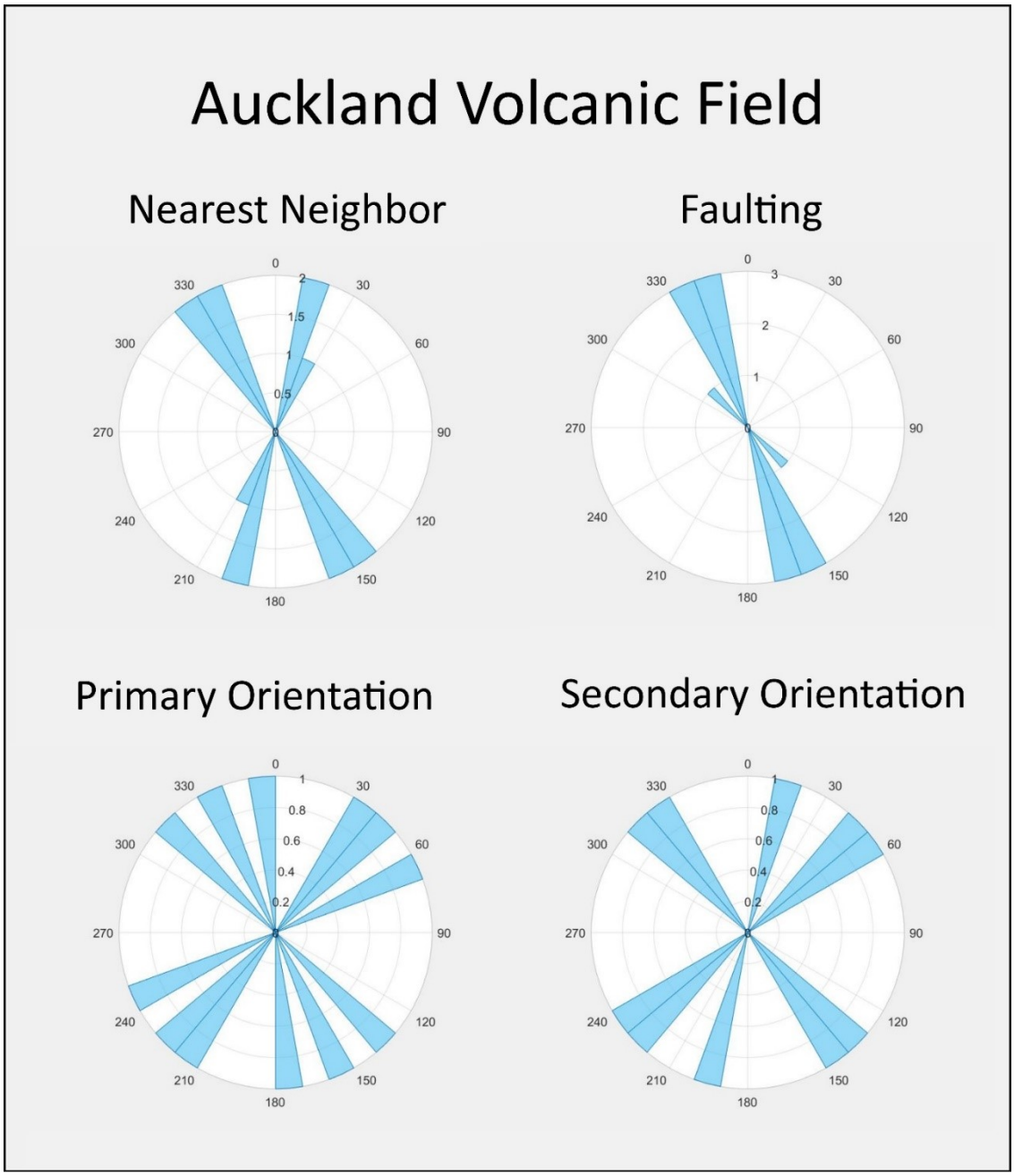

Figure 19 – Rose diagrams show orientation data for nearest neighbor, faulting, primary elongation orientation, and secondary elongation orientation in the Auckland Volcanic Field (New Zealand).

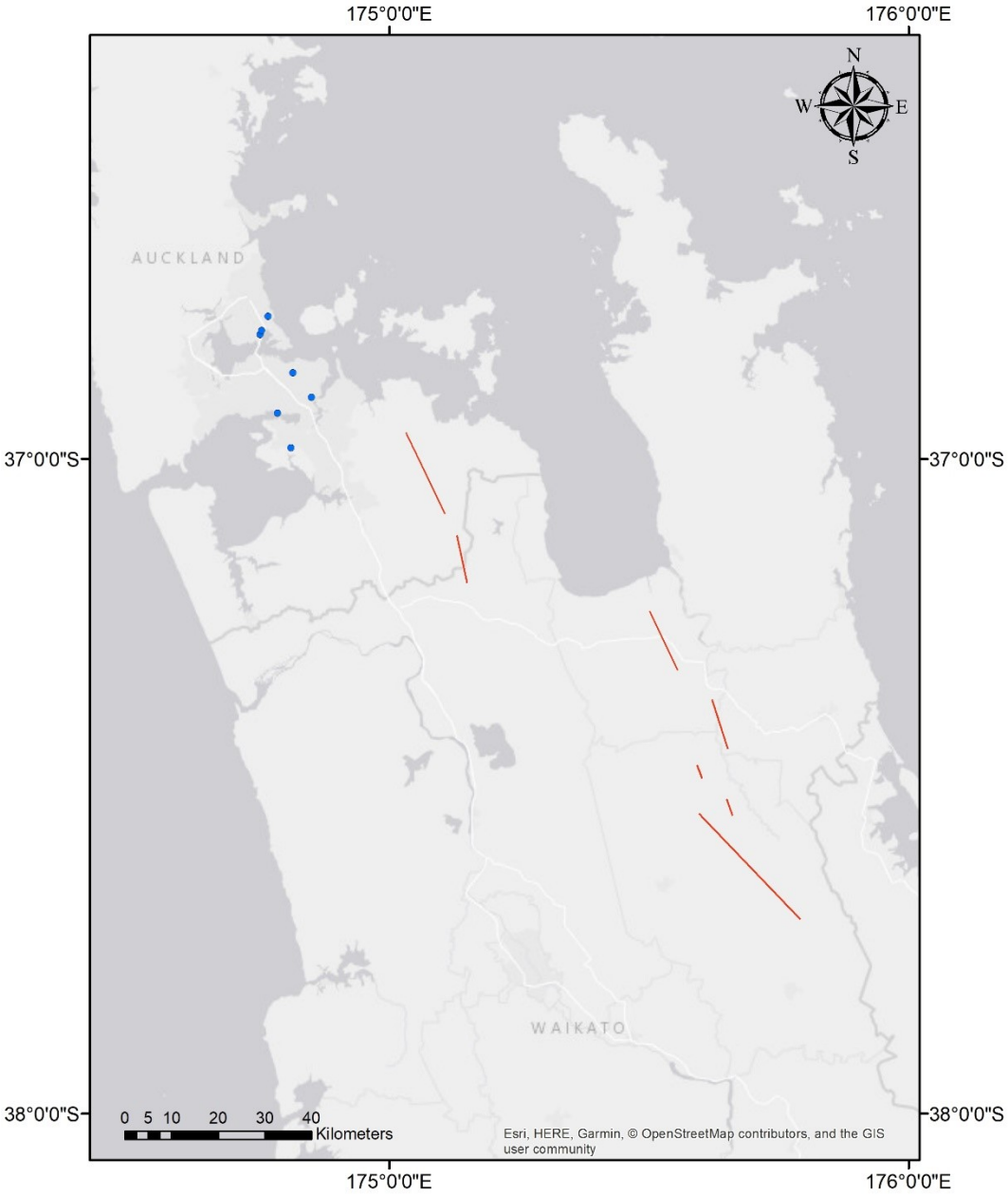

Figure 20 – Auckland Volcanic Field (New Zealand) Shows digitized fault lineaments (red lines) and maars (green dots) (Langridge, R.M., Ries, W.F., Litchfield, N.J., Villamor, P., Van Dissen, R.J., Barrell, D.J.A., Rattenbury, M.S., Heron, D.W., Haubrock, S., Townsend, D.B., Lee, J.M., Berryman, K.R., Nicol, A., Cox, S.C., et al., 2016).

Figure 21 – Shows nearest neighbor lines (light blue) between maars in the Auckland Volcanic Field (New Zealand).

Figure 22 - Shows nearest neighbor lineaments (light green) for aligned maars in the Auckland Volcanic Field (New Zealand).

Lamongan Volcanic Field

Lamongan Volcanic Field contains fourteen maars with measurable elongation. The maars of Lamongan Volcanic Field exhibit one strong primary elongation orientation mode from 179-11° (P_A, N=5), and one weak mode from 24-41° (P_C, N=3) (Figure 23 and Figure 24). Three of the maars were found to have secondary elongation orientations. There are no secondary elongation orientation modes among the Lamongan maars. Faulting data from Lamongan Volcanic Field exhibits two strong modes at 68-78° (F_A) and 135-150° (F_B). The nearest neighbor direction data in Lamongan has one strong mode from 144-155° (N_A) and one weak mode from 84-115° (Figure 25). Only the strong mode is supported by three or more aligned maars in field (Figure 26). Nearest neighbor mode N_A falls entirely within ten degrees of the edges of faulting mode F_B. No maar orientations found within primary elongation orientation modes are shared by either nearest neighbor or faulting data for this field.

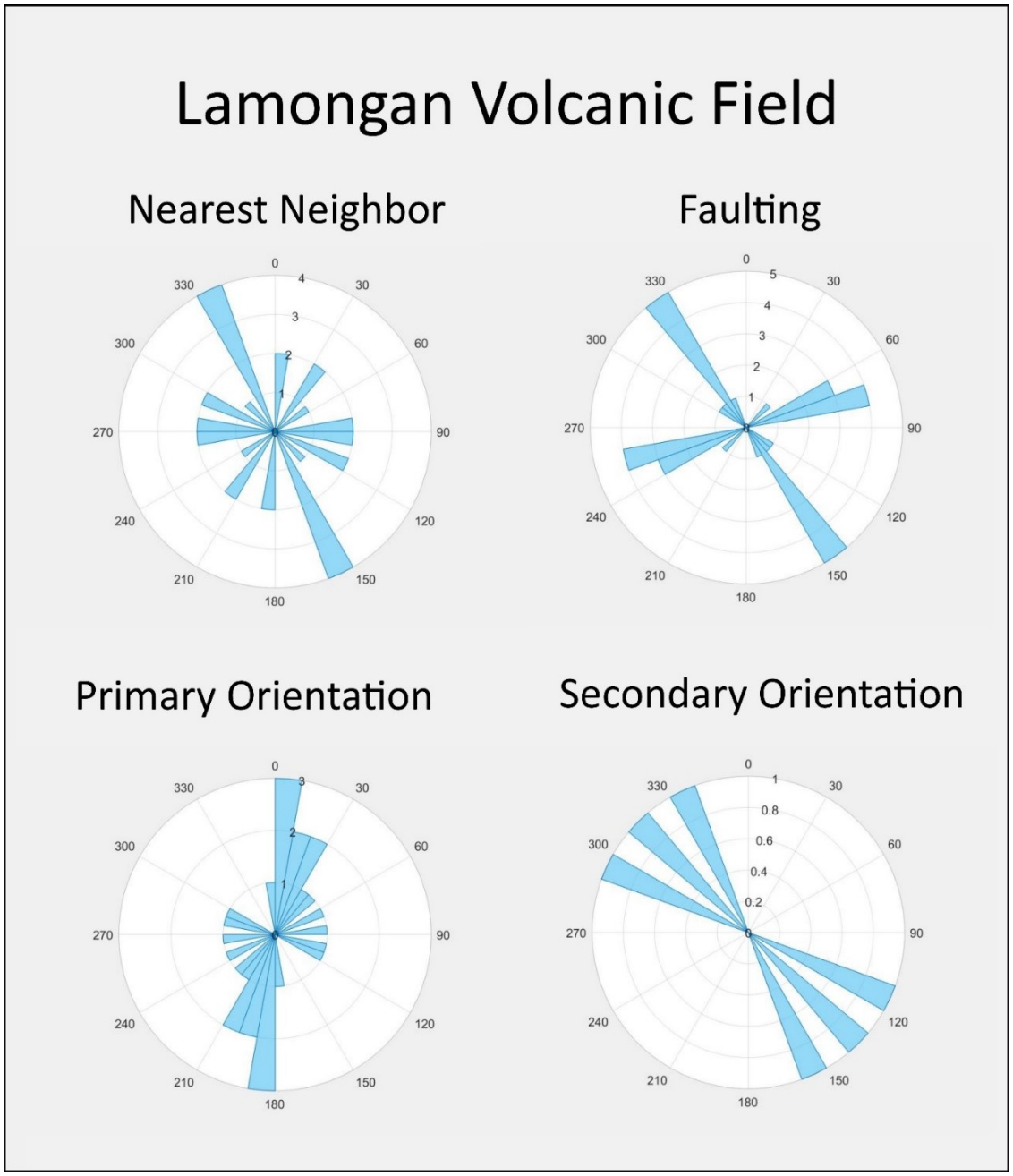

Figure 23 - Rose diagrams show orientation data for nearest neighbor, faulting, primary elongation orientation, and secondary elongation orientation in the Lamongan Volcanic Field (Indonesia).

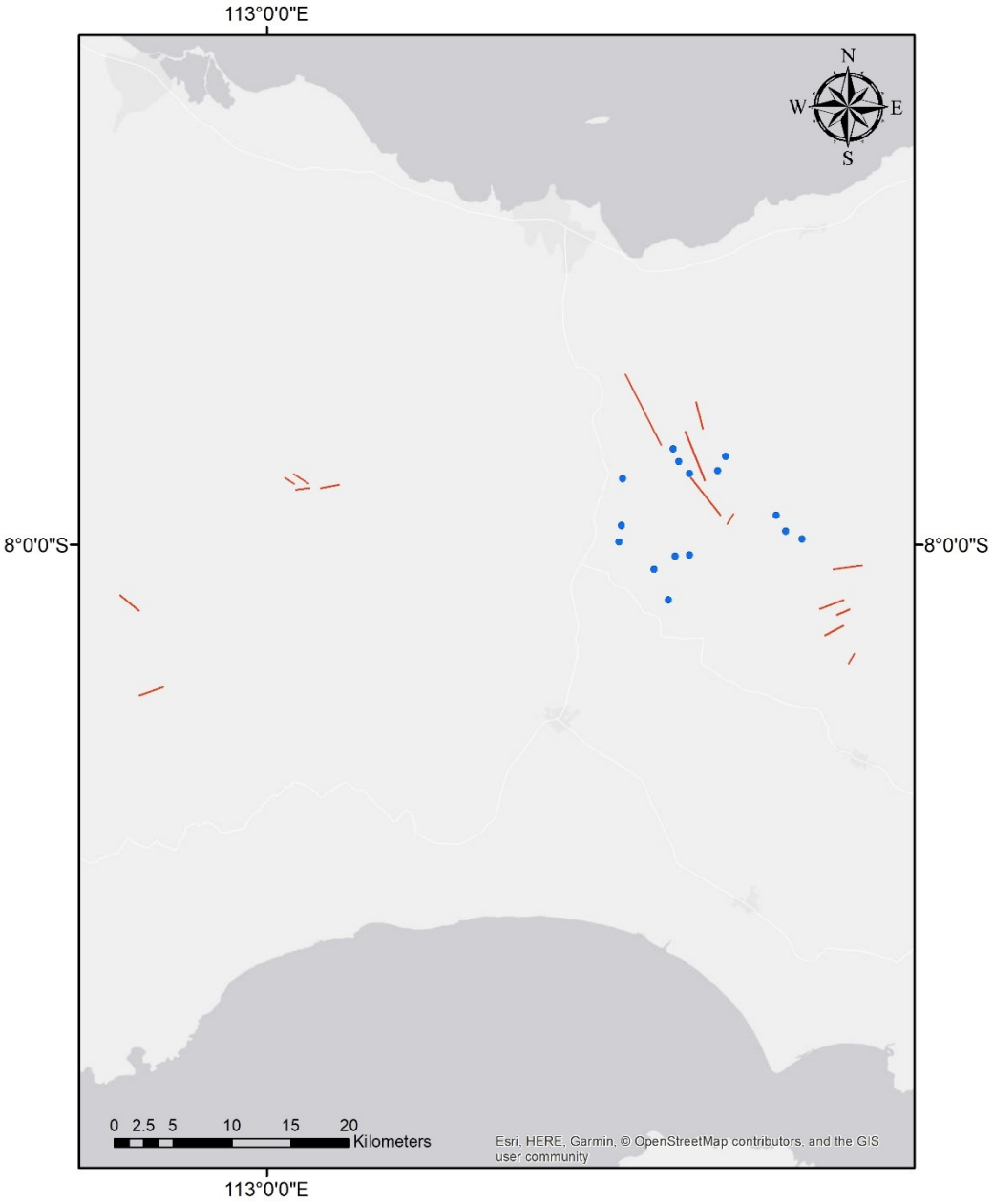

Figure 24 – Lamongan Volcanic Field (Indonesia) – Shows digitized fault lineaments (red lines) and maars (green dots) (Carn, S. A., 1999).

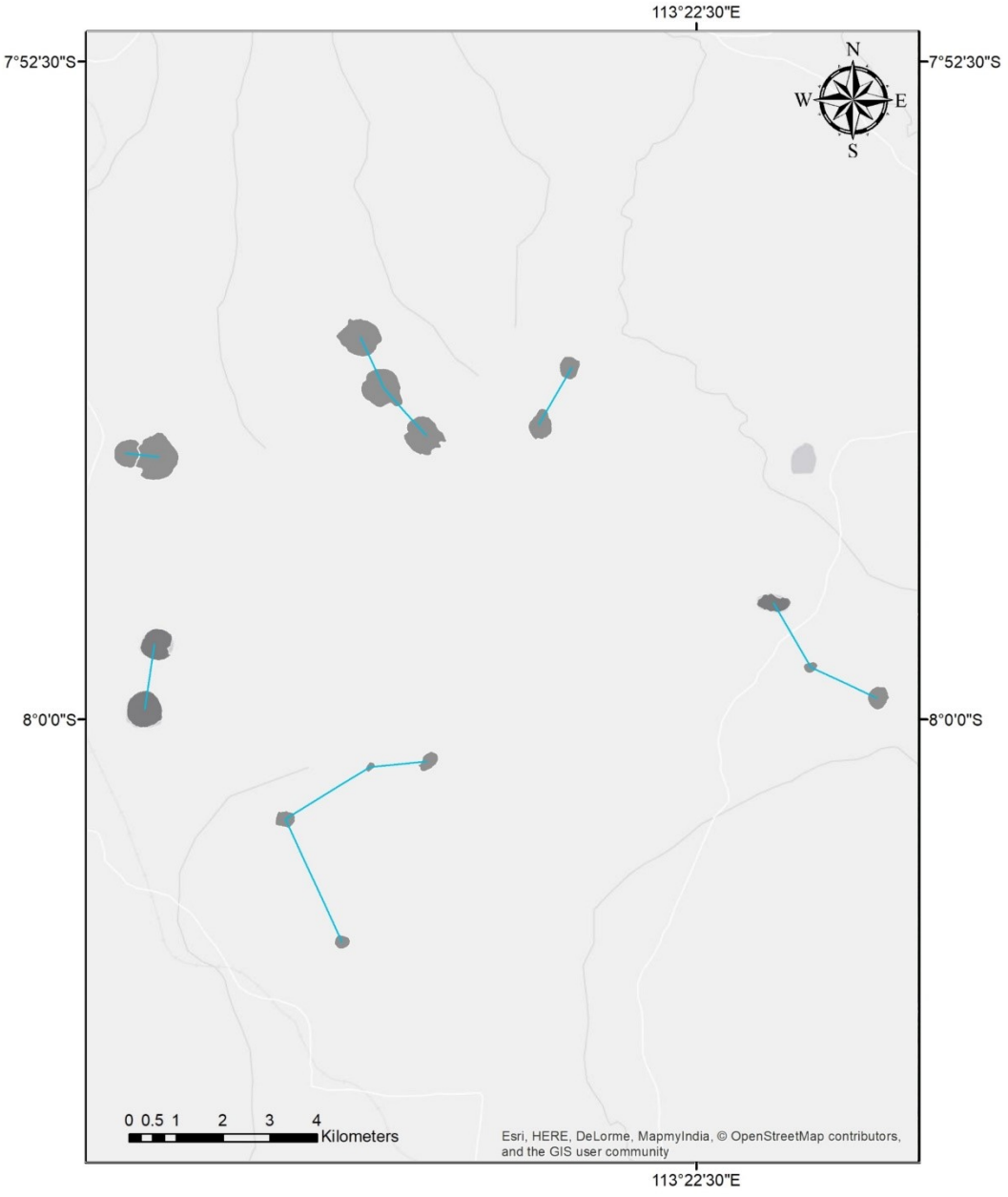

Figure 25 - Shows nearest neighbor lines (light blue) between maars in the Lamongan Volcanic Field (Indonesia).

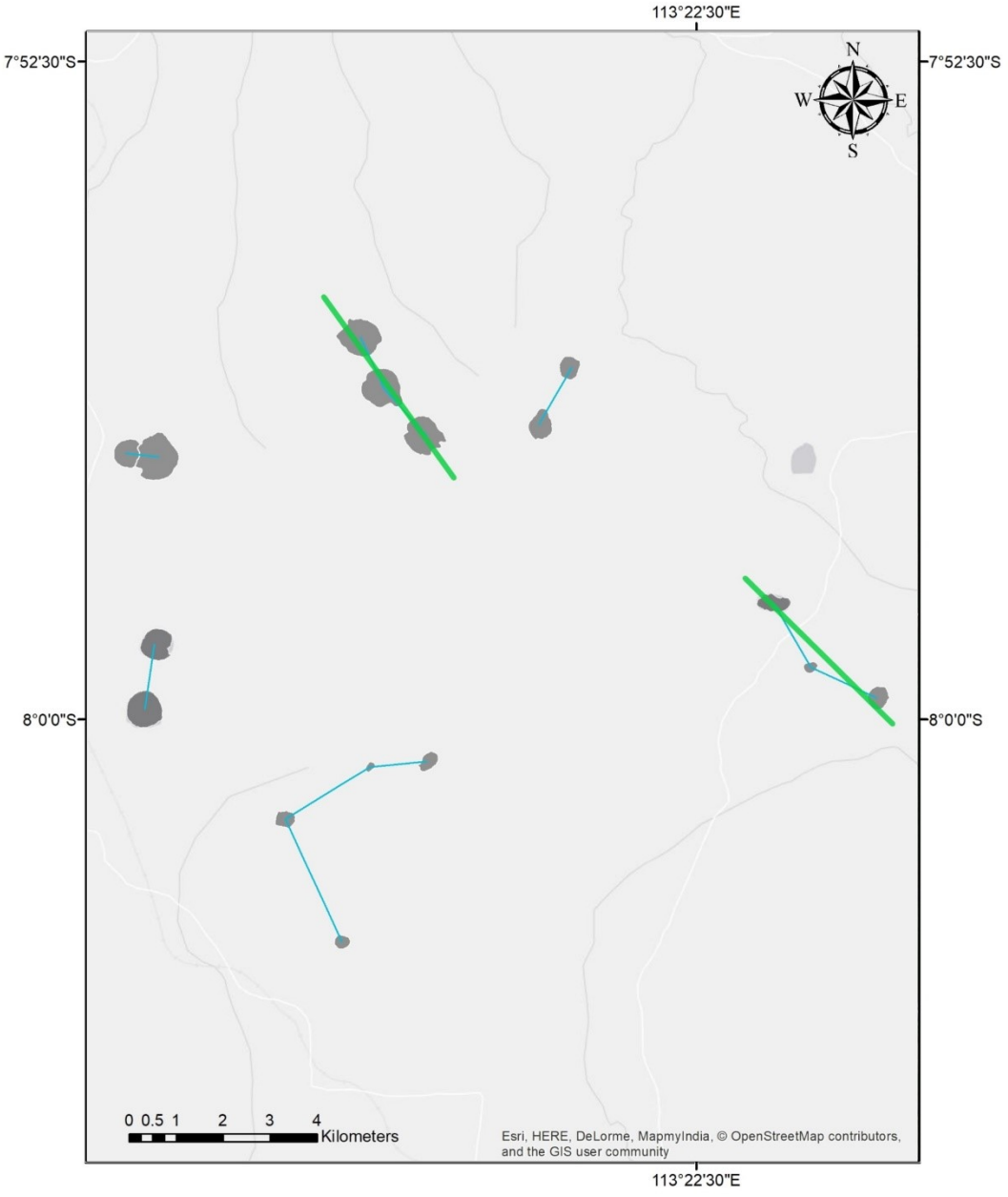

Figure 26 – Shows nearest neighbor lineaments (light green) for aligned maars in the Lamongan Volcanic Field (Indonesia).

Newer Volcanic Province

The Newer Volcanic Province contains 23 maars with complete rims and measurable elongation. The maars of the Newer Volcanic Province exhibit two strong modes and two weak modes in primary elongation orientation (Figure 27 and Figure 28). The strong modes are 9-41° (P_A, N=10) and 167-176° (P_B, N=3). The weak modes range from 104-136° (P_C, N=5) and 46-63° (P_D, N=3). Newer Volcanic Province secondary elongation orientation data exhibits a strong and weak mode. The strong mode is from 110-118° (S_A) and the weak is from 134-152° (S_B). Six of the maars were found to have secondary elongation orientations. The faulting modes exhibited by Newer Volcanic Province are 78-123° (F_A), 158-13° (F_B), and 123-140° (F_C). There are numerous nearest neighbor direction modes: 108-132°, 172-180°, 132-139°, 1-7°, 44-75°, and 160° (Figure 29 and Figure 30). However, only 108-132° (N_A), 132-132° (N_B), and 44-75° (N_C) are supported by three or more maars aligned with one another (Figure 31). Modes N_A and N_B are strong while mode N_C is weak. Of the primary maar elongation modes, the weak mode P_C is encompassed by faulting modes F_A and F_C, and nearest neighbor mode N_A. The weaker of the two strong primary elongation orientation modes P_B is accounted for by faulting mode F_B. About half of mode P_A is encompassed by faulting mode F_B. Finally, primary elongation orientation mode P_D is encompassed by nearest neighbor mode N_C. Part of nearest neighbor mode N_C also carries over to encompass the edge of primary elongation orientation mode P_A. All told, 18/23 maar primary elongation orientations share similar

orientations as faulting and nearest neighbor data. Including maars which are not part of maar modes, 20/23 maars are similar. Secondary maar elongation orientation mode S_A falls neatly within faulting mode F_A and secondary elongation orientation mode S_B falls mostly within faulting mode F_C (entirely within ten degrees of it).

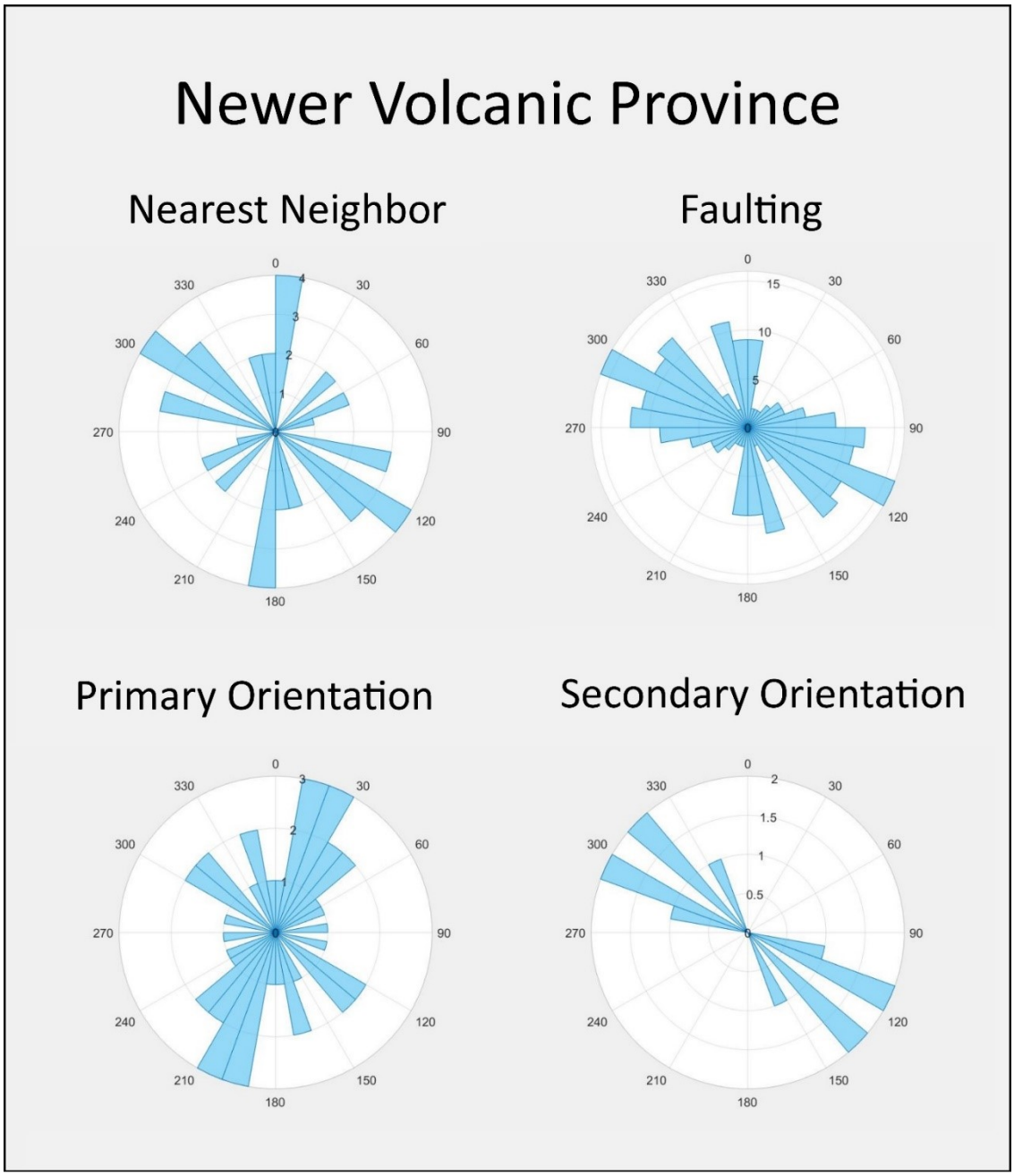

Figure 27 - Rose diagrams show orientation data for nearest neighbor, faulting, primary elongation orientation, and secondary elongation orientation in the Newer Volcanic Province (Australia).

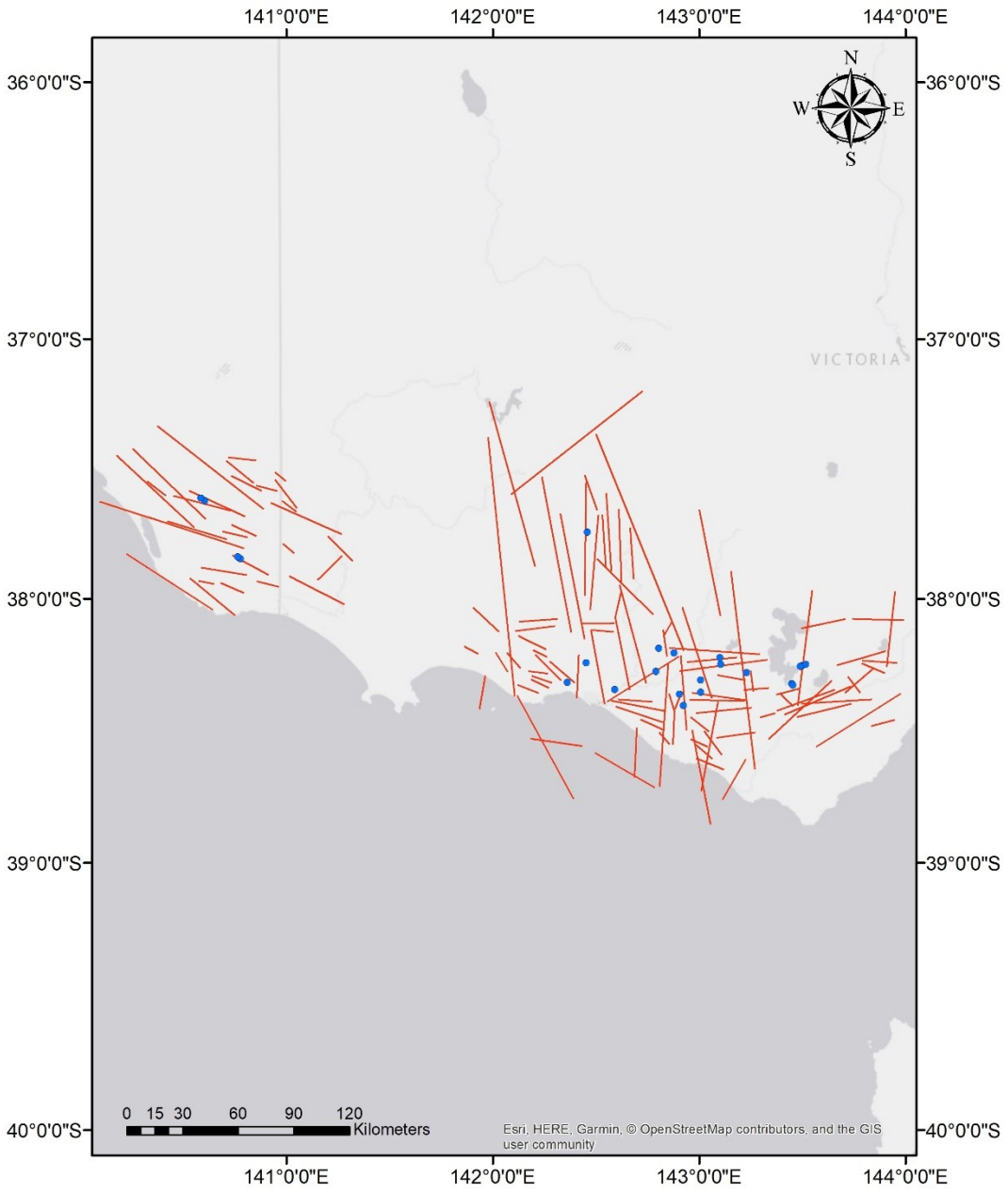

Figure 28 – Newer Volcanic Province (Australia) - Shows digitized fault lineaments (red lines) and maars (green dots) (Personal Communication Otterloo, J. V.).

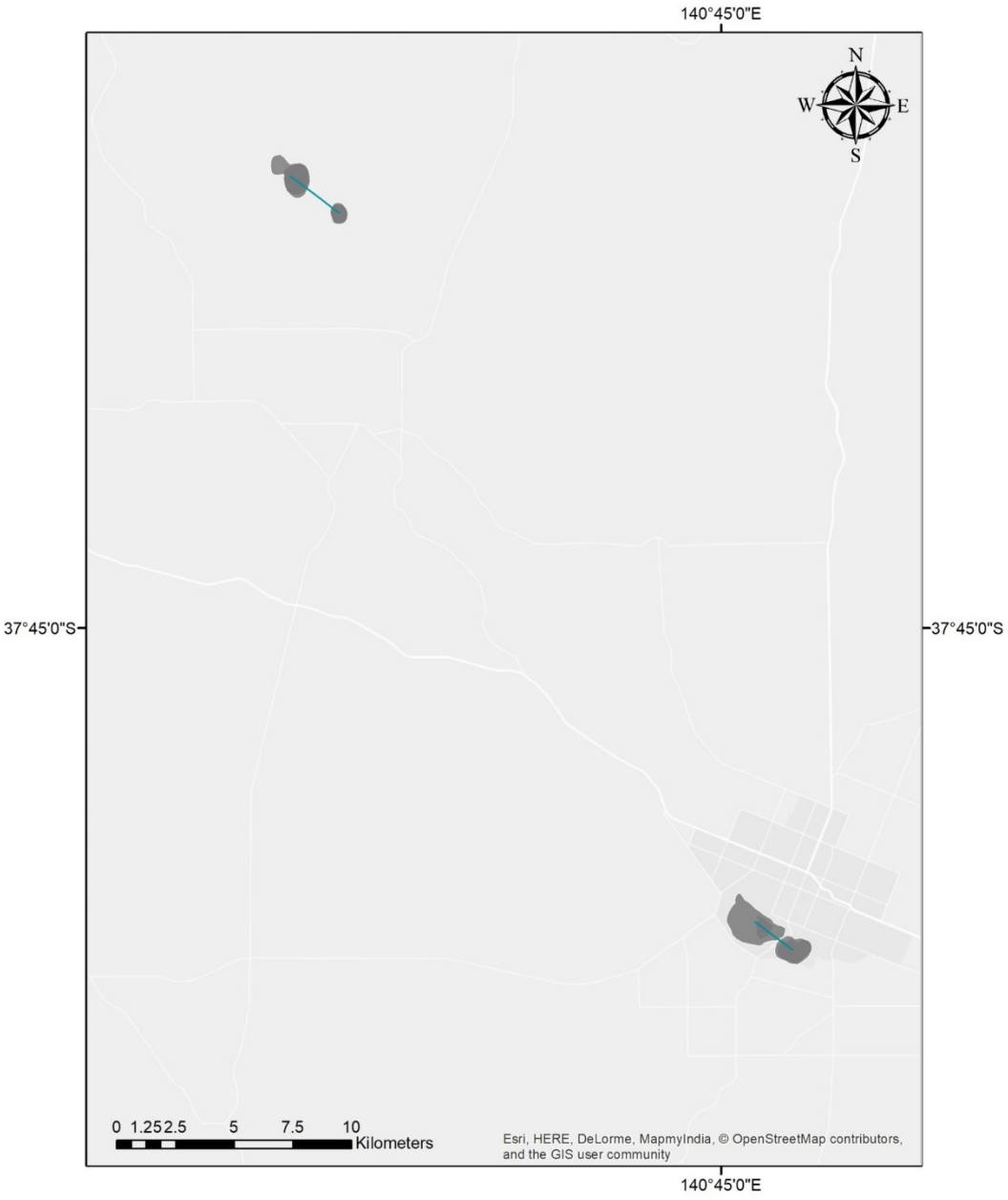

Figure 29 - Shows nearest neighbor lines (light blue) between maars in the west half of the Newer Volcanic Province (Australia).

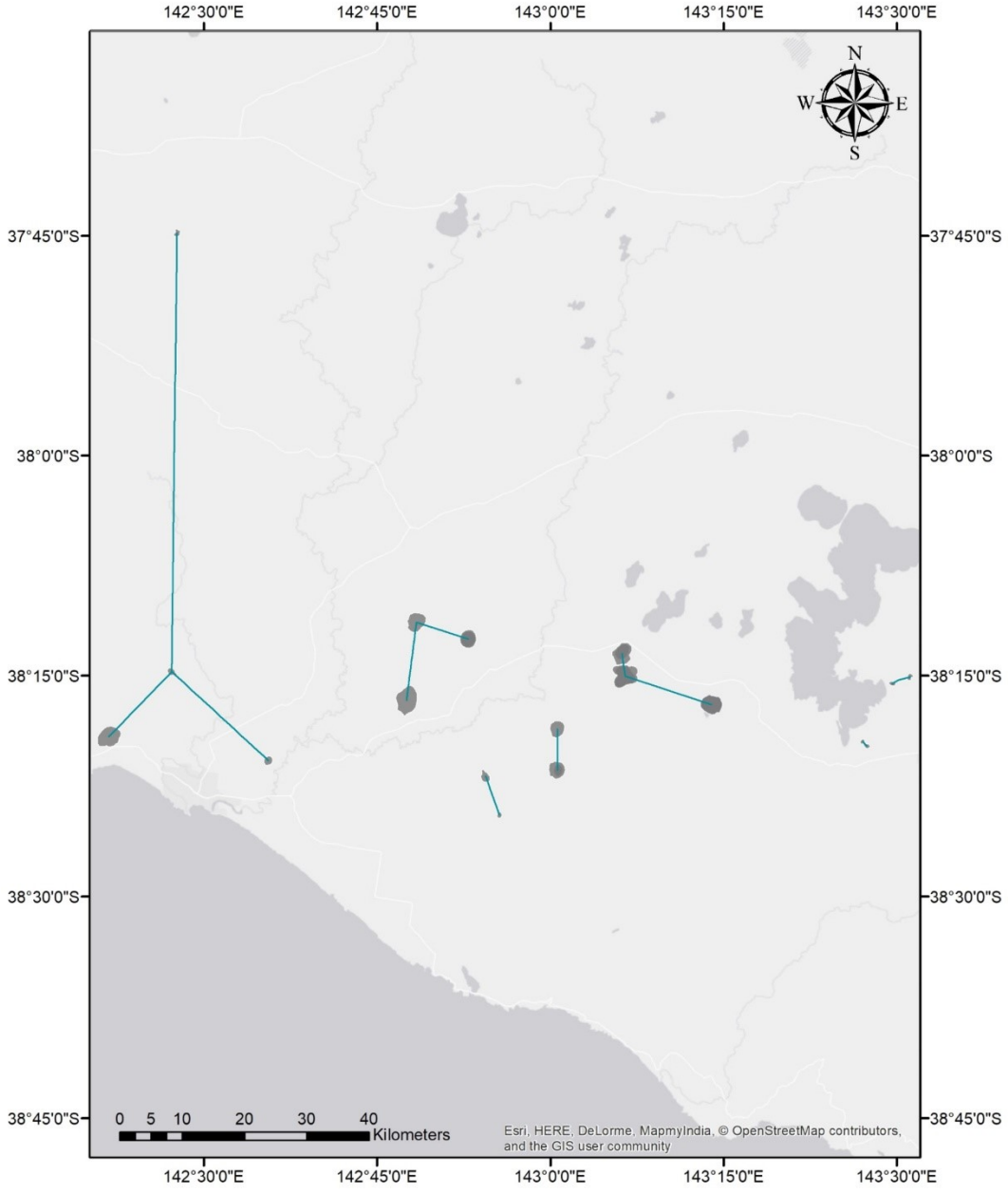

Figure 30 - Shows nearest neighbor lines (light blue) between maars in the east half of the Newer Volcanic Province (Australia).

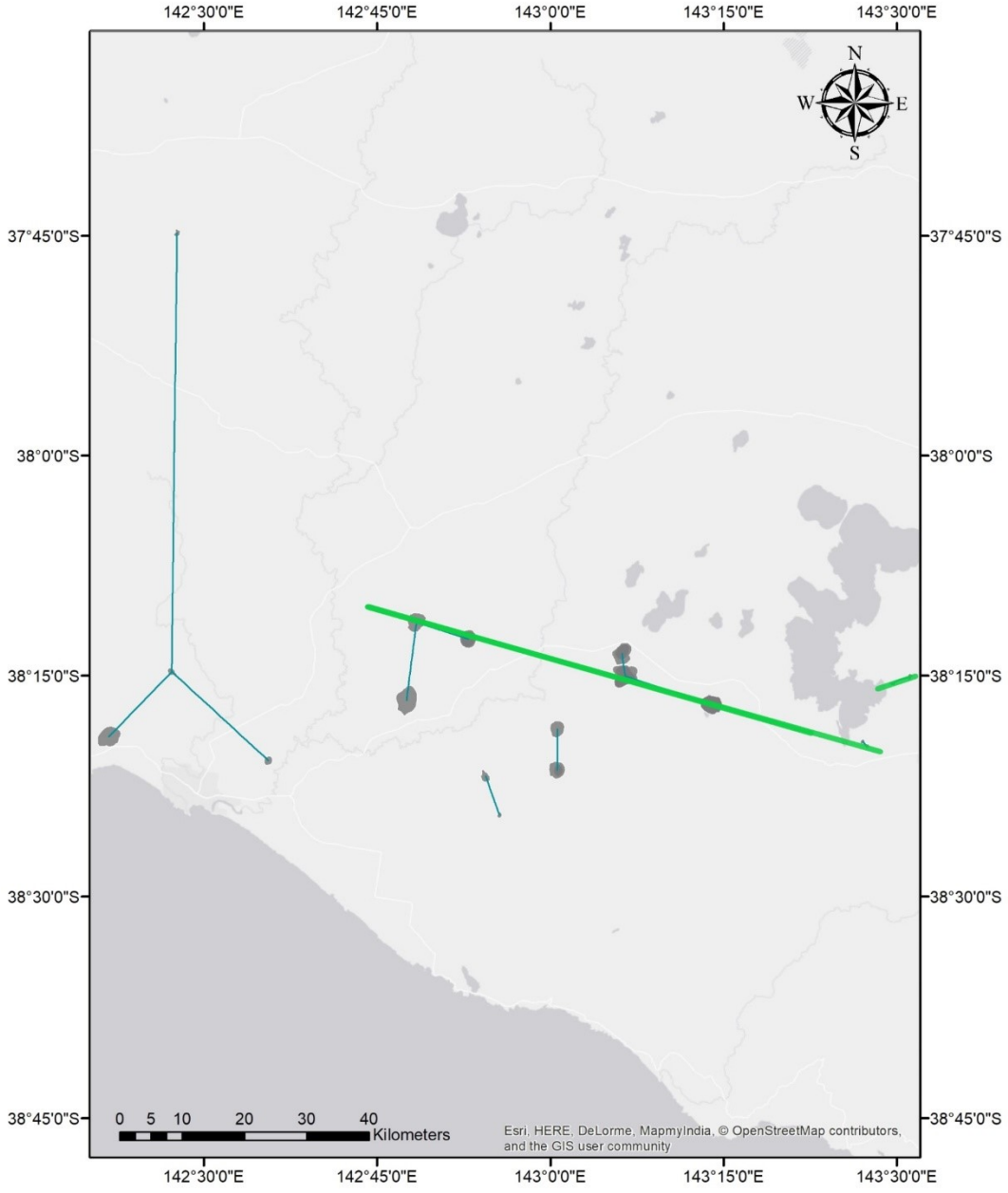

Figure 31 - Shows nearest neighbor lineaments (light green) for aligned maars in the eastern half of the Newer Volcanic Province (Australia).

Pali Aike Volcanic Field

The Pali Aike Volcanic Field contains 23 maars with measurable elongations. Pali Aike maars exhibit four strong modes in primary elongation orientation 136-148° (P_A, N=5), 1-13° (P_B, N=4), 81-96° (P_C, N=4), and 166-175° (P_D, N=4) (Figure 32 and Figure 33). One weak primary elongation orientation mode exists at 108-125° (P_E, N=3). Though the slope does dip below ten at another point in the primary elongation orientation line, this fell between two strong modes and is the product of their proximity. Secondary maar elongation orientation data exhibits two weak modes from 35-53° (S_A) and 85-105° (S_B). Eight of the maars were found to have secondary elongation orientations. Faulting data for Pali Aike exhibits three strong modes at 119-146° (F_A), 48-51° (F_B), and 71-74° (F_C). The nearest neighbor data for Pali Aike exhibits three strong modes from 132-163° (N_A), 87-98° (N_B), and 98-110° (N_C), as well as one weak mode from 60-76° (Figure 34). However, of these modes, only the strong are supported by maar alignment in field (Figure 35). While primary elongation orientation mode P_B has no matching modes in faulting or nearest neighbor data, all other primary elongation orientation modes are met with a complimentary fault or nearest neighbor mode. Primary elongation orientation modes P_A and P_E are matched by both faulting and nearest neighbor modes F_A and N_A. Primary elongation orientation mode P_C is matched in part by faulting mode F_C but is entirely covered by nearest neighbor mode N_B. Primary elongation orientation mode P_D is matched by the edge of nearest neighbor mode N_A. Lastly, nearest neighbor mode N_A also

encompasses primary elongation orientation mode P_F. As the only other field besides Newer Volcanic Province which exhibits secondary elongation orientation modes, it is interesting to note that mode S_A of secondary elongation orientation matches closely with mode F_B of faulting, and mode S_B of secondary elongation orientation matches mode N_B of the nearest neighbor data.

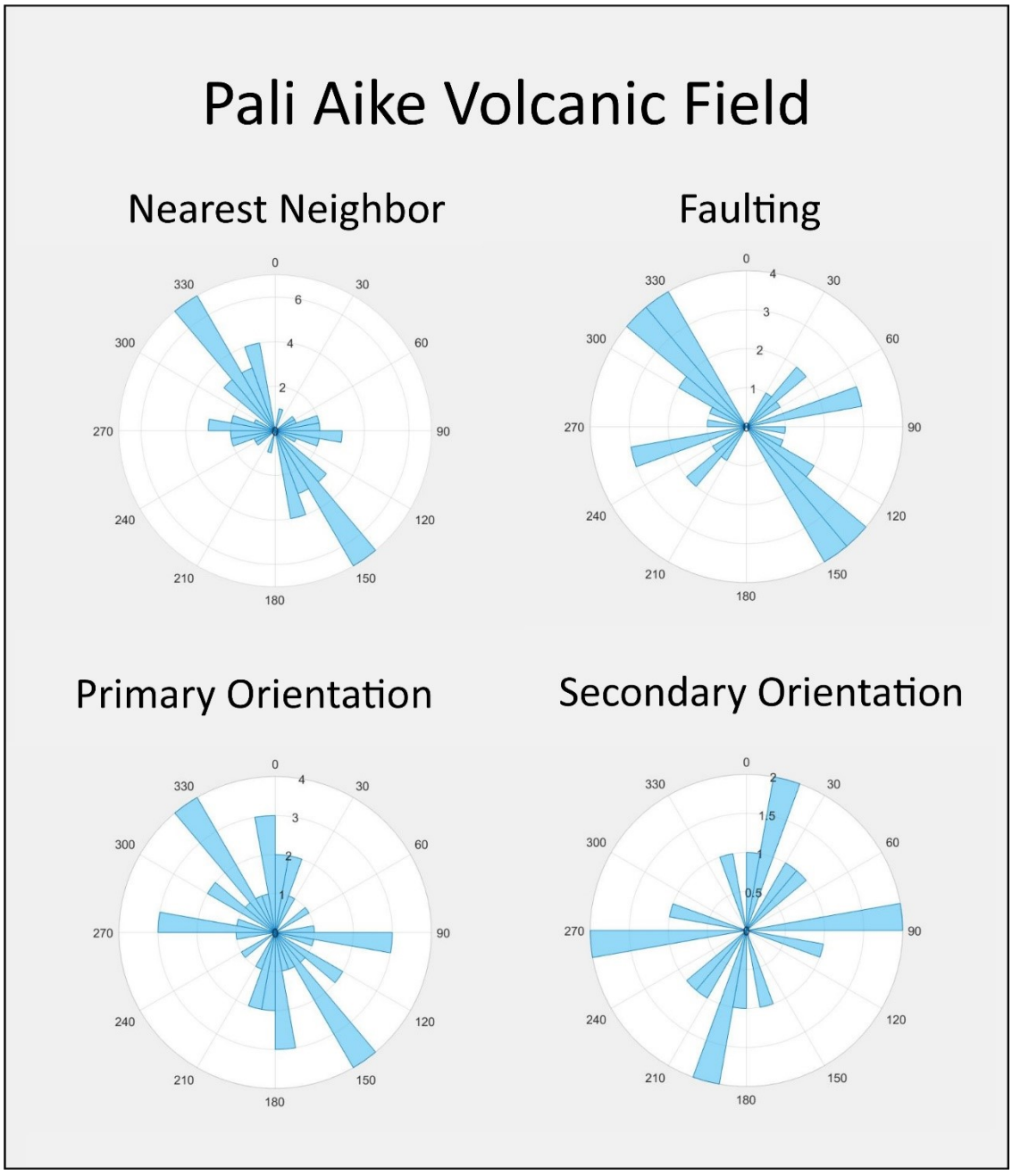

Figure 32 - Rose diagrams show orientation data for nearest neighbor, faulting, primary elongation orientation, and secondary elongation orientation in the Pali Aike Volcanic Field (Argentina).

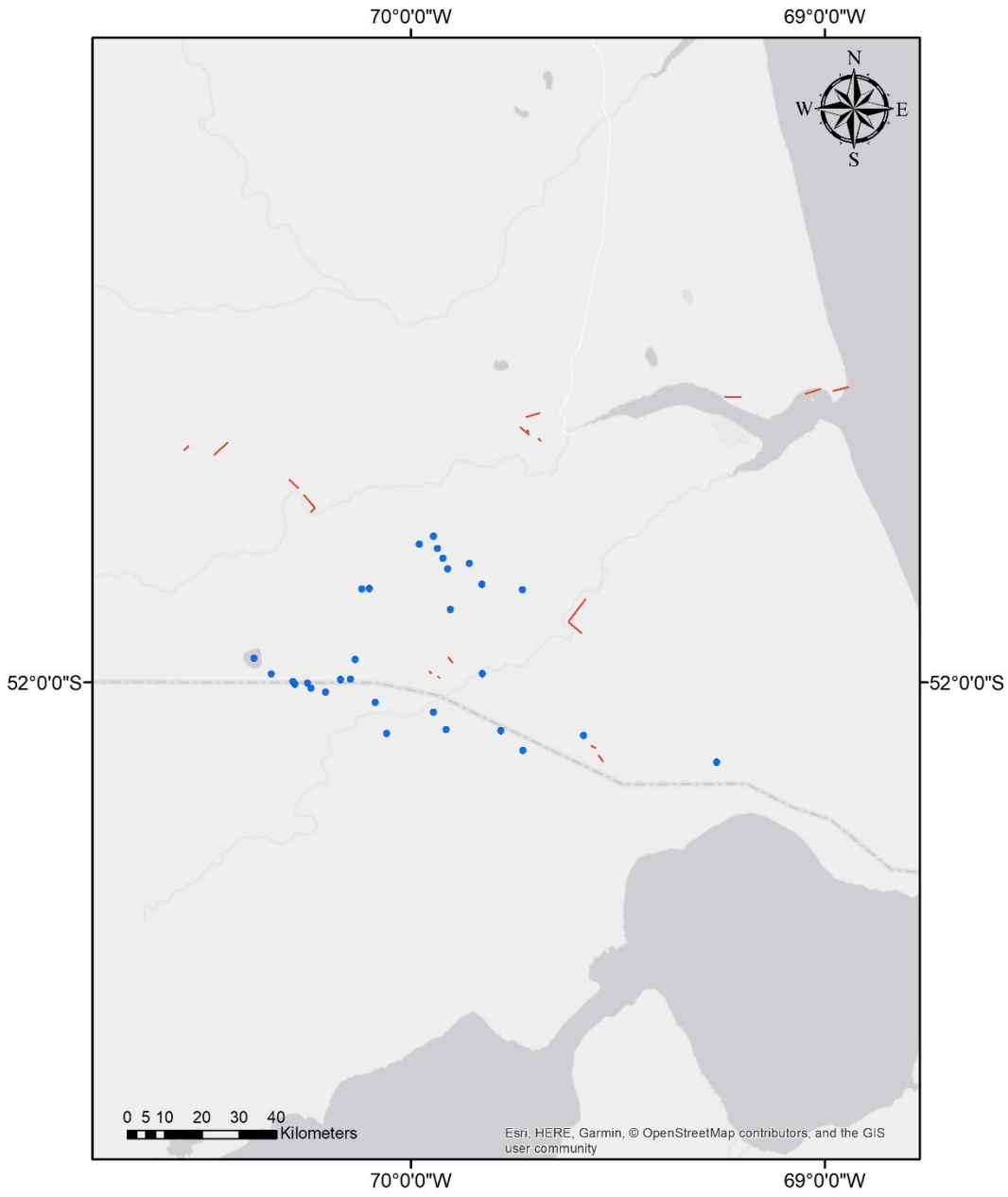

Figure 33 – Pali Aike Volcanic Field (Argentina) - Shows digitized fault lineaments (red lines) and maars (green dots) (Personal Communication Mazzarini, F.).

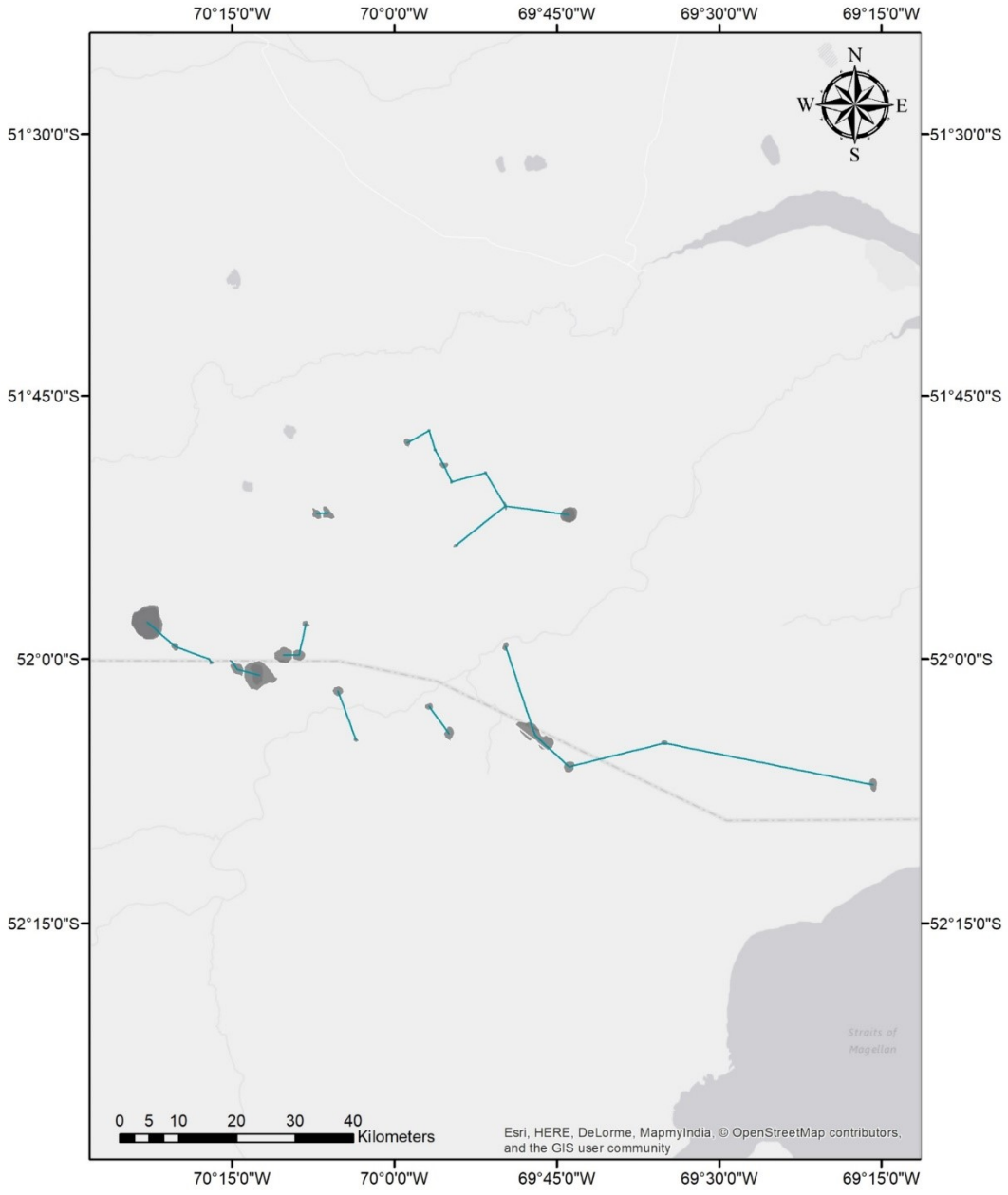

Figure 34 - Shows nearest neighbor lines (light blue) between maars in the Pali Aike Volcanic Field (Argentina).

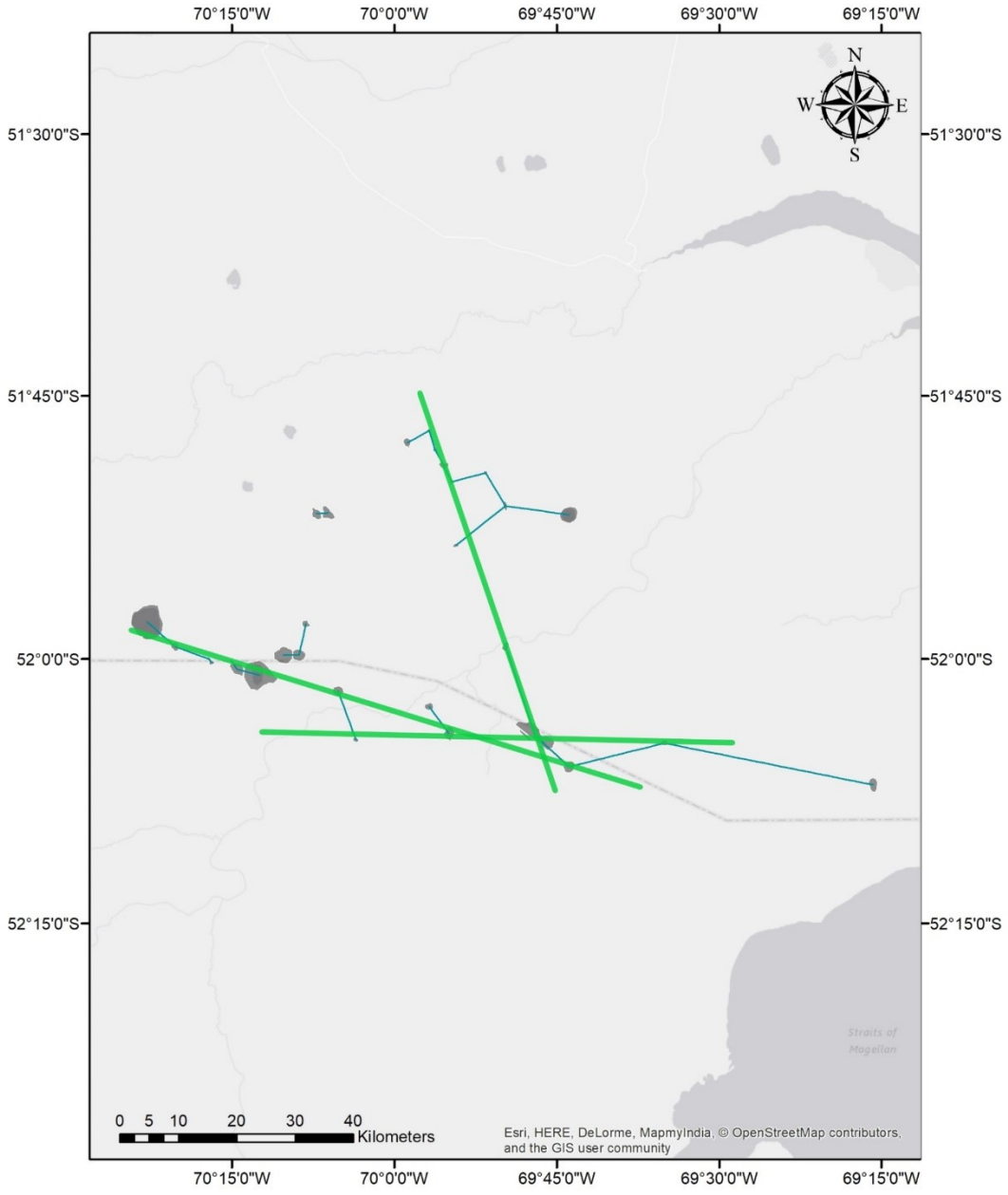

Figure 35 - Shows nearest neighbor lineaments (light green) between aligned maars in the Pali Aike Volcanic Field (Argentina).

Pinacate Volcanic Field

The Pinacate Volcanic Field, in Mexico, contains eight maars with measurable elongation orientations. The maars exhibit one strong mode in primary elongation orientation from 17-28° (P_A, N=3) (Figure 36 and Figure 37). No strong or weak modes in secondary elongation orientation data were found. Three of the maars were found to have secondary elongation orientations. Faulting data were found to have one strong mode from 127-153° (F_A). Nearest neighbor data exhibits one strong mode from 91-95° (N_A) supported in field and one weak mode from 28-48° (Figure 38). Only the strong mode is supported by three or more aligned maars (Figure 39). The primary elongation orientation mode does not match faulting or nearest neighbor orientations. Faulting and nearest neighbor orientations do not match. Two maars do match the faulting data, but they are not a part of any of the maar modes.

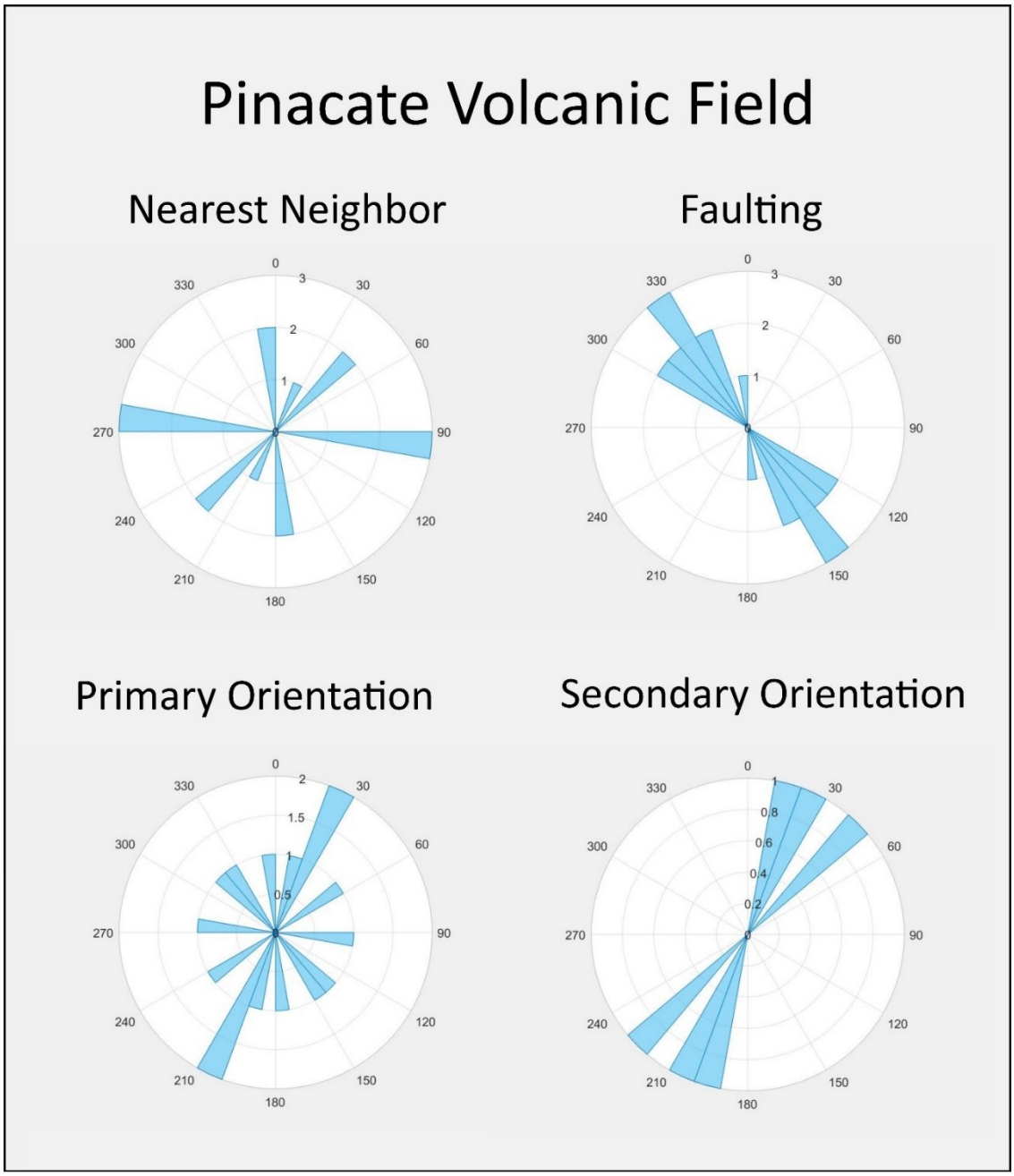

Figure 36 - Rose diagrams show orientation data for nearest neighbor, faulting, primary elongation orientation, and secondary elongation orientation in the Pinacate Volcanic Field (Mexico).

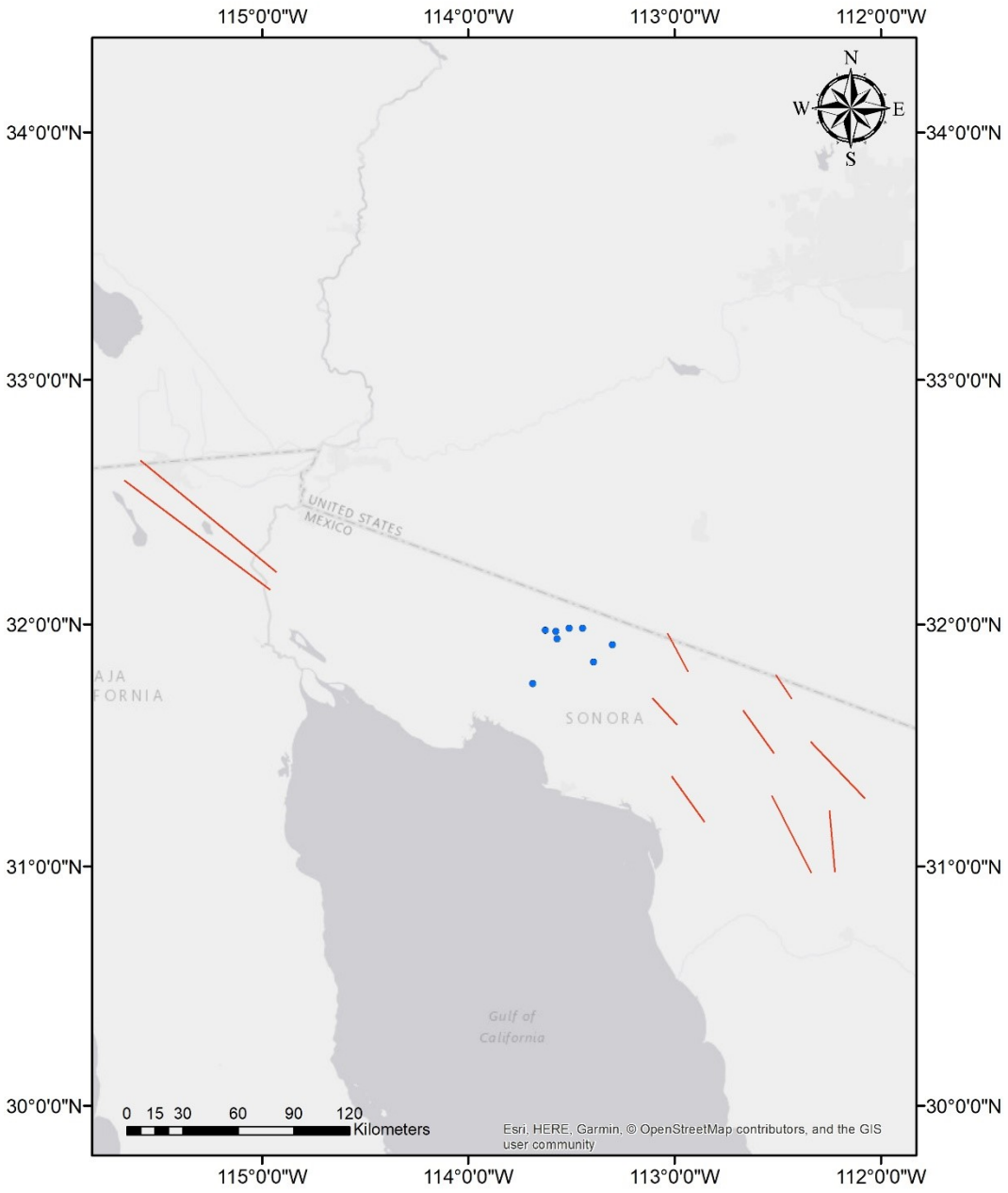

Figure 37 – Pinacate Volcanic Field (Mexico) - Shows digitized fault lineaments (red lines) and maars (green dots) (Padilla y Sánchez, R.J., Domínguez Trejo, I., López Azcárraga, A.G., Mota Nieto, J., Fuentes Menes, A.O., Rosique Naranjo, F., Germán Castelán, E.A., Campos Arriola, S.E., 2013).

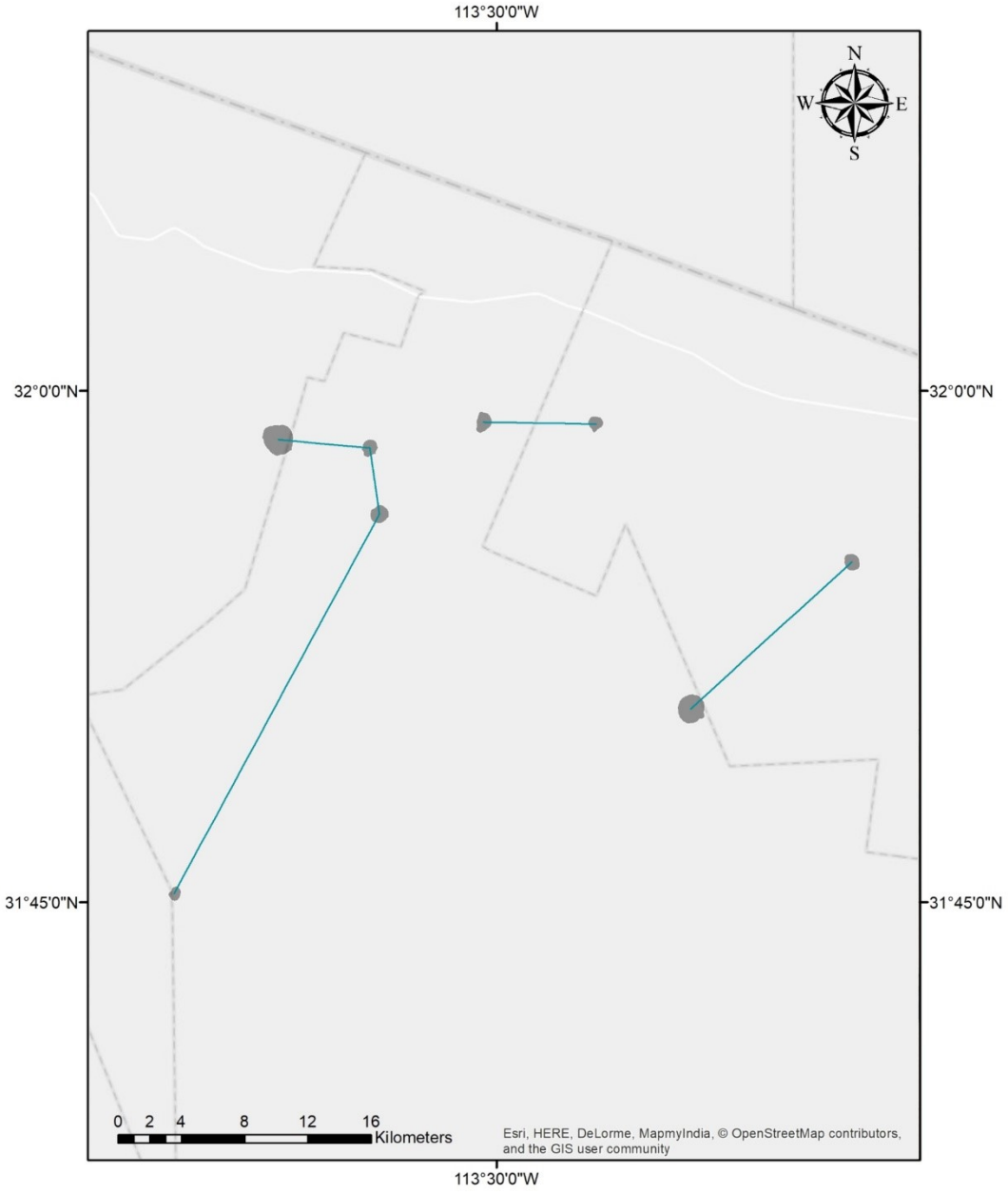

Figure 38 - Shows nearest neighbor lines (light blue) between maars in the Pinacate Volcanic Field (Mexico).

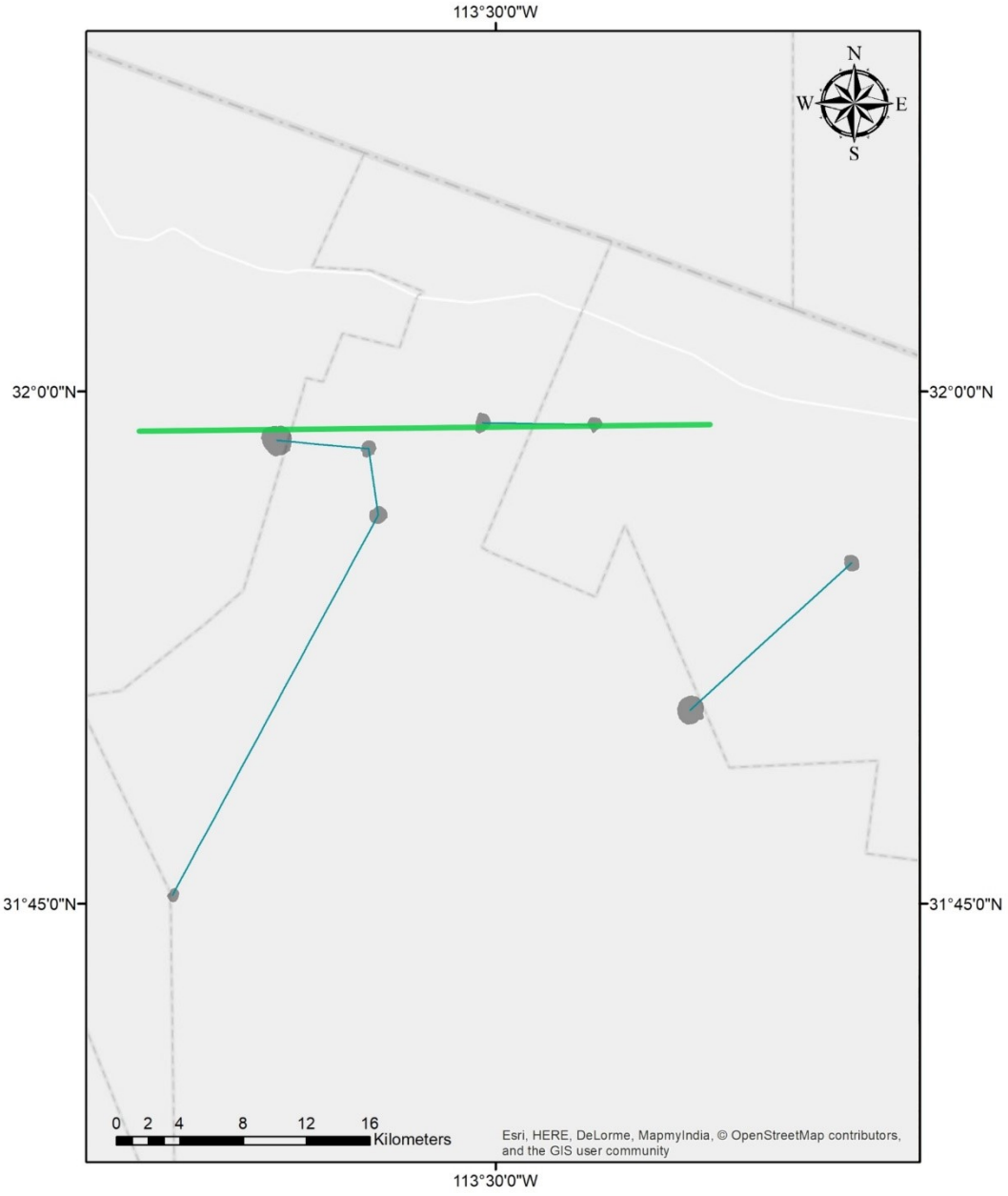

Figure 39 - Shows nearest neighbor lineaments (light green) between aligned maars in the Pinacate Volcanic Field (Mexico).

San Pablo City Volcanic Field

The San Pablo City Volcanic Field, in the Philippines, contains fourteen maars with measurable elongations. Primary maar elongation orientation data exhibits three strong modes from 4-8° (P_A, N=4), 31-40° (P_B, N=4) and 60-70° (P_C, N=4) and one weak mode from 97-114° (P_D, N=3) (Figure 40 and Figure 41). There are no secondary elongation orientation modes. Four of the maars were found to have secondary elongation orientations. There are three strong modes among the faulting data from 27-68° (F_A), 177-18° (F_B), and 90° (F_C). Three strong modes were found in nearest neighbor data from 59-62° (N_A), 153-161° (N_B), and 167-173° (Figure 42). Only the first two are supported by three or more aligned maars in field (Figure 43). Each of the four maar modes have a similar faulting or nearest neighbor mode. Primary elongation orientation mode P_A exhibits a similar orientation as faulting mode F_B. Faulting mode F_A shares a similar orientation with the maars of primary elongation orientation mode P_B. Primary elongation orientation mode P_C is similar to nearest neighbor mode N_A and faulting mode F_A. Primary orientation mode P_D has overlap with faulting mode F_C, but only for one maar's elongation orientation. In summary, there are 10/14 maars in modes with similar orientations as faulting or nearest neighbor data. If all maars are considered, regardless of maar modes, then 12/14 maars can be found with similar primary elongation orientations to faulting and nearest neighbor data. Nearest neighbor and faulting data also exhibit overlap in this field between modes F_A and N_A.

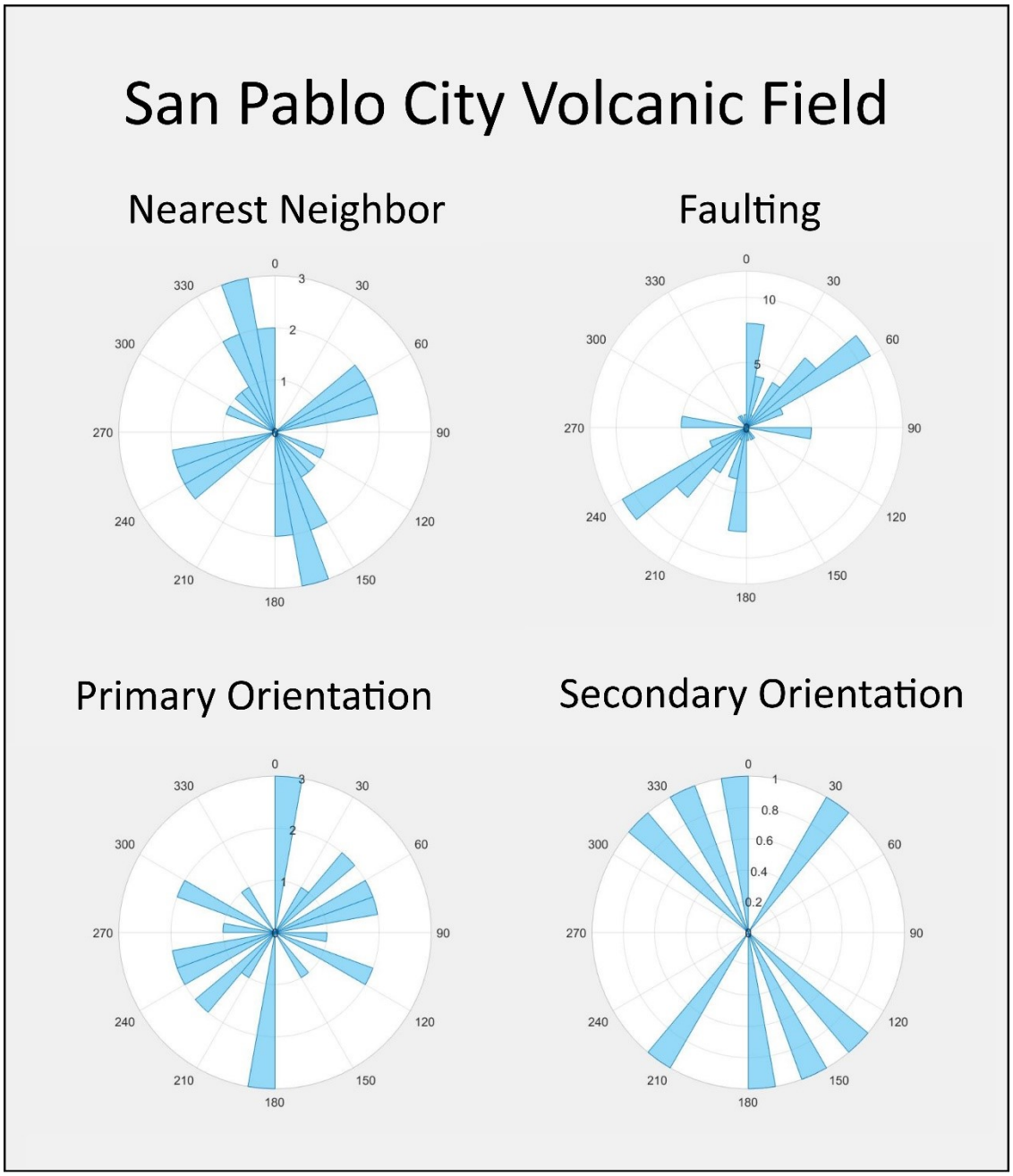

Figure 40 - Rose diagrams show orientation data for nearest neighbor, faulting, primary elongation orientation, and secondary elongation orientation in the San Pablo City Volcanic Field (Philippines).

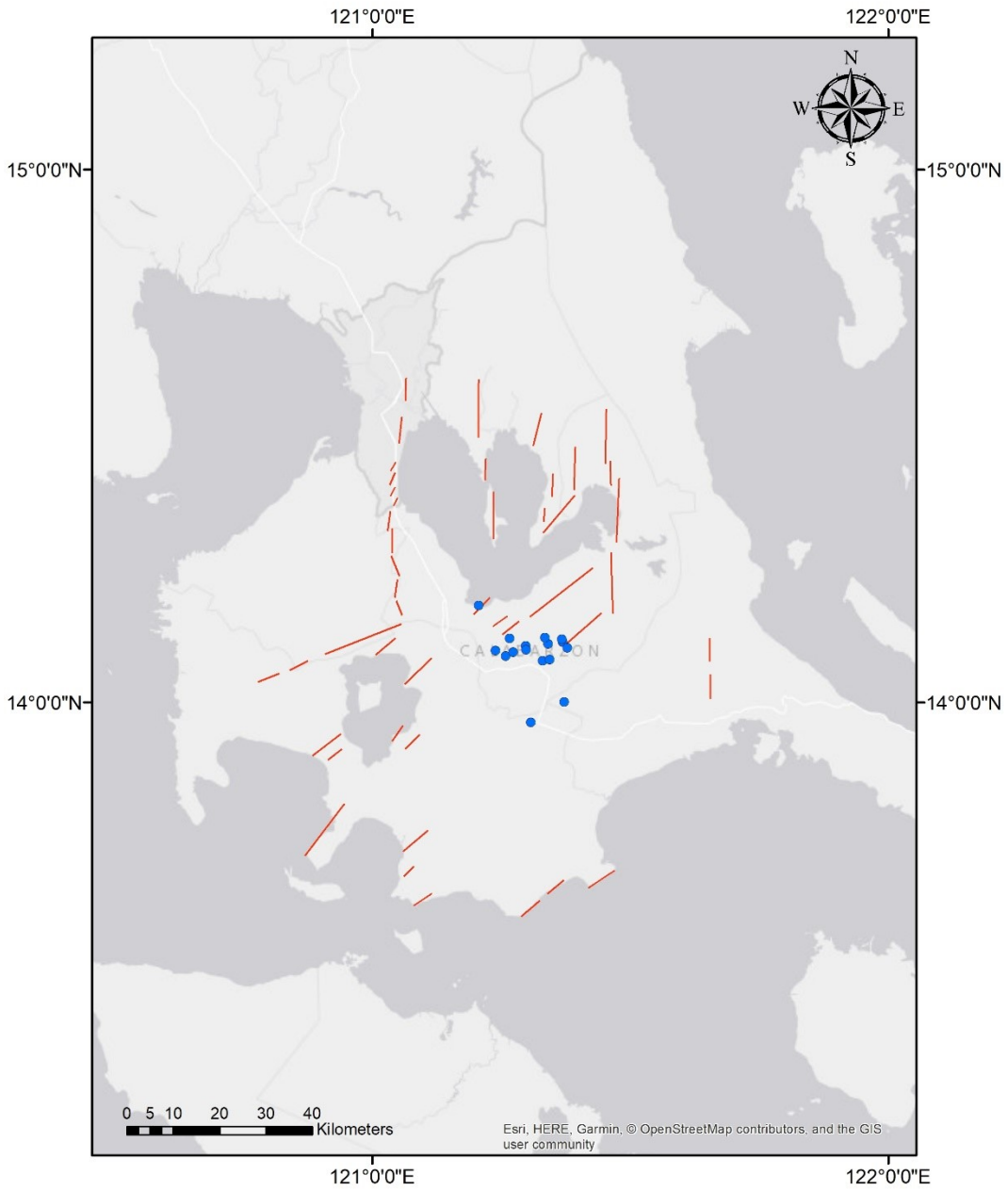

Figure 41 – San Pablo City Volcanic Field (Philippines) - Shows digitized fault lineaments (red lines) and maars (green dots) (Förster et al., 1990; Vogel et al. 2006; Tsutsumi, H. and Perez, J.S., 2013)

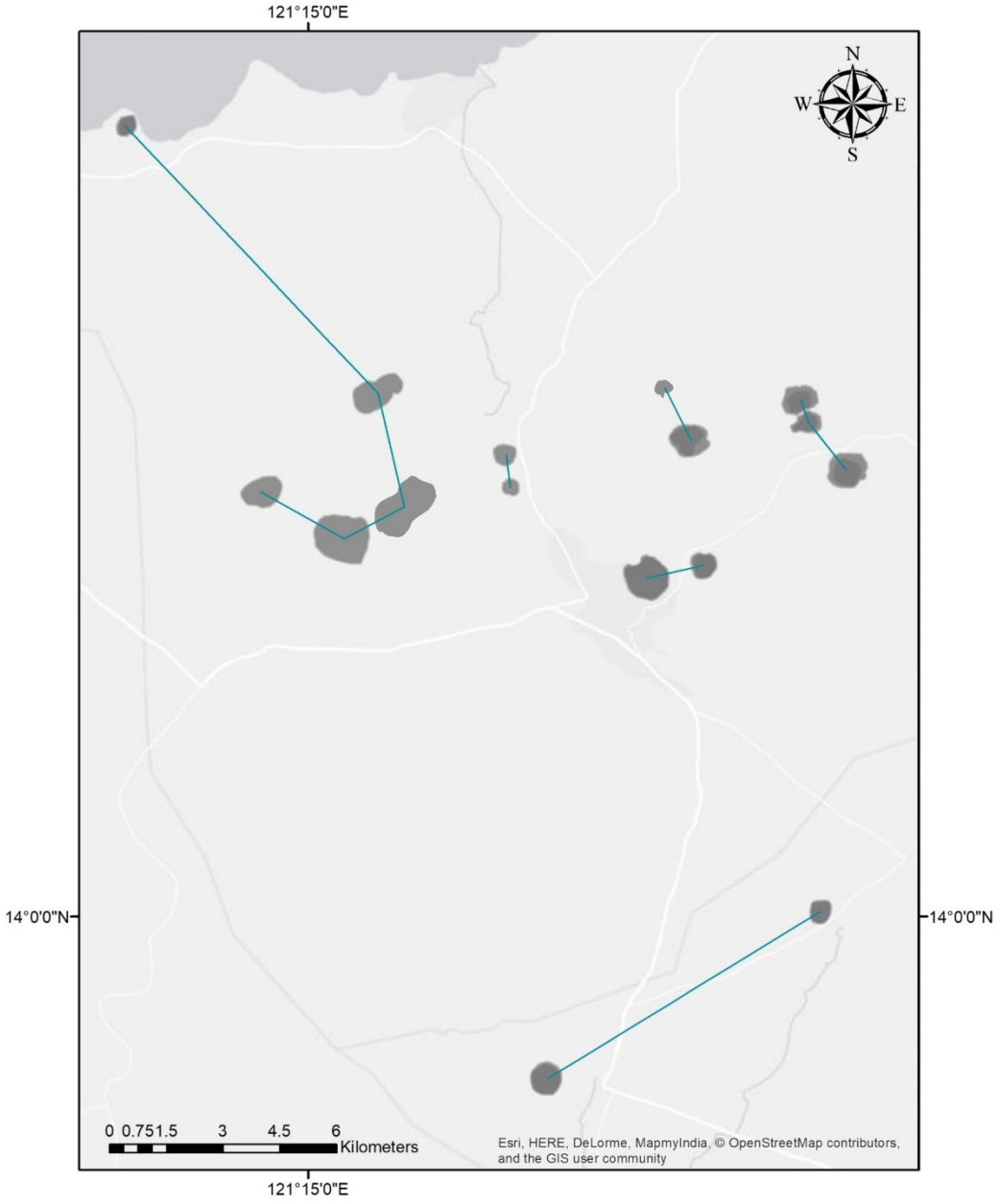

Figure 42 - Shows nearest neighbor lines (light blue) between maars in the San Pablo City Volcanic Field (Philippines).

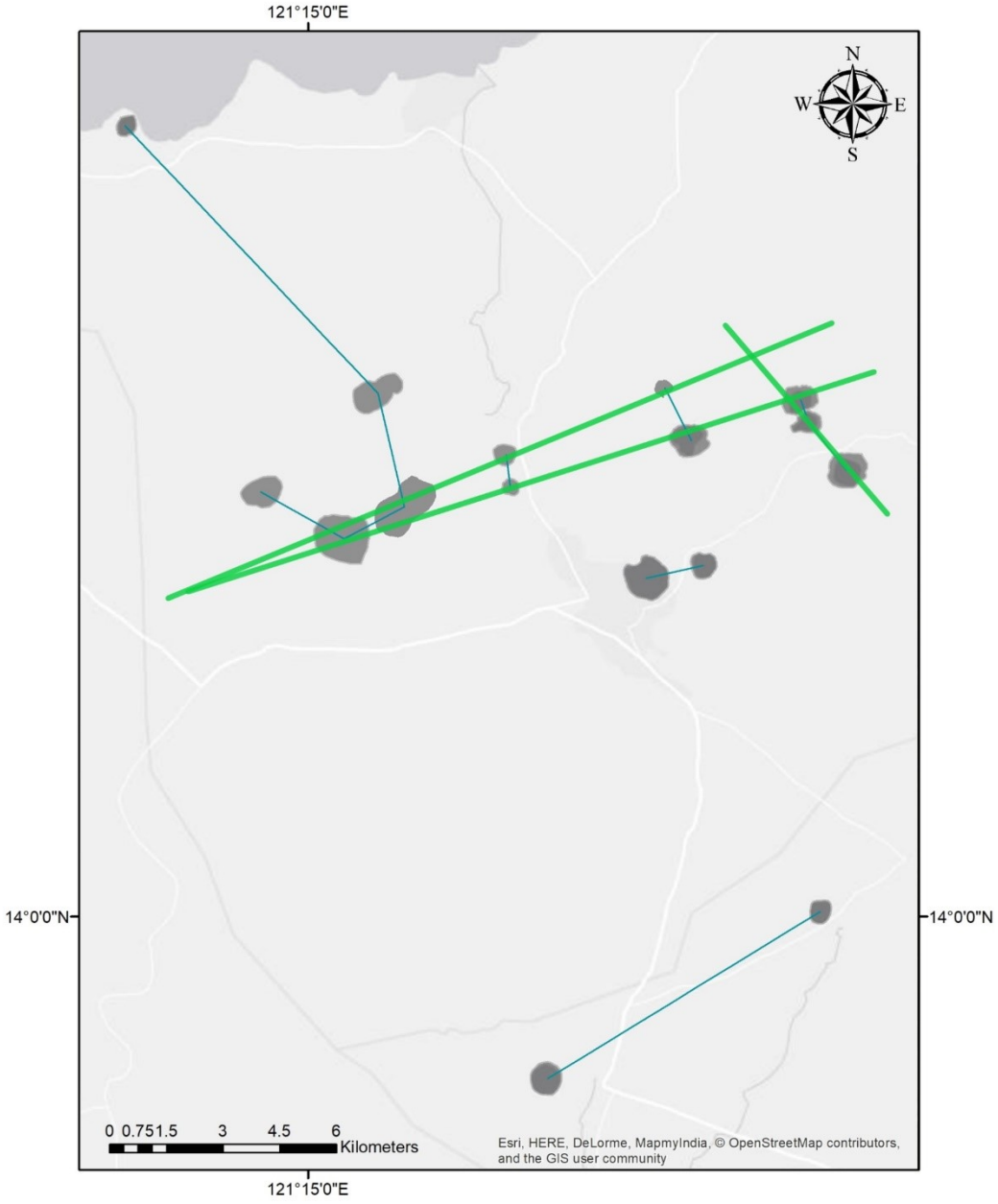

Figure 43 - Shows nearest neighbor lineaments (light green) between aligned maars in the San Pablo City Volcanic Field (Philippines).

Serdán Oriental Volcanic Field

The Serdán Oriental Volcanic Field, in Mexico, contains nine maars with measurable elongations. One strong mode was found in primary elongation orientation data from 70-77° (P_A, N=3) (Figure 44 and Figure 45). Four of the maars were found to have secondary elongation orientations. No secondary elongation orientation modes were identified. Faulting data exhibits two strong modes from 118-154° (F_A) and 5-13° (F_B). Nearest neighbor direction data has two strong modes from 158-170° and 142°, neither of which are supported in the field by three or more aligned maars (Figure 46). The maars of Serdán Oriental have only one primary elongation orientation mode P_A which is in no way matched by faulting modes or nearest neighbor modes. Three of the maars share similar primary elongation orientations as faulting and nearest neighbor data, but do not fall under a maar mode.

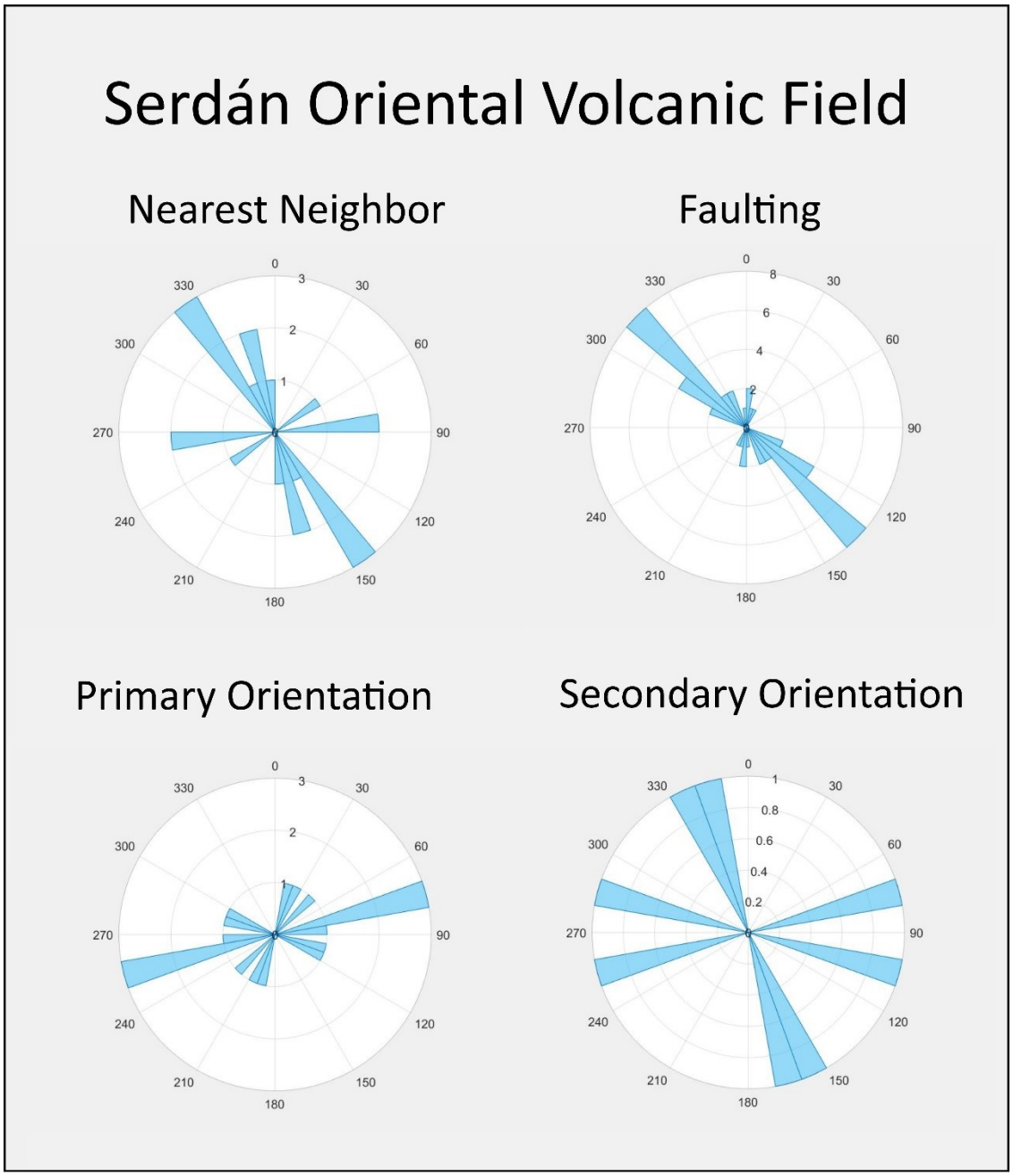

Figure 44 - Rose diagrams show orientation data for nearest neighbor, faulting, primary elongation orientation, and secondary elongation orientation in the Serdán Oriental Volcanic Field (Mexico).

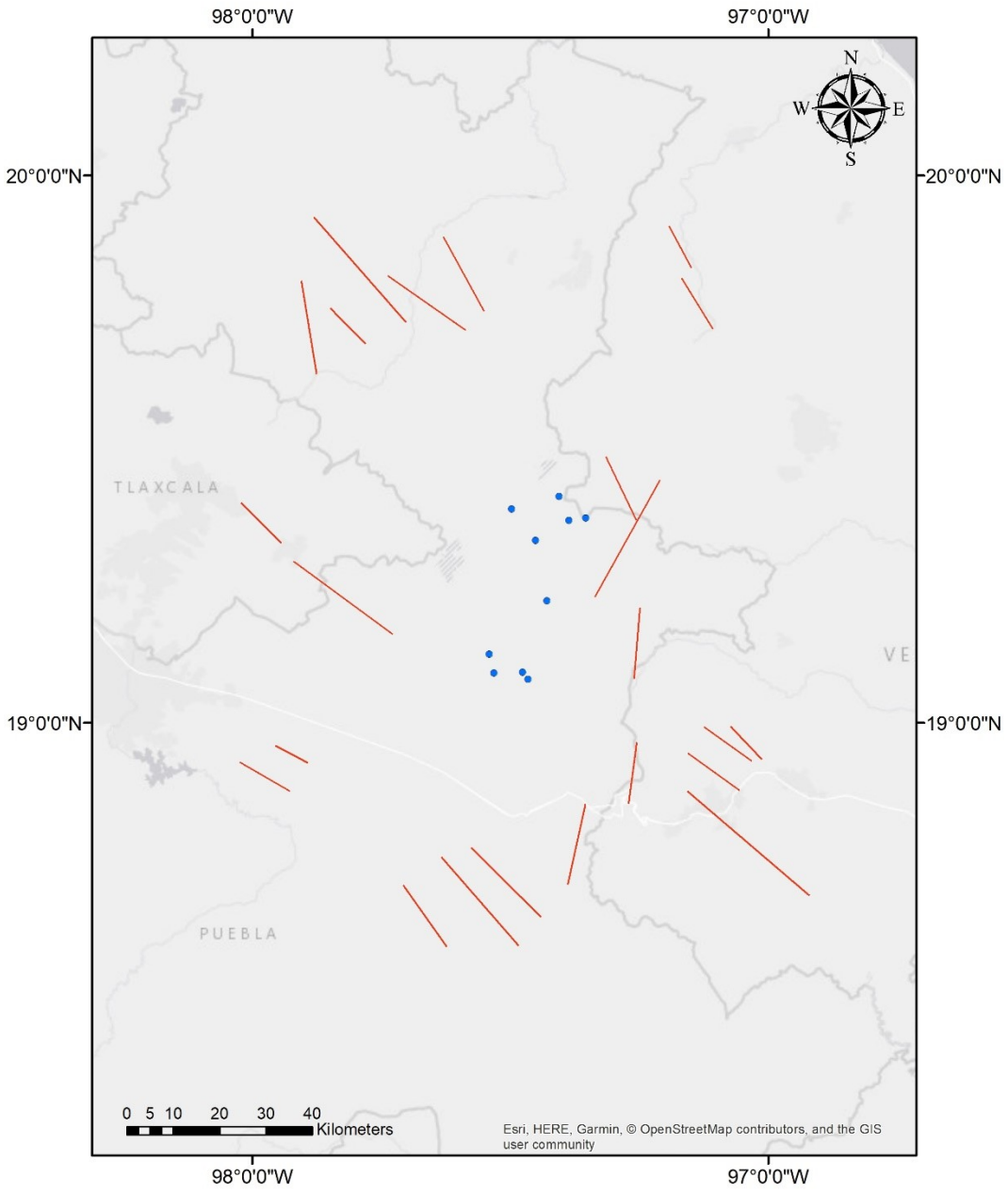

Figure 45 – Serdán Oriental Volcanic Field (Mexico) - Shows digitized fault lineaments (red lines) and maars (green dots) (Padilla y Sánchez, R.J. et al., 2013)

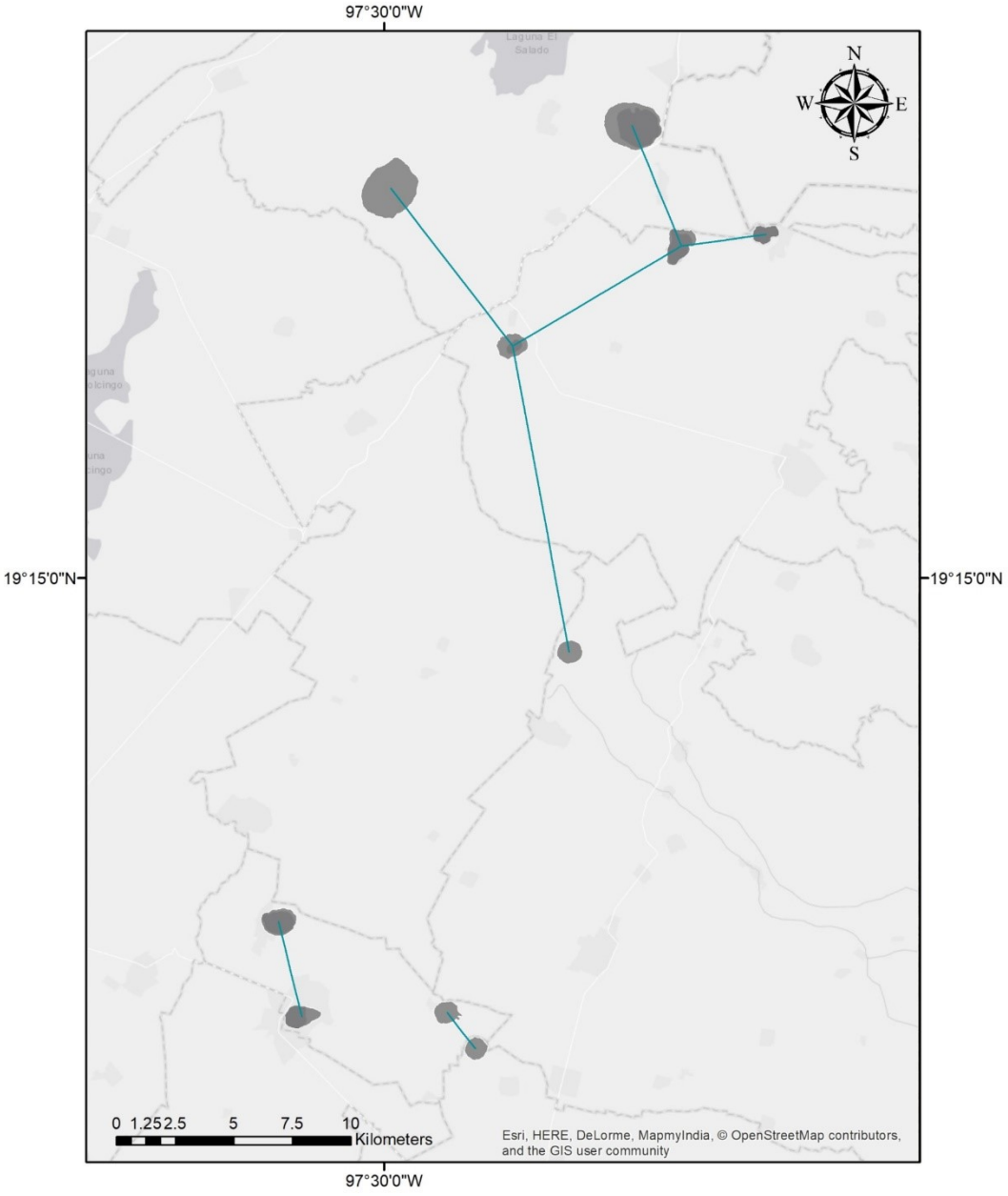

Figure 46 - Shows nearest neighbor lines (light blue) between maars in the Serdán Oriental Volcanic Field (Mexico).

CHAPTER 5

DISCUSSION

Before discussing maar elongation orientation, it is important to establish nearest neighbor analysis as an effective means of identifying structures and regional stresses. Previous work by Connor and Aubele (1992), Mazzarini and D'Orazio (2003), Cebria et al. (2011), and Hernando et al. (2014) has identified a correlation between regional structures and alignment of volcanic cones and vents. In each of these studies, it was found that volcanic features within a field exhibit evidence of structural control in their geographic distribution as a result of regional stresses. In the formation of mafic volcanic cones, vents, and maars, magma rises to the surface from an underground source by tabular dikes and sills resulting in linear trends of vents at the surface. The physical expression, i.e. the shape of landform, of each of these features is related to eruption history, but the process by which they are supplied magma is the same (Lorenz and Haneke, 2004). Research regarding dike propagation has shown that dikes within volcanic edifices are often aligned with the regional tectonic stress field, that is, perpendicular to the least compressive stress (Acocella and Neri 2009). This is because dikes can either utilize pre-existing faults as pathways to get magma to the surface, if the current stress regime is favorable, or create new pathways. Since the distribution of features is owing to the supply geometry (dike position and orientation), it is expected that maar craters would exhibit evidence of structural control in their distribution. In this study faults in

each field were compared with lineaments identified by nearest neighbor results. In each field, to qualify for consideration, a nearest neighbor mode had to exhibit both a mode as defined previously (methodology section), and a visible lineament comprised of three or more maars in field with an orientation within ten degrees of that of the mode.

All fields studied here exhibited nearest neighbor modes, and six of the seven fields were found to have three or more maars aligned in a direction supporting at least one or more of the nearest neighbor modes identified (Auckland, Lamongan, Newer Volcanic Province, Pali Aike, Pinacate, and San Pablo City). Of the six fields where lineaments were identified, four were found to have some overlap with faulting modes for those fields (Lamongan, Newer Volcanic Province, Pali Aike, and San Pablo City). Thus, in 66% of the fields where potential structural controls were identified via nearest neighbor analysis, at least one of the nearest neighbor lineament orientations also correlated with observed faulting. All exposed faulting may not be representative of the regional structures present during the time of the maars' formation. Additionally, if the stress regime at the time of maar formation did not produce extension of faults, existing structures may not have been favorable pathways for magma to propagate. Nearest neighbor analysis, however, reveals the structural controls and stresses that acted on the maars during formation. Inclusion of this data helps to ensure that regional stresses and structures are accurately represented. It is interesting to note that each of the fields with larger maar populations (4/7) showed overlap between nearest neighbor and faulting

data. Since identification of modes in nearest neighbor analysis is dependent upon the number of maars available to analyze, this break in the data may be a reflection of maar population.

The next most important topic is maar elongation. The presence of elongation in maars is a documented characteristic, typical of the volcanic feature (Ort and Carrasco-Núñez, 2009; Graettinger, 2018). However, it has yet to be determined whether that elongation is the product of regional structural control, the result of host rock properties, or more local influences. For this study, less than 5% of the maars with crater rims suitable for elongation orientation analysis were rejected for insufficient elongation (Table 2). This demonstrates the predisposition of maar craters toward elongation. Table 3 shows that 74% of all maars which exhibit elongation fall within elongation modes. In the two largest fields, 91% of all elongate maars are part of primary elongation orientation modes. When just the strong modes are considered, 55% of all maars are part of primary elongation orientation modes. In just the two largest fields, this number increases to 65%. These numbers reveal that maars in a field will commonly present similar primary orientations of elongation. What follows is a closer look at each of these cases and how they are relevant to the others.

Table 2 - A Summary of Maar Elongation

Field Name	Maars Digitized	Maars Used for Elongation	Elongation for Field	Maars Rejected for Insufficient Elongation	
Auckland Volcanic Field	7	6	1.26	1	Orakei
Lamongan Volcanic Field	16	14	1.27	1	Gunungparang
Newer Volcanic Province	23	23	1.31	0	
Pali Aike Volcanic Field	30	23	1.36	0	
Pinacate Volcanic Field	8	8	1.22	0	
San Pablo City Volcanic Field	16	14	1.28	1	Sampaloc
Serdán Oriental Volcanic Field	10	9	1.34	1	Maar II (Unnamed)

Table 3 – Elongate Maars in Modes

Field Name	Maars Used for Elongation	Maars in Modes	Percentage of maars in modes
Auckland Volcanic Field	6	0	0%
Lamongan Volcanic Field	14	10	71%
Newer Volcanic Province	23	21	91%
Pali Aike Volcanic Field	23	21	91%
Pinacate Volcanic Field	8	3	38%
San Pablo City Volcanic Field	14	12	86%
Serdán Oriental Volcanic Field	9	3	33%

The fields analyzed can be divided into three distinct groups. There are the fields which have few if any maars that share primary elongation orientations (Auckland, Pinacate, and Serdán Oriental), fields with many maars that share similar primary elongation orientations but few that match faulting or nearest neighbor data (Lamongan), and fields which have high numbers of maars that share similar primary elongation orientations as well as large numbers of maars that match faulting and nearest neighbor data (Pali Aike, San Pablo City, and Newer Volcanic Province). Each of these three groups

possesses distinguishing features, besides the number of maars that fall in modes, which group them together and set them apart from the others.

Auckland, Pinacate, and Serdán Oriental each have fewer than ten maars (the lowest counts found in this study). In all three fields, no maars in modes match faulting or nearest neighbor modes. Additionally, no nearest neighbor modes for either Auckland or Pinacate were found to match faulting modes (Serdán Oriental has no nearest neighbor modes that qualify). These fields all exhibit an exceptionally low number of maars in modes, ranging from 0-37%. Essentially, each of these fields shows very little in the way of correlation between any of the considered variables. The three fields do not share similar tectonic settings or distances to exposed faults. While each of these fields shares a distinct lack of correlation between maar primary elongation orientation, maar location, and fault orientation, it is possible that the root cause of the lack in modes belongs to their shared low number of maars. In order for a mode to be identified, even a weak one, three or more data points must be found within twenty degrees of one another. While this is an easy requirement to meet for other fields, in these three, a mode would have to contain more than 30% of the maars measured. This is important considering that, across all fields, the average primary elongation orientation mode contains only 22% of the maars in field. It is possible that the lack of modes is related to the number of maars. Since the identification of modes in maar primary elongation orientation is pivotal for any correlation between elongation orientation and orientations identified in faulting and

nearest neighbor data, it was decided that these fields would not be considered for further analysis. It is important to note that analysis of these fields has not been halted because they lack modes. An absence of modes would be just as meaningful as the presence of modes, in a given field. They have been removed from further testing because the number of maars these fields contain is insufficient to confirm the absence of modes. Despite their ineligibility for additional analysis, each of these fields still yielded valuable data on the occurrence and distribution of primary and secondary maar elongations. Each field was found to contain maars with both primary and secondary elongation orientations, the orientations of the maars' elongations covered a wide range of orientations in each field, and none of the fields were found to have a majority of maar elongation orientations in any single orientation.

Lamongan Volcanic Field contains fourteen maars. Of those maars, 71% fall within primary elongation orientation modes. However, unlike the other three fields which exhibit high populations of maars within primary elongation orientation modes, none of Lamongan's maars fall within both primary elongation orientation and faulting or nearest neighbor modes. Furthermore, only one maar (not in a mode) can be found with a primary elongation orientation that matches that of a faulting mode. The nearest neighbor mode for this field is matched by faulting, but has no maars which share its orientation. This is why Lamongan volcanic field is in a group of its own. It has a large enough population of maars, most of which are part of primary elongation orientation

modes, but the maars found in those modes do not align with faulting or nearest neighbor direction data. Looking back to Figure 5, a satellite image of the Lamongan Volcanic Field, the maars are all centered around the Lamongan Volcano; they appear to be distributed radially around the stratovolcano. The presence of the volcano may have influenced the local stress regime and overridden more regional stresses and structural controls (Acocella and Neri, 2009). If maar shape was structurally controlled, this could explain the absence of primary elongation orientation modes following faulting. However, it does not explain why no maar primary elongation orientations match nearest neighbor data. Nearest neighbor data for the region reflects the stresses and structures that acted on the maars at the time of formation. The presence of radial lineaments, about the Lamongan volcano, in that nearest neighbor data indicates that they were placed under the influence of stresses produced by the volcano's presence. The absence of maars with elongation orientations similar to nearest neighbor lineaments shows that that stress did not impact the maars' elongation orientations. Also, none of the maars found within nearest neighbor lineaments shared a primary elongation orientation with that lineament.

The last group is comprised of fields which have both high numbers of maars in primary elongation orientation modes (Newer Volcanic Province, Pali Aike, and San Pablo City; Average 82%), and high numbers of those maars which share similar primary elongation orientations as nearest neighbor and faulting orientations (average 82% of field). In each of these fields, there are nearest neighbor trends that are corroborated by

faulting, demonstrating that regional structural controls played a part in the formation of these maars, particularly their geographic distribution. With Newer Volcanic Province, there are multiple examples of maars directly crosscut by faulting (Figure 47). In these nine maars, the primary elongation orientation never matches the coincident fault. While many maars can be found with primary elongation orientations similar to the orientation of faults and nearest neighbor lineaments in the Newer Volcanic Province, these maars do not compose the lineaments their elongation orientations are similar to. In Pali Aike and San Pablo City, maars with primary elongation orientations similar to the nearest neighbor lineaments they compose are similarly infrequent.

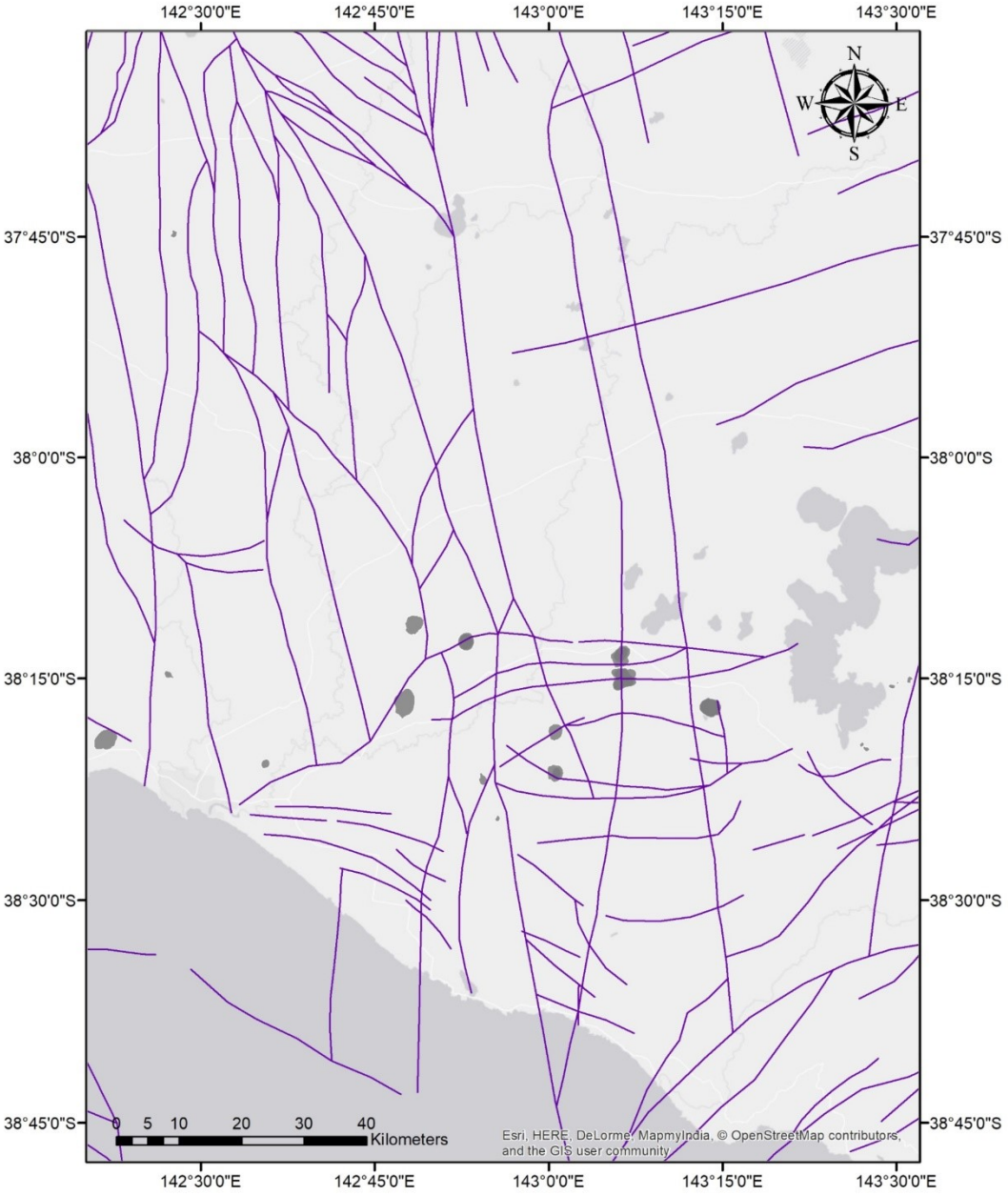

Figure 47 – Shows faulting along the western side of the Newer Volcanic Province (Australia). Several maars occur immediately along faults but do not have primary elongation orientations that match the fault.

Out of the all fields, only 17% of maars found in nearest neighbor lineaments shared a primary elongation orientation with the lineament they composed (Table 4). When just the larger fields were taken into account, the percentage was the same. More than half of the maars in these fields exhibit similar elongation orientations as faulting and nearest neighbor trends, but the orientation of the maar's primary elongations show no bias towards the trend that determined their placement. While this evidence alone does not rule out the possibility of regional structural controls influencing the elongation of maar craters, it does demonstrate that the structural controls which determine maar placement are not the same as those acting on elongation. The percentage of maars which falls within primary elongation orientation modes for the four largest fields (84% averaged) makes a strong case for the existence of preferred elongation orientations. However, in each field, the maars which make up these primary elongation orientation modes are scattered throughout the field. There is little to no spatial clustering of similarly oriented maars. It does not appear that there is any correlation between where a maar is and the orientation of its elongation.

Table 4 - A Summary of Maars in Nearest Neighbor Lineaments

Field Name	Maars in Nearest Neighbor Lineaments	Primary Orientations Matching Lineament Found In
Auckland Volcanic Field	3	0
Lamongan Volcanic Field	6	0
Newer Volcanic Province	9	3
Pali Aike Volcanic Field	16	3
Pinacate Volcanic Field	4	1
San Pablo City Volcanic Field	9	1
Serdán Oriental Volcanic Field	0	0

Finally, Table 5 shows that the percentage of each maar population (primary elongation orientation) found to match nearest neighbor and faulting modes closely approximates the percentage of area covered by those modes out of 360^{o}. The percentage of each field covered by nearest neighbor and faulting data almost always surpasses the percentage of maars for that field which were found to share a similar primary elongation orientation with it. If regional structural controls did influence the elongation orientation of maar craters, a much larger portion of the maars in each field would be found with similar elongation orientations as faults and nearest neighbor

lineaments. When the modes are restricted to exclude the ten-degree buffer to either side, the percentage of maars with similar orientations to faulting and nearest neighbor modes decreases across the board. If regional structural controls governed the primary elongation orientations of these maars, most of the maars would fall under these modes. Additionally, while none of the fields had a sufficient number of maars exhibiting secondary maar elongation orientations to make a quantitative statement about their behavior, the occasional presence of secondary elongation orientations in maars found in nearest neighbor lineaments further reduces the feasibility of structural control over these features. Secondary elongation orientations indicate that maar craters grow in more than one direction during an eruption. It is possible that this is the result of a change in stress field while the eruption is underway (Le Corvec, N., Muirhead, J.D., and White, J.D.L., 2018). While secondary elongation orientations could be produced by regional structures, the fact that neither the primary or secondary orientations of maars frequently align with the lineaments they compose or the faults that cut them indicates otherwise. Considering this evidence, alongside that of the Lamongan Volcanic Field, it becomes clear that other factors must be considered for determining the controls on maar elongation.

Table 5 – Faulting and Nearest Neighbor Range Compared to Maars with Similar Primary Elongation Orientations

	Including 10° buffer		Excluding 10° buffer	
Volcanic Fields	Area covered by faulting and nearest neighbor	Maars with similar orientation	Area covered by faulting and nearest neighbor	Maars with similar orientation
Auckland Volcanic Field	33%	50%	11%	17%
Lamongan Volcanic Field	48%	7%	17%	0%
Newer Volcanic Province	94%	87%	71%	52%
Pali Aike Volcanic Field	75%	74%	39%	43%
Pinacate Volcanic Field	39%	38%	17%	25%
San Pablo City Volcanic Field	75%	86%	38%	57%
Serdán Oriental Volcanic Field	53%	33%	38%	22%

If the orientation of maar elongation is not controlled by regional structures, it becomes necessary to consider alternative influences, such as local and shallow stress regimes which may be a result of host rock material strength, the influence of the explosive eruption itself, stress produced by overlying layers prior to eruption, or the nature of the hydrology present at the time of maar formation.

It may be that there are both deep and shallow stress fields influencing different parts of maar formation. A deep stress field which determines placement through

structural control, and a shallow one which plays a role in the elongation of maars. Considering that shallow sill complexes primarily form when dikes encounter the contact between areas of strongly contrasting rigidity (Van den Hove, J., Grose, L., Betts, P. G., Ailleres, L., Van Otterloo, J., & Cas, R. A. F., 2017), and that most of the fields analyzed were hosted in sediments atop bedrock (Table 1), it is highly likely that the sources of magma for these maars were directed at depth by pre-existing structures and then diverged near the surface. If this was the case, it could explain how a maar could to be placed by a deep governing structural control and shaped by another control at the surface. Additionally, based on the lack of clustering in maar elongation orientations geographically, these stresses are either extremely localized, or there are other factors at play in maar formation. Recent research by Le Corvec et al. (2018) indicates that the initial explosion which begins the maar eruption could alter the stress field around the maar and divert the dike which feeds it. This change in stress field, and dike diversion, would influence the elongation orientation of maars. Because of the high numbers of maars found to exhibit similar elongation orientations, elongation orientations could be functions of inconsistencies in the local geology, possibly due to which layers were exposed at the time and place of formation or the fracturing of the rock in the surrounding area. However, this is unlikely considering that most of the fields exhibit fairly consistent geology throughout. If the stress field was found to exist prior to the formation of the maar, it is possible that the shape is controlled by the distribution of the magma

before it erupted. Localized and smaller scale fracturing of the uppermost layer intruded could be the source to a preexisting shallow stress field which might produce directions in which elongation is more likely. Shallow stress fields could dictate the direction in which magma propagation is most likely, or channel the energy of explosions preferentially.

Lorenz (2003) explained that irregularity of the root zone in maars can be attributed to explosions which largely follow the trend of the feeder dike. While the dike supplies the magma necessary for the eruption to take place, phreatomagmatic eruptions also require a supply of water (Ort and Carrasco-Núñez, 2009). Variation in water availability can lead to multiple explosion foci or migration of foci over the course of an eruption (Lorenz, 2003; Ort and Carrasco-Núñez, 2009; White and Ross, 2011; Le Corvec, 2018). The presence of a shallow stress field could influence the distribution of magma, or water, altering the area where explosions can take place (and the overall crater shape). Alternatively, if explosions propagate along the path of the dike, and the dike itself is at an angle other than 90^{o}, it is reasonable that the surface expression would be elongate in a direction other than parallel to the dike.

Additional analysis of these data, and expanded datasets focused on these more localized influences would help narrow down the controls on maar elongation orientation. The limited number of maars available for study in a given field makes statistical analysis of a single field difficult. However, due to the limited number of maars with preserved crater rims and the structural differences between fields, it is unlikely that future studies

will be able to produce larger maar populations without sacrificing accuracy. Future studies might work to incorporate data unique to each individual maar such as surface fracturing, feeder dike trend, local geology, and local hydrology. Alternatively, experimental re-creation of maar eruptions could help elucidate which variables have an effect on the overall crater shape. This approach has the advantage of allowing for control over which potential controls are present during an eruption and direct measurement of the outcome. The current understanding of maar eruptions leaves a substantial void in current hazard mapping and safety protocols. Identification of the factors leading to maar elongation orientation will prove beneficial to these and other studies by helping to identify the directions these eruptions are likely to propagate. Future research into occurrence and magnitude would also benefit these studies.

CHAPTER 6

CONCLUSIONS

The distribution of maar elongation orientations found in this study shows that maars tend to exhibit similar elongation orientations within a field. Data collected also demonstrates that maars, like vents and cones, are subject to structural control with regards to their geographic location. Although maars can be found in nearest neighbor lineaments, they rarely exhibit primary elongation orientations similar to the lineaments they compose. Furthermore, maars which shared similar primary elongation orientations with other maars were not found to be grouped close together geographically with those maars. Overall, the number of maars in each field which share primary elongation orientations with faults and nearest neighbor lineaments is not sufficient to suggest regional structural control over primary elongation orientation in any field. The tendency of maars to exhibit similar primary elongation orientations within a field, coupled with the lack of correlation with structural controls shows that the elongation orientations of maars are likely governed by more local controls such as shallow stress fields, local geology, magma distribution, dike trend, or even stresses created by the explosions as the eruption unfolds.

APPENDIX

Table Showing Maar Orientation Data Across All Fields

Name of Field	Maars Digitized	Maars Used for Elongation	Maars in Modes	Maars Matching faults or NN	Maars Matching in modes	Maars in Strong Modes	Maars matching in strong modes
Auckland Volcanic Field	7	6	0	3	0	0	0
Lamongan Volcanic Field	16	14	10	1	0	6	0
Newer Volcanic Province	23	23	21	20	18	13	10
Pali Aike Volcanic Field	30	23	20	17	15	17	12
Pinacate Volcanic Field	8	8	3	3	0	3	0
San Pablo City Volcanic Field	16	14	12	12	10	9	9
Serdán Oriental Volcanic Field	10	9	3	3	0	3	0

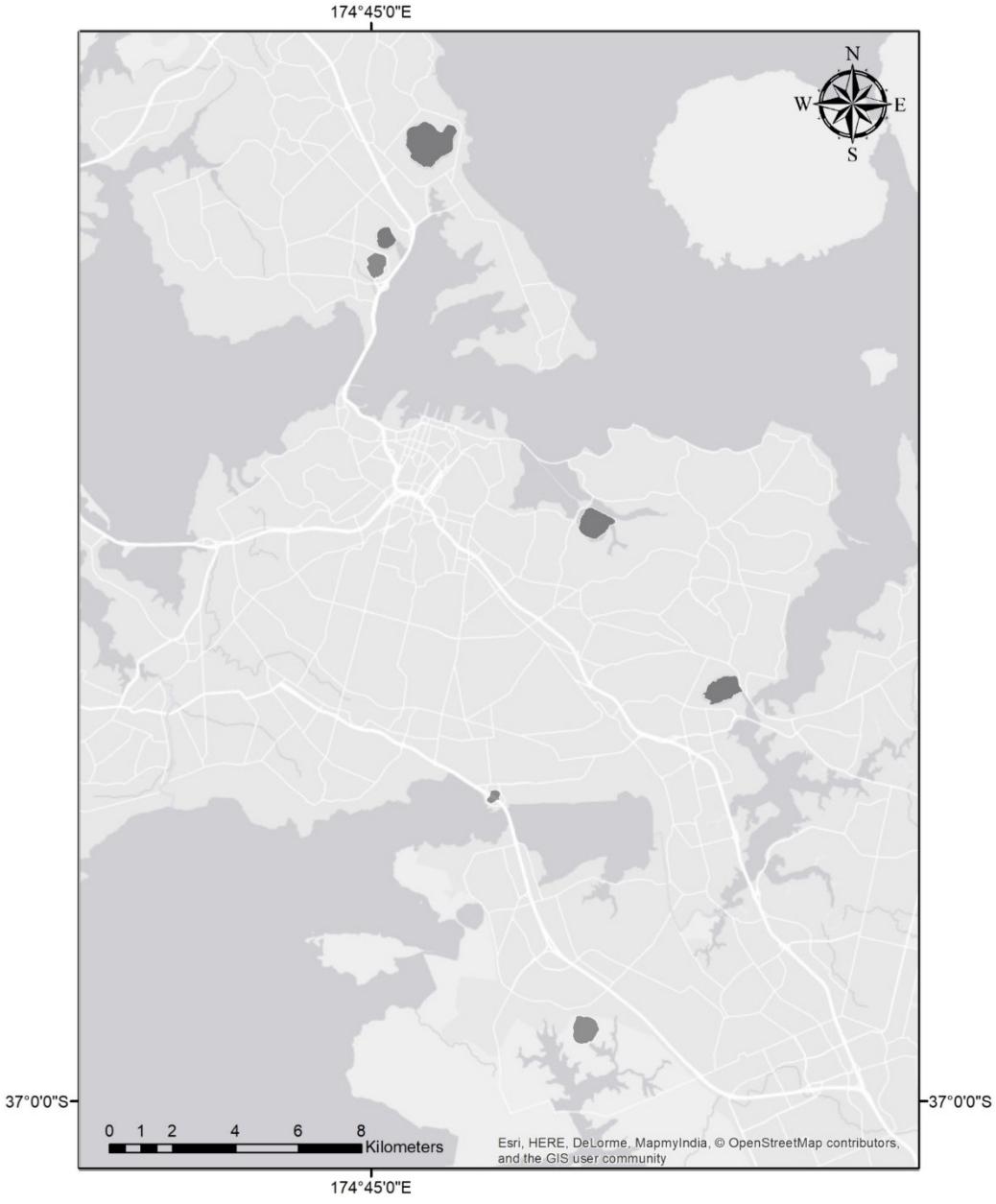

Auckland Volcanic Field (New Zealand) – Shows all maars digitized.

Auckland Volcanic Field (New Zealand) – Shows all maars used for measuring primary orientation. Any maars in primary orientation modes are highlighted.

Auckland Volcanic Field (New Zealand) – Highlighted maars fall both within primary orientation modes, and exhibit a similar orientation as faulting and nearest neighbor modes.

Auckland Volcanic Field (New Zealand) – Dark grey maars were found to exhibit secondary orientations.

Auckland Volcanic Field (New Zealand) – Highlighted maars were found to exhibit secondary orientations which were both in a mode, and similar to faulting and nearest neighbor modes.

Auckland Volcanic Field (New Zealand) – Highlighted maars make up secondary orientation modes.

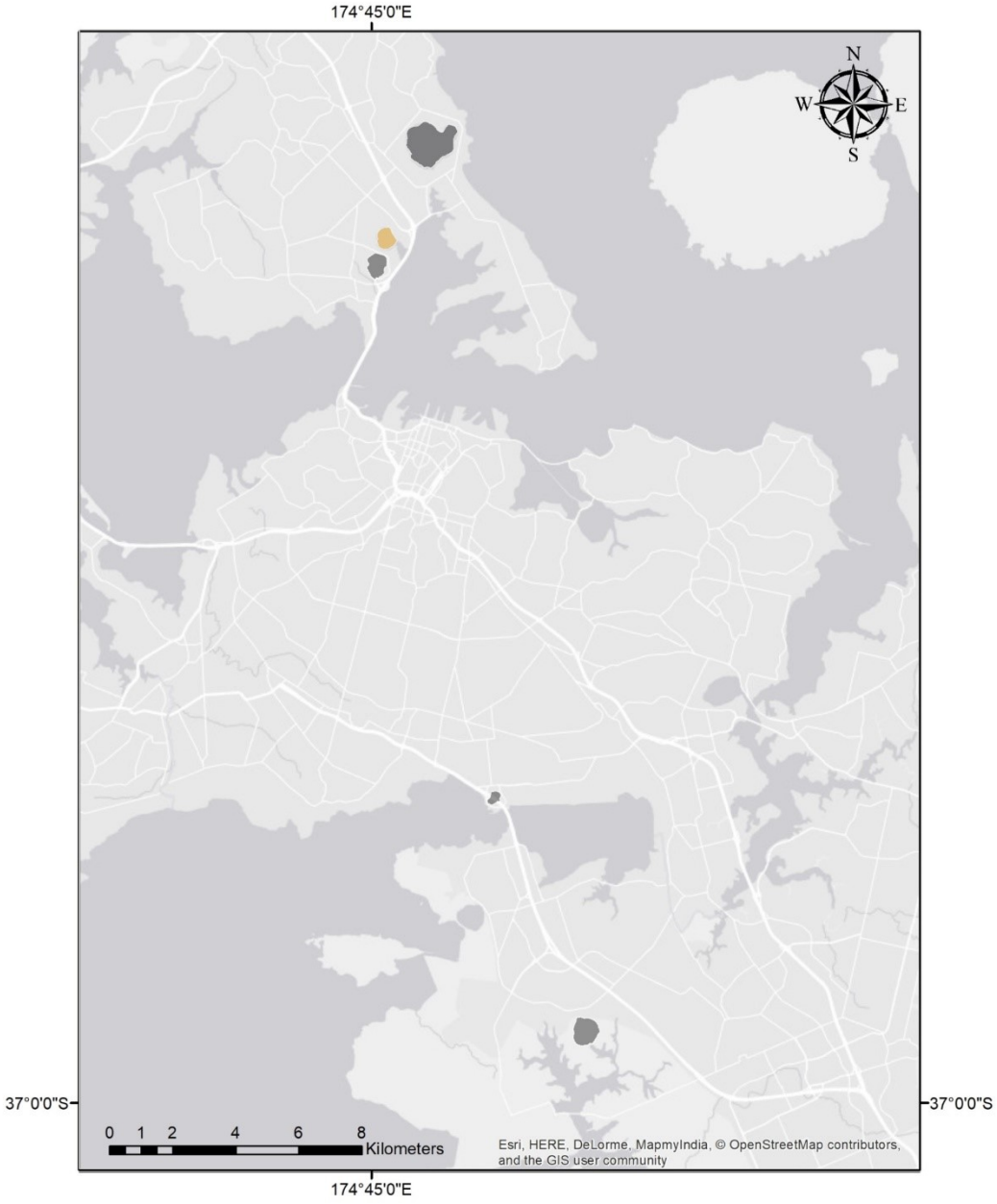

Auckland Volcanic Field (New Zealand) – Highlighted maars were found to have secondary orientations similar to faulting and nearest neighbor modes. The yellow maars fall within at least 10^{o} of nearest neighbor modes.

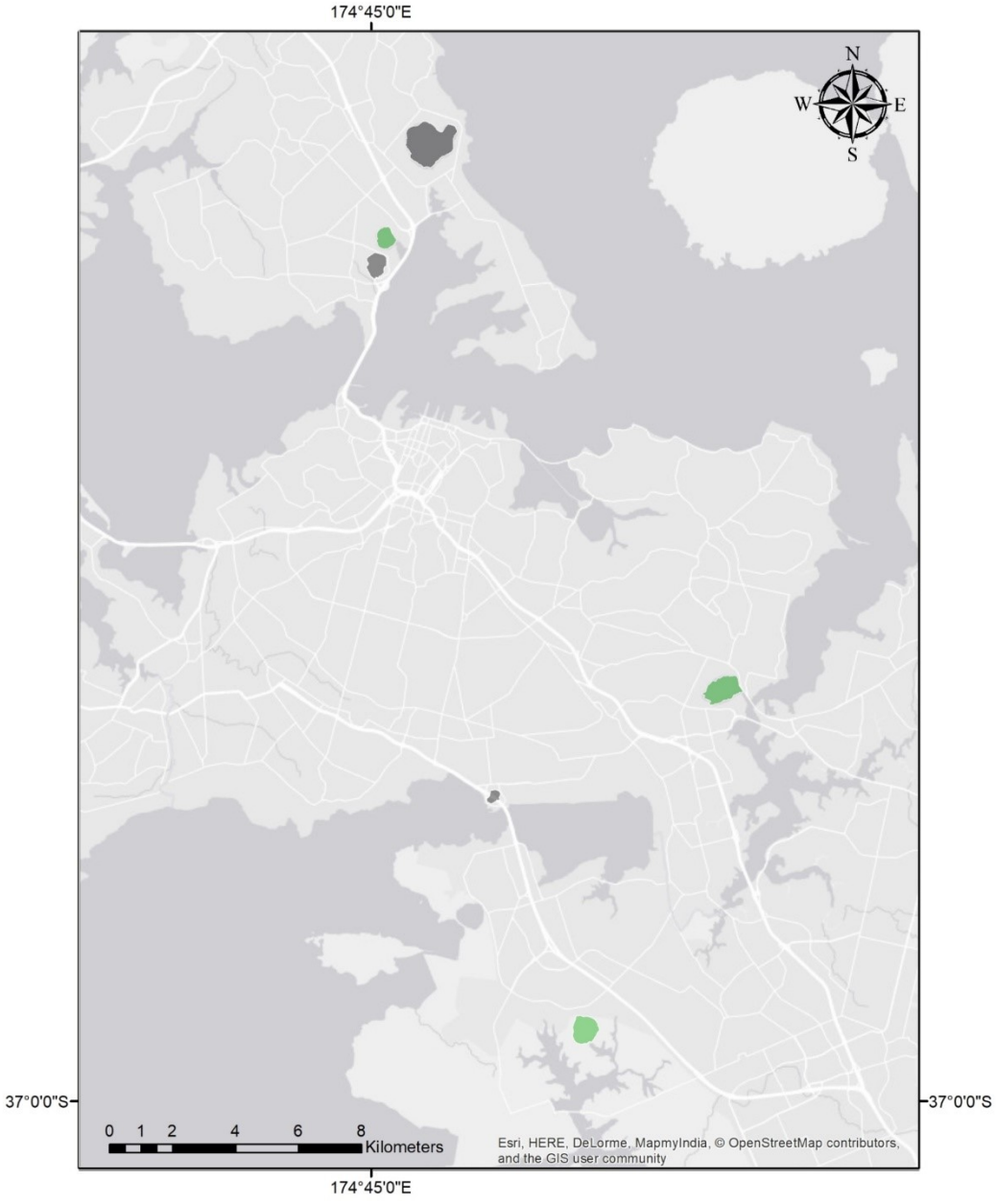

Auckland Volcanic Field (New Zealand) – Shows maars with similar primary orientations as faulting and nearest neighbor modes. The green maars fall within 10^{o} of faulting modes.

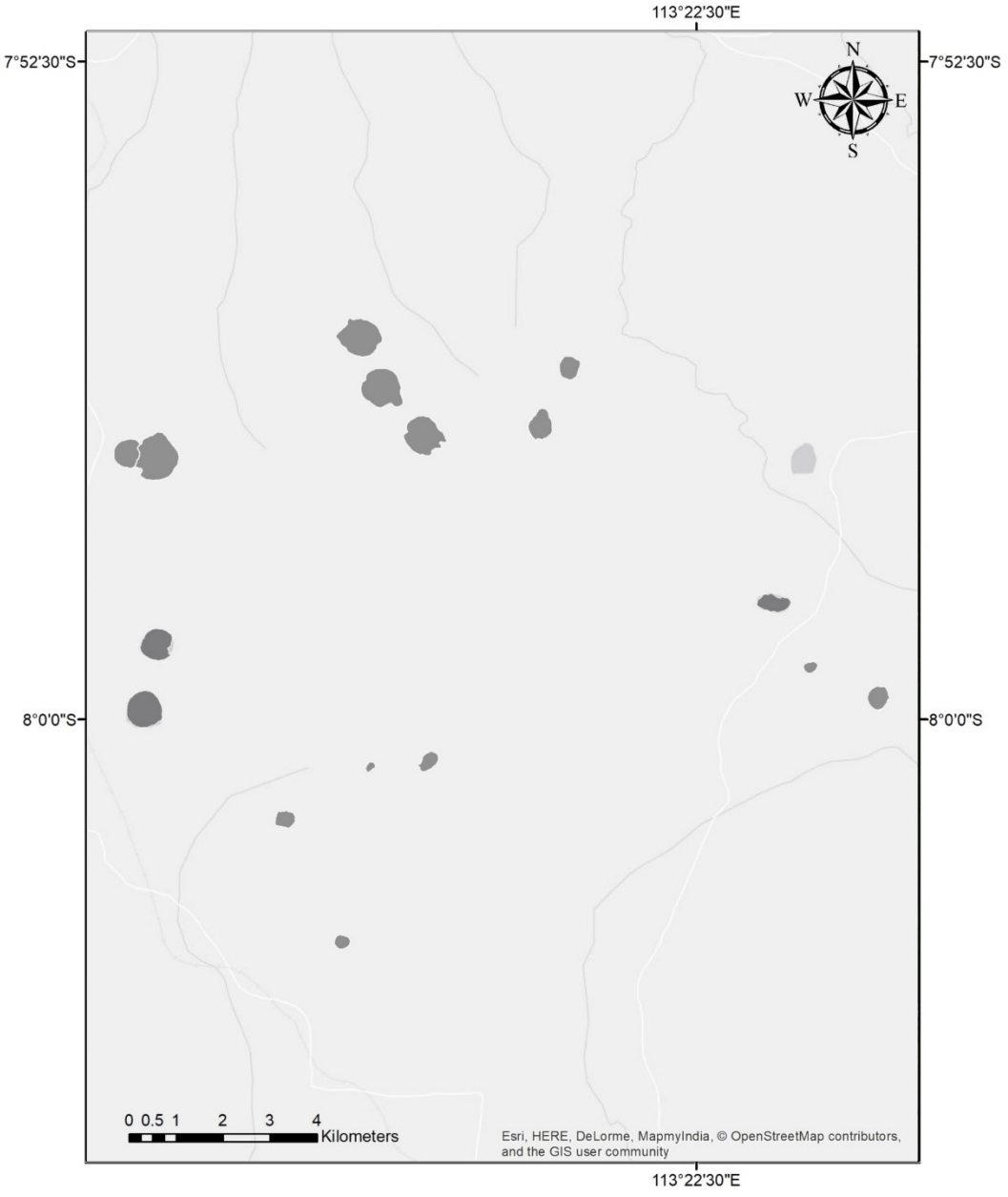

Lamongan Volcanic Field (Indonesia) – Shows all maars digitized for use in the field.

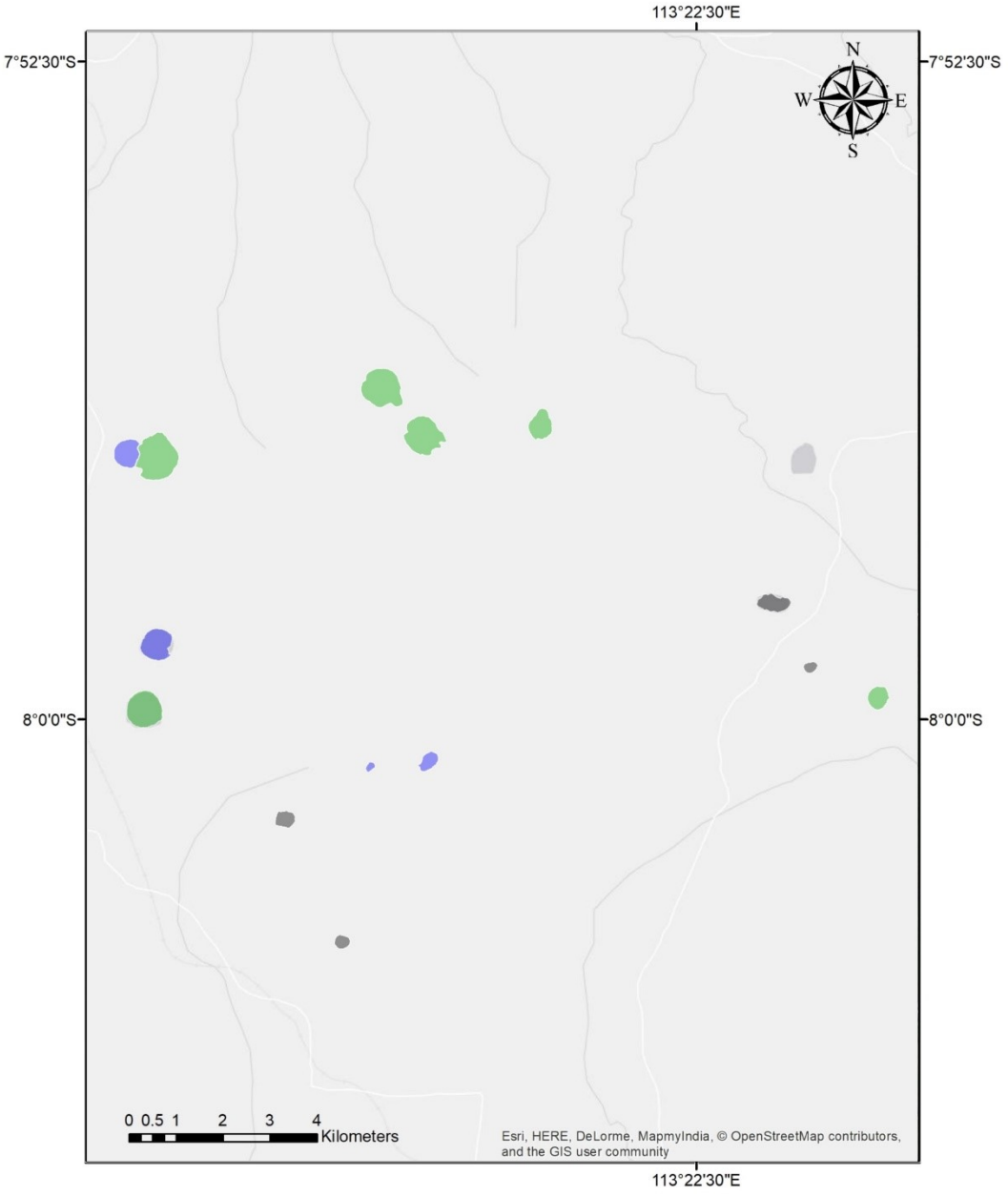

Lamongan Volcanic Field (Indonesia) – Shows maars used for calculating primary orientation. Green maars fall within Mode P_A, blue maars fall within Mode P_B.

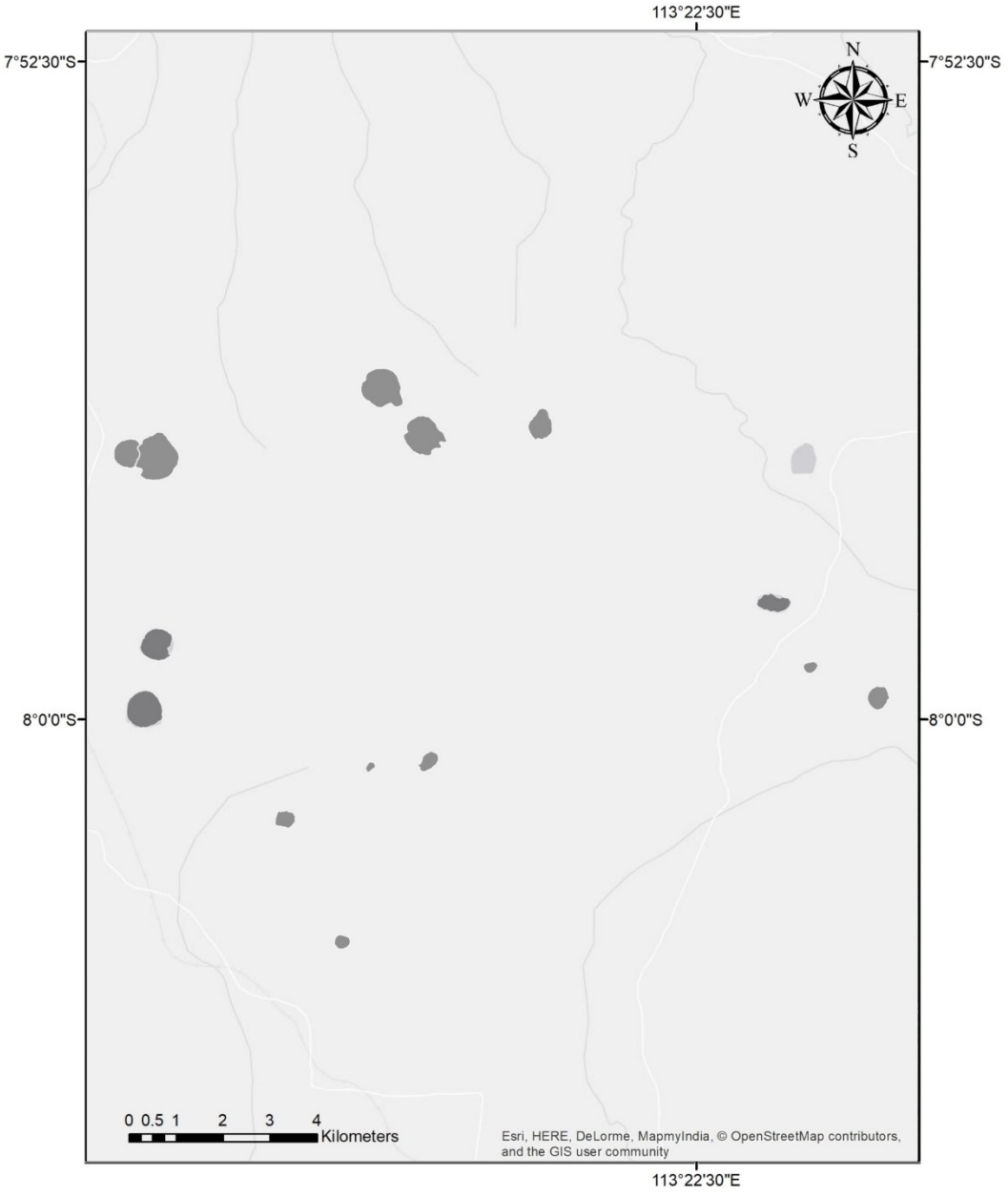

Lamongan Volcanic Field (Indonesia) – Highlighted maars both fall within primary orientation modes and exhibit primary orientations that fall within 10^{o} of faulting and nearest neighbor modes.

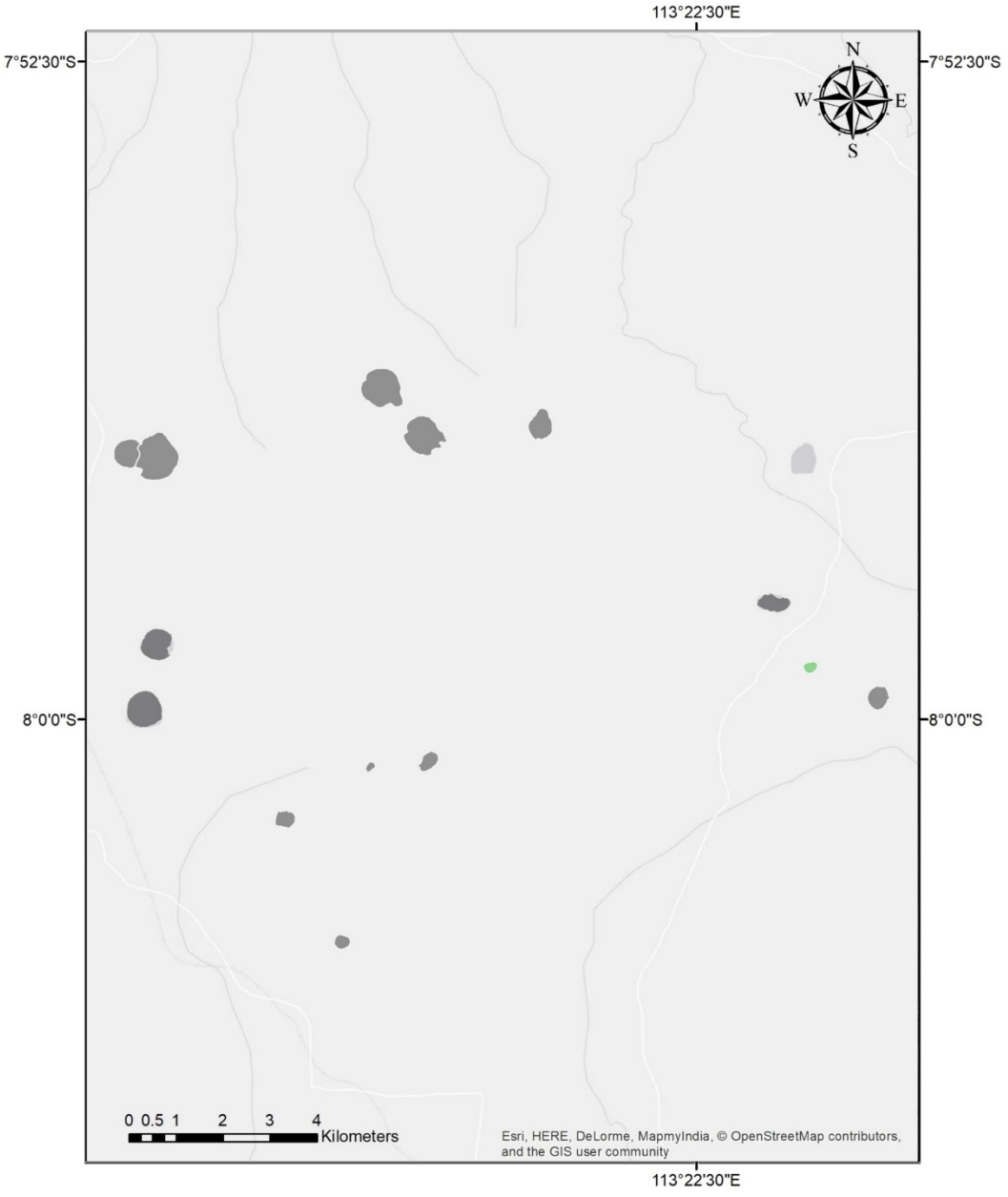

Lamongan Volcanic Field (Indonesia) – Highlighted maars exhibit primary orientations that fall within 10^{o} of faulting and nearest neighbor modes. The green maars fall within 10^{o} of faulting modes.

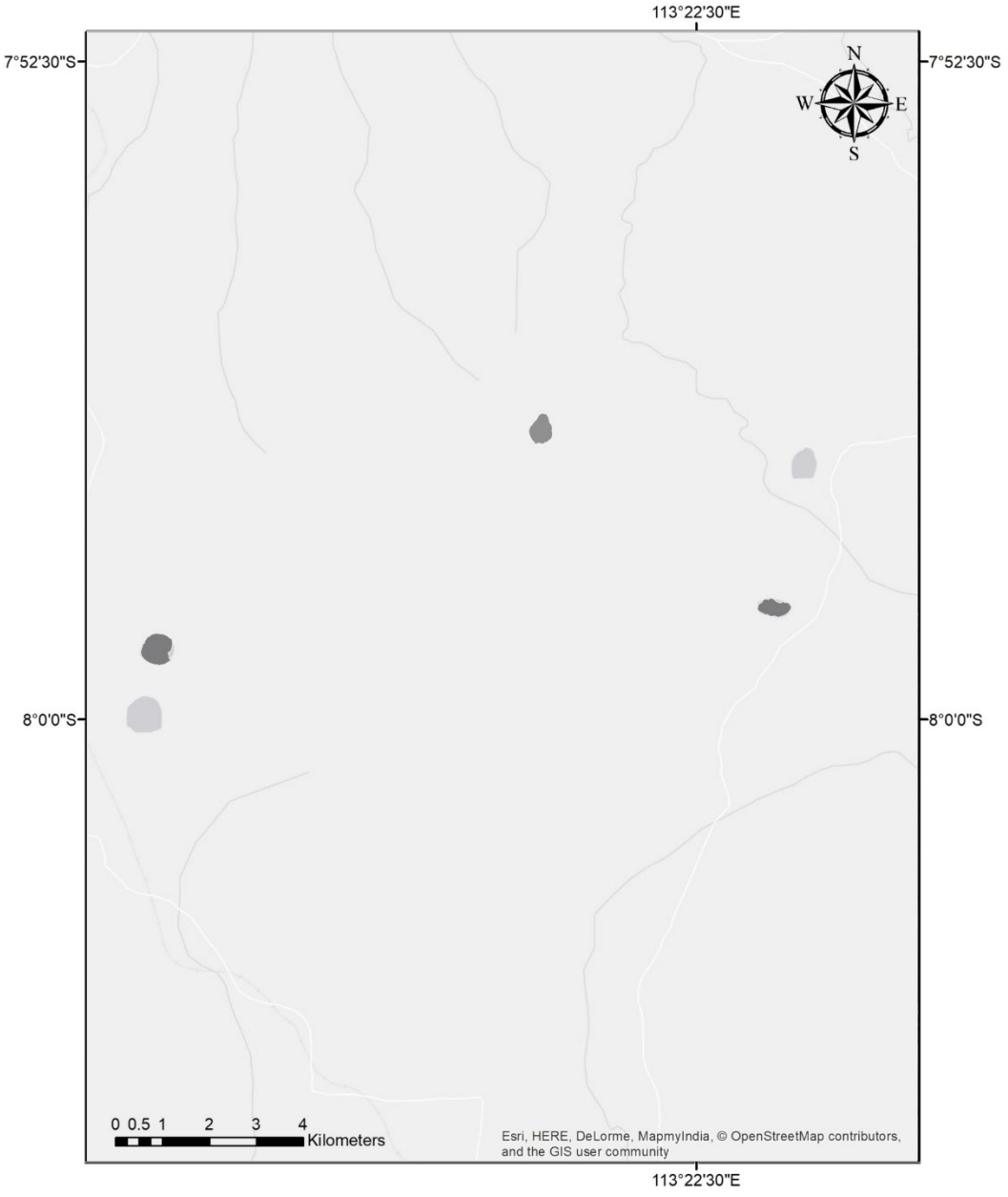

Lamongan Volcanic Field (Indonesia) – Shows maars which exhibit secondary orientations.

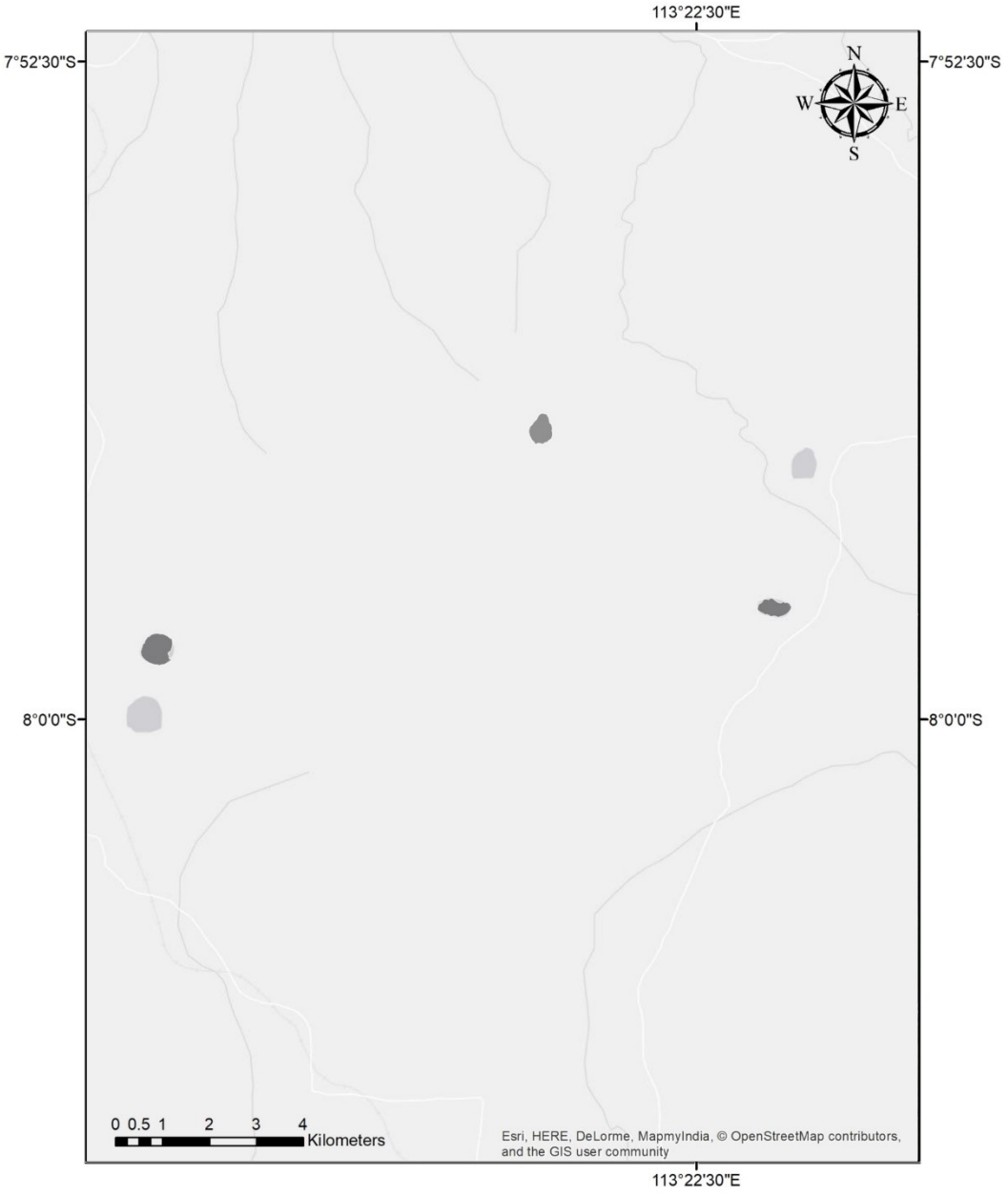

Lamongan Volcanic Field (Indonesia) – Highlighted maars are both a part of secondary orientation modes and fall within 10^{o} of faulting and nearest neighbor modes.

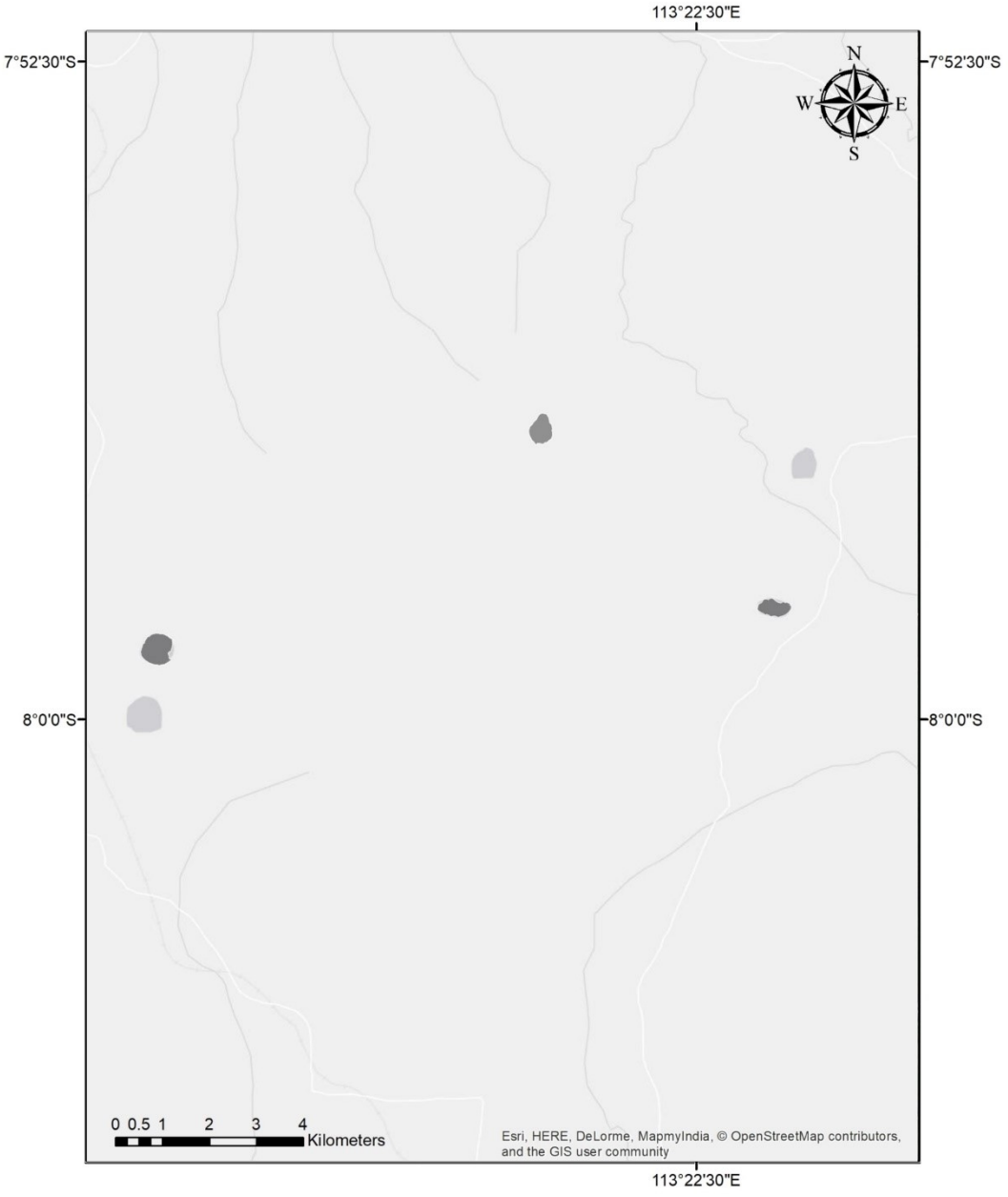

Lamongan Volcanic Field (Indonesia) – Highlighted maars make up secondary orientation modes.

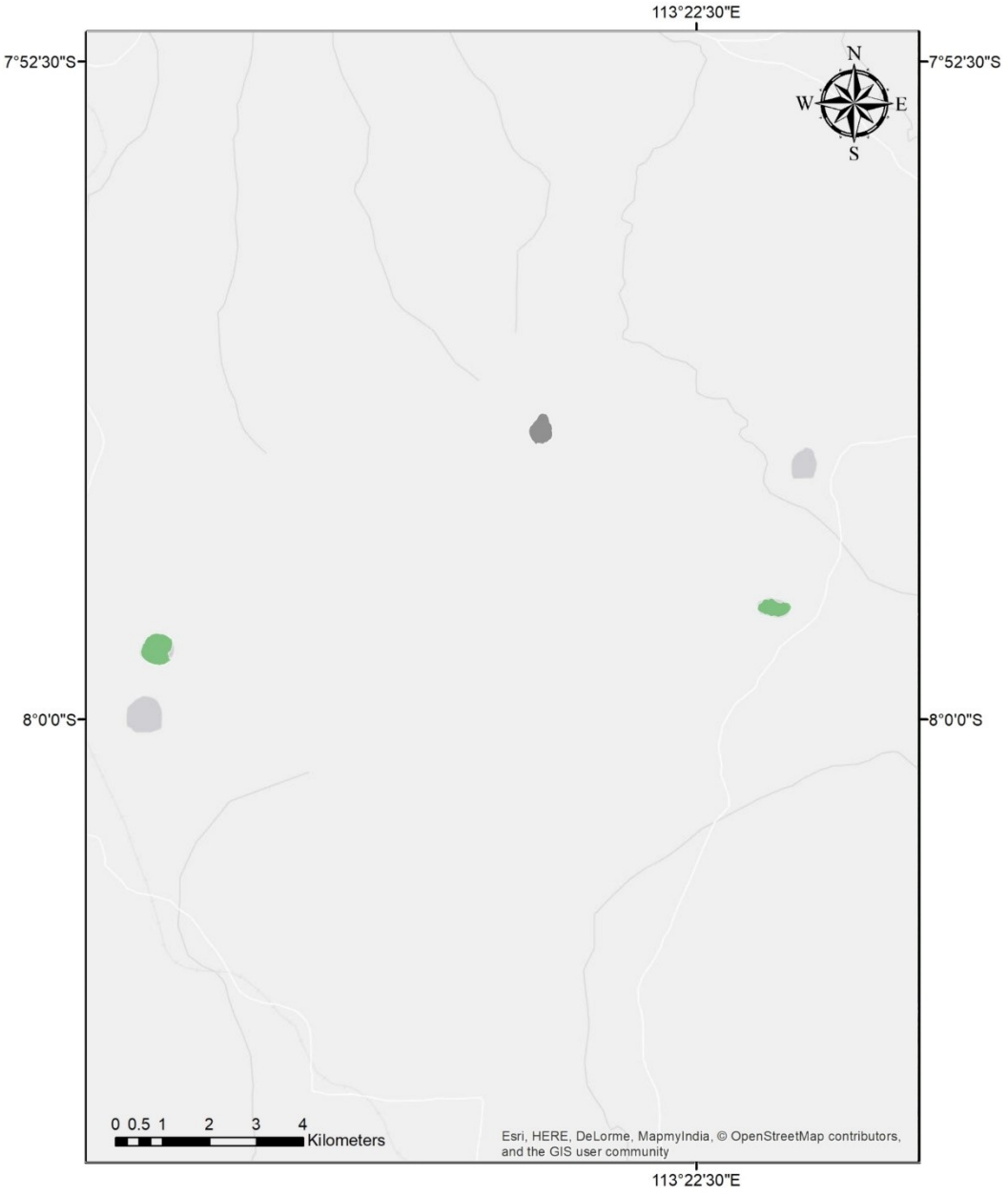

Lamongan Volcanic Field (Indonesia) – Highlighted maars exhibit secondary orientations that fall within 10^{o} of faulting and nearest neighbor modes. The green maars have orientations that fall within faulting modes.

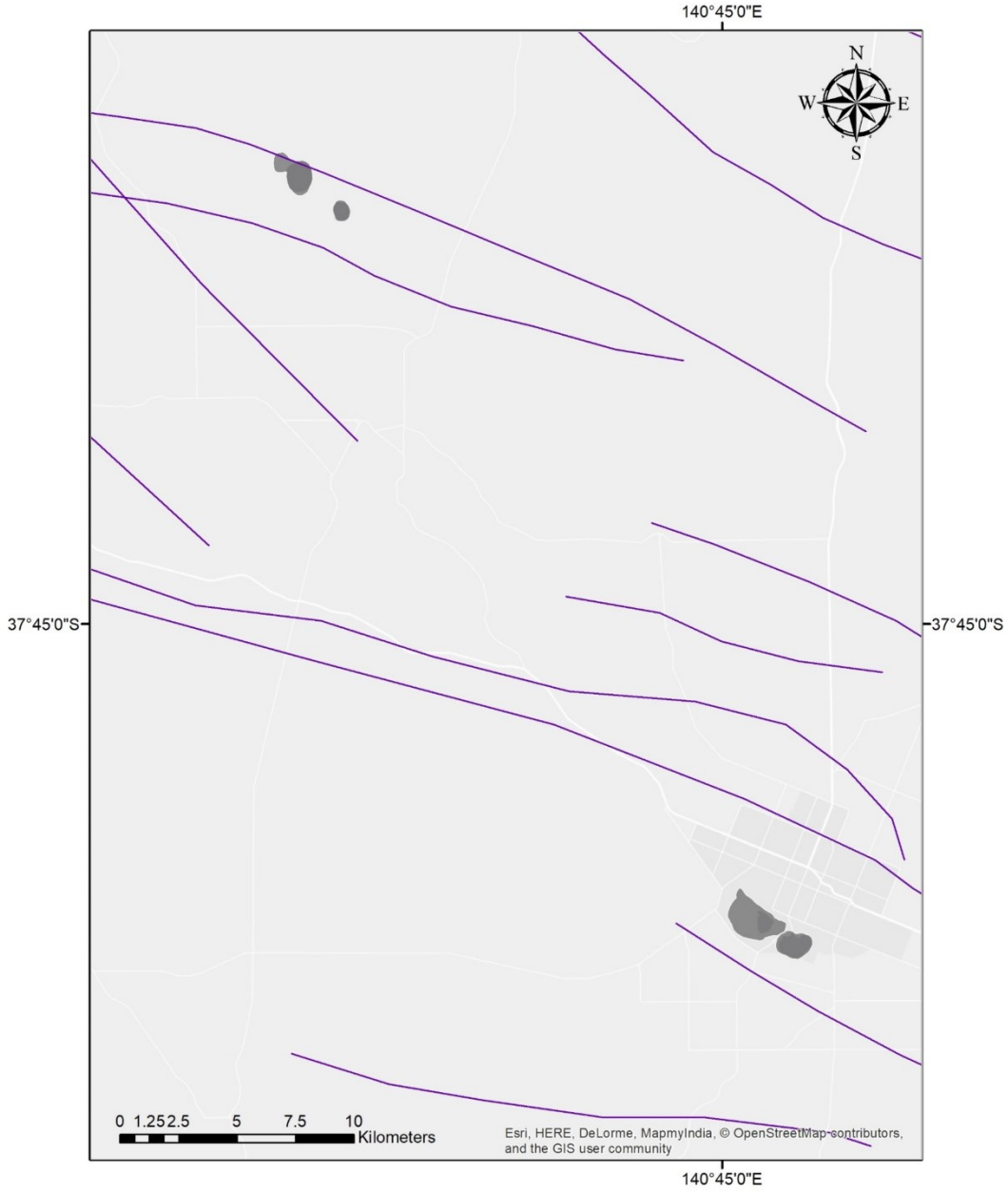

Newer Volcanic Province (Australia) (Left) – Shows faulting lineaments digitized for the field.

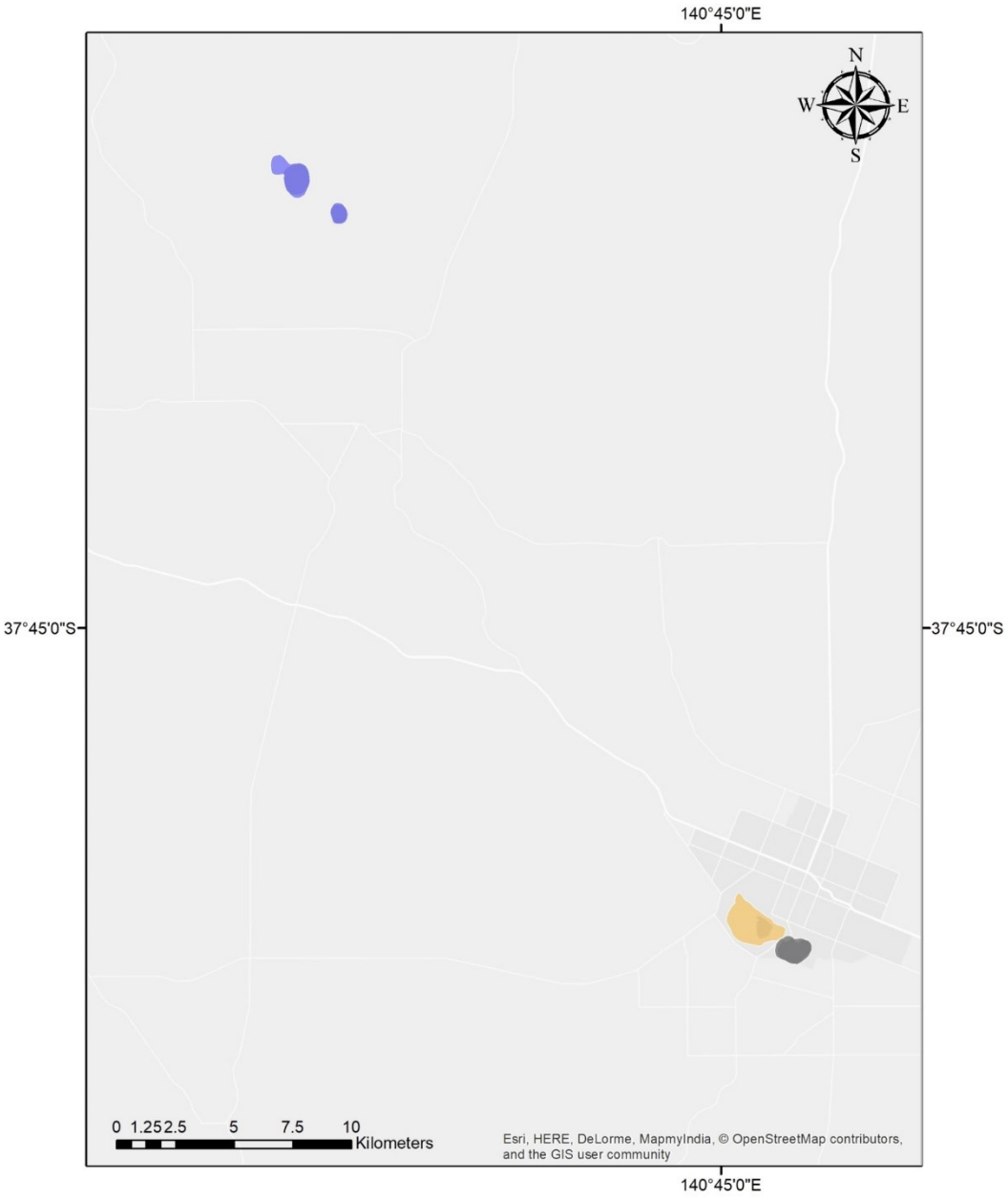

Newer Volcanic Province (Australia) (Left) – Shows maars used for calculating primary orientation modes. Highlighted maars fall within primary orientation modes. Blue maars fall within primary orientation mode P_B, yellow maars fall within primary orientation mode P_C.

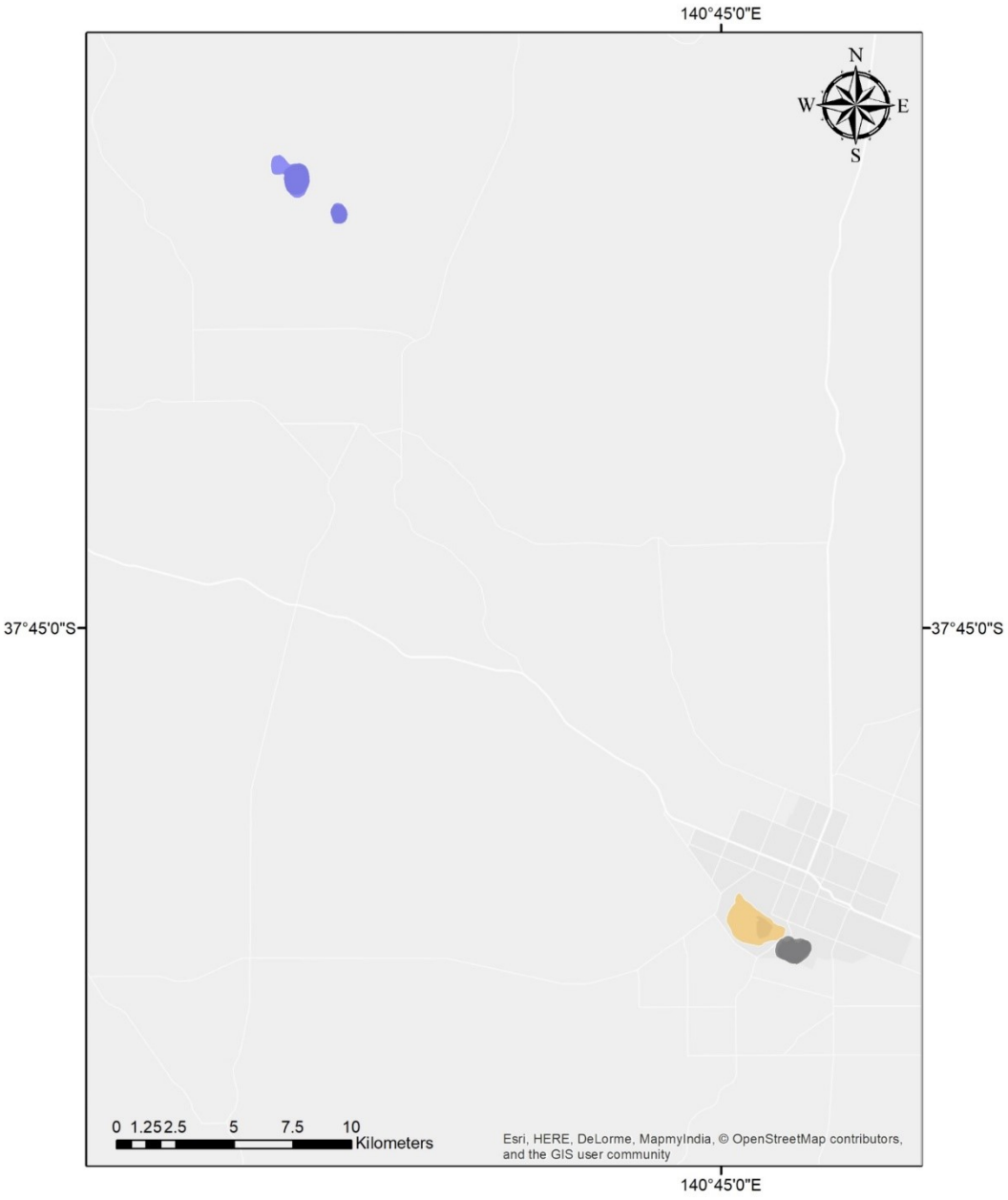

Newer Volcanic Provence (Australia) (Left) – Highlighted maars both fall within primary orientation modes and exhibit similar primary orientations as faulting and nearest neighbor modes. Blue maars fall within primary orientation mode P_B, yellow maars fall within primary orientation mode P_C.

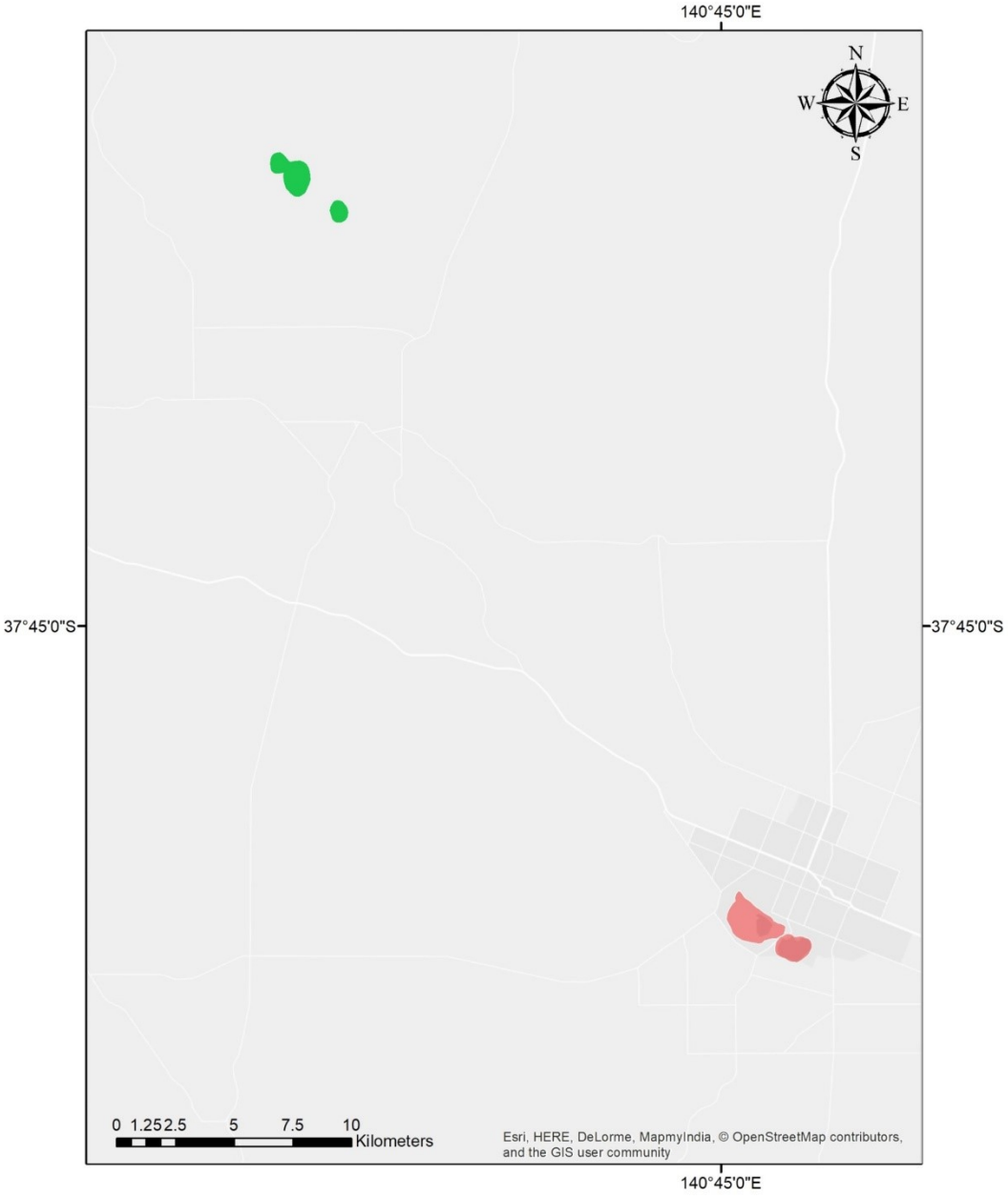

Newer Volcanic Province (Australia) (Left) – Shows maars with primary orientations similar to faulting and nearest neighbor modes. Highlighted maars' primary orientations fall within 10^{o} of faulting and nearest neighbor modes. Green maars fall within faulting modes while red maars fall within nearest neighbor and faulting modes.

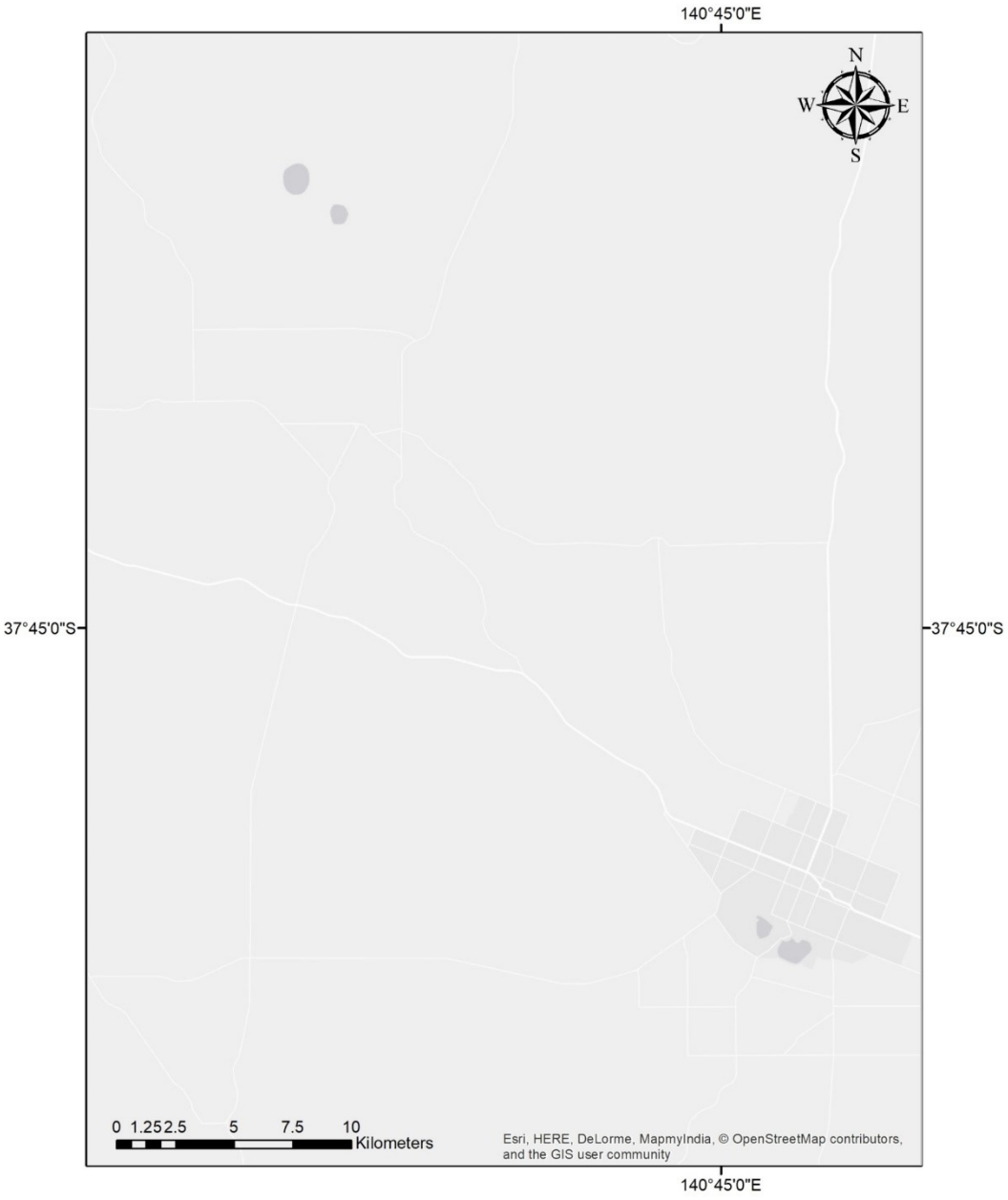

Newer Volcanic Province (Australia) (Left) – Dark grey maars were found to exhibit secondary orientations.

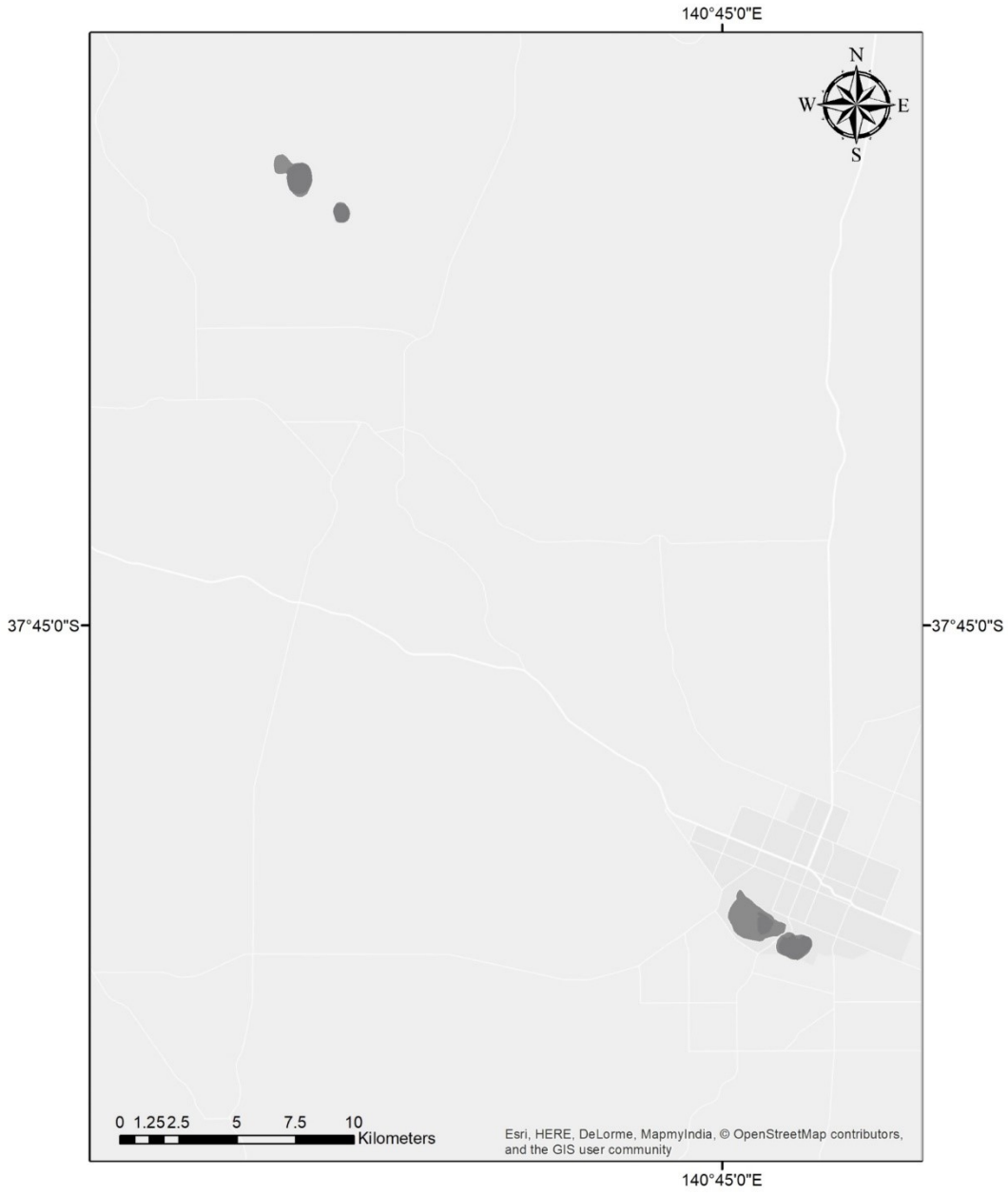

Newer Volcanic Province (Australia) (Left) – Dark grey maars represent maars digitized for use in the field.

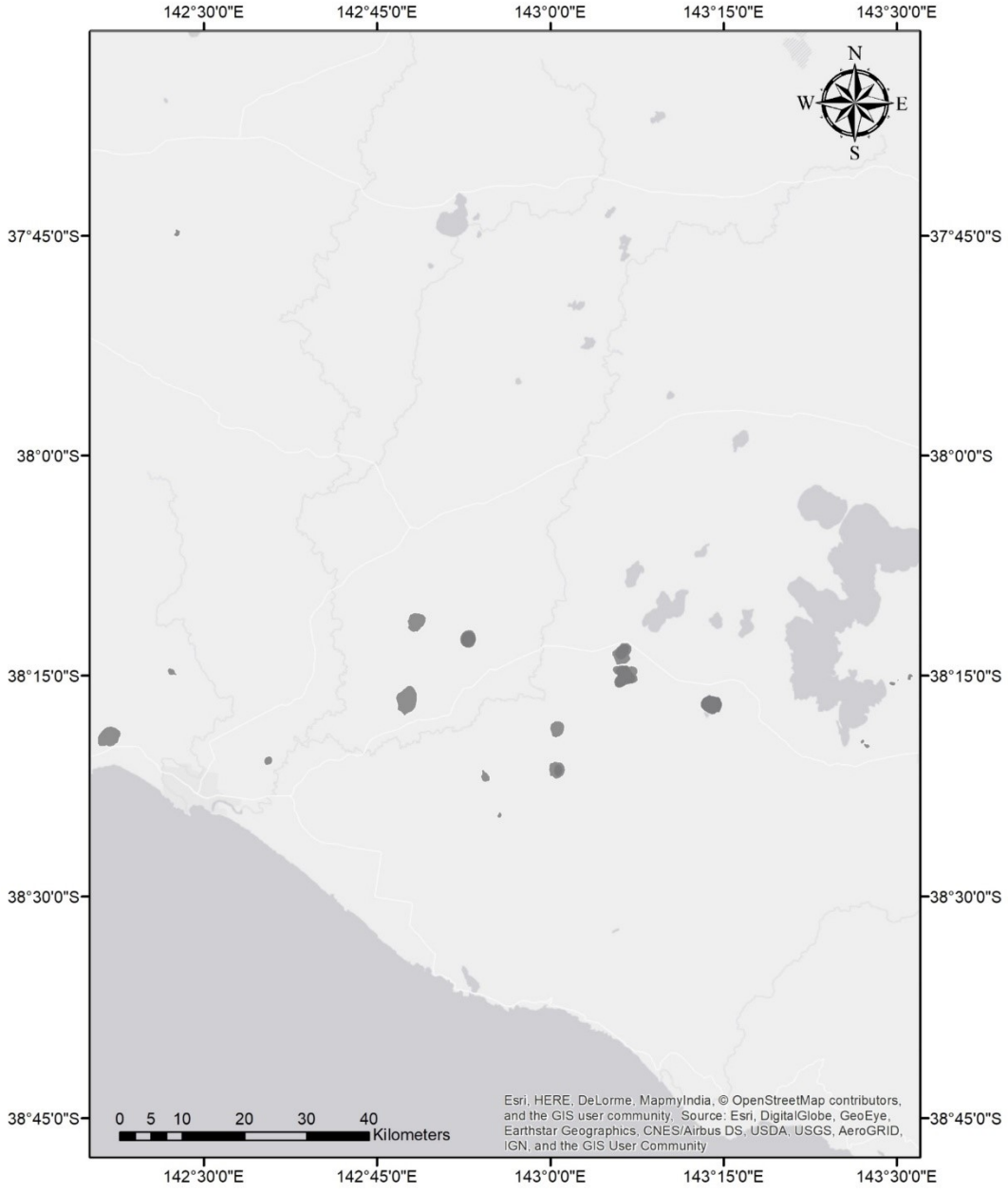

Newer Volcanic Province (Australia) (Right) – Shows all maars digitized for use in the field.

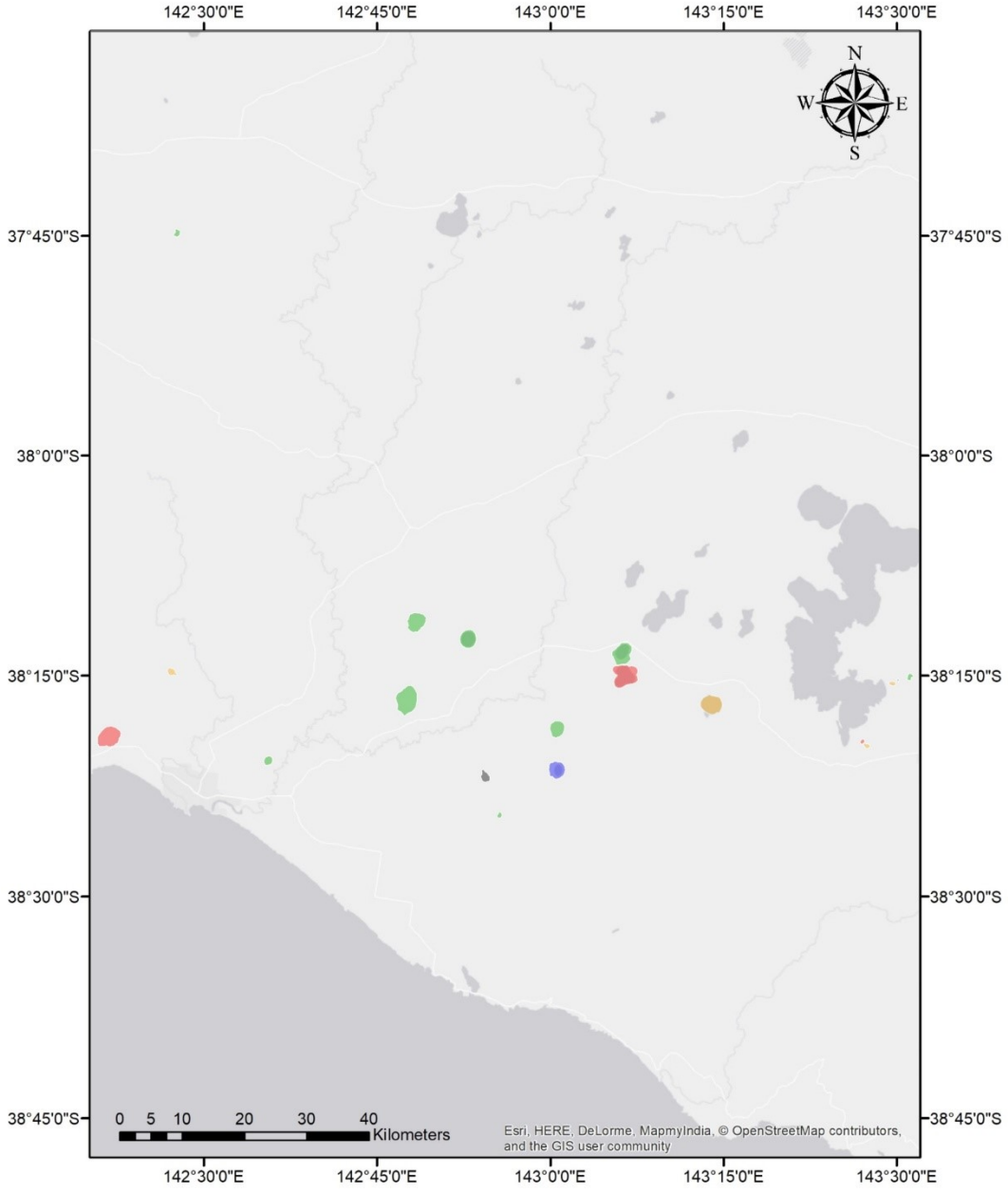

Newer Volcanic Province (Australia) (Right) – Shows all maars used for calculating primary orientation modes. Highlighted maars fall within primary orientation modes. Green maars make up P_A, blue modes P_B, yellow maars P_C, and orange maars P_D.

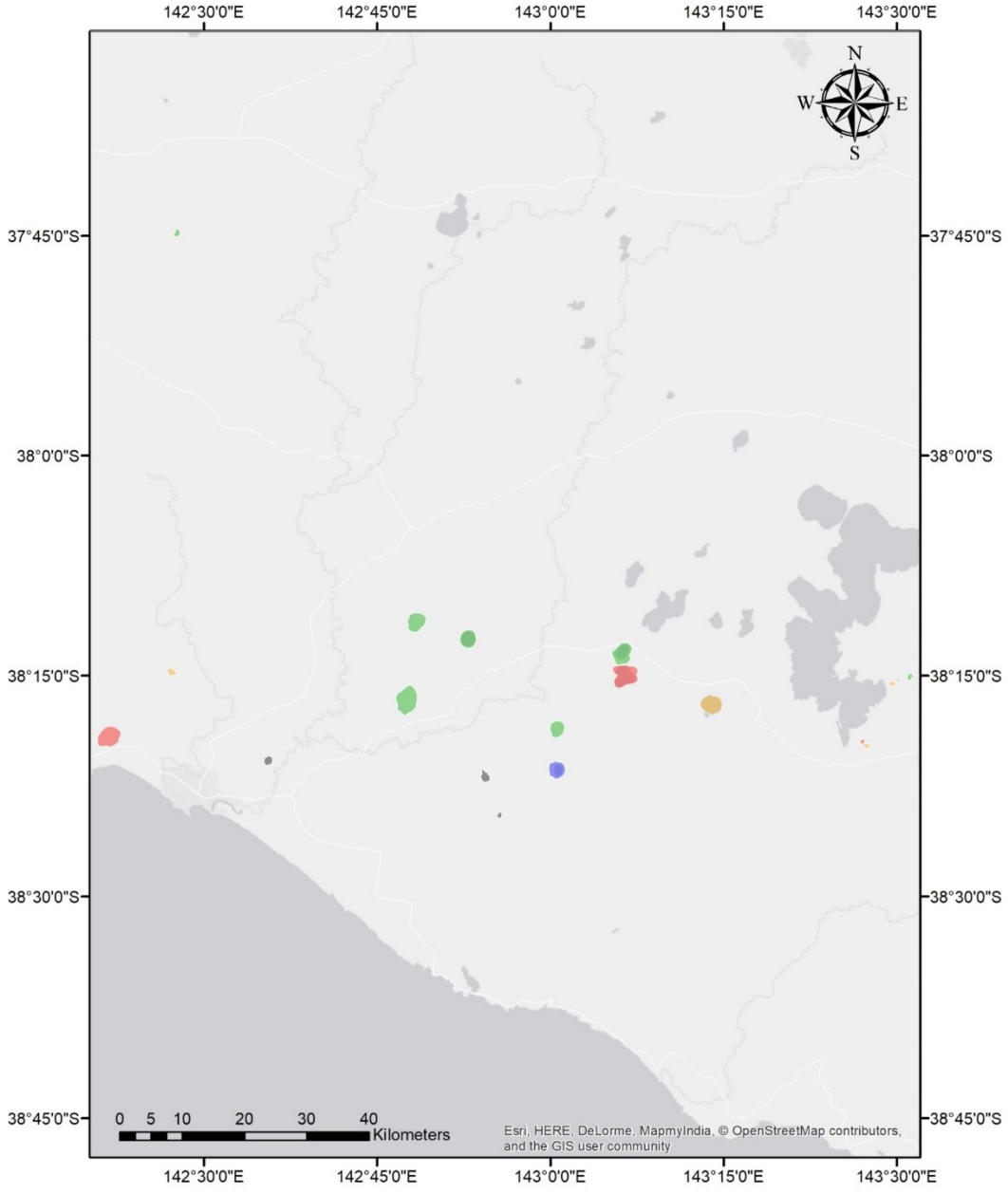

Newer Volcanic Province (Australia) (Right) – Shows maars which both make up primary orientation modes and exhibit similar primary orientations as faulting and nearest neighbor modes. Green maars make up P_A, blue modes P_B, yellow maars P_C, and orange maars P_D.

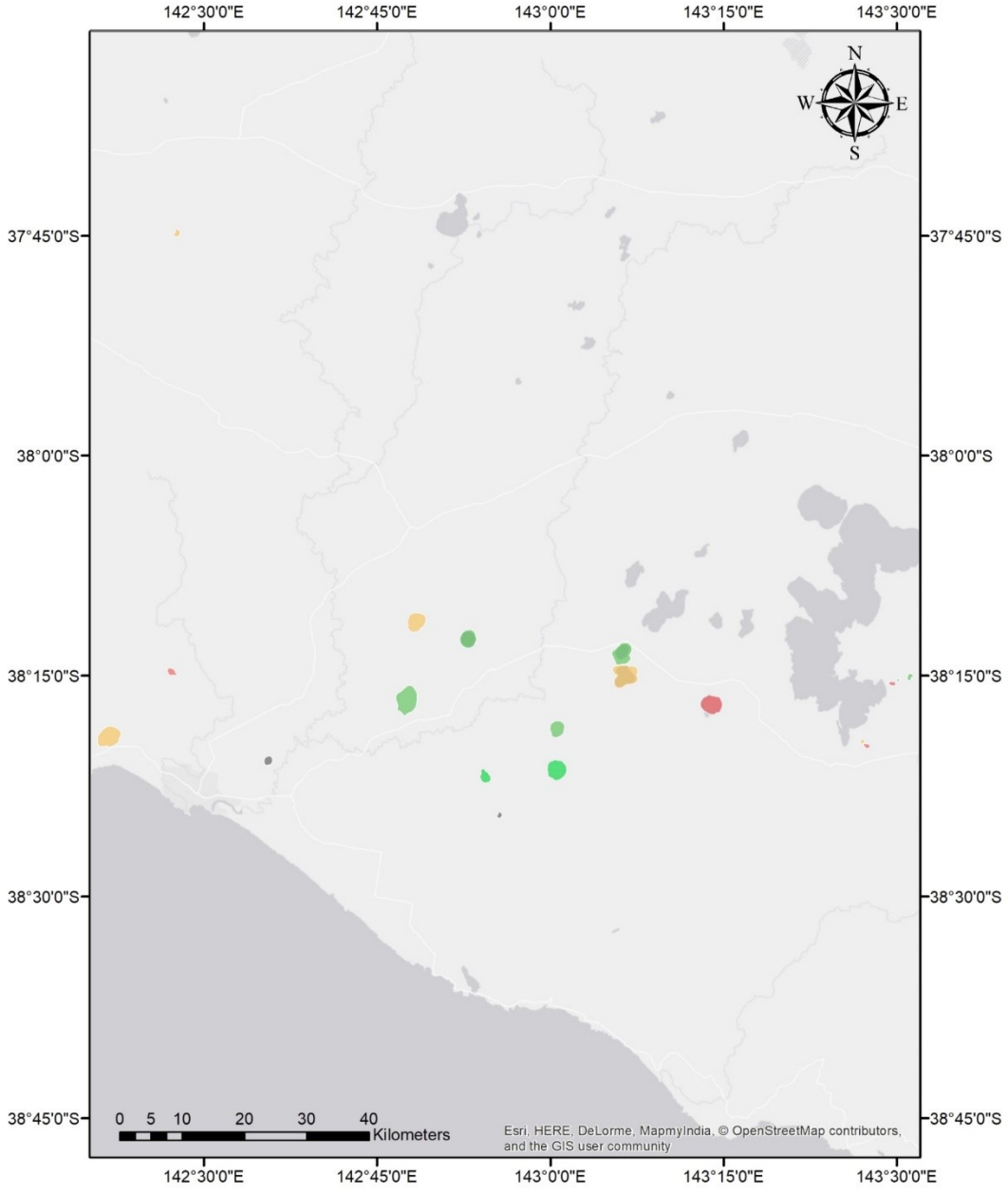

Newer Volcanic Province (Australia) (Right) – Shows maars with similar primary orientations as faulting and nearest neighbor modes. Green maars fall within 10^{o} of faulting modes, Yellow within nearest neighbor modes, and red maars fall under both.

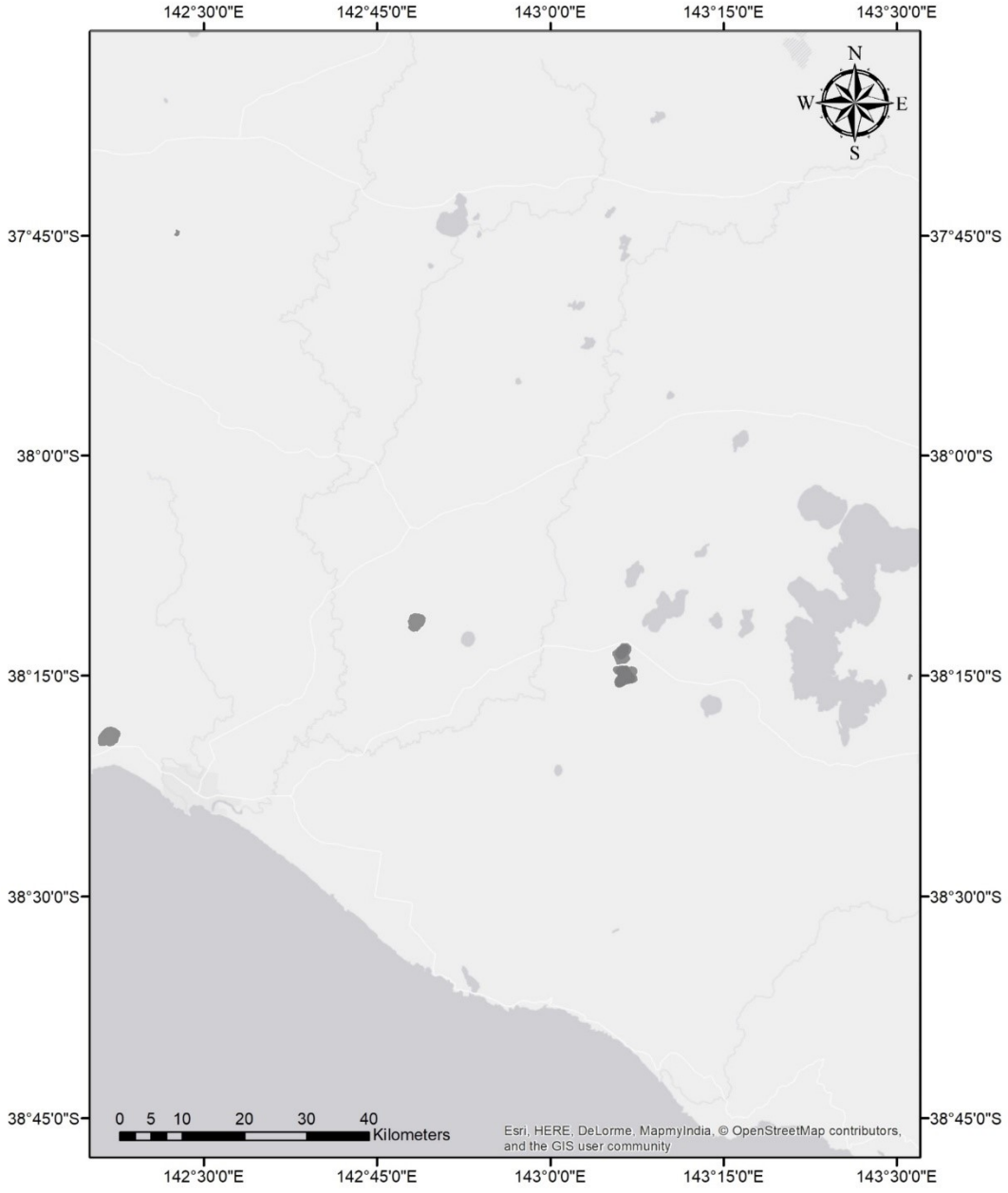

Newer Volcanic Province (Australia) (Right) – Dark grey polygons show maars which exhibit secondary orientations.

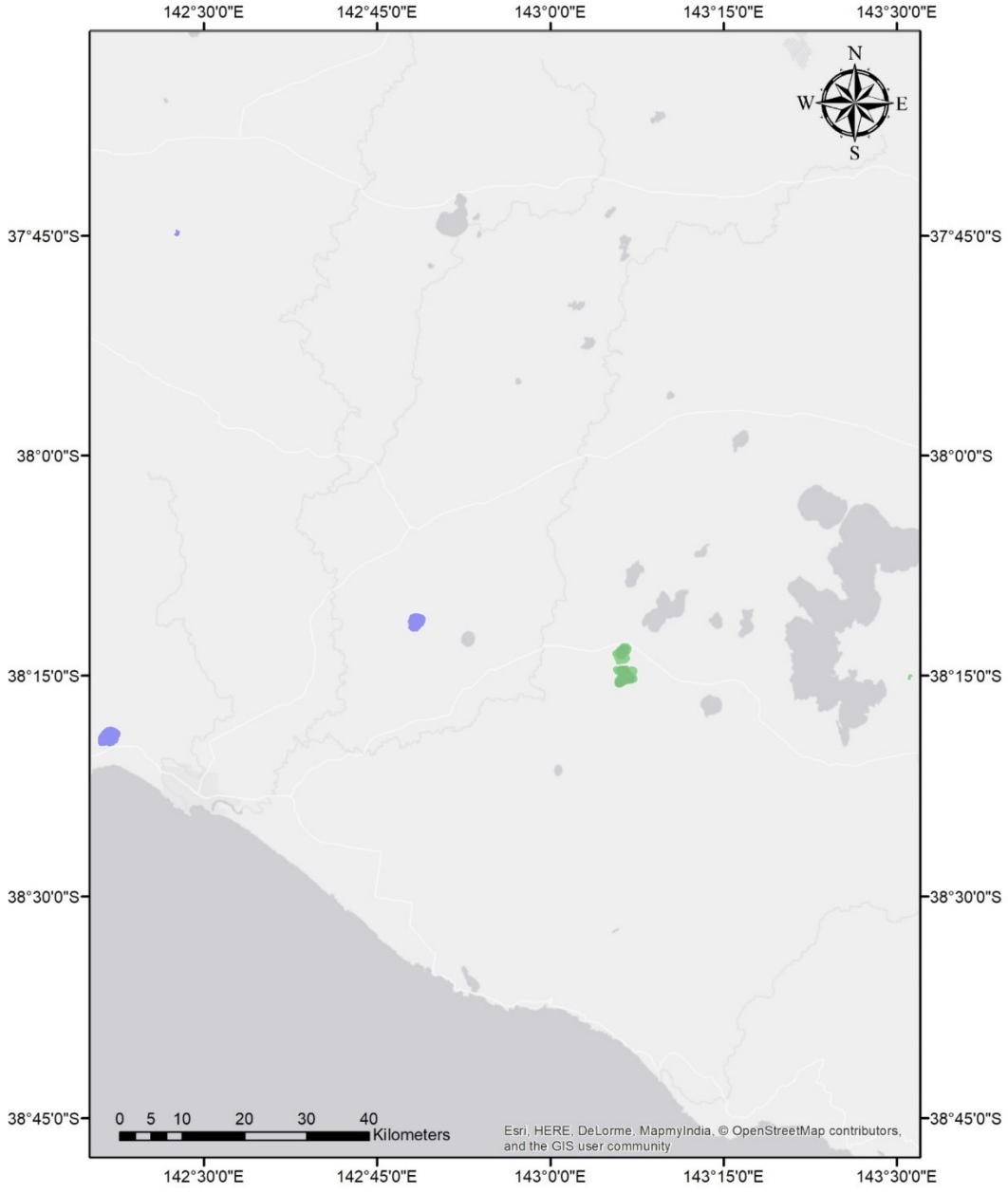

Newer Volcanic Province (Australia) (Right) – Shows maars with secondary orientations that fall within secondary orientation modes. Green maars make up Mode S_A while blue are in S_B.

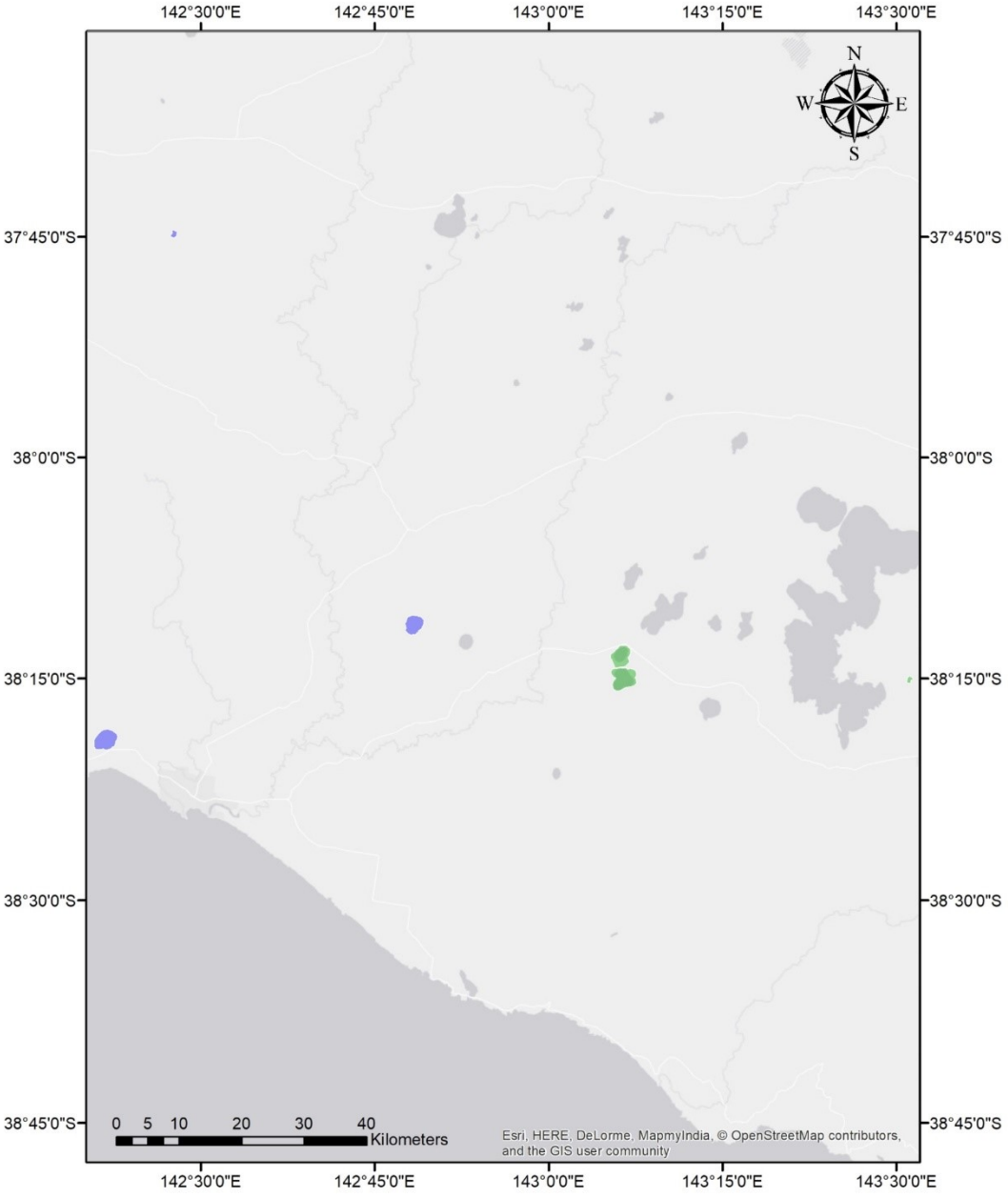

Newer Volcanic Province (Australia) (Right) – Shows maars that both fall in secondary orientation modes and share similar orientations as faulting and nearest neighbor modes. Green maars make up Mode S_A while blue are in S_B.

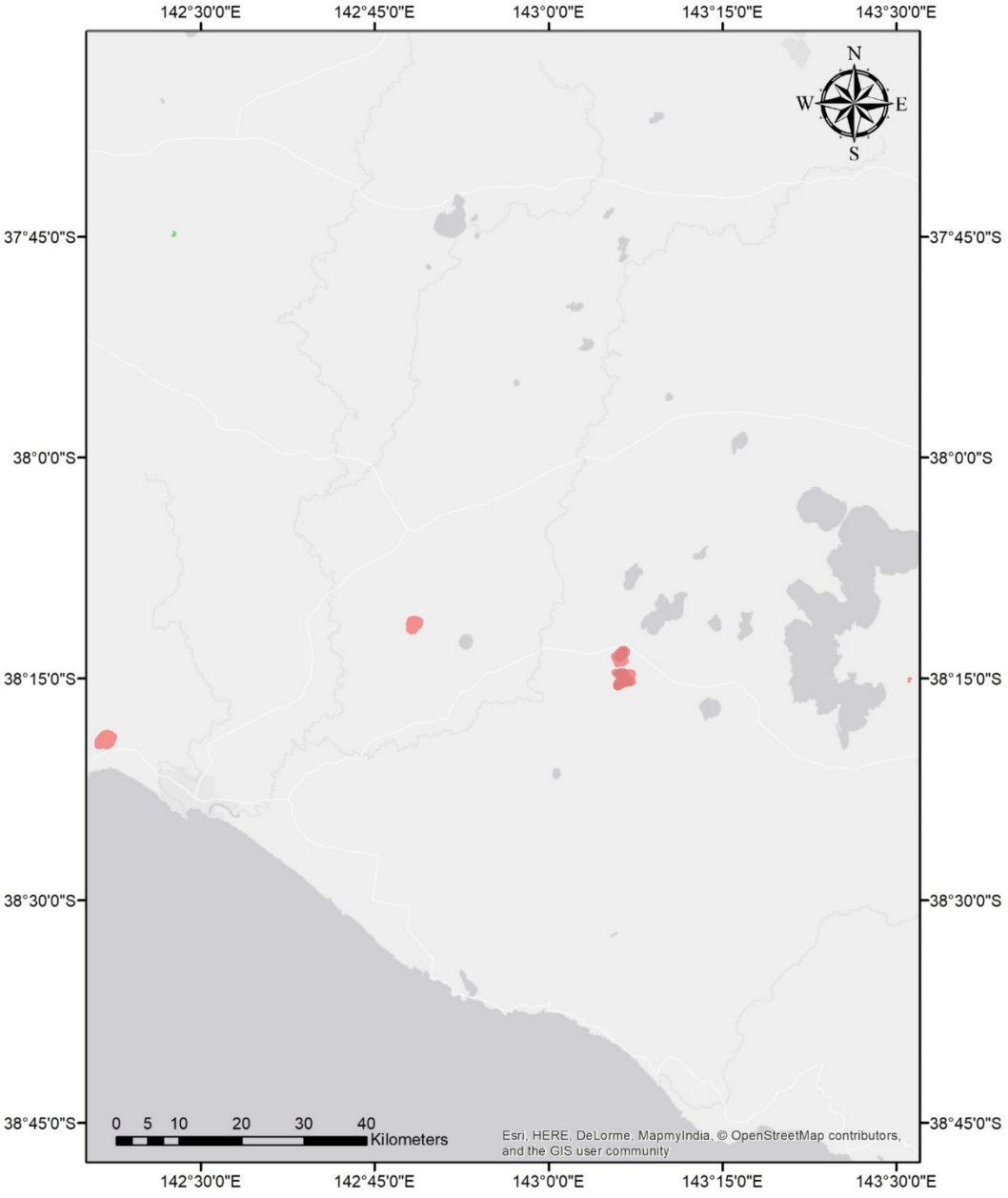

Newer Volcanic Province (Australia) (Right) – Shows maars with secondary orientations that are similar to faulting and nearest neighbor modes. Maars highlighted red exhibit secondary orientations within 10^{o} of both faulting and nearest neighbor modes. Green maars have secondary orientations similar to faulting modes.

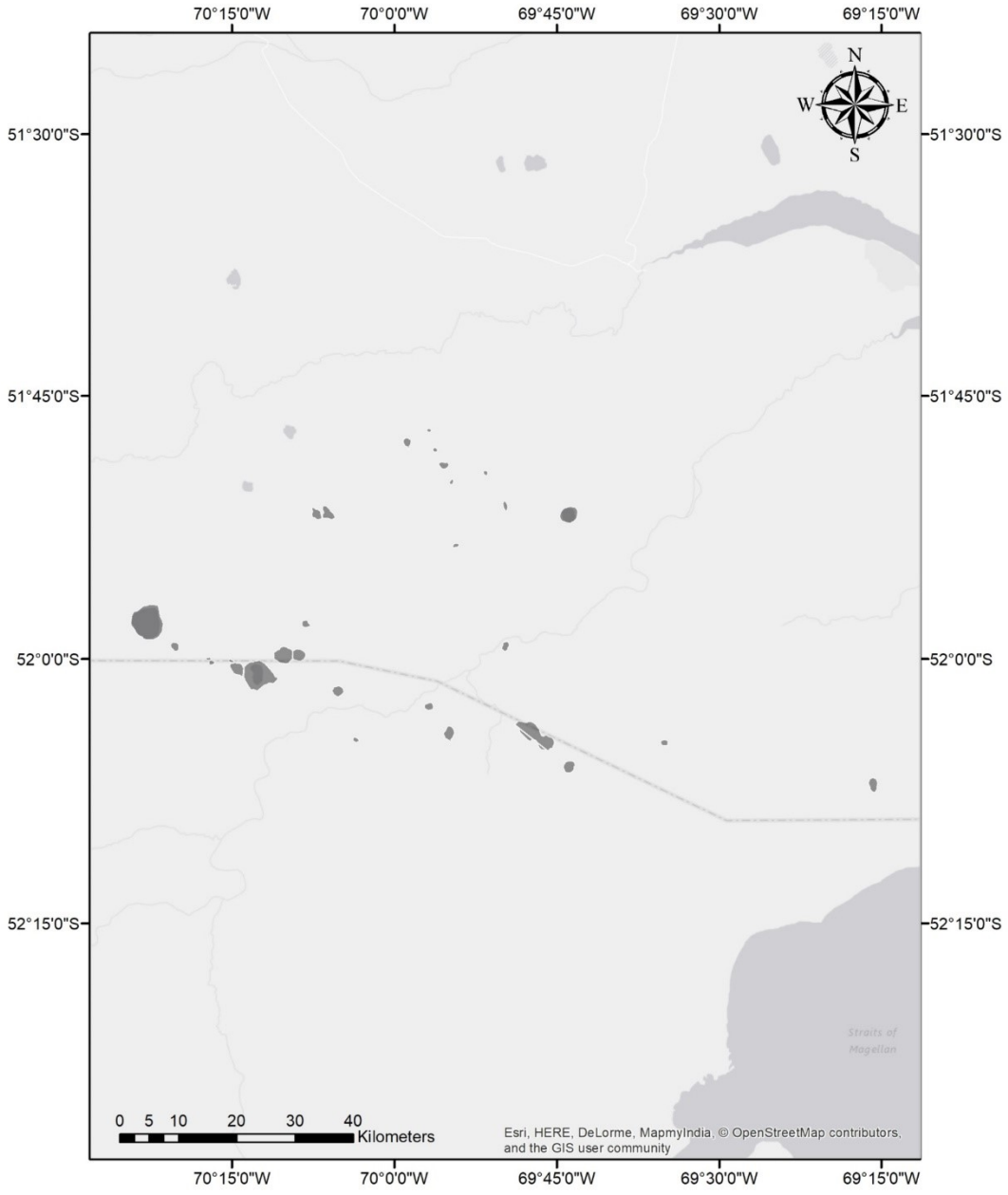

Pali Aike Volcanic Field (Argentina) – Shows all maars digitized for use in the field.

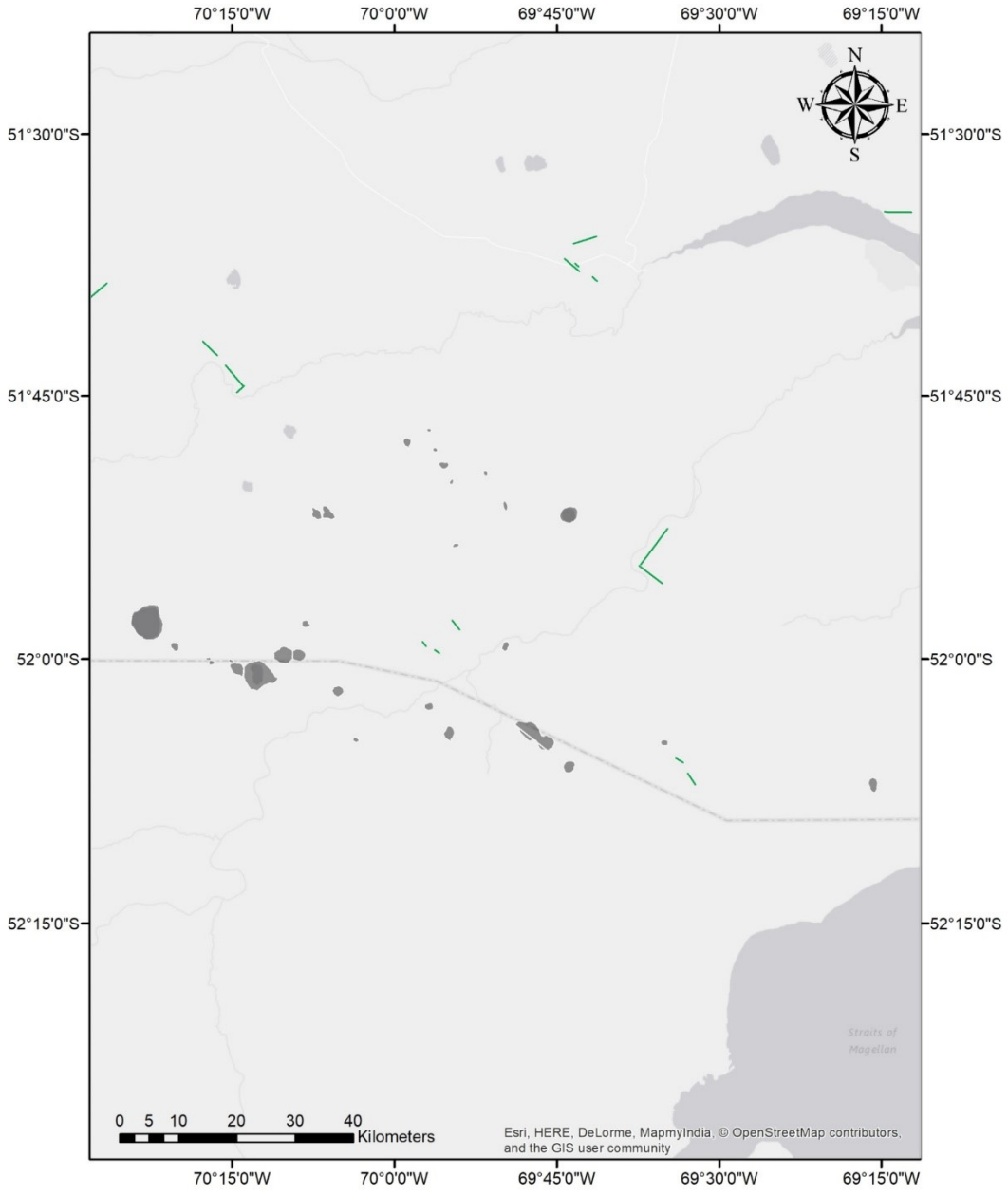

Pali Aike Volcanic Field (Argentina) – Shows faults digitized for analysis in this field.

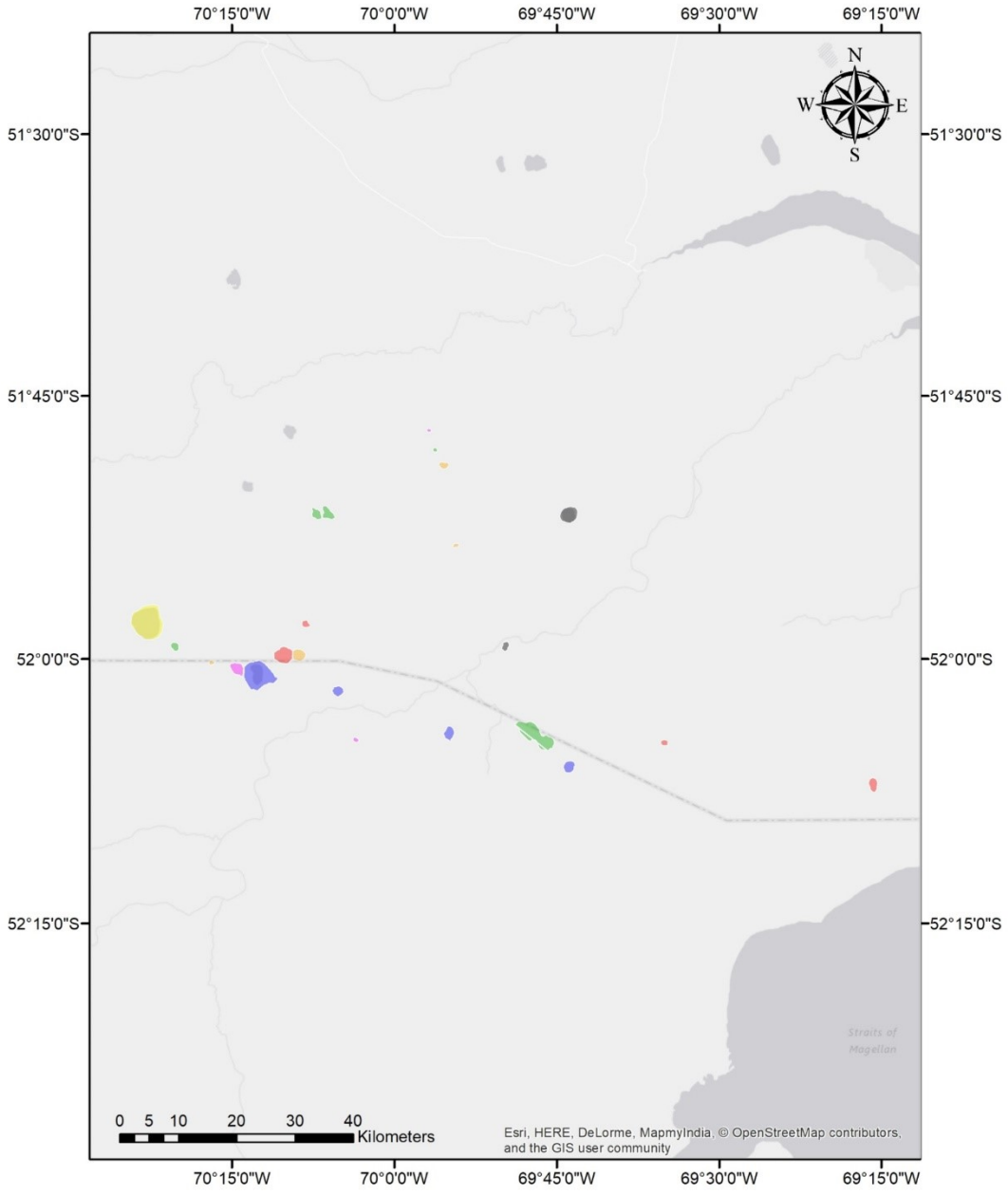

Pali Aike Volcanic Field (Argentina) – Shows maars analyzed for primary orientation modes. Highlighted maars fall within primary orientation modes. Green maars represent mode P_A, blue P_B, yellow P_C, orange P_D, and pink P_E.

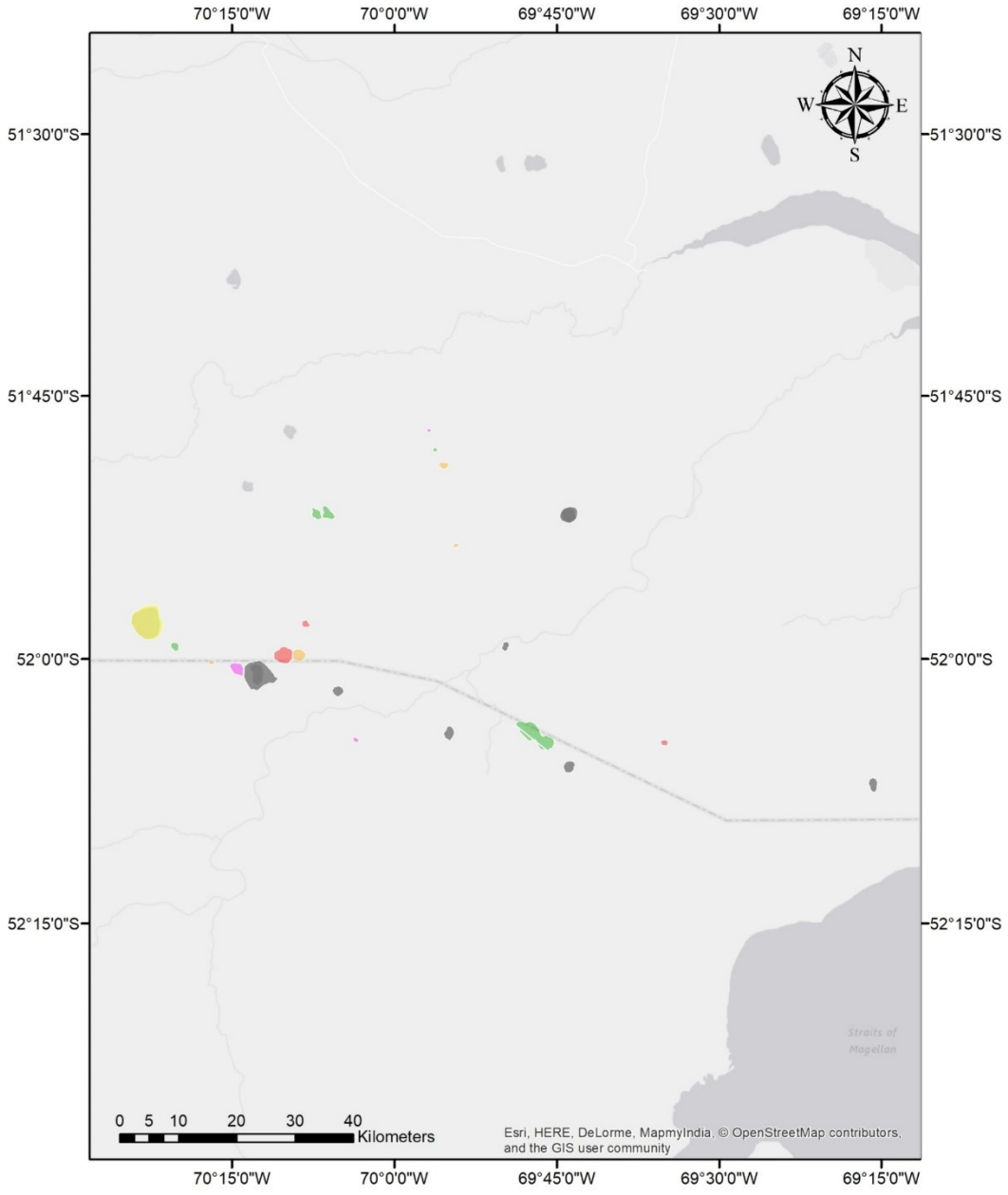

Pali Aike Volcanic Field (Argentina) – Shows maars which both fall within primary orientation modes and exhibit orientations similar to faulting and nearest neighbor modes. Green maars represent mode P_A, blue P_B, yellow P_C, orange P_D, and pink P_E.

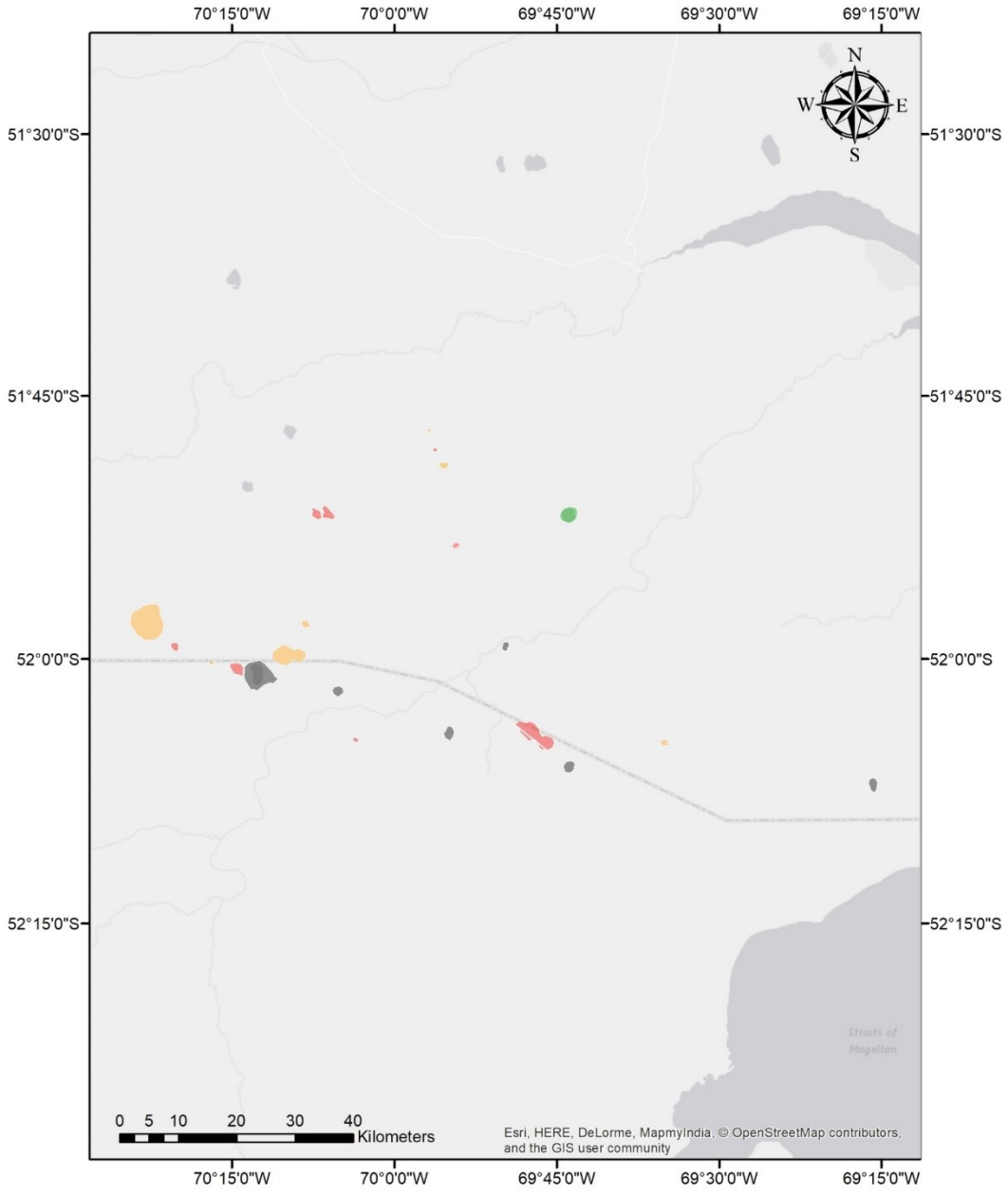

Pali Aike Volcanic Field (Argentina) – Shows maars with orientations that fall within 10^{o} of faulting and nearest neighbor modes. Green maars have orientations similar to faulting modes, yellow are similar to nearest neighbor modes, and red have similar orientations to both.

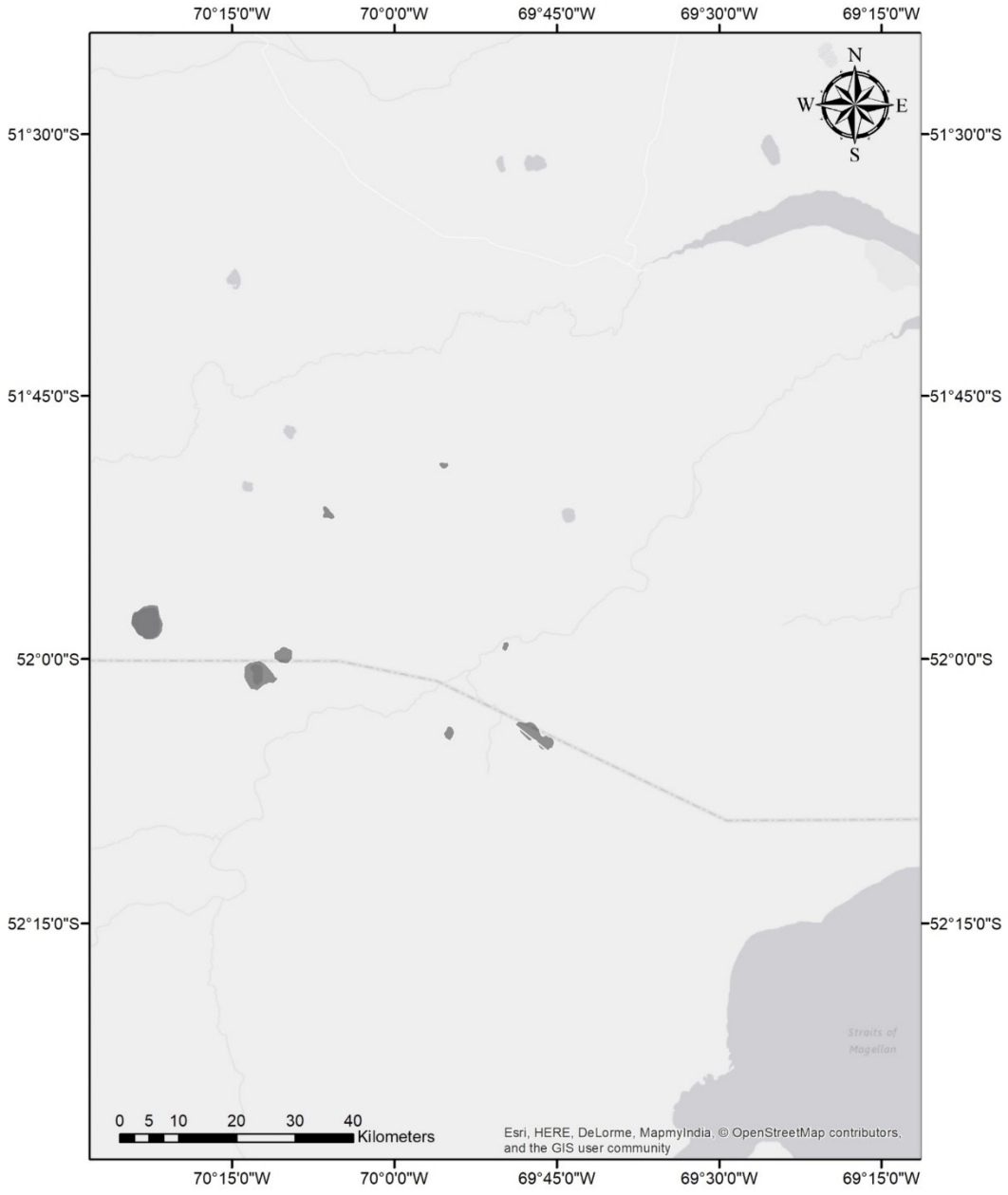

Pali Aike Volcanic Field (Argentina) – Dark gray polygons show maars which exhibit secondary orientations.

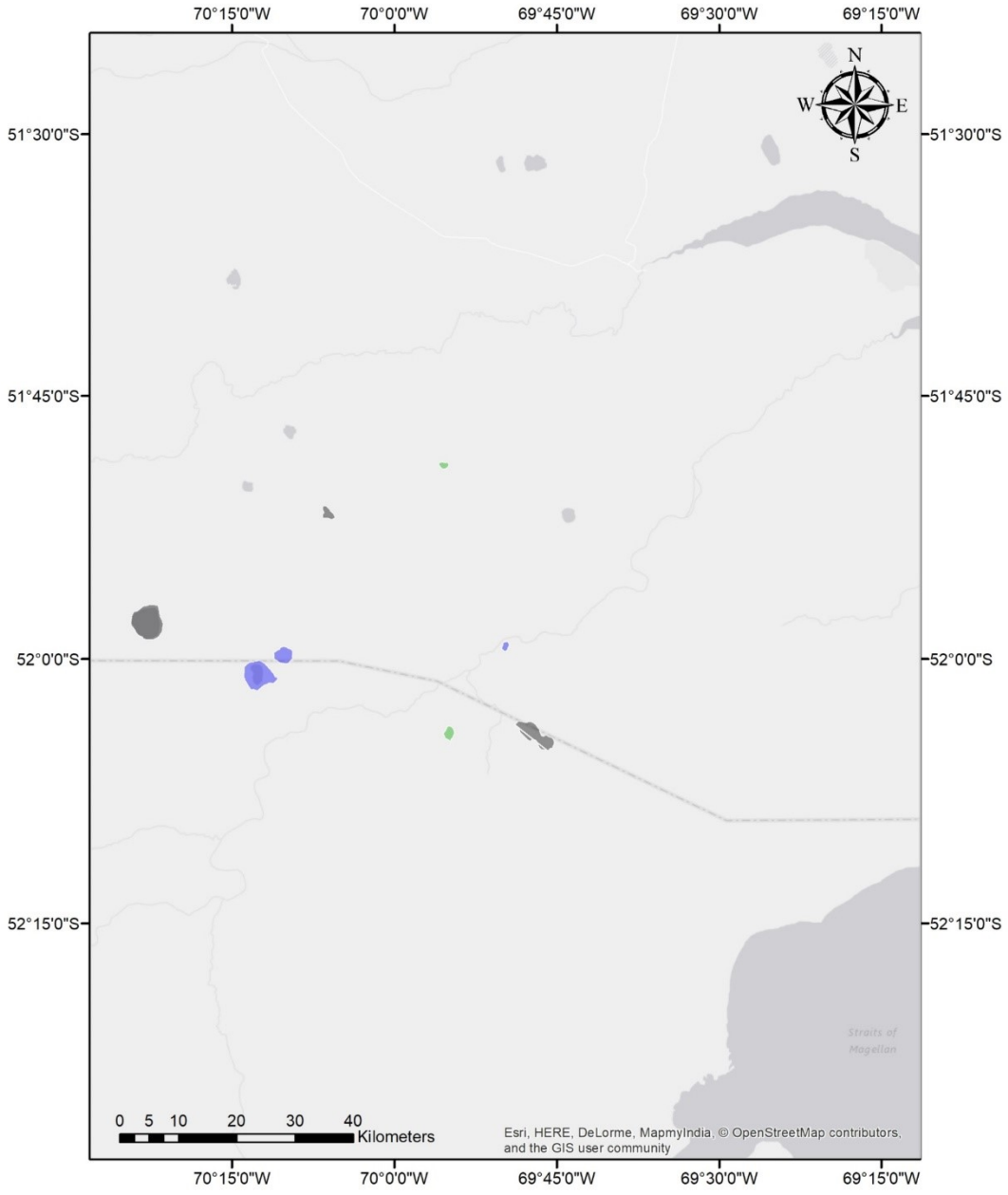

Pali Aike Volcanic Field (Argentina) – Shows maars which both fall within secondary orientation modes and exhibit similar orientations as faulting and nearest neighbor modes. Green maars fall within mode S_A, while blue maars fall in S_B.

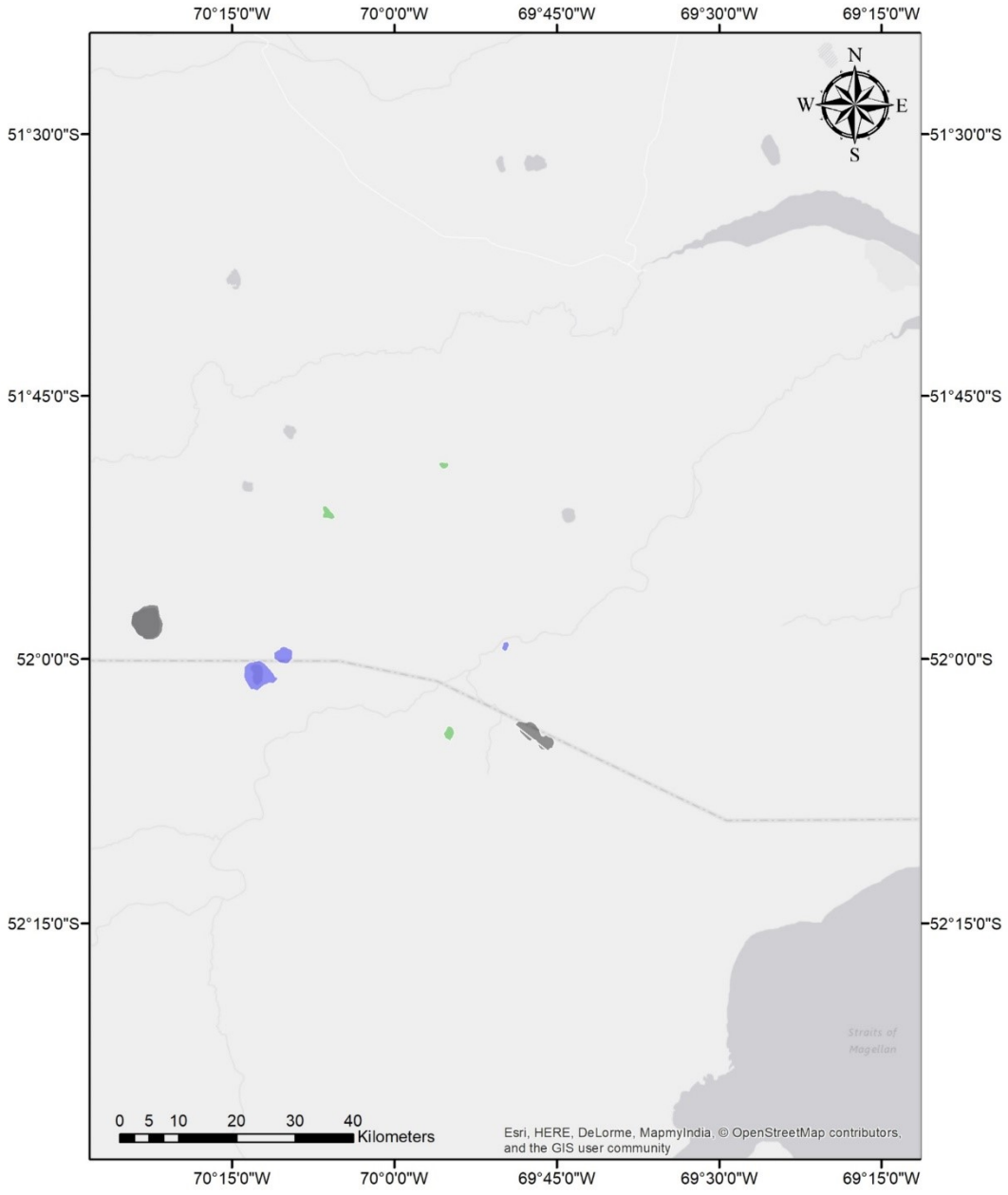

Pali Aike Volcanic Field (Argentina) – Shows maars used for calculating secondary orientation modes. Green maars fall within mode S_A, while blue maars fall in S_B.

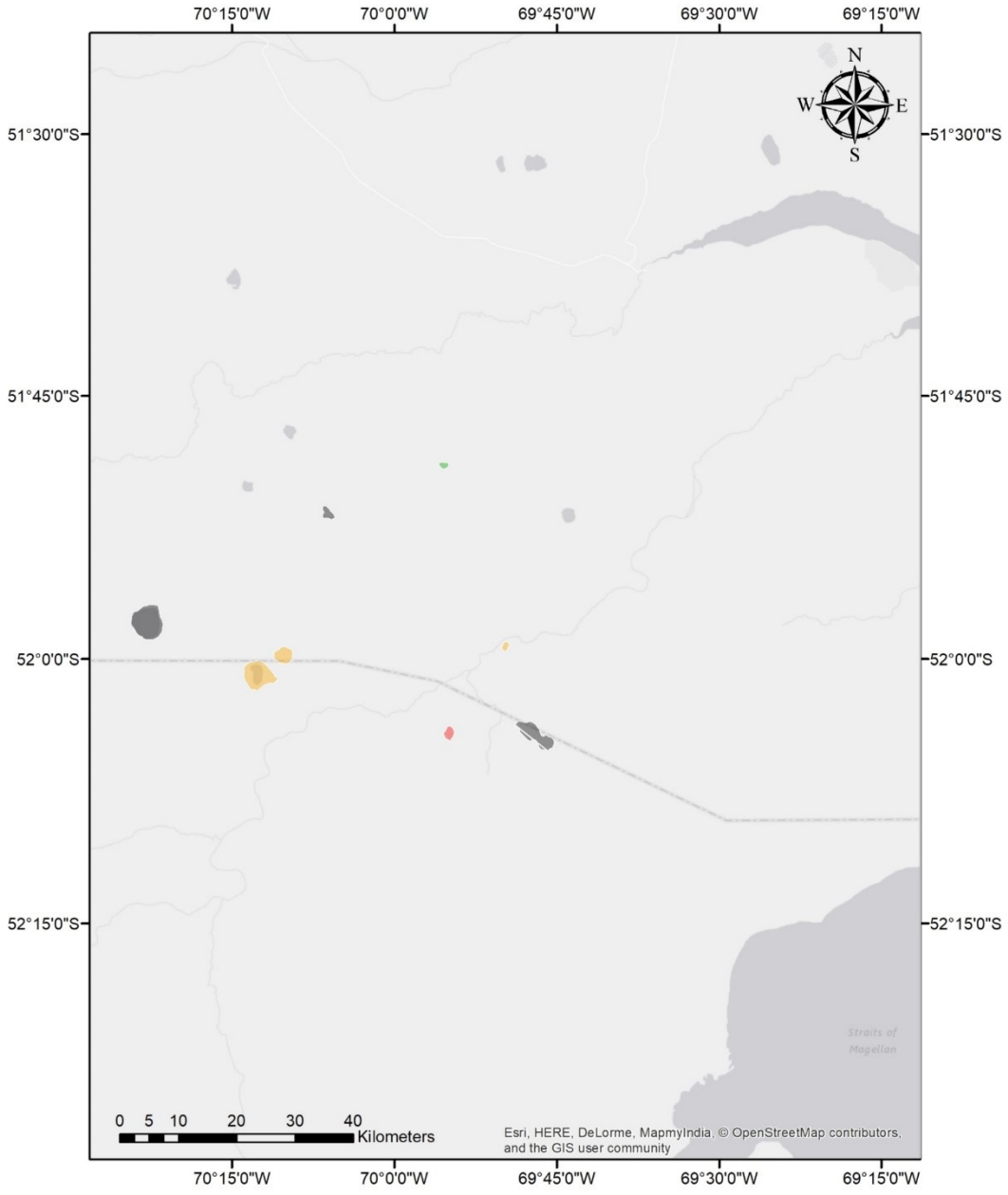

Pali Aike Volcanic Field (Argentina) – Highlighted maars exhibit secondary orientations which also share a direction with faulting and nearest neighbor modes. Green maars fall within faulting modes, yellow within nearest neighbor, and red under both.

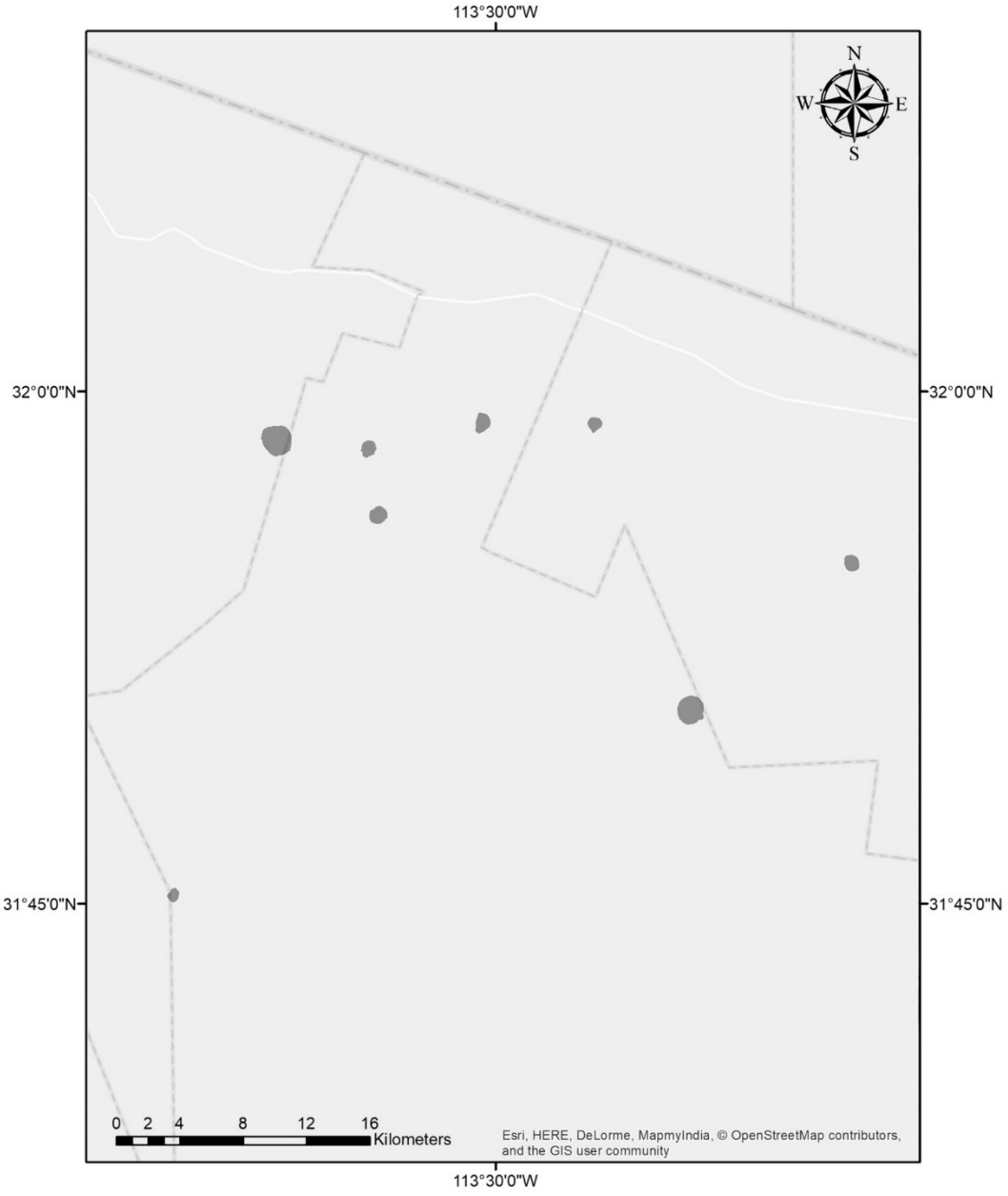

Pinacate Volcanic Field (Mexico)– Dark gray polygons show maars digitized for analysis in this field.

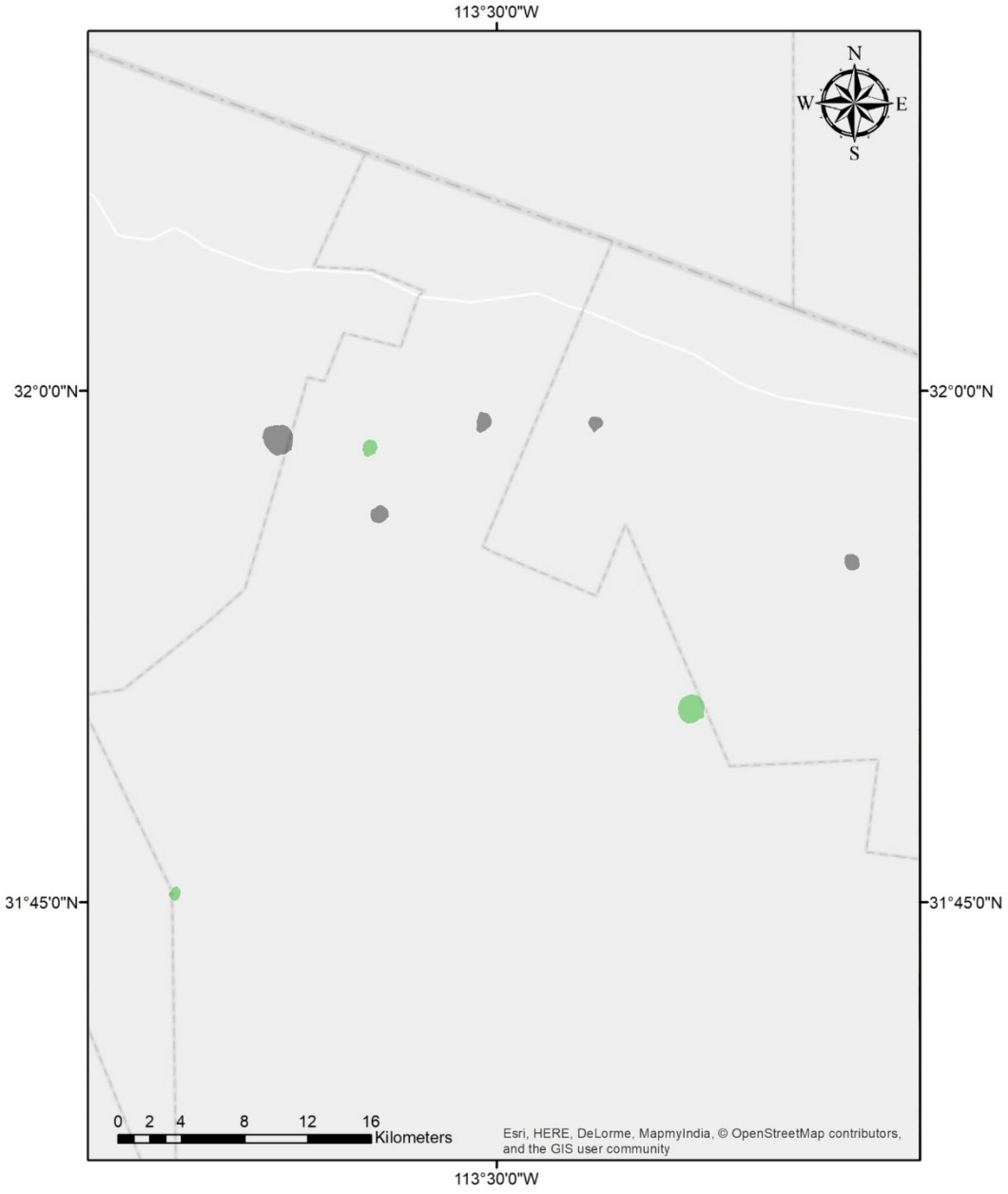

Pinacate Volcanic Field (Mexico) – Shows maars used in calculating primary orientation modes. Green maars make up mode P_A.

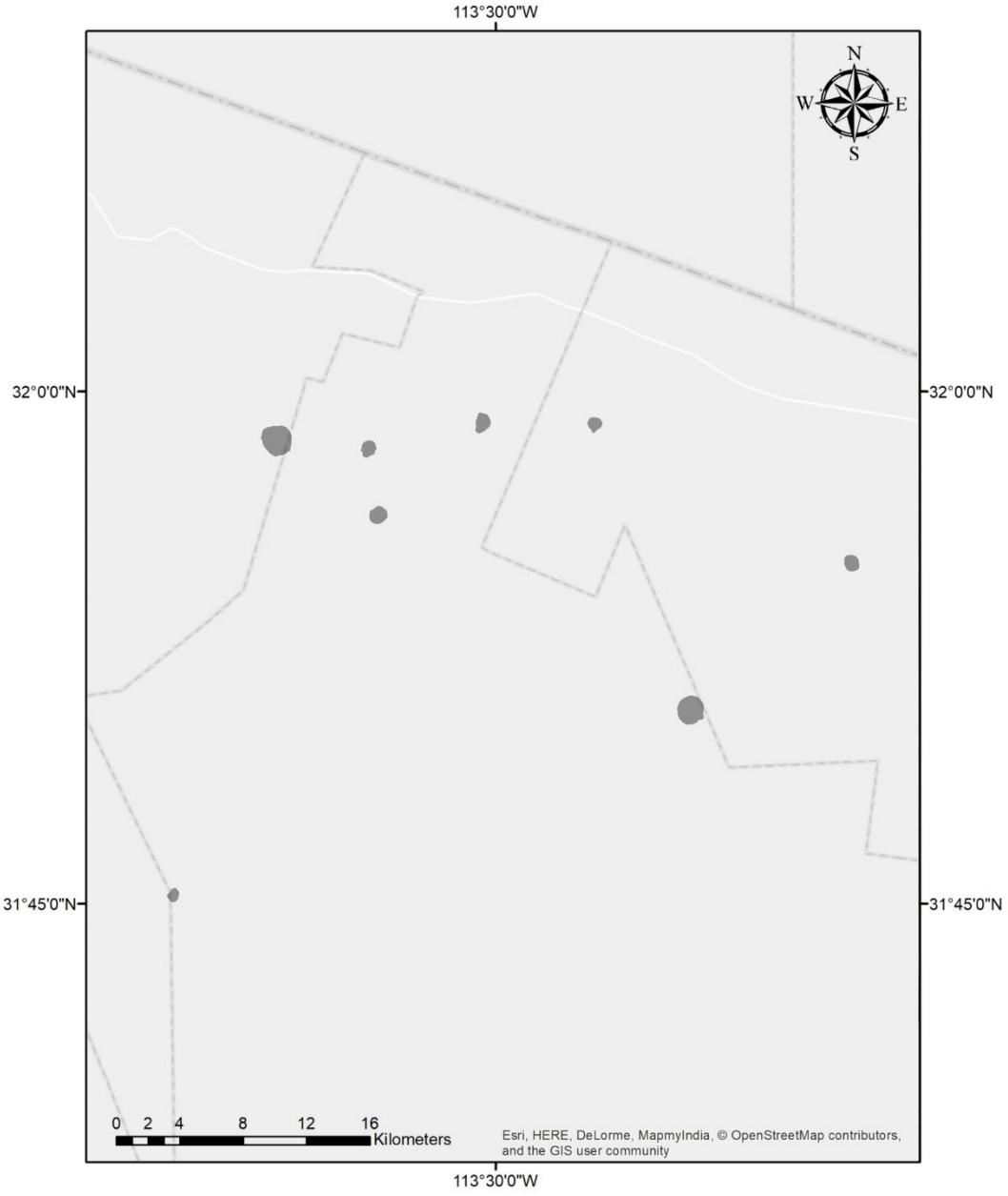

Pinacate Volcanic Field (Mexico) – Highlighted maars both fall within primary orientations modes and have an orientation similar to faulting and nearest neighbor modes.

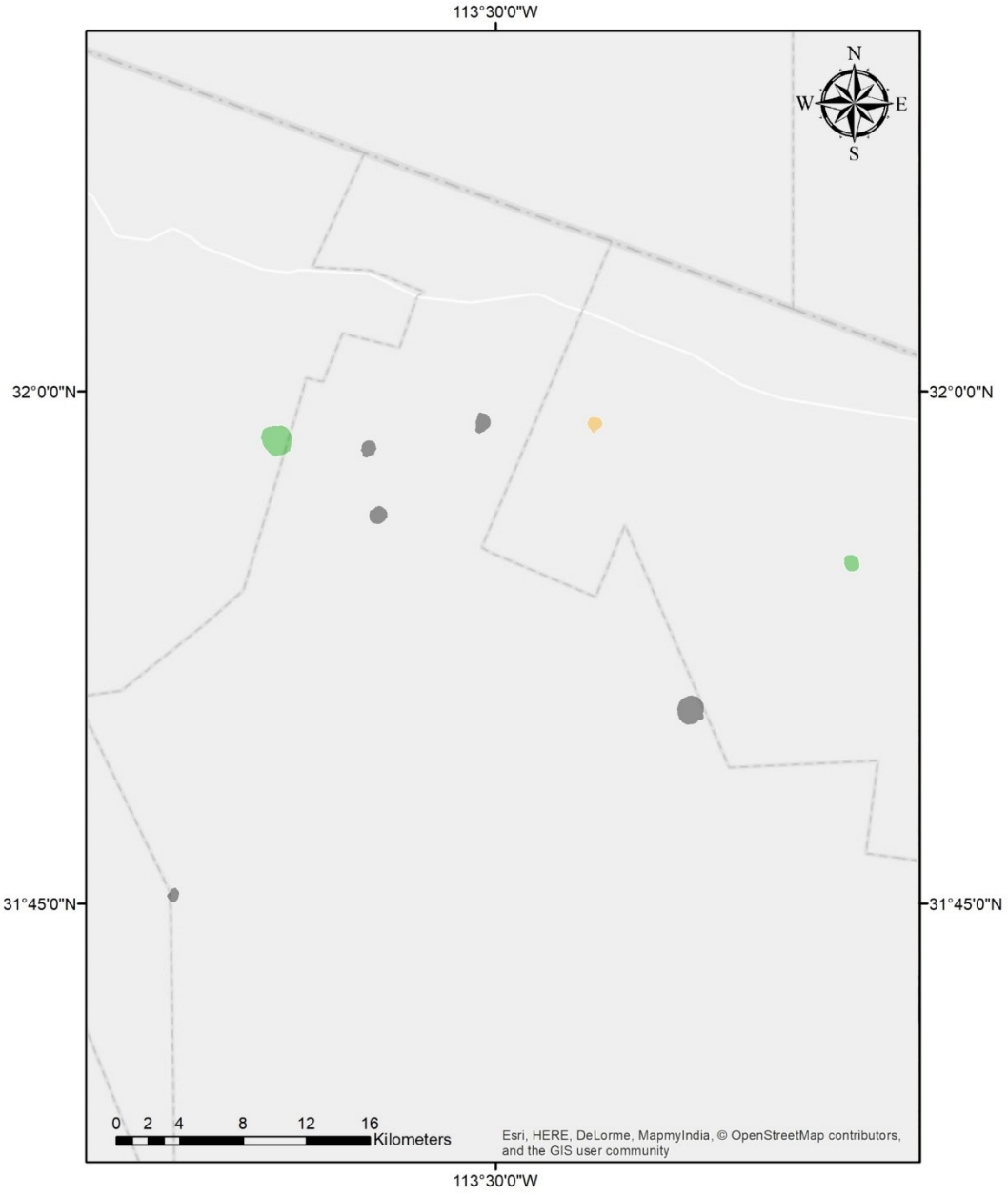

Pinacate Volcanic Field (Mexico) – Highlighted maars exhibit primary orientations within 10^{o} of faulting or nearest neighbor modes. Green maars fall within faulting modes, yellow within nearest neighbor, and red under both.

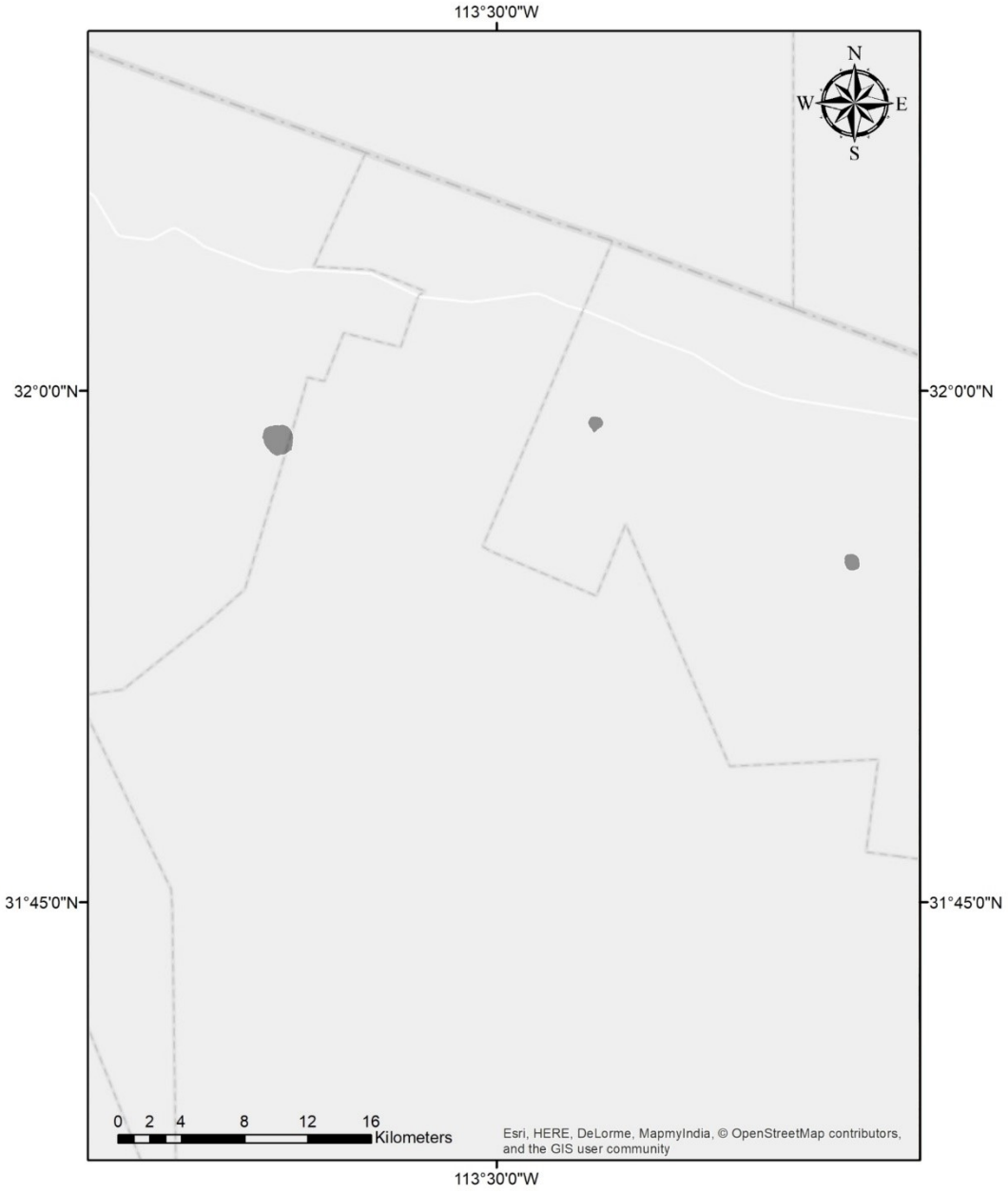

Pinacate Volcanic Field (Mexico) – Dark gray polygons show maars which exhibit secondary orientations.

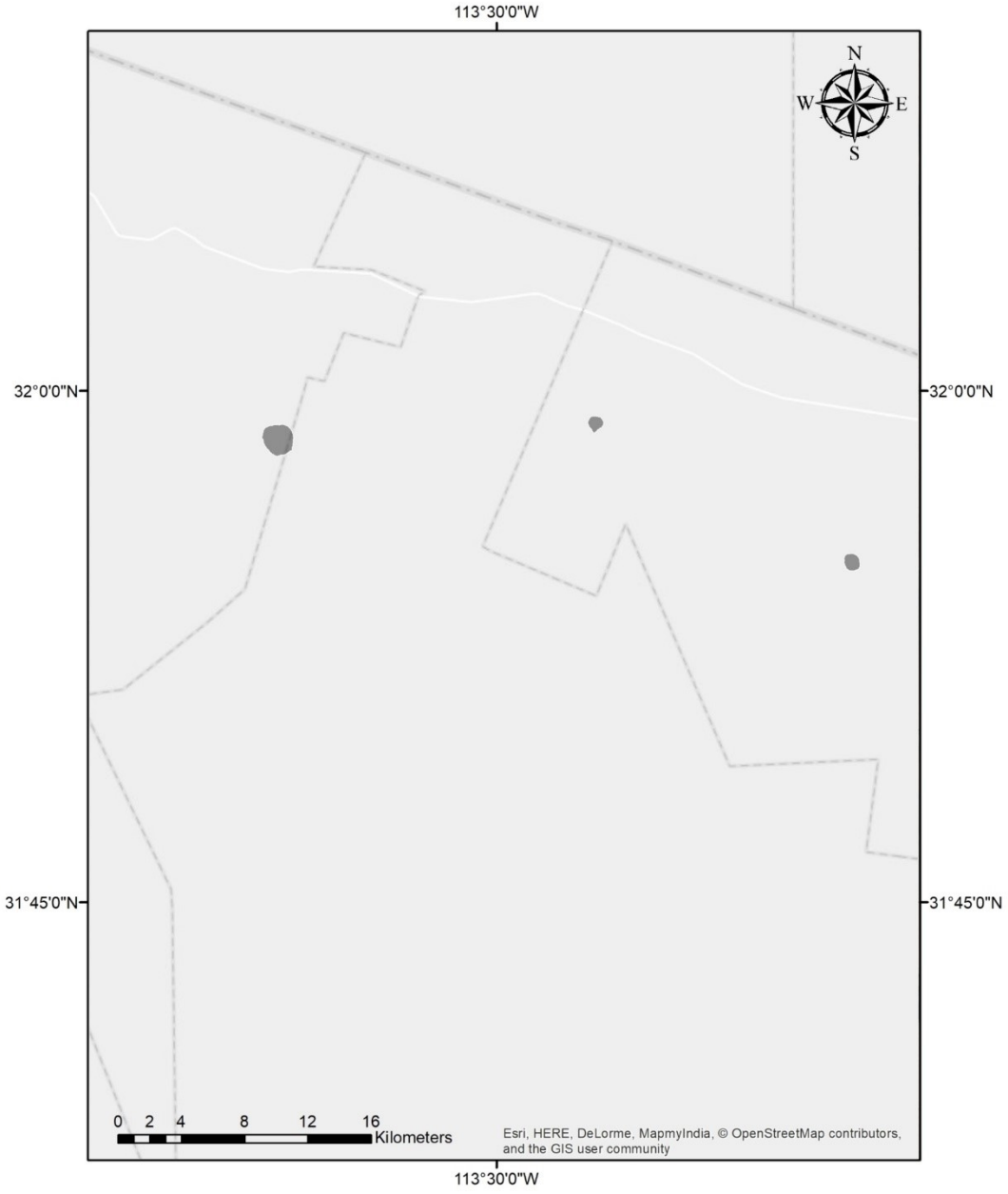

Pinacate Volcanic Field (Mexico) – Shows maars with secondary orientations which both fall within modes, and share similar orientations as faulting and nearest neighbor modes.

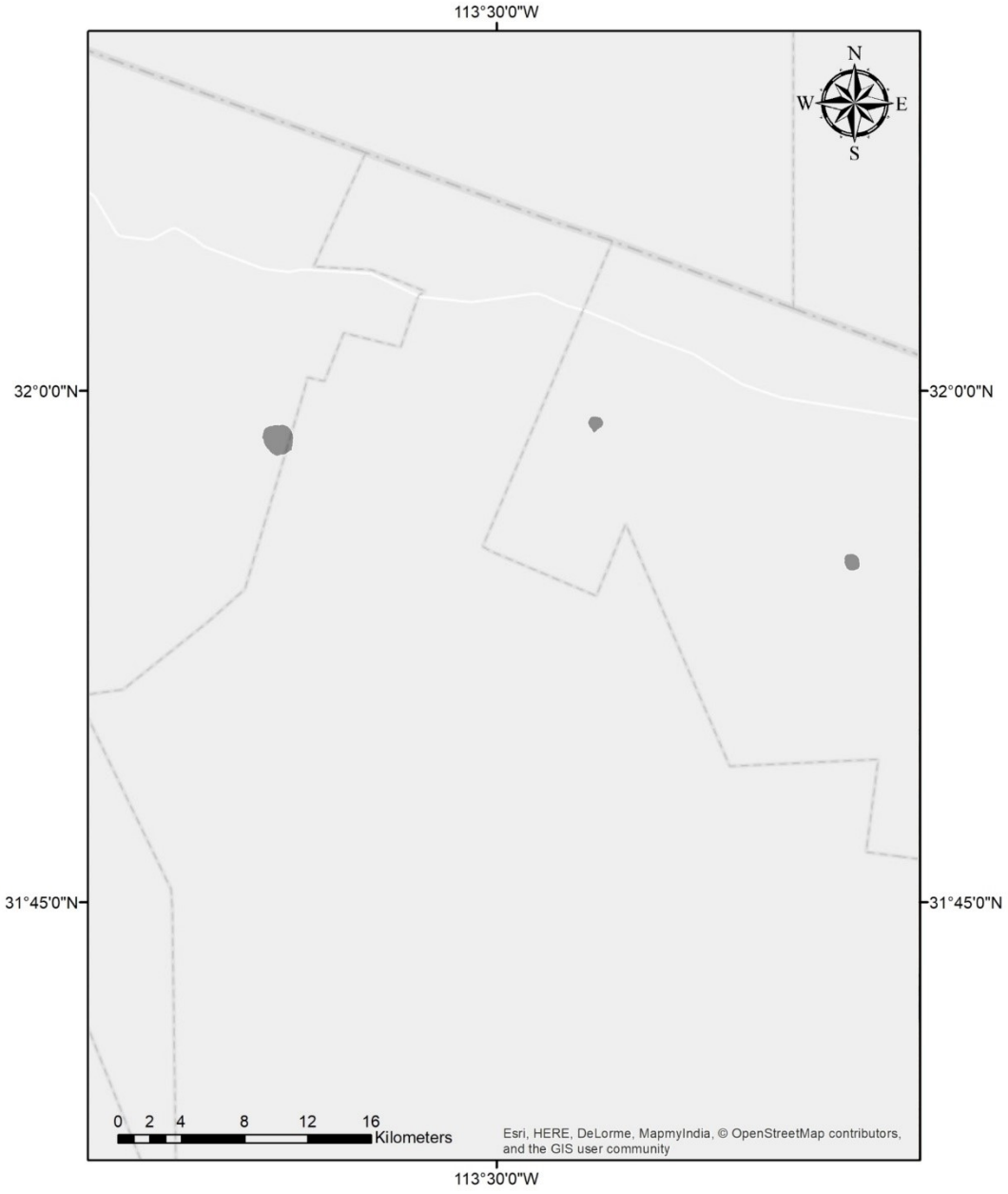

Pinacate Volcanic Field (Mexico) – Highlighted maars fall within secondary orientation modes.

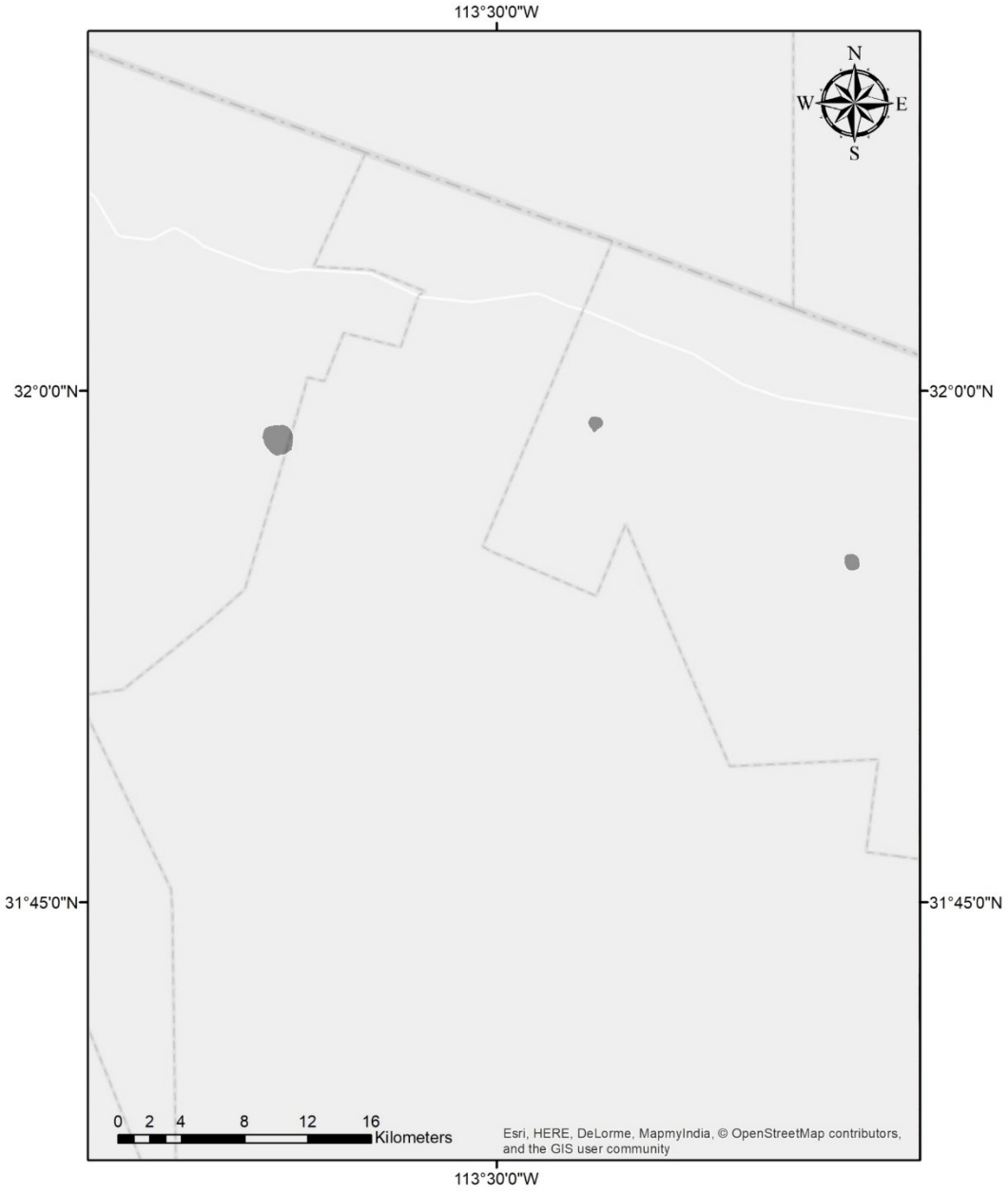

Pinacate Volcanic Field (Mexico) – Highlighted maars have secondary orientations similar to faulting and nearest neighbor modes.

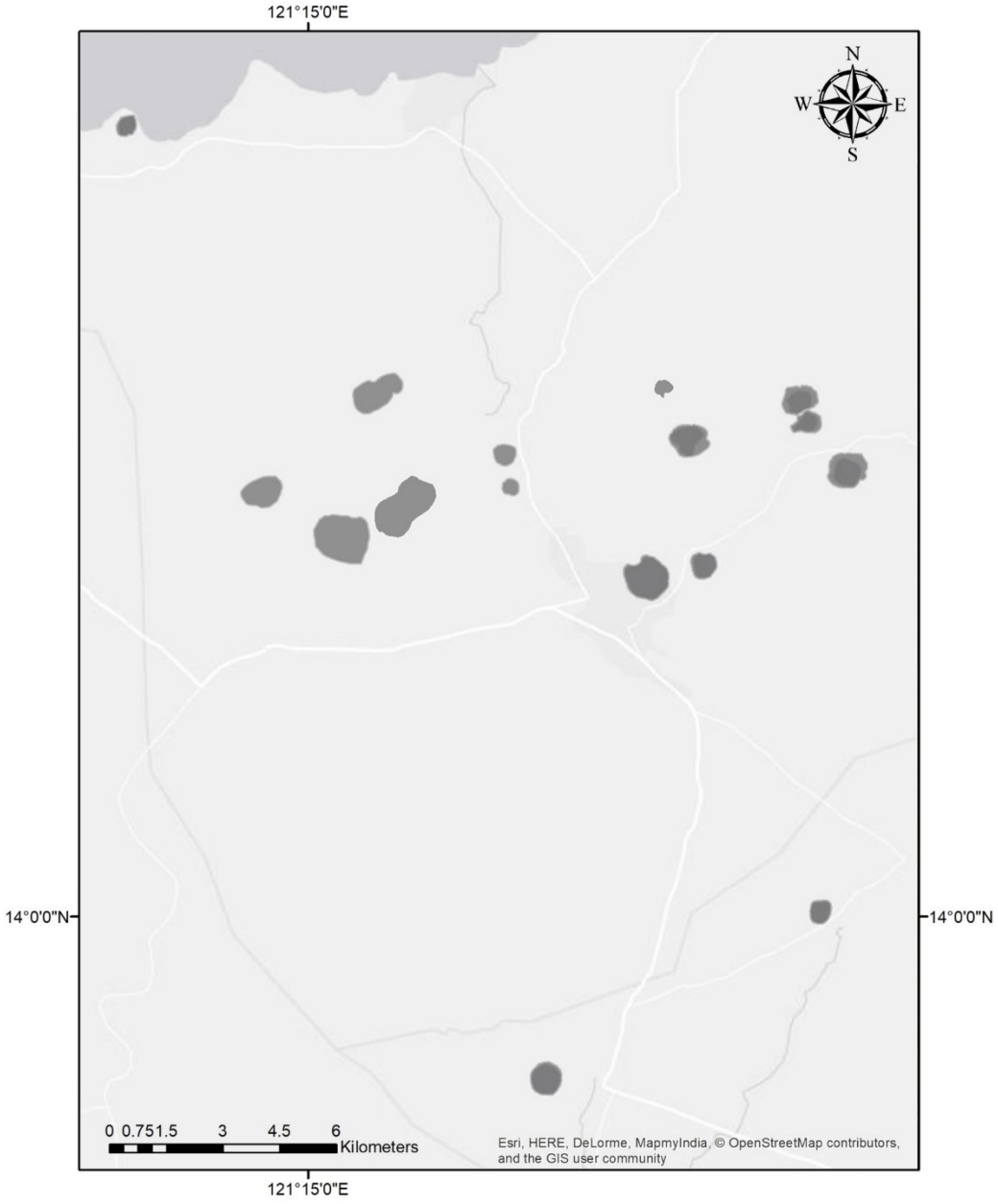

San Pablo City Volcanic Field (Philippines) – Dark gray polygons show all maars digitized for analysis in this field.

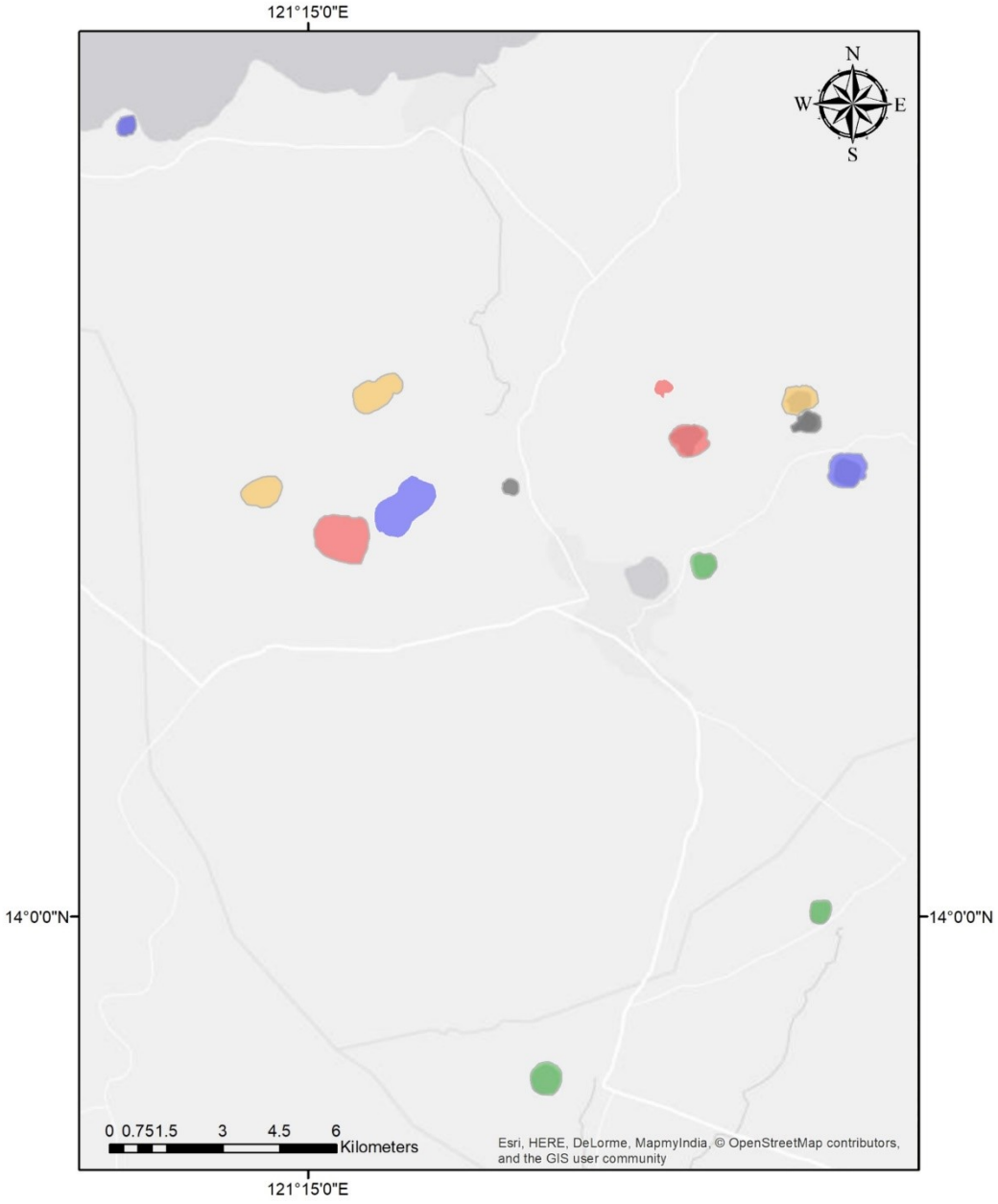

San Pablo City Volcanic Field (Philippines) – Shows maars used for calculating primary orientation modes. Green maars fall within mode P_A, blue P_B, yellow P_C, and red P_D.

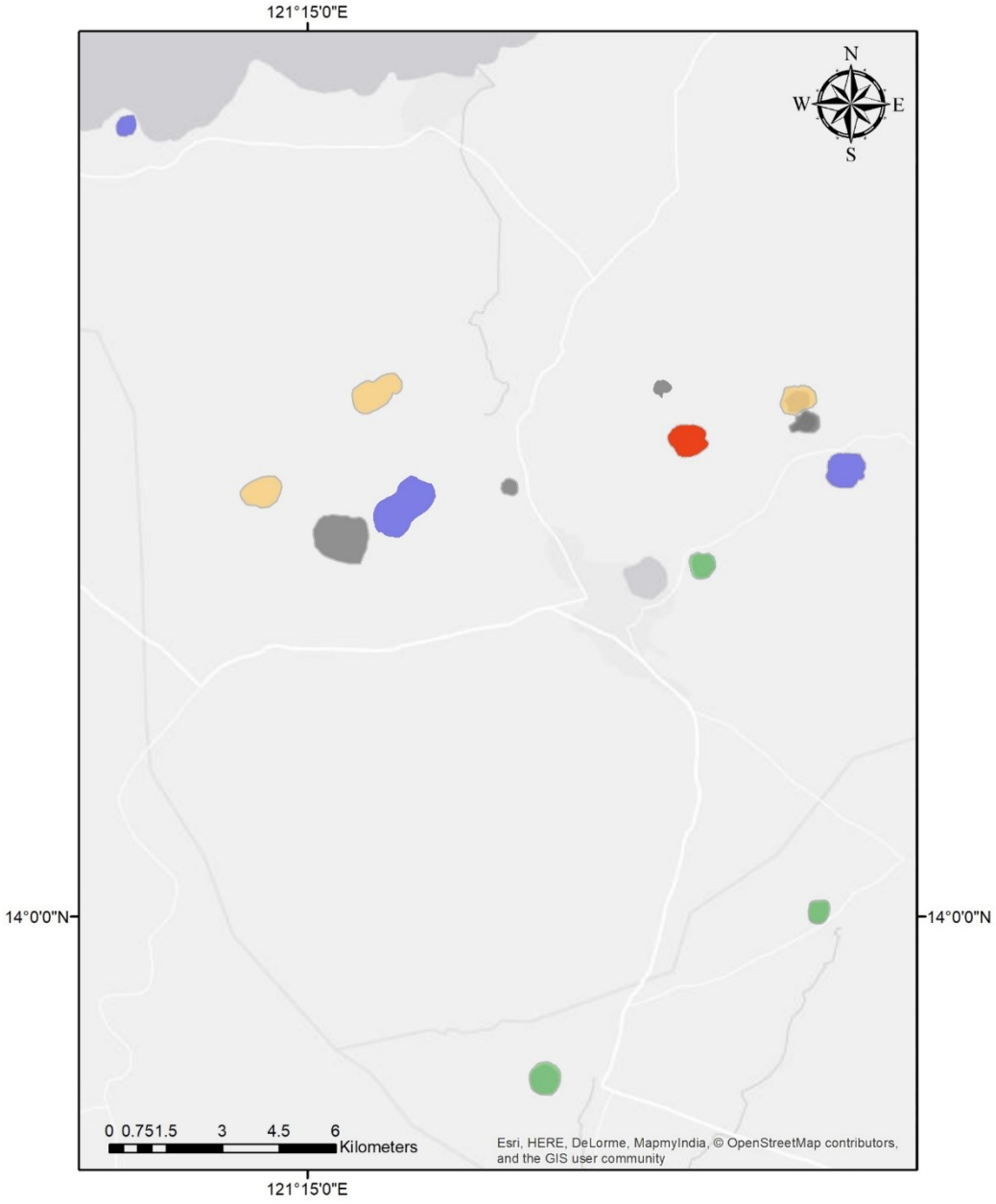

San Pablo City Volcanic Field (Philippines) – Highlighted maars both fall within primary orientation modes and have an orientation similar to faulting and nearest neighbor modes. Green maars fall within mode P_A, blue P_B, yellow P_C, and red P_D.

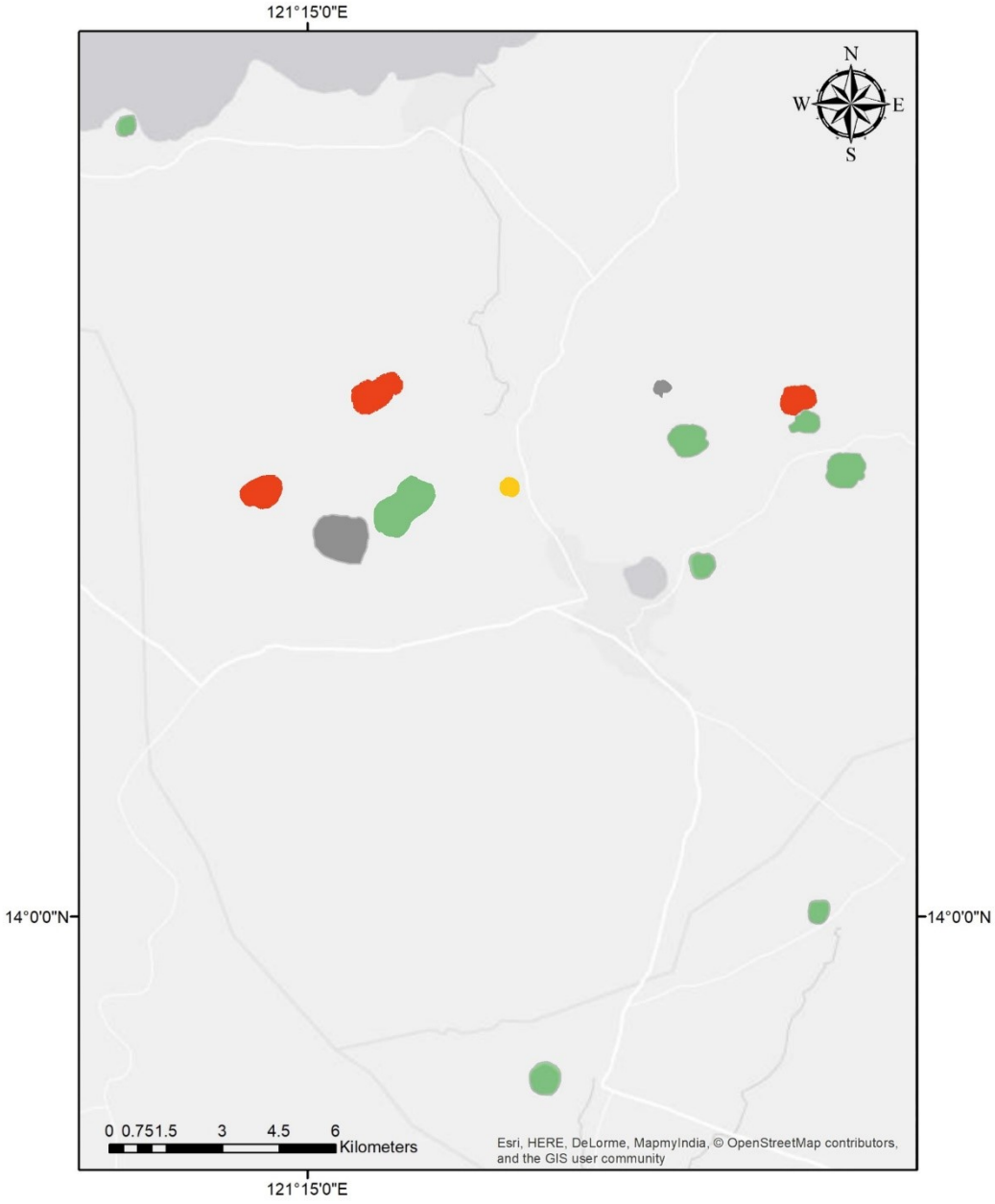

San Pablo City Volcanic Field (Philippines) – Highlighted maars exhibit similar orientations as faulting and nearest neighbor modes. Green maars fall under faulting modes, yellow under nearest neighbor, and red under both.

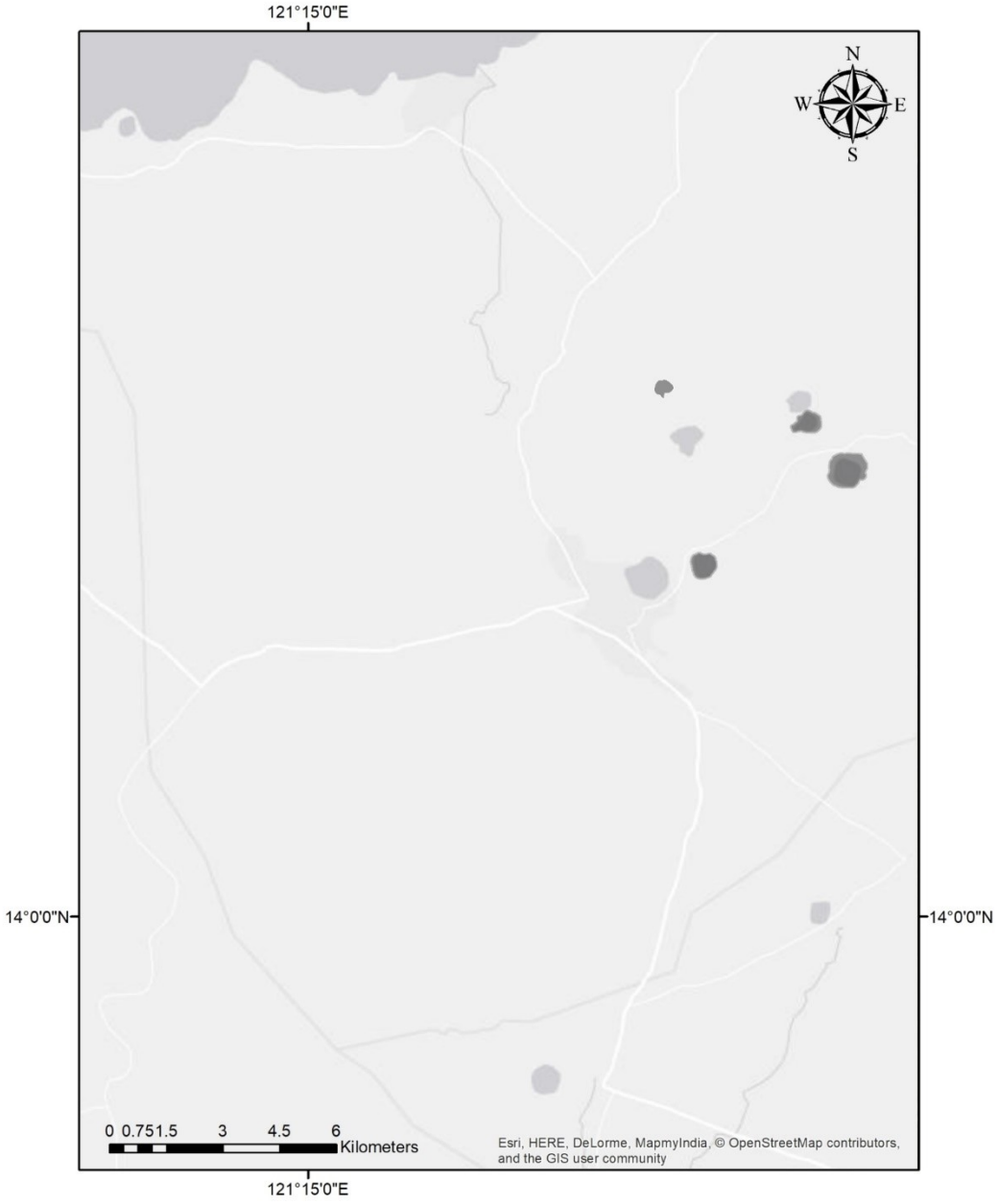

San Pablo City Volcanic Field (Philippines) – Dark gray polygons represent maars with secondary orientations.

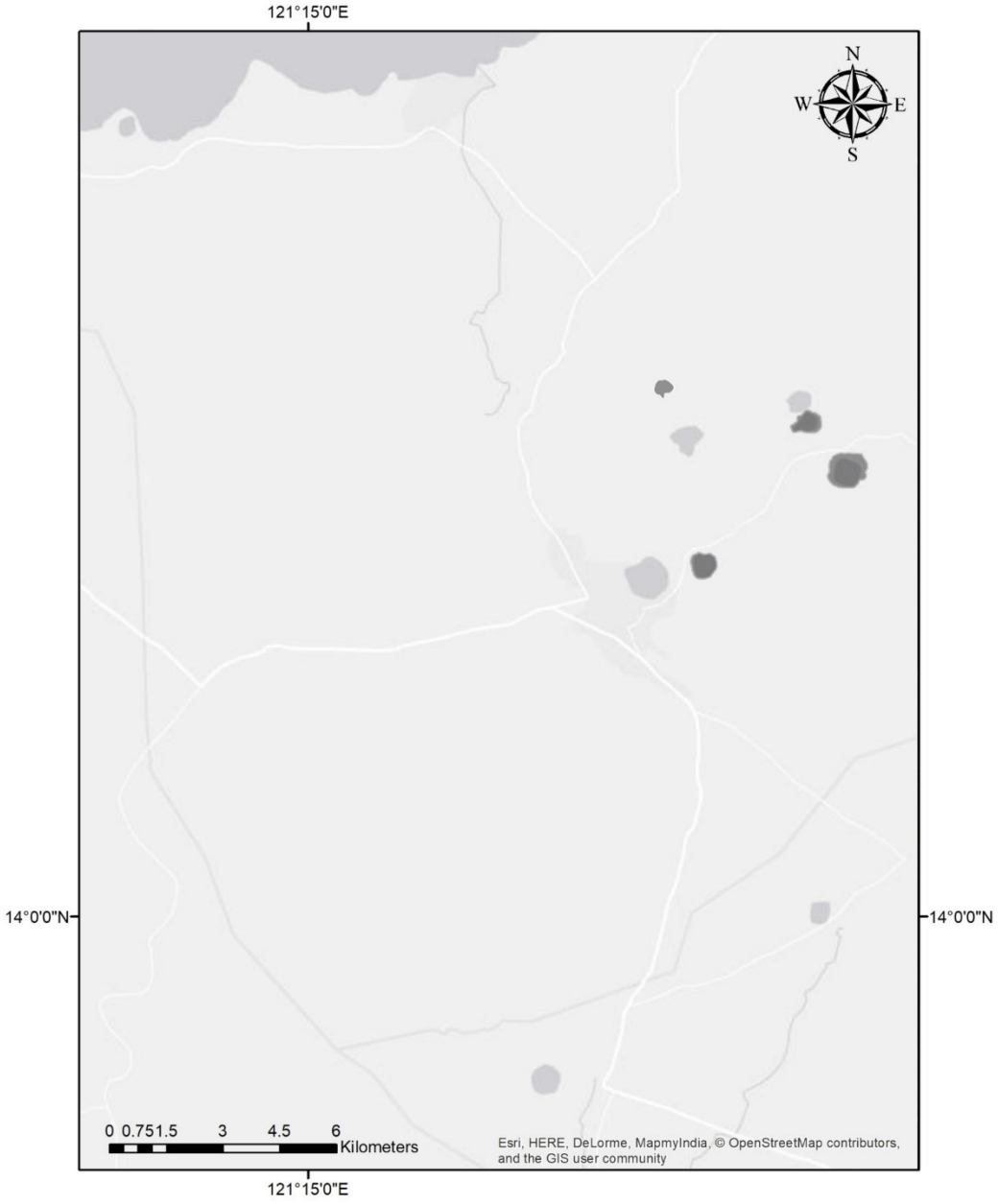

San Pablo City Volcanic Field (Philippines) – Highlighted maars both fall within secondary orientation modes and have a similar orientation to faulting and nearest neighbor modes.

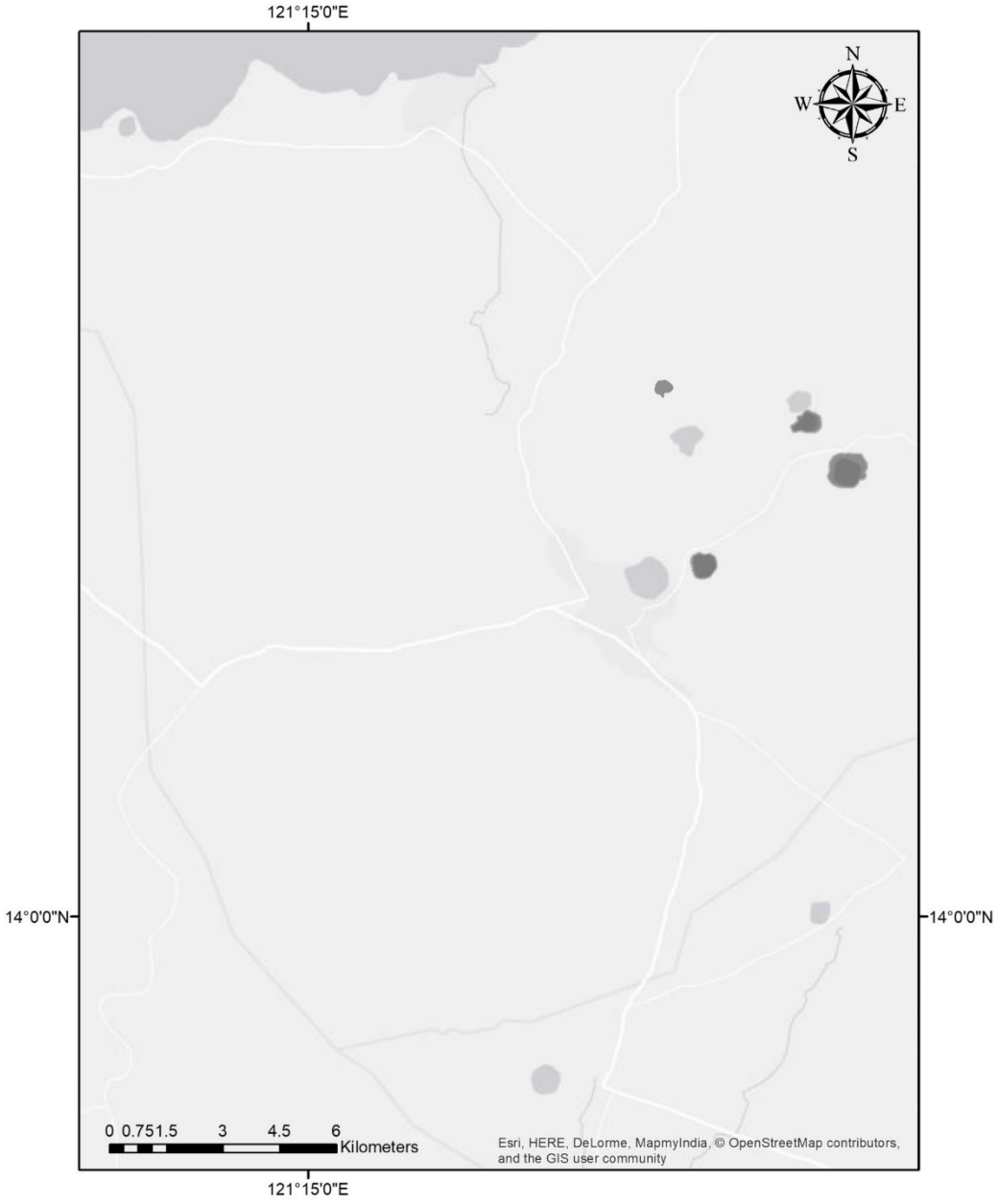

San Pablo City Volcanic Field (Philippines) – Highlighted maars fall within secondary orientation modes.

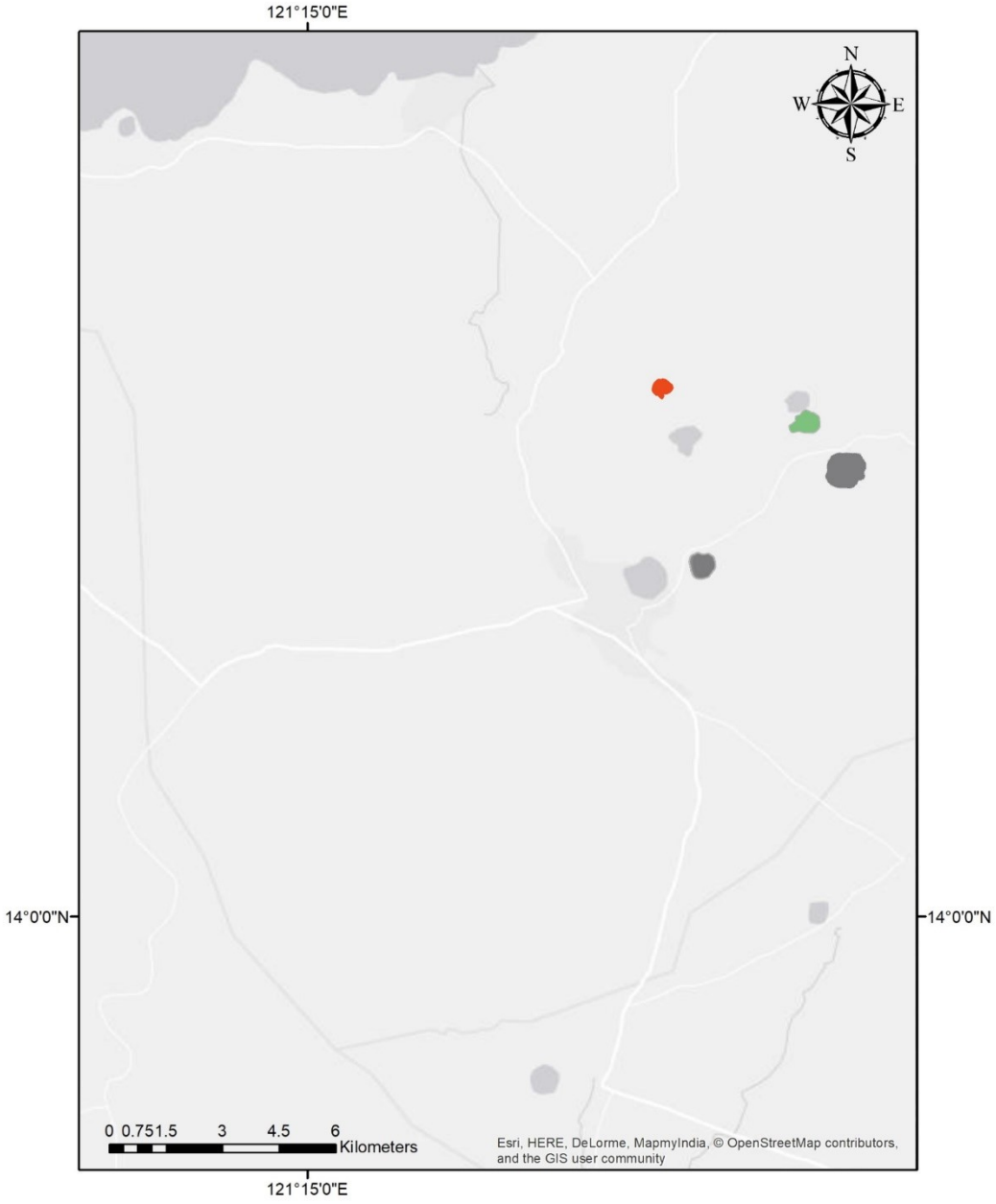

San Pablo City Volcanic Field (Philippines) – Highlighted maars exhibit secondary orientations within 10^{o} of faulting and nearest neighbor modes. Green maars fall under faulting modes, yellow under nearest neighbor, red under both.

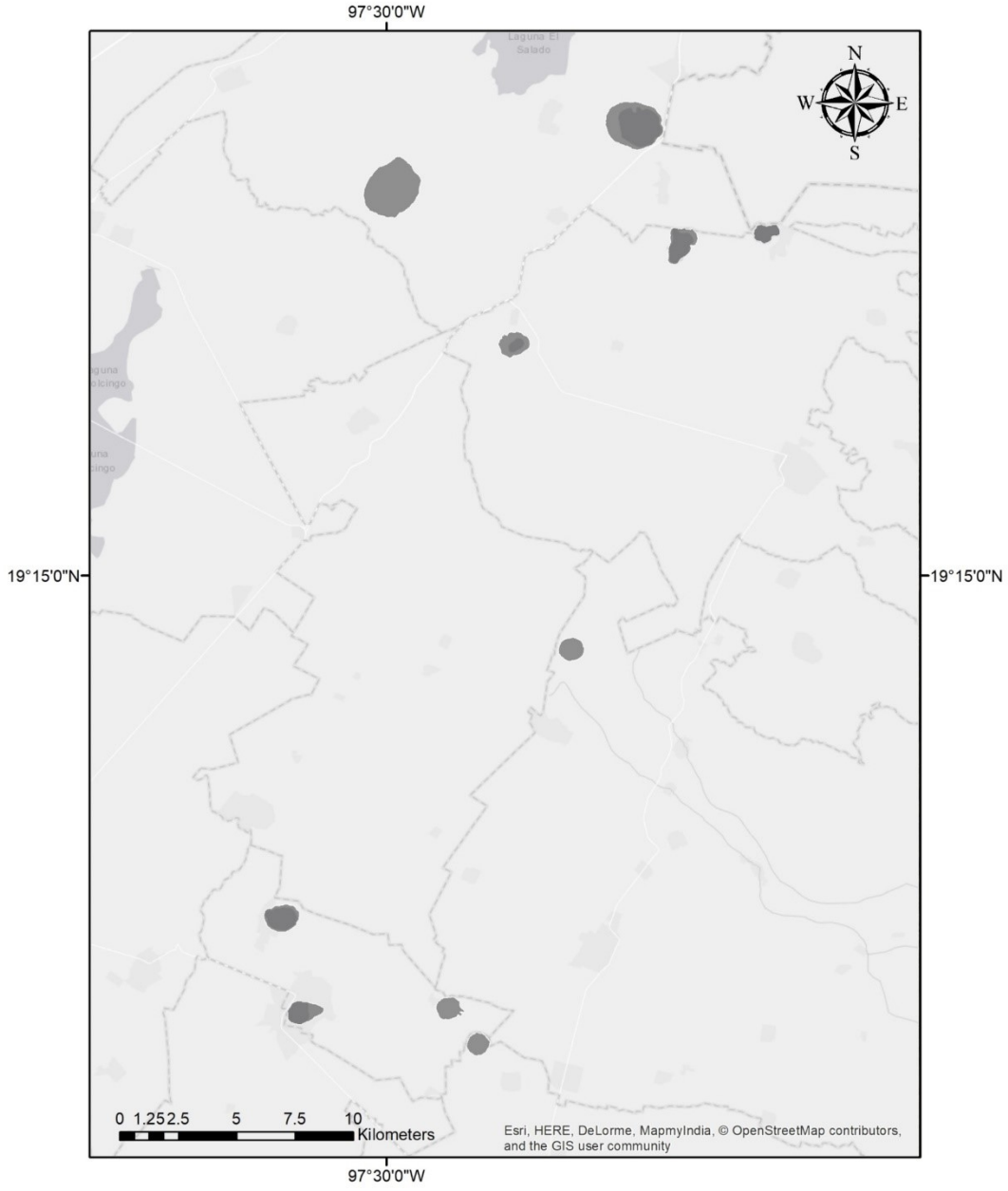

Serdán Oriental Volcanic Field (Mexico) – Dark gray polygons show maars digitized for analysis in this field.

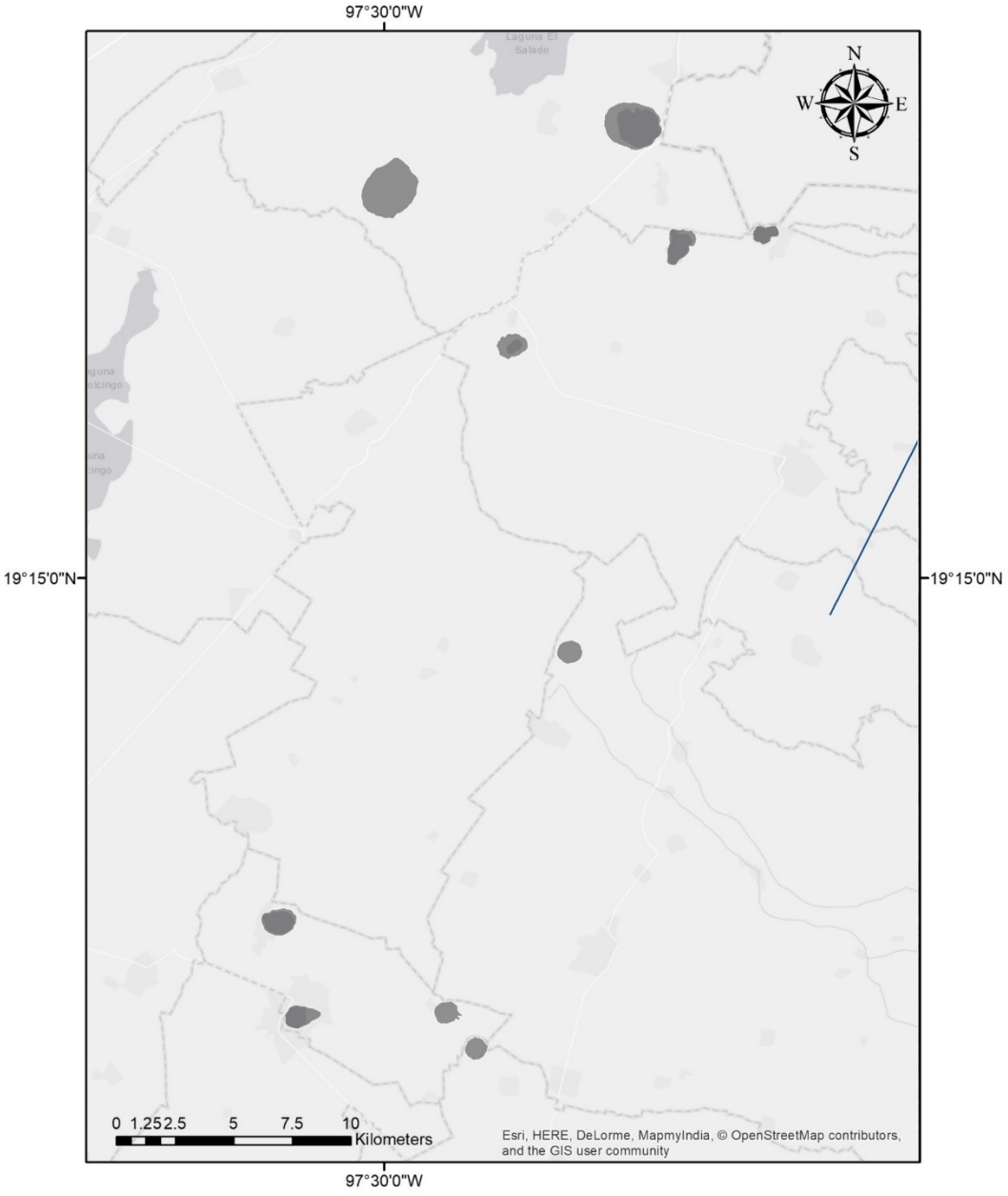

Serdán Oriental Volcanic Field (Mexico) – Shows faults digitized for analysis in field (not all faults are pictured).

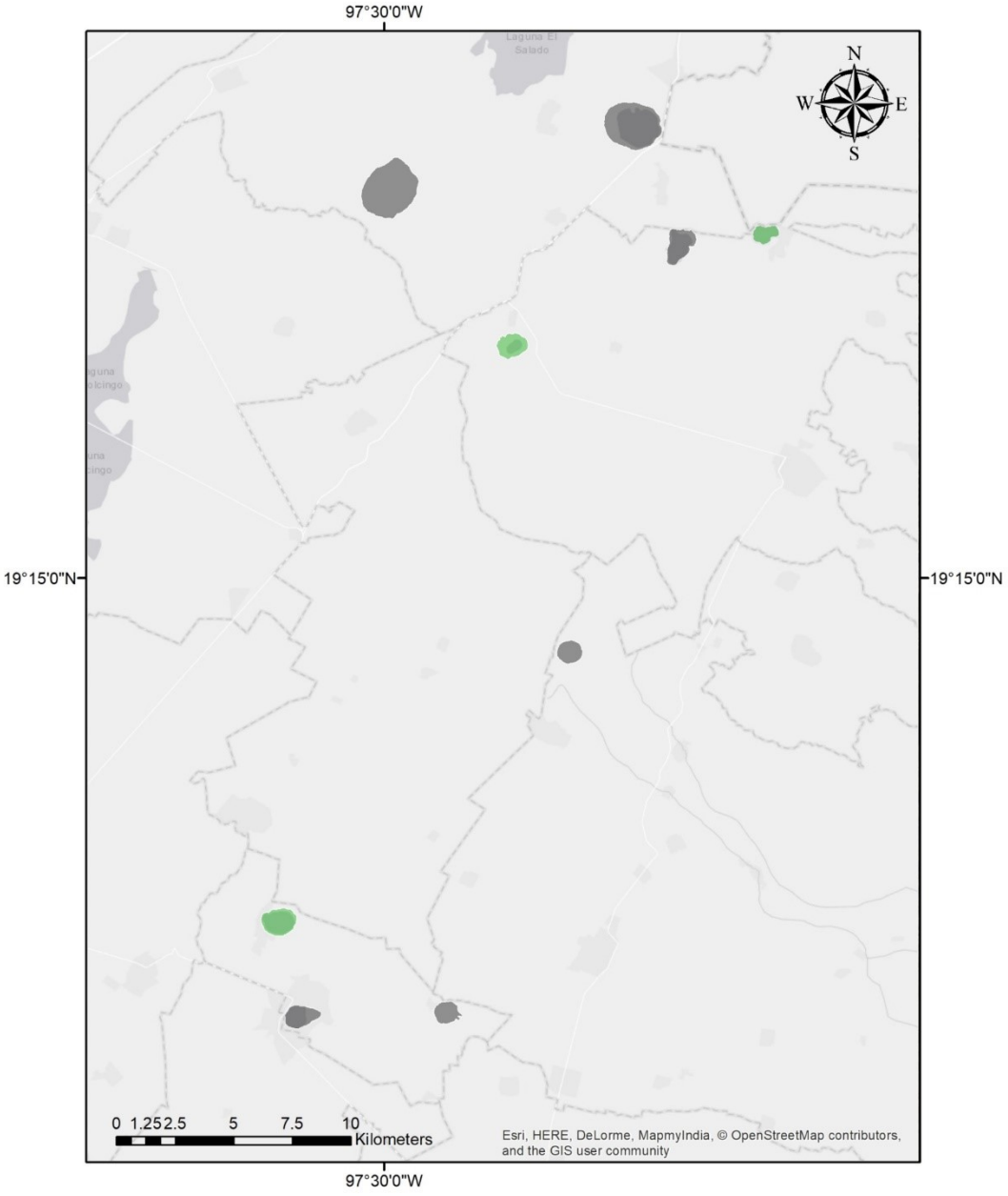

Serdán Oriental Volcanic Field (Mexico) – Shows maars used for calculating primary orientation modes. Highlighted maars fall within primary orientation modes. Green maars fall under mode P_A.

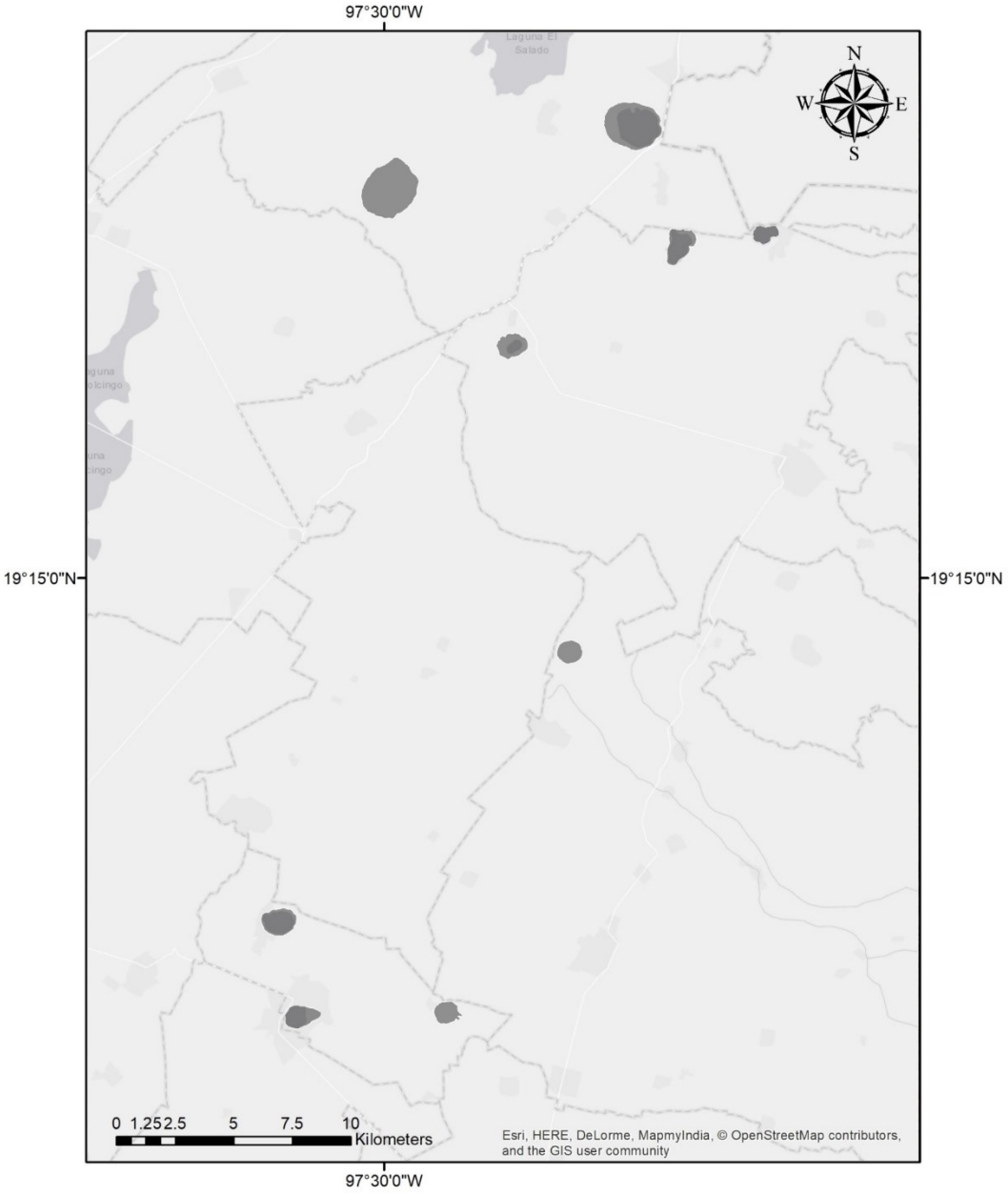

Serdán Oriental Volcanic Field (Mexico) – Highlighted maars both fall under primary orientation modes and exhibit primary orientations similar to the orientation of faulting and nearest neighbor modes.

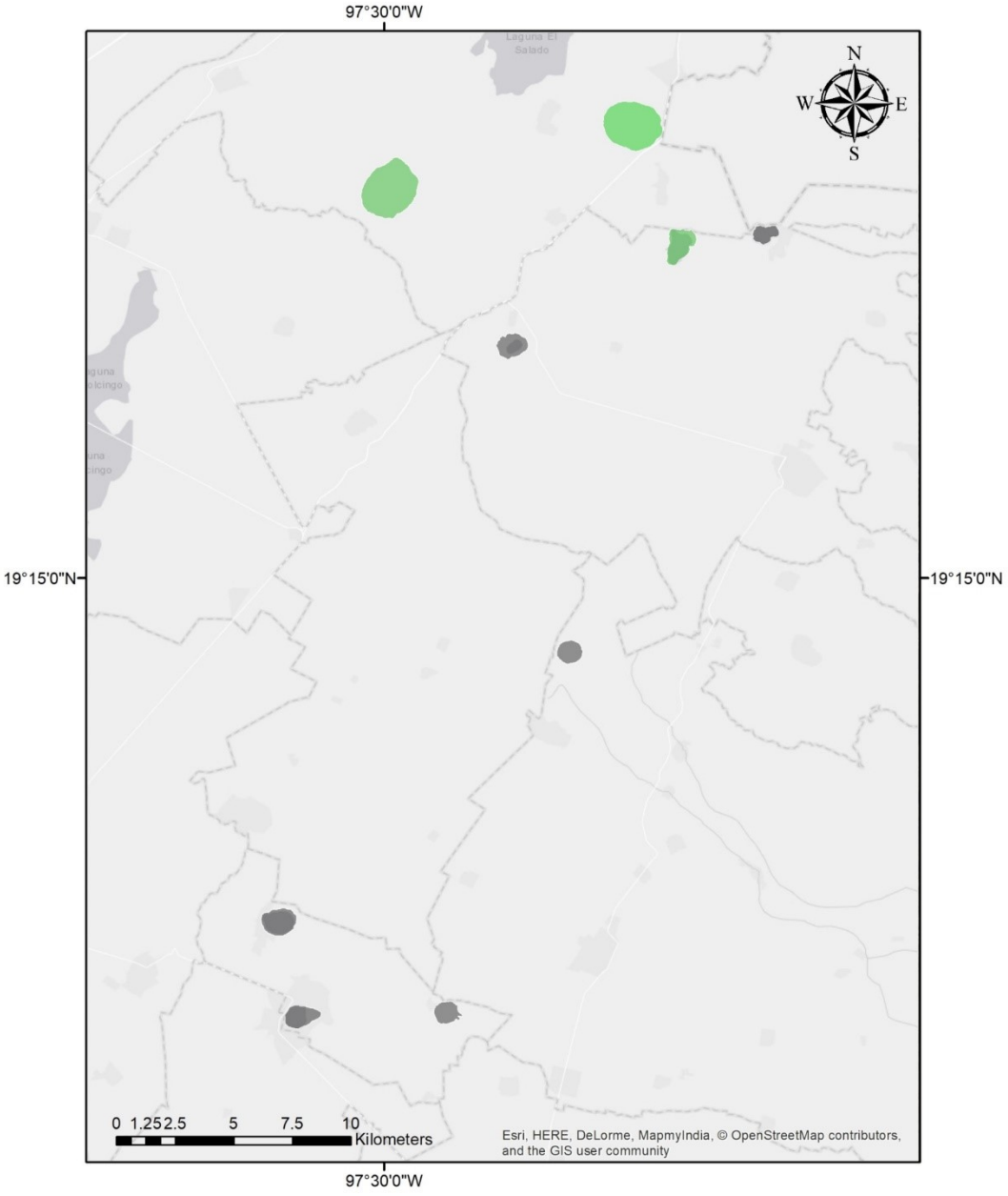

Serdán Oriental Volcanic Field (Mexico) – Highlighted maars exhibit similar orientations as faults and nearest neighbor modes. Green maars have orientations similar to faulting, yellow are similar to nearest neighbor modes, and red fall under both.

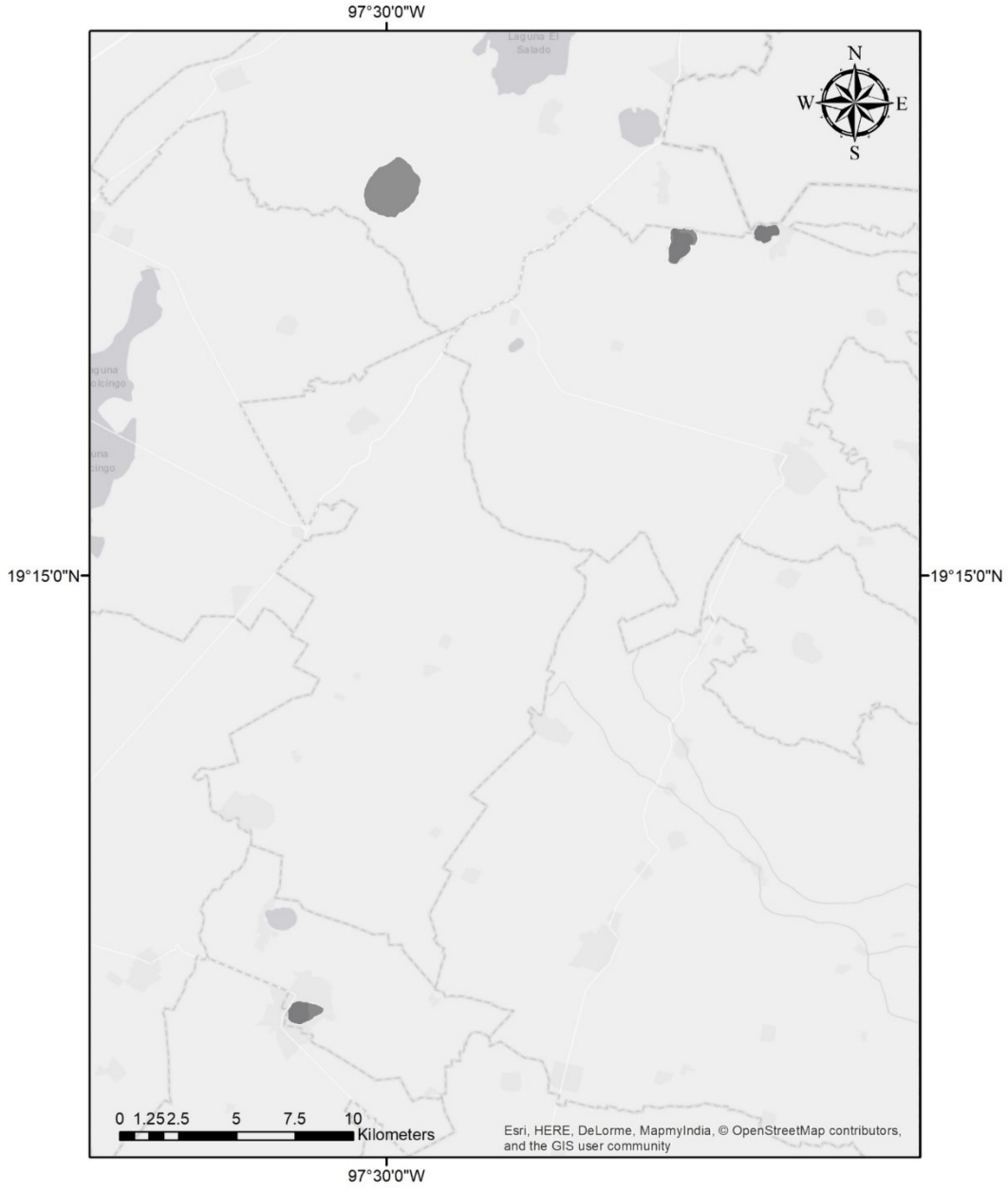

Serdán Oriental Volcanic Field (Mexico) – Dark gray polygons show maars which exhibit secondary orientations.

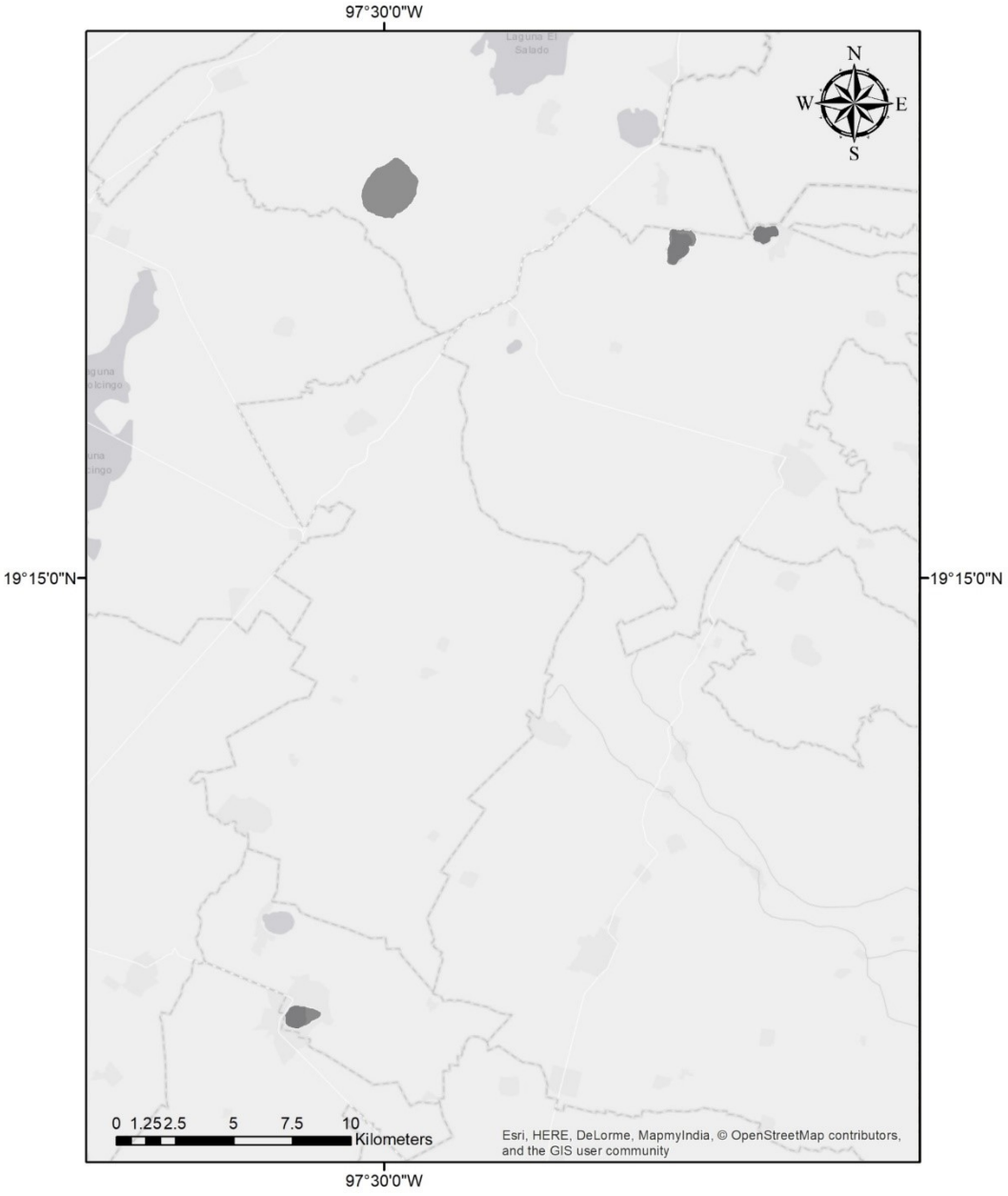

Serdán Oriental Volcanic Field (Mexico) – Highlighted maars both fall under secondary orientation modes and share similar orientations as faulting and nearest neighbor modes.

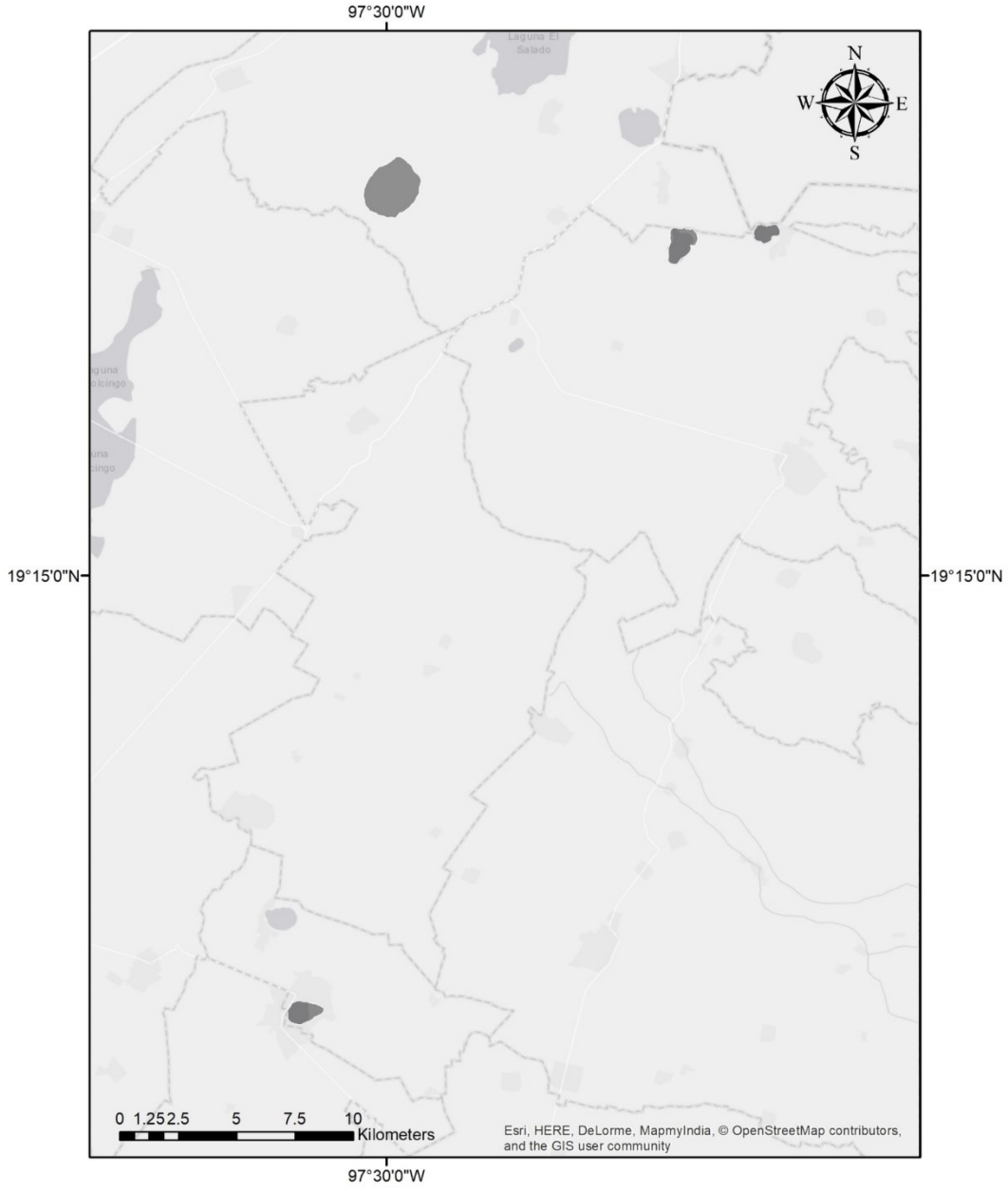

Serdán Oriental Volcanic Field (Mexico) – Highlighted maars fall under secondary orientation modes.

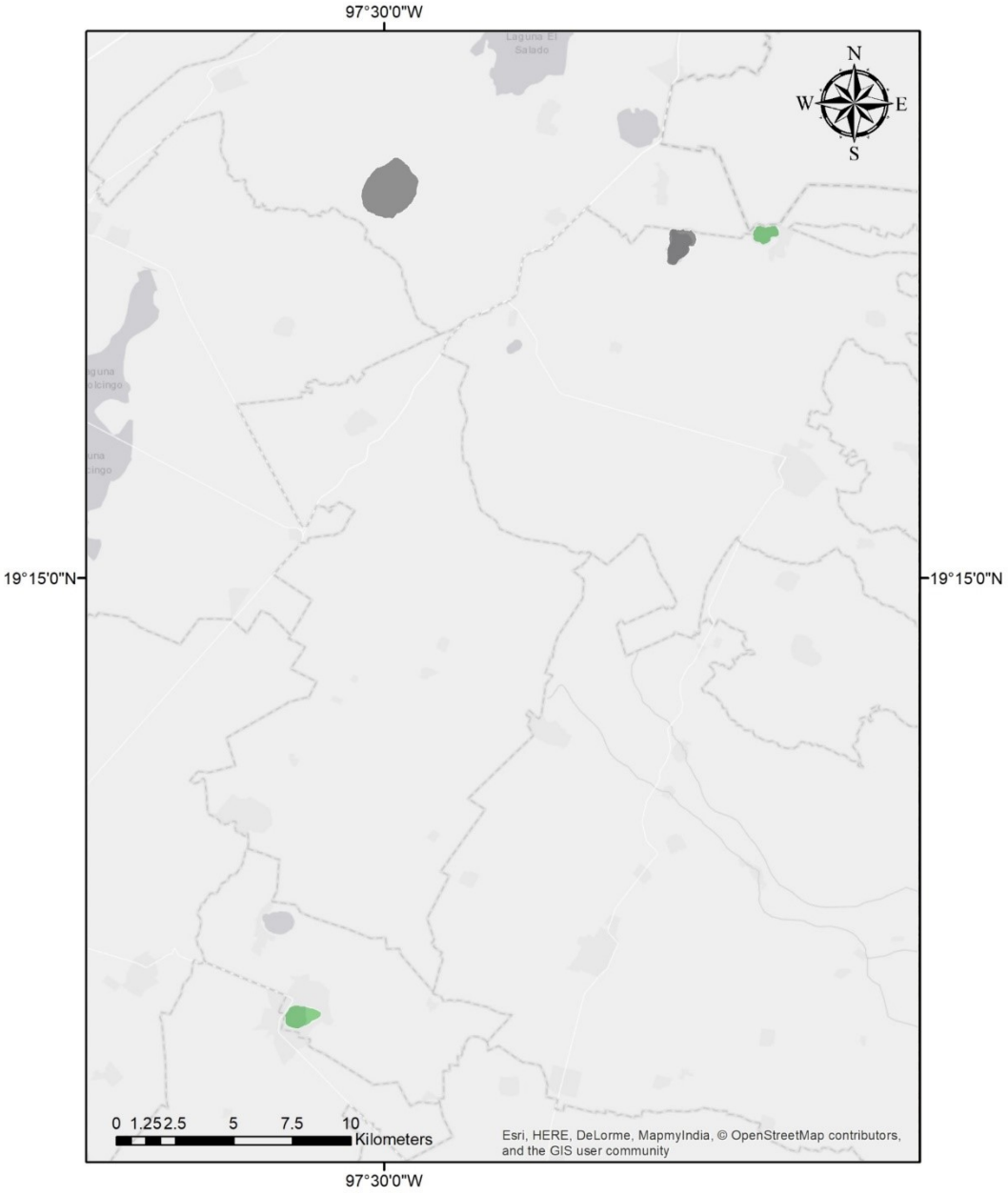

Serdán Oriental Volcanic Field (Mexico) – Highlighted maars exhibit secondary orientations similar to faulting and nearest neighbor modes. Green maars fall within 10^{o} of faulting modes.

REFERENCES

Acocella, V., & Neri, M. (2009). Dike propagation in volcanic edifices: Overview and possible developments. Tectonophysics, 471(1–2), 67–77. https://doi.org/10.1016/j.tecto.2008.10.002

Acocella, V., Korme, T., Salvini, F., & Funiciello, R. (2003). Elliptic calderas in the Ethiopian Rift: Control of pre-existing structures. Journal of Volcanology and Geothermal Research, 119(1–4), 189–203. https://doi.org/10.1016/S0377-0273(02)00342-6

Boyce, J. (2013). The Newer Volcanics Province of southeastern Australia: A new classification scheme and distribution map for eruption centres. Australian Journal of Earth Sciences, 60(4), 449–462. https://doi.org/10.1080/08120099.2013.806954

Carn, S. A. (1999). Application of synthetic aperture radar (SAR) imagery to volcano mapping in the humid tropics: A case study in East Java, Indonesia. Bulletin of Volcanology, 61(1–2), 92–105. https://doi.org/10.1007/s004450050265

Carn, S. A. (2000). The Lamongan volcanic field, East Java, Indonesia: Physical volcanology, historic activity and hazards. Journal of Volcanology and Geothermal Research, 95(1–4), 81–108. https://doi.org/10.1016/S0377-0273(99)00114-6

Carrasco-Núñez, G., Ort, M. H., & Romero, C. (2007). Evolution and hydrological conditions of a maar volcano (Atexcac crater, Eastern Mexico). Journal of Volcanology and Geothermal Research, 159(1–3), 179–197. https://doi.org/10.1016/j.jvolgeores.2006.07.001

Cassidy, J., & Locke, C. A. (2010). The Auckland volcanic field, New Zealand: Geophysical evidence for structural and spatio-temporal relationships. Journal of Volcanology and Geothermal Research, 195(2–4), 127–137. https://doi.org/10.1016/j.jvolgeores.2010.06.016

Cebriá, J. M., Martín-Escorza, C., López-Ruiz, J., Morán-Zenteno, D. J., & Martiny, B. M. (2011). Numerical recognition of alignments in monogenetic volcanic areas: Examples from the Michoacán-Guanajuato Volcanic Field in Mexico and Calatrava in Spain. Journal of Volcanology and Geothermal Research, 201(1–4), 73–82. https://doi.org/10.1016/j.jvolgeores.2010.07.016

Connor, C.B., and Aubele, J.C., 1992, Evidence of regional structural controls on vent distribution: Springerville volcanic field, Arizona: Journal of Geophysical Research: Solid Earth, 97, p. 12349–12359.

Defant, M. J., De Boer, J. Z., & Dietmar, O. (1988). The western Central Luzon volcanic arc, the Philippines: two arcs divided by rifting? Tectonophysics, 145(3–4), 305–317. https://doi.org/10.1016/0040-1951(88)90202-8

Ferrari, L., Conticelli, S., Vaggelli, G., Petrone, C.M., and Manetti, P., 2000, Late Miocene volcanism and intra-arc tectonics during the early development of the Trans-Mexican Volcanic Belt: Tectonophysics, 318, p. 161–185, doi: 10.1016/S0040-1951(99)00310-8.

Förster, H., Oles, D., Knittel, U., Defant, M. J., & Torres, R. C. (1990). The Macolod Corridor: A rift crossing the Philippine island arc. Tectonophysics, 183(1–4), 265–271. https://doi.org/10.1016/0040-1951(90)90420-D

García-Abdeslem, J., & Calmus, T. (2015). A 3D model of crustal magnetization at the Pinacate Volcanic Field, NW Sonora, Mexico. Journal of Volcanology and Geothermal Research, 301, 29–37. https://doi.org/10.1016/j.jvolgeores.2015.05.001

Graettinger, A.H. (2018). Trends in maar crater size and shape using the global Maar Volcano Location and Shape (MaarVLS) database. Journal of Volcanology and Geothermal Research.

Gutmann, J. T. (2002). Strombolian and effusive activity as precursors to phreatomagmatism: Eruptive sequence at maars of the Pinacate volcanic field, Sonora, Mexico. Journal of Volcanology and Geothermal Research, 113(1–2), 345–356. https://doi.org/10.1016/S0377-0273(01)00265-7

Hernando, I. R., Franzese, J. R., Llambías, E. J., & Petrinovic, I. A. (2014). Vent distribution in the Quaternary Payún Matrú Volcanic Field, western Argentina: Its relation to tectonics and crustal structures. Tectonophysics, 622, 122–134. https://doi.org/10.1016/j.tecto.2014.03.003

Kereszturi, G., Németh, K., Cronin, S. J., Procter, J., & Agustín-Flores, J. (2014). Influences on the variability of eruption sequences and style transitions in the Auckland Volcanic Field, New Zealand. Journal of Volcanology and Geothermal Research, 286, 101–115. https://doi.org/10.1016/j.jvolgeores.2014.09.002

Kharazizadeh, N., Schellart, W.P., Duarte, J.C., and Hall, M., 2017, Influence of lithosphere and basement properties on the stretching factor and development of extensional faults across the Otway Basin, southeast Australia. Marine and Petroleum Geology, v. 88, p. 1059–1077, doi: 10.1016/j.marpetgeo.2017.08.034.

Ku, Y. P., Chen, C. H., Song, S. R., Iizuka, Y., & Shen, J. J. S. (2009). A 2 Ma record of explosive volcanism in southwestern Luzon: Implications for the timing of subducted slab steepening. Geochemistry, Geophysics, Geosystems, 10(6). https://doi.org/10.1029/2009GC002486

Langridge, R.M., Ries, W.F., Litchfield, N.J., Villamor, P., Van Dissen, R.J., Barrell, D.J.A., Rattenbury, M.S., Heron, D.W., Haubrock, S., Townsend, D.B., Lee, J.M., Berryman, K.R., Nicol, A., Cox, S.C., et al., 2016, The New Zealand Active Faults Database. New Zealand Journal of Geology and Geophysics, 59, p. 86–96, doi: 10.1080/00288306.2015.1112818.

Le Corvec, N., Muirhead, J.D., & White, J.D.L. (2018), Shallow magma diversions during explosive diatreme-forming eruptions: Nature Communications, v. 9, p. 1459, doi: 10.1038/s41467-018-03865-x.

Lesti, C., Giordano, G., Salvini, F., & Cas, R. (2008). Volcano tectonic setting of the intraplate, Pliocene-Holocene, Newer Volcanic Province (southeast Australia): Role of crustal fracture zones. Journal of Geophysical Research: Solid Earth, 113(7), 1–11. https://doi.org/10.1029/2007JB005110

Lewis, S. D., & Hayes, D. E. (1989). Plate convergence and deformation, North Luzon Ridge, Philippines. Tectonophysics, 168(1–3), 221–237. https://doi.org/10.1016/0040-1951(89)90377-6

Lorenz, V. (2003). Maar-Diatreme volcanoes, their formation, and their setting in hard-rock or soft-rock environments. Geolines, 15, 72–83.

Lorenz, V., & Haneke, J. (2004). Relationship between diatremes, dykes, sills, laccoliths, intrusive-extrusive domes, lava flows, and tephra deposits with unconsolidated

water-saturated sediments in the late Variscan intermontane Saar-Nahe Basin, SW Germany. Geological Society, London, Special Publications, 234(1), 75–124. https://doi.org/10.1144/GSL.SP.2004.234.01.07

Lynch, D.J., Musselman, T.E., Gutmann, J.T., & Patchett, P.J. (1993), Isotopic evidence for the origin of Cenozoic volcanic rocks in the Pinacate volcanic field, northwestern Mexico: Lithos, 29, p. 295–302, doi: 10.1016/0024-4937(93)90023-6.

Mazzarini, F. (2003). Faulting in the Pali Aike Volcanic Field. Unpublished raw data.

Mazzarini, F., & D'Orazio, M. (2003). Spatial distribution of cones and satellite-detected lineaments in the Pali Aike Volcanic Field (southernmost Patagonia): Insights into the tectonic setting of a Neogene rift system. Journal of Volcanology and Geothermal Research, 125(3–4), 291–305. https://doi.org/10.1016/S0377-0273(03)00120-3

Ort, M. H., & Carrasco-Núñez, G. (2009). Lateral vent migration during phreatomagmatic and magmatic eruptions at Tecuitlapa Maar, east-central Mexico. Journal of Volcanology and Geothermal Research, 181(1–2), 67–77. https://doi.org/10.1016/j.jvolgeores.2009.01.003

Otterloo, J. V. (2017). Faulting in the Newer Volcanic Province. Unpublished raw data.

Padilla y Sánchez, R.J., Domínguez Trejo, I., López Azcárraga, A.G., Mota Nieto, J., Fuentes Menes, A.O., Rosique Naranjo, F., Germán Castelán, E.A., & Campos Arriola, S.E., 2013, National Autonomous University of Mexico Tectonic Map of Mexico GIS Project, American Association of Petroleum Geologists GIS Open Files series. http://www.datapages.com/gis-map-publishing-program/gis-open-files/geographic/files/Padilla_Tectonic_Map_of_Mexico_2013.zip

Ross, P. S., Delpit, S., Haller, M. J., Németh, K., & Corbella, H. (2011). Influence of the substrate on maar-diatreme volcanoes - An example of a mixed setting from the Pali Aike volcanic field, Argentina. Journal of Volcanology and Geothermal Research, 201(1–4), 253–271. https://doi.org/10.1016/j.jvolgeores.2010.07.018

Suter, M., Quintero, O., & Johnson, C. A., (1992). Active faults and state of stress in the central part of the Trans-Mexican Volcanic Belt, Mexico 1. The Venta de Bravo Fault. Journal of Geophysical Research, 97, p. 11983, doi: 10.1029/91JB00428.

Tsutsumi, H. & Perez, J.S., 2013. Large-scaleactive fault map of the Philippine fault based on aerial photograph and interpretation. Active Fault Research, 39, 29-37.

Turrin, B. D., Gutmann, J. T., & Swisher, C. C. (2008). A 13 +/-3 ka age determination of a tholeiite, Pinacate volcanic field, Mexico, and improved methods for 40Ar/39Ar dating of young basaltic rocks. Journal of Volcanology and Geothermal Research, 177(4), 848–856. https://doi.org/10.1016/j.jvolgeores.2008.01.049

Van den Hove, J., Grose, L., Betts, P. G., Ailleres, L., Van Otterloo, J., & Cas, R. A. F. (2017). Spatial analysis of an intra-plate basaltic volcanic field in a compressional tectonic setting: South-eastern Australia. Journal of Volcanology and Geothermal Research, 335, 35–53. https://doi.org/10.1016/j.jvolgeores.2017.02.001

Vogel, T.A., Flood, T.P., Patino, L.C., Wilmot, M.S., Maximo, R.P.R., Arpa, C.B., Arcilla, C.A., & Stimac, J.A., 2006, Geochemistry of silicic magmas in the Macolod Corridor, SW Luzon, Philippines: Evidence of distinct, mantle-derived, crustal sources for silicic magmas: Contributions to Mineralogy and Petrology, 151, p. 267–281, doi: 10.1007/s00410-005-0050-7.

White, J. D. L., & Ross, P. S. (2011). Maar-diatreme volcanoes: A review. Journal of Volcanology and Geothermal Research, 201(1–4), 1–29. https://doi.org/10.1016/j.jvolgeores.2011.01.010

VITA

Cody Nichols received his Bachelor of Science in Geology and Chemistry at Northwest Missouri State University in May of 2015. Three years later, he received his Master of Science in Environmental and Urban Geoscience at the University of Missouri-Kansas City in May of 2018. While at the University of Missouri-Kansas City he held a graduate teaching assistantship and taught the Understanding the Earth Lab for two of his three years enrolled. As an undergraduate student at Northwest Missouri State University, he held an undergraduate teaching assistantship and assisted with teaching the Earth Science and Botany Labs. While working on his master's thesis, Cody was selected to present his research at the IAVCEI 2017 Scientific Assembly. Cody is a member of the International Association of Volcanology and Chemistry of the Earth's Interior.